Large Deformation Structural Performance of Double Skin Composite Construction using British Steel's "Bi-Steel"

by

Brett McKinley M.Eng.

Thesis submitted to City University for the degree of Doctor of Philosophy

Department of Civil Engineering, School of Engineering
City University, London

December 1999

Table of Contents

Figures

Tables

Plates

Acknowledgements

The research detailed in this thesis has been conducted at the Department of Civil Engineering, City University and was funded by an EPSRC CASE award with British Steel plc and the Steel Construction Institute as industrial partners. The author wishes to thank his supervisor Professor Laurie F. Boswell for the continued help, guidance and support throughout the duration of this research. The author would also like to thank the technical staff of the Department of Civil Engineering for their continued assistance and without whom, it would not have been possible to conduct this work. Thanks go to Mr. Tony Jones, Mr. Les Ansdell, Mr. Paul Mennell, Mr. Jim Rose, Mr. Ahmed Saeed and Mr. Graham Gatehouse. Dr. Stuart Robson and Mr. Neil Woodhouse are also thanked for their survey measurements using digital photogrammetry and the subsequent signal processing.

Thanks are also expressed to Dr. J. Tolleczko, formerly of SCI, who initiated this research programme, Mr. H.G. Bowerman, of SCI, for continuing the support and allowing the research to be carried out and to British Steel plc for providing the steel specimens and financial contributions for this research. Finally, the support and understanding of family and friends throughout this period has been very important to the author.

Declaration

I declare that the work contained within this thesis is all my own work except where explicit reference is given. I also hereby give consent to the library for this thesis, in whole or in part, to be copied without the need to seek permission from the author.

Signed: 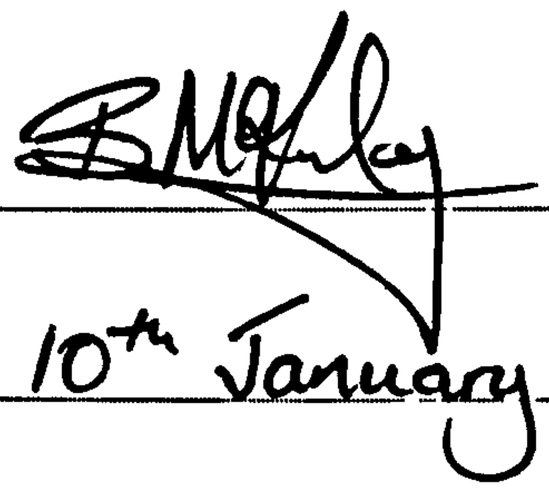 Brett McKinley

Date: 10th January 2000

Synopsis

Double skin composite construction consists of two relatively thin steel plates with the space between filled with, usually, normal weight concrete. The transfer of shear between the steel and concrete is possible through the use of steel shear connectors that are welded to the steel plates.

A study of previously published information revealed that the areas to market double skin composite construction would be submerged tube tunneling and floating offshore structures, particularly those used for the storage of crude oil.

Double skin composite construction was traditionally fabricated with headed studs, as used in composite bridge construction. These were welded to each of the steel plates which were then temporarily held in place whilst the concrete was cast. This method of construction was costly in time and labour so British Steel Plc and The Steel Construction Institute developed an idea of using continuous friction welded bars. These connect to both plates to form a continuous steel structure. By manufacturing steel panels, up to 12m by 3m in a factory environment that requires no additional formwork allows great savings in time and labour during the construction process.

Research on Bi-Steel, as it is known, is being carried out on numerous fronts with that detailed in this thesis being part of it. This thesis covers the overall performance aspects of strength and stiffness throughout the elastic and plastic regions of deformation and includes local buckling of the compression plate.

Analytical solutions are developed for all aspects dealt with by this thesis which are supported with an experimental test programme. The test programme uses 16 full-scale, wide beam specimens that are tested in three point bending. The first series of tests carried out, which used the first two prototype Bi-Steel panels, compared the existing method of construction of double skin composites with Bi-Steel, the new method of construction. The second series of tests, divided into two parts, helped to develop the strength, stiffness and local buckling equations.

The first series of tests showed that Bi-Steel was structurally the better performer. This was due to the continuous nature of the steelwork, which allowed the full strength of the steel to be achieved and structural continuity even after buckling failure. The traditional method of constructing DSC was no weaker or less stiff than its Bi-Steel counterpart, but the headed shear studs prematurely pulled out of the concrete.

The second test series, which only used Bi-Steel panels, showed that an Euler analysis can be carried out to determine the buckling load of the compression plate. It also showed that the post yield gain in strength of the panels was due to strain hardening of the steel tension plate.

In conclusion, it has been structurally and financially beneficial to develop Bi-Steel. The factory fabrication of the steelwork increases quality control and the unit type product allows easy on-site assembly. The structural performance of Bi-Steel is now well understood with few areas left to study which are now being addressed. The first design code has now been produced by SCI for the design of Bi-Steel components.

Key to Symbols

Geometric Properties

A_1	Cross sectional area of plate 1
A_2	Cross sectional area of plate 2
A_c	Cross sectional area of concrete
b	Width of element
d	Distance between centroids of plate 1 and plate 2
D	Diameter of shear connector
g	Gravitational acceleration
h_c	Height of concrete
l	Length
l_e	Effective length
L	Span
n_x	Number of connectors in direction of x
n_y	Number of connectors in direction of y
s_x	Spacing of connectors in direction of x
s_y	Spacing of connectors in direction of y
t_1	Thickness of plate 1
t_2	Thickness of plate 2
y	Distance from centroid to a point on a section
y_1	Distance from neutral axis to centroid of plate 1
y_2	Distance from neutral axis to centroid of plate 2
z	Depth of neutral axis from interface of steel plate 1 and concrete

Physical Properties

δ	Shear deflection of shear connector
Δ_1	Composite deflection of double skin composite element
Δ_2	Shear deflection of double skin composite element
Δ_T	Total deflection of double skin composite element
E_c	Young's modulus of concrete
E_s	Young's modulus of steel
ε_1	Longitudinal strain in plate 1
ε_2	Longitudinal strain in plate 2
ε_c	Longitudinal strain in concrete
ε_{e1}	Longitudinal strain at edge of plate 1
ε_{e2}	Longitudinal strain at edge of plate 2
ε_{t1}	Transverse strain in plate 1
ε_{t2}	Transverse strain in plate 2
f_1	Stress in the plate 1
f_2	Stress in the plate 2
f_c	Stress in concrete
f_{y1}	Tensile strength of plate 1
f_{y2}	Tensile strength of plate 2
f_c	Tensile strength of shear connector
f_{cu}	Concrete cube compressive strength
G	Shear modulus of core
G'	Effective shear modulus of core
H	Post Yield Strength Coefficient

I	Second moment of area
I_b	Second moment of area of shear connector
k	Modulus of foundation
κ	Curvature
K	Bending stiffness
m	Modular ratio
n	Strain hardening exponent
π	Pi
ρ	Density
σ	Post yield stress
υ	Poisson's Ratio
υ'	Shear strain

Force and moment properties

F_1	Force in plate 1
F_2	Force in plate2
F_{cu}	Force in concrete
M	Moment
M_y	Yield moment of resistance
M_{py}	Post yield moment of resistance
P	Applied force
P_E	Euler buckling load
V	Shear force

Chapter 1 Introduction and Literature Review

1.1 Introduction

Double Skin Composite construction (DSC), alternatively known as Steel-Concrete-Steel Sandwich construction (SCS), is formed from two relatively thin steel plates infilled with concrete. Connection between the steel and concrete is maintained through the use of mechanical shear connectors. The steel plates are aligned in the plane of bending such that one is in tension and the other in compression when subjected to flexure. A typical arrangement is shown in Figure 1.1.

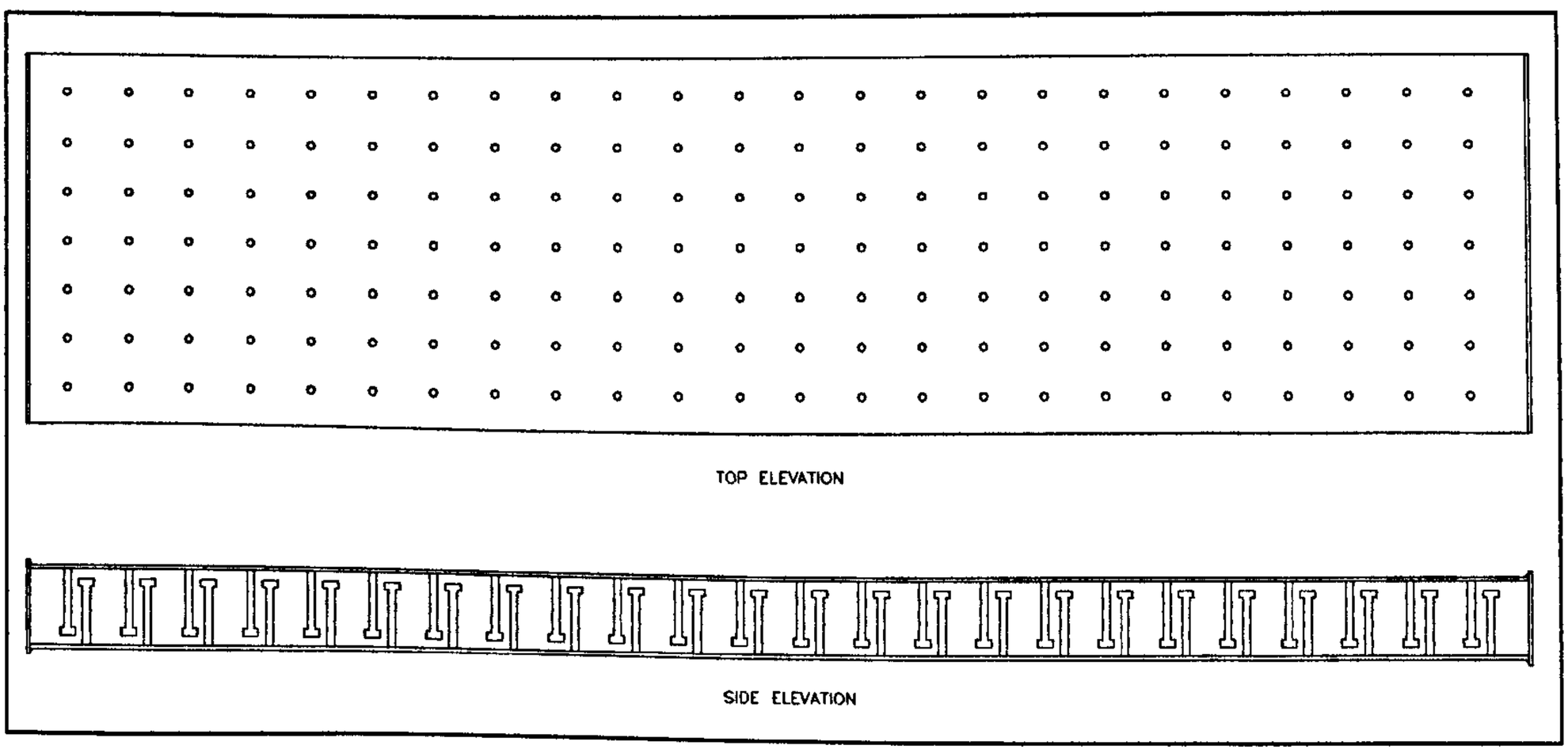

Figure 1.1. Typical Double Skin Composite Arrangements.

There have been a number of different forms of shear connection suggested, but the existing primary form is the shear stud used in composite bridge deck construction (Plate 1.1). Other methods of providing shear connection are rolled sections such as angles [Machida (1992a)] and web plates [Noriji (1986)]. No other reinforcement is necessary.

Plate 1.1. TRW Nelson shear studs.

'Bi-Steel'[1] is a development of the idea of DSC differing in the form of the shear connector. A continuous bar forms the connection and is friction welded simultaneously at both ends to the steel (Plate 1.2). The fabrication of the panels requires specialist tooling which is currently undergoing commissioning trials at British Steel, Scunthorpe.

The bright steel bars are held into a chuck with a cam mechanism. The whole chuck then moves between the steel plates where it is spun at speeds of approximately 2500 rpm. Load is applied to the outside of the panel, which creates sufficient friction to generate the heat required to weld the bar to the plate. During this process, the length of the bar becomes shorter by 6mm. This is due to burn off, which can be mistaken for a poor quality weld (Plate 1.2).

---

[1] 'Bi-Steel' and any associated equipment are patent protected products of British Steel

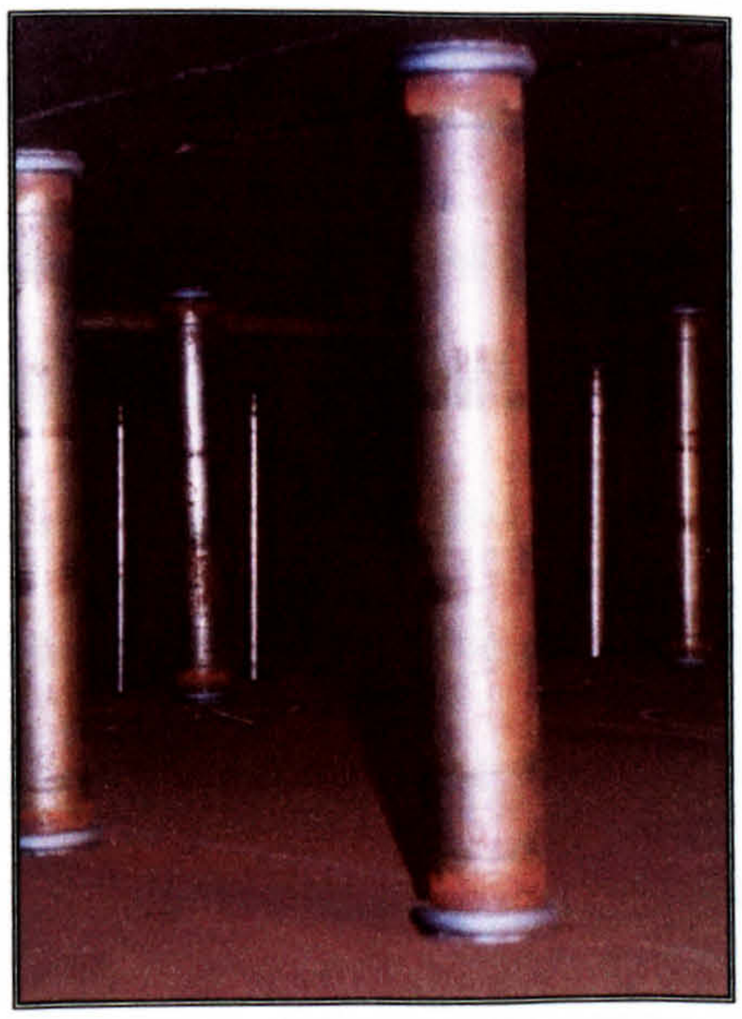

Plate 1.2. Bi-Steel continuous shear connectors.

1.2 Review of Published Information

It is intended that this review of published information be a comprehensive background of research knowledge that has been previously carried out in the areas of double skin composite construction and their applications. Particular attention is given to the development of composite structures, as that is the intention of this thesis, with regard for its use in offshore structures where it is thought that double skin composite construction could be of benefit. In carrying out the investigations for this study any further areas where this form of construction may be of benefit have been included.

Four areas are reviewed which are considered relevant to the eventual use of DSC and these are:

1. A Need for Further Research,
2. Applications,
3. Loading and,
4. Double Skin Composite Construction Research.

'A Need for Further Research' details information that influences the progress of research within the field of DSC. *'Applications'* includes any information on possible uses of DSC that could be identified when marketing the product. *'Loading'* provides information relating to the loads that structures may be subjected to when used in the areas identified in *'Applications'*. Any work that is directly involved with research in the field of double skin composite construction will be found in the fourth section. All four of these sections will be

brought together in the *'Conclusions'* section of this Chapter which provide direction to the research in DSC.

1.2.1 A Need for Further Research

The Steel Construction Institute (1994) identified the research that had been carried out on DSC particularly with respect to the strength of various elements. However, the research was not sufficiently comprehensive to enable DSC to be used in major construction projects. The main conclusions, which were made by SCI were:

1. Engineers are generally unaware of DSC as a form of construction. If they were aware of DSC it was thought to be expensive and liable to corrosion in comparison to reinforced concrete,

2. Existing research was fragmented with regard to the type of shear connector hence there was insufficient information to develop design guidelines. This has now been partly addressed with the publication of a design guide [Narayanan (1994)] and,

3. Research had focused on the strength of elements with little regard to how the elements may be fabricated commercially. This is currently being addressed by British Steel with its 'Bi-Steel' project.

This meant a market study be carried out in order to assess whether or not there was a requirement for DSC. If it was found to be viable then a design publication was required for engineers to use and finally a marketing strategy to promote the product. These are aspects that have been covered by The Steel Construction Institute in the development of Bi-Steel. In carrying these out SCI

have published a design guide on the existing forms of DSC as well as developing Bi-Steel, and a design guide for that is now in draft form (August 1999). Some of the results presented in this thesis have been used in the preparation of the design guide.

A report [CRINE (1998)] has highlighted the ways in which the oil industry can achieve lower capital costs of 30% savings. Also, the report contained the requirements for a reduction of up to 50% in operating costs by the year 2015. There is, therefore, a need to reduce costs throughout the industry. The information contained within this thesis shows how this may be achieved in construction by using Bi-Steel, which by ease and speed of construction reduces construction costs by 15 – 40 % compared with traditional methods of fabrication for steel offshore structures.

Other structures to benefit from the use of DSC are submerged tube tunnels where large lengths of tunnel segments are constructed in dry docks. These are then fitted with bulkheads, floated into position and then ballast is added to sink them onto the sea/river bed. Reinforced concrete is typically used but requires extensive shuttering, often being slip-formed. A DSC submerged tube tunnel would not require shuttering as it provides its own by using the steel skins.

The study carried out by the Steel Construction Institute (1994) also identified a use for double skin composite construction in double skin offshore structures. Floating, Production, Storage and Offloading vessels (FPSO's) were targeted for a study to compare the various forms of construction:

1. Stiffened steel plate,

2. Reinforced Concrete and,

3. Double Skin Composite.

It was found that by using double skin composite construction there were structural and construction benefits that lead to financial savings of 15% and 40% over stiffened steel plate and reinforced concrete construction methods, respectively.

1.2.2 Applications

The original concept of DSC was developed during design considerations of the Conwy submerged tube tunnel on the A55, North Wales [Wright (1991)]. Common practice for this type of tunnel was to use reinforced concrete covered by a thin sheet of steel for water proofing. Considerable research was carried out in the University of Wales, Cardiff [Narayanan (1987), Wright (1991a/b), Edwards (1990)] investigating the possibility of incorporating the strength of the steel into the design. Ultimately, normal construction methods were used for the final design of the Conwy tunnel.

Caissons particularly vulnerable to impact, say from ships around bridge piers, would also benefit from DSC construction. DSC would provide an easy connection for a cutting edge on the lower edge of the caisson even if one were required, the steel plate of the caisson providing an alternative. The steel skin forms a water-tight barrier for the water to be pumped out from within, which can then be filled with concrete.

1.2.2.1 Offshore Structures

Bottom Founded Structures are the traditional way of positioning offshore structures by sitting the structure on the sea bed. Although this provides great stability it can lead to massive structures as the water depth increases. However, most of these are tubular structures where DSC would not be a viable alternative. There are a few cases where there could be benefits and these are presented in what follows:

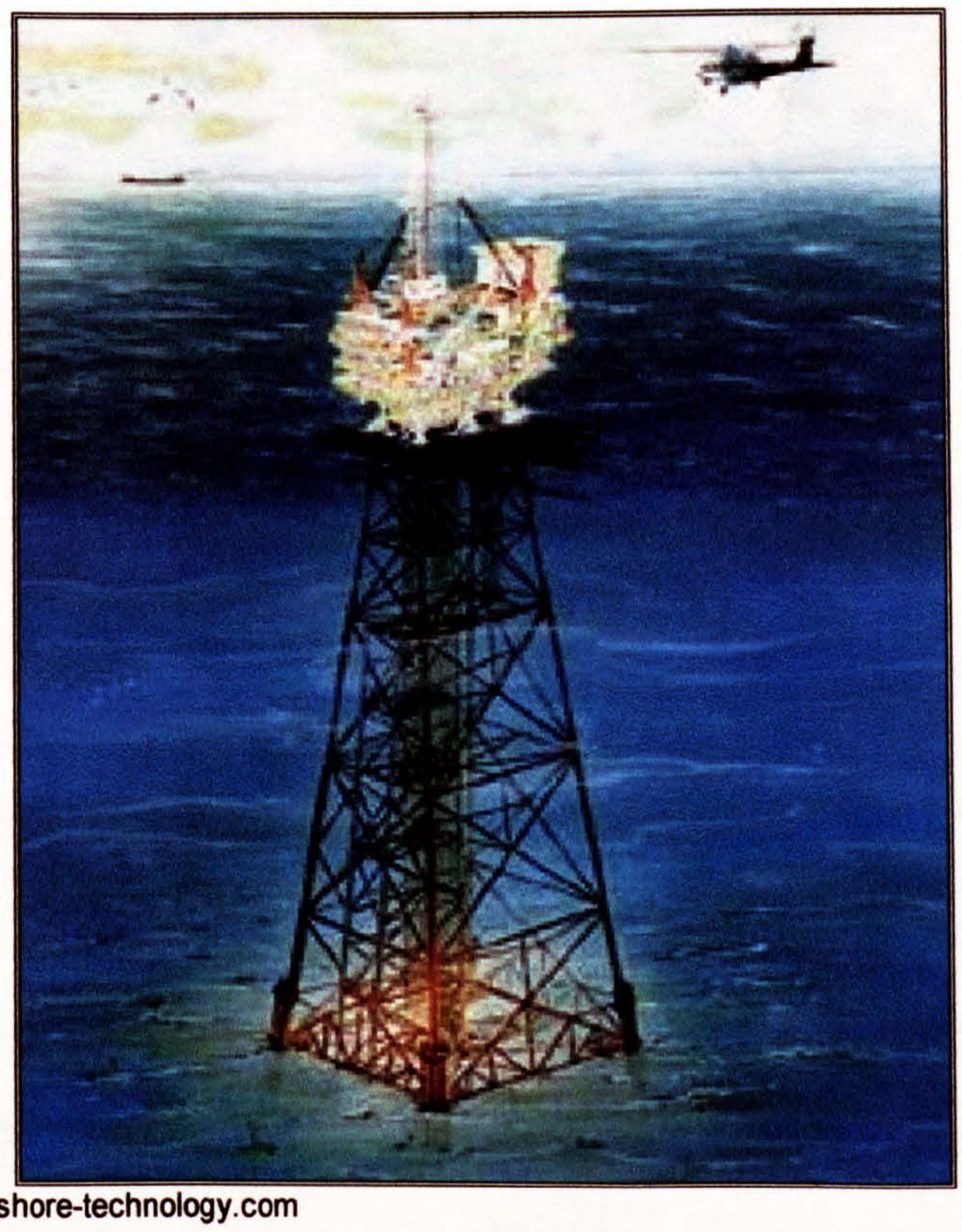

Photo courtesy of www.offshore-technology.com

Plate 1.3. Typical Bottom Founded tubular structure.

- Gravity Based Structures (GBS).

Gravity Based Structures rely on their weight to hold their position on the sea bed of an oil and gas exploration field, this weight being a combination of its own weight and ballast. The use of these structures in places such as the Alaskan and Canadian Beaufort Sea where sea ice is common appears to be a

natural choice due to their bulk. Being constructed from reinforced concrete and the large amounts of ballast they posses gives them this bulk to resist sea ice impacts and movements.

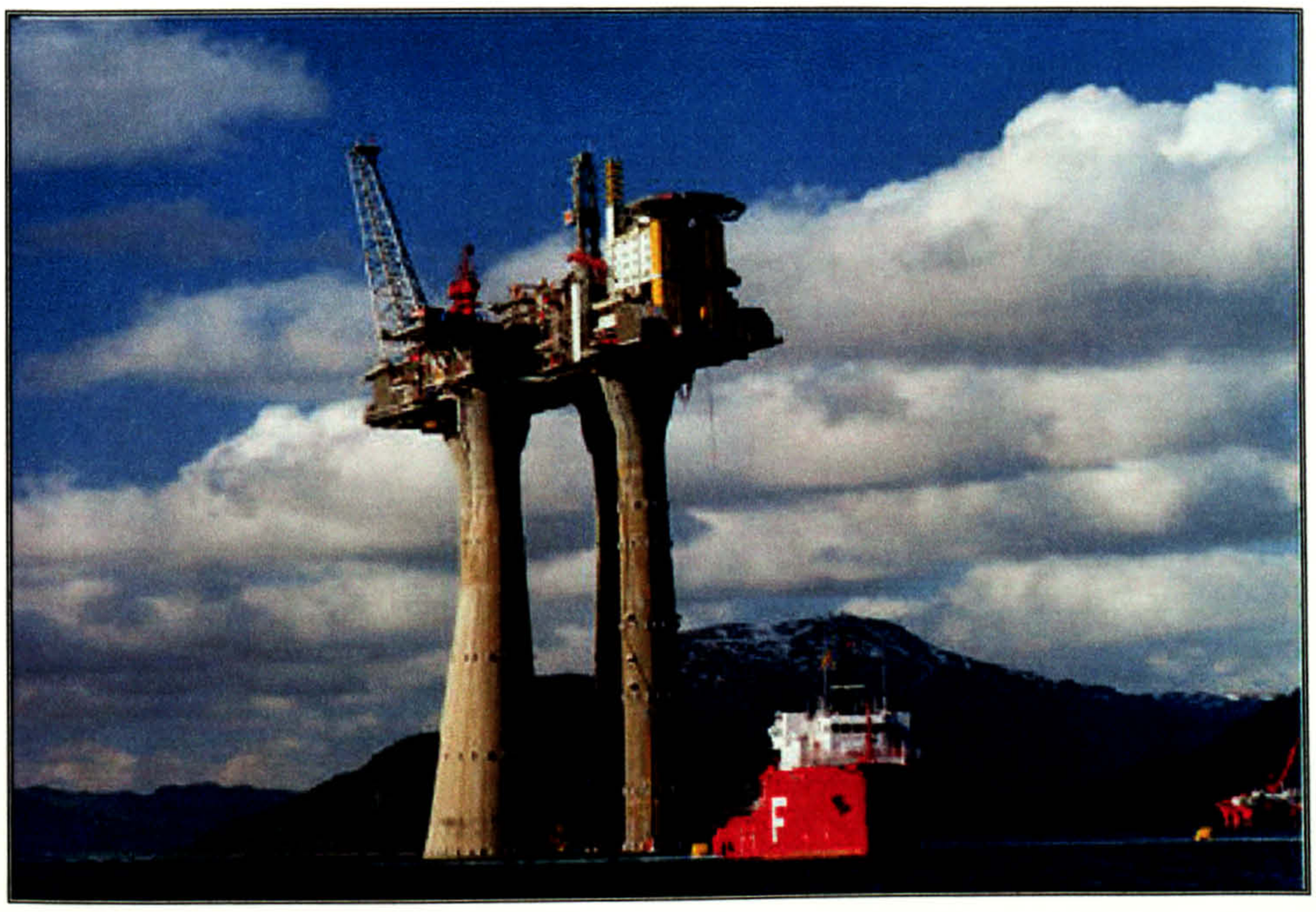

Photo courtesy of A/s norske shell exploration (www.shell.no).

Plate 1.4. Gravity Base Structure showing massive leg construction.

As existing reserves are depleted and the oil prices remain low and competitive, the oil companies are being forced to find cheaper methods of extraction than previously used. Also, new reserves are being found in deeper water such as the West of Shetland Atlantic Frontier zone where at least 5 billion bbl oil are said to be recoverable [Hughes (1995)]. Norway is reaching further north where water depths in the Voring Plateau region reach 800 to 1200 metres. These factors require the development of *Floating Production Systems* since bottom founded structures become uneconomic at such depths.

There are a number of types of floating offshore structure where DSC might be useful within their construction, in whole or in part.

- Floating Production Storage and Offloading units (FPSO).

FPSO's are ship shaped structures and can either be purpose built or converted barges. They are moored in position via the use of a turret mounted at or near the bow and naturally weather vane. Due to the nature of this mooring the vessel is allowed to pitch and roll and hence drilling is unable to be carried out. The first use of a FPSO was in 1977 when the 'Castellon' was installed off the Spanish coast.

Photo courtesy of www.offshore-technology.com

Plate 1.5. FPSO moored in position.

Since FPSO's include storage facilities for crude oil any new vessel constructed needs to be of double skin. This provides a great opportunity to prove and market DSC as an alternative form of construction since floating production has a foreseeable future.

Comparisons of FPSO's constructed from Bi-Steel, plated steel or concrete [SCI (1994)] show the Bi-Steel alternative to be slightly heavier than the steel but considerably lighter than the concrete alternatives. However, the benefits

of manufacture and construction make it the cheapest and fastest method to construct. Costs of the Bi-Steel alternative were 15% and 40% lower than the steel and concrete alternatives respectfully.

- Semi-submersible Platforms.

Semi-submersible Platforms float with most of their hull under the wave zone and are therefore little affected by wave motions. These motions are still not small enough to allow wells to be mounted on board but drilling can be carried out remotely using flexible lines and risers that pass down to the sea bed.

Photo courtesy of www.offshore-technology.com

Plate 1.6. Semi-submersible Platform showing pontoons.

The hull is generally made up from two rectangular shaped pontoons with four cylindrical hollow legs. The deck is approximately 20 metres above sea level and consists of conventional topsides. The Argyll semi-submersible was the first to be used along with the previously mentioned Castellon FPSO.

- FOBOX

FOBOX is a new generation of floating, drilling, production and storage vessel designed for use in waters of up to 3000m depth. Harland and Wolff (1999) have designs for 600000 and 2000000 barrel, storage vessels. The large panels which form the sides of this system provide opportunity for the use of DSC.

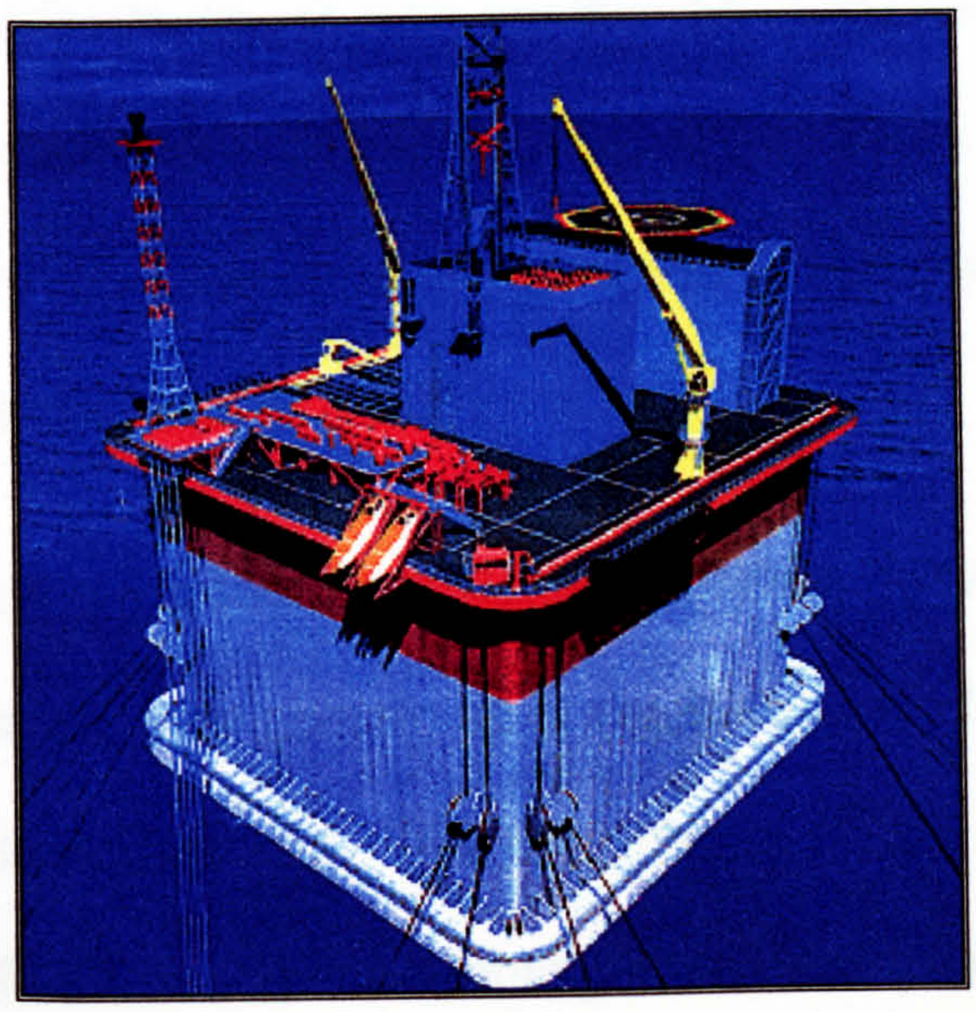

Photo courtesy of www.harland-wolff.co.uk

Plate 1.7. FOBOX floating platform (courtesy of Harland & Wolff).

- Tension Leg Platforms (TLP).

A TLP is structurally similar to a semi-submersible, the main difference occurring in the mooring system. A TLP is moored by a set of vertical pre-tensioned wires that remain in tension under all loading and weather conditions. Typical drafts of TLP's are of the order of 50 metres.

SCI (1994) also reported on a comparison of construction methods between semi-submersibles and TLP's. The most viable scheme was found to use DSC for the pontoons and plated steel for the columns of the hull structure. The use

of DSC for the columns was found to introduce complicated connections between the pontoons and columns.

Until 1995 there had been 21 semi-submersibles, 27 FPSO's and 4 TLP's in operation. Another 6, 11 and 3 respectively were undergoing construction at the same time. It was predicted that up to 100 mobile production units would be required by the year 2000 [www.Bluewater-Offshore.com (1998)]. Current information gives 47 FPSO's in use with another 24 under construction, a total number that has approximately doubled in the last four years. Thirty percent of this total is in the North Sea, an opportunity for the British market in terms of construction and potential use for DSC.

Of all the various floating production systems available, FPSO's are generating the most interest because they contain all of the systems (oil production, storage and offloading) in one unit. This is confirmed by the number of FPSO's in use or under construction. Their capability to be deployed in water depths of 30 - 1000 metres and in all weather conditions [Henery (1995)] making them particularly versatile.

Another advantage of using DSC for the construction of oil containing vessels is the lack of additional stiffening required when compared with normal steel structures. As all forms of double skin composites have all of their local stiffening internally then no additional stiffeners are necessary on the interior surfaces of the tanks. As the surface is now smooth it becomes much easier to clean hence reducing time spent in dock and therefore reducing costs.

The use of DSC in the construction of a GBS has been considered [Isaacson (1988)]. The testing of large scale specimens to resist the high magnitude

forces subjected by ice loads showed that DSC followed theoretical predictions up to ultimate loads.

1.2.2.2 Other Structures

Other areas that may benefit from the use of DSC are those where impact or abrasion resistance is required. The steel plate on the opposite side to the point of impact has a large restraining effect on punching shear [Shukry (1990)]. This makes DSC resistant to projectiles and high intensity local loading. Also, the steel provides protection to the concrete subjected to abrasion by waves or sea ice. Structural elements that may utilise this effect are:

- Ice resisting walls [Nojiri (1986), Ellis (1993)].
- Ice breaker hulls particularly in the area around the bow. The U.S. Coast Guard has carried out measurements [St. John (1992)] of ice loads exerted on the bow of Polar Class ice breakers.
- Military bunkers/ shelters
- Nuclear reactor containment vessels require thick concrete shells to contain radioactivity in the event of an explosion or leak. The external steel plate provides integrity in the event of an explosion.

1.2.3 Double Skin Composite Construction Research

The two main fields in which DSC could be used have been identified and these are for submerged tube tunnels [Narayanan (1987), Edwards (1990), Wright (1991)] and for offshore structures [Hordyk (1994)]. Research into the suitability of DSC for submerged tube tunnels has led to the publication of a design guide by the Steel Construction Institute [Steel Construction Institute (1997)]. The use of DSC in the form of 'Bi-Steel' in the offshore industry was developed to enable steel plate to be a competitor with reinforced concrete [Steel Construction Institute (1994)].

The previously published research of DSC structural elements has been broken down into a number of categories:

Failure Modes

DSC elements

Shear Connectors and Reinforcement

Fatigue Loading

Construction Methods

Economics

1.2.3.1 Failure Modes

The failure of single span DSC elements are broadly described by three different modes of failure:

- *Flexural deformations* are indicated by the upper concrete and steel remaining in compression whilst the lower steel plate is in tension. Final failure involves yielding of the steel and crushing of the concrete although the order in

which this happens can differ. An element with a high steel content (p=4%) will fail by crushing of the concrete followed by yielding of the tensile steel plate. All other beams, with steel contents less than 4% failed by yield of the steel plate [Nojiri (1986)].

Flexural failure is preceded by cracking, which originates from or near to the location of the shear connectors near the load point. As these cracks appear there is a simultaneous slight and sudden increase in the deflections and steel strains at mid-span. The slip between the concrete and the steel plate increases non-linearly with load although the deflections increase in a linear manner. The beams show considerable ductility until final failure when the compression concrete begins to crush. The serviceability limits may not be satisfied throughout the beam due to the presence of the cracks [Oduyemi (1989)].

Hassinen (1989) and Narayanan (1994) give the flexural capacity of a double skin composite element as the axial capacity of the tension steel plate acting about the centroid of the compression steel plate:

$$M_R = A_s f_y (h - t) \qquad \textbf{Equation 1.1}$$

where A_s is the area of a single steel plate (assumes both plates equal thickness),

f_y is the steel yield strength,

h is the concrete depth and,

t is the steel plate thickness.

- *Vertical Shear Failure* occurs as the dowel action capacity of the steel plate, the tensile capacity of the shear connectors or their welds are reached.

This mode of failure develops an inclined crack that originated as a flexural crack within the shear span. The crack propagates towards the load point, flattening at the neutral axis and continuing with further increase in load. If sufficient shear reinforcement is provided then failure in this manner can be prevented. Adequate numbers of long studs can achieve this.

The vertical shear capacity of DSC beams without shear reinforcement will be dependant upon the strength of the concrete, the tensile steel area, the shear span/effective depth ratio and the tensile connection ratio [Oduyemi (1989)]. Hassinen (1989) agreed with the empirically derived solution for the shear resistance of a double skin composite panel that has been developed by C-Fer [Adams (1987)]:

$$V_R = \frac{1.35 f_c b d \rho^{0.5}}{(a/d)^{1.3}}$$ **Equation 1.2**

where f_c is the concrete cube strength,

b is the width of the beam,

d is the depth between the centroids of the steel plate,

ρ is the connection ratio, which is equal to the shear connector shear strength divided by the steel plate tensile strength and,

a is the length of the shear span.

- *Horizontal Shear Failure* occurs suddenly when the shear capacity of the connectors or studs is reached. Failure by this mechanism occurs at the steel concrete interface and can be prevented through the provision of a sufficient number of connectors to give a shear resistance greater than the axial load expected in the steel plate. Fewer cracks appeared during this mode of failure

when compared to a flexural failure [Oduyemi (1989)]. Shear failure can be preceded by slip between the steel and concrete, which can be controlled by the stiffness of the shear connectors. A more detailed study is made later in the Chapter.

Local buckling of the top steel plate may precede the above failure modes if the spacing of the shear connectors is too great. Equating the Euler buckling load to the yield load of the steel plate gives limiting values of spacing/plate thickness ratio (s/t) of 25 and 50 for simply and fixed supported beams respectively. Experimental limiting values of 33 and 50 were found and hence a design value of 30 for all cases has been suggested as good practice [Oduyemi (1989)].

1.2.3.2 DSC Elements

Previously published information has covered a number of different types of structural elements. These have been broken down into basic groups for review and include:

- Beams,
- Axially and Eccentric loaded columns,
- Corners, junctions and sections and,
- Shear connectors and reinforcement.

Beam Elements form the largest concentration of DSC research with a considerable number of samples having been tested. Most of these were subjected to static load conditions with other undergoing quasi-static and fatigue loading. Element dimensions, that have been tested in previous

research, range from small scale to full size. Noriji (1986) tested beam elements of 600(l) x 300(b) x 300(h) up to 1500 x 900 x 360 in various test arrangements of 3-point or 5-point loading. Machida (1992) tested beams up to 3200(l) x 250(b) x 300(h), in four point bending.

A number of *Flexure and Shear Resisting Mechanisms* that are at work within DSC beam elements have been suggested. Some of these suggestions are direct contradictions of each other in the conclusions that they have drawn. Most agree that DSC sections can be designed and behave using existing reinforced concrete (RC) theories with some additional detailing [Nojiri (1986), Edwards (1990), Hordyk (1994)]. The additional detailing relates to the shear connector design in order to ensure that the section retains its composite nature. Hordyk (1994) supported the experimental test results with non-linear analysis.

Strains at the intersection of the steel plate and concrete can be used to calculate the position of the neutral axis. Its position calculated from strains by Machida (1992b) during elastic loading showed that it did not remain in the same position as would be expected from elastic beam theory. However, the strains up to the point of yield from Nojiri (1986) were reported as agreeing well with those calculated in conventional RC theory where assumptions of "plane sections remain plane" are made.

It was also reported that the measured strains in the transverse sections did not obey the principles due to Poisson's ratio. Transverse sections were not in equilibrium as shown by the calculation of longitudinal forces of the steel plates.

An experimental investigation of eight beams to determine the flexure and shear resisting mechanisms was carried out [Machida (1992b)]. The beam dimensions were:

Span = 2000 (3No), 2600 (1No), 3200 (2No) and 2900mm (2No)

Width = 300mm

Depth = 250mm

The variable parameters were the shear span/depth ratio (a/d) and the steel plate thickness (t).

In beams with larger shear span to depth ratio ($a/d \cong 4.0$) the cracks originate from connectors near the support at an angle near to 45°. They continue horizontally until changing direction, again at 45°, towards the load point causing failure. Beams with smaller shear span to depth ratios (a/d = 2) exhibited tied arch behaviour before collapse provided that there was sufficient shear connection. The formation of the truss or tied arch occurs with compression elements (struts), acting either side of the diagonal shear cracks. This was evident by a gradual reversal of the strains in the steel plate, near the load and support points as the steel plate yields. Hence it was concluded that DSC beams do not have the same load carrying mechanism as RC beams [Machida (1992a); (1992b)].

However, Nojiri (1986) questioned these results after carrying out tests which directly compared DSC beams with RC beams. A number of tests on two span continuous beam elements showed that flexural cracks appeared at the load point with inclined shear cracks then developing from the edge of the support plate. These cracks continued to the edge of the centre load plate. It was from

this point that a truss mechanism was assumed to be acting. Failure occurred due to crushing of concrete struts at the lower end after the tensile steel plate had yielded at and around the load point. Therefore, it was found that although DSC beams did behave in a truss type manner, it showed that RC beams did so also and, therefore, the two methods of construction behave similarly.

The load carrying capacity of the beam will also increase after yielding of the shear reinforcement. This is partly demonstrated by an increase in the deflections over those calculated using beam theory. Beams with larger a/d ratios gave better correlation suggesting that the mechanism at work is flexural [Machida (1992a)].

The point at which the shear connector is welded to the steel plate is subjected to stress concentrations due to the forces exerted by the compression struts. The stage at which these become apparent depends on the ratio a/d. For large values (a/d=4) the stress concentrations appeared after shear cracking and vice versa. For a/d = 3.5 with additional vertical webs no stress concentrations were found possibly suggesting that the webs prevented their formation [Machida (1992a)].

A number of parametric studies have previously been carried out and can be divided into a number of categories. These categories are:

- steel ratio or content (p)
- overall ductility
- confinement
- shear connector spacing

- concrete strength

Load/deflection curves [Oduyemi (1989)] for beams with a change in tension steel area indicate linearity until the steel begins to yield. After yield there is no increase in load carrying capacity although all beams indicate considerable ductile behaviour. A reduction in the tension steel ratio leads to an increase in overall ductility of a DSC beam. This is further proven by the tension steel strains that increase as the steel ratio decreases.

These findings have been further qualified by Nojiri (1986), Edwards (1990), Wright (1991) as they found that a reduction in the steel ratio led to an increase in the beam ductility.

Increasing the steel ratio (p=1-4%) with a constant length/depth ratio decreases the difference between calculated and test failure loads [Nojiri (1986)]. The flexural capacity was calculated either by:

1. Neglecting the compressive steel plate.

2. Including the compressive steel plate.

The method of determining which of these to use was by experience on what had been considered in a particular test. It was found that these methods overestimated the capacity of the beam by 3%, with a standard deviation of 9%. No reason was given to explain why it might be possible to use two alternative methods for determining the flexural strength of a double skin composite beam.

The ductile behaviour was observed during the testing of various DSC beams, Nojiri (1986), Edwards (1990), Wright (1991) and Oduyemi (1989) believed that a reduction in the steel area, particularly on the tension plate, led to an increase

in the ductility. Without any additional shear reinforcement the beams tested by Nojiri (1986) all failed in a brittle manner. The exception to this occurred in a beam of low steel content (p=1%) which exhibited considerable ductility and continued to carry the increasing load after the steel plate had yielded. Strain hardening of the tensile steel plate was suggested as the cause of this. The inclusion of shear reinforcement improved the situation as all beams failed in a ductile manner with deflections reaching 4% of the span.

A direct comparison with similar reinforced concrete beams showed that they all failed in a brittle manner. This may suggest that the DSC form of construction increased the ductility of a beam provided that the steel content remains low or additional shear reinforcement is included.

However, Edwards (1990) found that DSC beams exhibited considerable ductility throughout the range of shear span/depth ratios tested.

Roberts et al. (1996) described the testing of beam specimens and compared the results to theoretical predictions made in accordance with a recently published design guide [Narayanan (1994)]. The test specimens were subjected to relatively high shear force to bending moment ratios in order to assess the ability of long shear studs for resisting transverse shear. It was found that they were and that the theoretical predictions gave satisfactory results for lower bound solutions, as may be used in design. Also calculated was a limit to the stud spacing to plate thickness ratio for buckling considerations. This was given as 45 and assumed that buckling would occur at 1.5 times the allowable stress in the compression plate.

In order to assess the effects of an element contained within a structure (i.e. continuous span) the concrete can be confined by the addition of end plates. Two tests were carried out which showed that confinement is taken into account by increasing the effective cube strength in proportion to the degree of confinement [Hordyk (1994)]. Roberts (1996) suggested that in order to provide sufficient resistance to slip, then 20% of the shear connectors should be placed beyond the centreline of the support.

As the amount of shear connection on the tension steel plate is reduced, so does the maximum strain achievable. Hence, there becomes a point where the steel is unable to develop its full yield strength and failure of the beam occurs due to shearing of the connectors. A reduction in shear connection also reduces the stiffness of the beam [Wright (1991), Oduyemi (1989)].

A reduction in the shear connection on the compression steel plate has little effect on the strength or ductility of DSC beams. This is due to the connectors being fixed in concrete subjected to high compression and hence they can develop high strength and stiffness [Wright (1991)].

The strength of the concrete had little effect on the failure mode of the DSC beams [Wright (1991)]. However, low strength concrete allowed early crushing in over reinforced sections. If an insufficient number of connectors are provided then low strength concrete will prematurely cause the beam to fail by *horizontal* shear.

Testing and analysis was carried out for elements in axial compression [Hordyk (1994)]. The results showed that DSC compression elements can also be designed similarly to reinforced concrete elements.

Column tests [Edwards (1990)] failed through buckling or yielding of the compression plate. Some concrete crushing did occur. No concrete cracking occurred since load eccentricity was not great enough to produce tension. Analysis of test results shows conventional RC and composite theories can be used.

Columns increased in ultimate load capacity with increased steel provided there were adequate studs (spacing/plate thickness < 50) [Wright (1991)]. Stud pull out strength was related to their length and to the concrete strength. Concrete strength had little effect on behaviour but effected the level of failure. Slip is important to DSC, if composite action is to be achieved, and is resisted by adequate shear connection.

Beam-columns lost ductility with increasing axial load. Reducing top connection had little effect, but reducing the amount of bottom connection increased the slip and the deflection. Increased steel (top or bottom) increased the capacity provided sufficient studs are provided to carry the additional forces [Wright (1991)].

Hordyk (1994) carried out large scale tests on 1.8m and 2.9m diameter cylinders with total wall thickness of between 40mm and 60mm. These showed that local buckling strengths are significantly increased when compared to an all steel cylinder of similar weight. This is due to a decrease in the effective buckling length caused by the presence of the concrete and a corresponding restriction of deformations.

Some tests have also been carried out on various corners, junctions and other sections in an attempted to model DSC in practical applications [Narayanan

(1987), Edwards (1990)]. The bulk of this research was performed for the aforementioned submerged tube tunnel across the River Conwy. The scale of the samples varied depending on the size of the element to be modelled. Corners and junctions tended to be close to or at full scale whilst a complete tunnel section was scaled at a fifth full scale.

A tunnel corner was modelled [Narayanan (1987), Edwards (1990)] and subjected to closing and opening tests. Closing tests showed some cracking of concrete on the outer tensile corner. The tensile steel plate separated from the concrete almost instantly as the opening load was applied. Failure occurred as the short studs pulled out from the concrete and the longer studs yielded at the steel plate. Large portions of the element remained intact giving this form of construction benefits when used in areas subjected to blast loading.

Junction tests failed due to separation of steel on tension corners in a similar manner to the corner sections. Corners with radii improve the situation over squared corners [Edwards (1990)].

An element modelling a tunnel wall between points of contraflexure (full scale) [Narayanan (1987)] was subjected to a static load test. Failure of the element occurred due to shear cracking at 1/4 shear span and by the studs shearing in the tension zone. The peak measured shear failure load (475kN) was some 70% greater than calculated (280kN).

A single, one fifth scale tunnel sample [Edwards (1990)] was subjected to two tests of vertical and horizontal (50% of vertical) loading simulating actual loading conditions. Failure occurred due to shear cracking of the concrete at an upper internal corner, which was then repaired for a repeat test. The

second test failed in the same area although new cracks appeared showing that the repaired section was effective.

Different types of shear connector and methods of providing additional reinforcement have also previously been investigated. The most widespread in use are the conventional stud connectors used in composite bridge deck construction. These transfer the shear across the section when the opposing plates are brought together. Other types found in use are generally limited to single research projects looking to validate the use of such a connection system. These include the use of rolled sections (particularly angles) [Machida (1992a)], web plates and straight bars [Nojiri (1986)]

A number of other possible forms of shear connector were identified as part of an application study (Figure 1.2) [Steel Construction Institute (1994)]. The most viable included those mentioned above plus:

- Bent bars, forming a trapezoidal shape and welded to each steel plate,
- Trough sections, forming inclined webs between the steel plates,
- Hot rolled sections, forming webs between the steel plates and the flanges reducing stresses at the junction for increased fatigue performance,
- Cold rolled sections, again forming perpendicular webs and,
- T-sections, welded to each steel plate and overlapping when each plate is brought together in a similar manner to conventional studs.

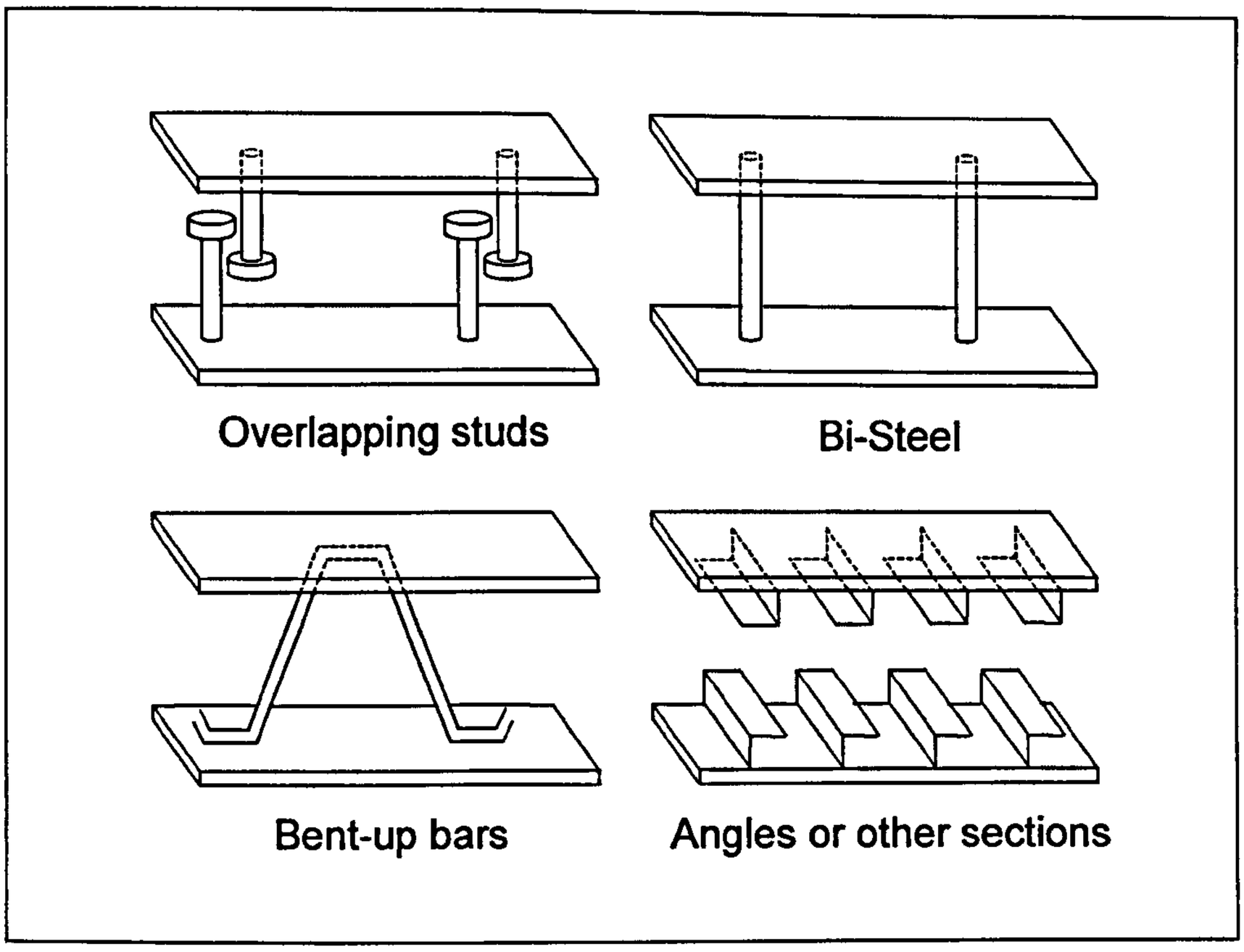

Figure 1.2. Different forms of shear connector.

However, the cost and construction considerations for these alternatives generally make them non-viable. It was found that the cost of the end product depended heavily on the amount of material used in the shear connection. Also the amount of welding necessary to connect a rolled section is large in comparison to studs and bars, which again increases the cost.

Nojiri (1986) also investigated the possible use of alternative forms of shear connection in beams, which included long studs, web plates and bent-up bars. The long studs improved both the strength and stiffness characteristics of the beam. The use of vertical webs increased the strength of the beam, but had no effect on the stiffness. Bent-up bars were placed to cross the diagonal cracks at right angles. A lack of anchorage and fixing in the tensile zone prevented any reasonable results from being obtained.

The different modes of failure of a DSC element were discussed earlier in 'Failure Modes'. It has been shown that the shear connectors can have a considerable influence on which of these modes occurs in the element.

It is widely considered [Hordyk (1994); Wright (1991); Oduyemi (1989); Steel Construction Institute (1997)] that if there are an insufficient number of connectors then the structural integrity between the concrete and the steel can be lost. This would be indicated by relative slip between the concrete and the steel skin eventually causing the connector to bend. Alternatively, it may pull out of the concrete, fail in tension, or cause the weld attaching it to the steel skin to fail. The element would therefore failure in *Horizontal Shear* instead of in *Flexure*.

However, if there are a sufficient number of studs to transmit the loads to the steel plate, failure of the element will occur in a *flexural* or *buckling* manner [Hordyk (1994)]. This will happen by either tensile yielding of the steel or by compression buckling of the steel, which occurs between adjacent studs. Therefore, the spacing of the connectors has to be considered along with their number. It is insufficient to provide one of these criteria alone in order to assure a *flexural* failure.

The connectors can be used as transverse shear reinforcement in a DSC element [Hordyk (1994)] provided that they are long (i.e. they reach across the section) [Wright (1991)]. This increases the shear capacity of the concrete, which would be unlikely to fail in a correctly proportioned section anyway.

Although concrete can fail in shear if an insufficient reinforcement is provided, a DSC section would have a large amount of residual strength due to the steel

plates. These would have a residual shear capacity and ductility enabling large deformations to occur without overall failure of the element.

The other form of failure that may occur is of the connector itself. Narayanan (1987) investigated the different failures of TRW Nelson stud connectors at two different lengths. The short stud connectors (less than 125mm) failed by cracking of the concrete followed by the studs pulling out from the block. The long connectors (greater than 125mm) failed through the yielding of the stud material.

Oduyemi (1989) shows the effect of varying the amount of shear connection on load/mid span deflections for DSC beams. It was suggested that in order to calculate the required number of connectors their capacity should be taken as:

- 55% of the connector pull out force for those located on the tensile steel plate.
- 80% for those located on the compressive steel plate.

This reduction in the connector capacities was attributed to:

1. Work hardening of the steel increasing the ultimate moment at failure and hence increasing the force the connectors transmit to the concrete.
2. The capacity of the connector being reduced in cracked concrete.
3. The capacity of the connector being reduced by having to resist axial tension due to diagonal shear in the bottom layer.

This research helped develop the Steel Construction Institute design guide SCI-P-131 [Narayanan (1994)], although the magnitude of the tensile plate connector capacity has been amended to 60% of the pull out strength of the

connector. Allowances have been made in the design guide for the pull out force to be based on the smaller of:

1. the tensile strength of the connector

$$0.8 f_c \left(\frac{\pi D^2}{4} \right)$$ **Equation 1.3**

where f_c is the tensile strength of the shear connector and,

D is the diameter of the shear connector.

2. the pull-out force of the connector from the concrete

$$0.29 \alpha D^2 \left(f_{ck} E_{cm} \right)^{0.5}$$ **Equation 1.4**

where f_u is ultimate tensile strength of the stud

f_{ck} is the concrete cylinder strength

E_{cm} is the secant modulus of the concrete

$\alpha = 0.2 h/d + 1$ when $3 \leq h/d \leq 4$ or $\alpha = 1$ when $h/d > 4$

h is the height of the stud.

Equation 1.3 and Equation 1.4 allow for failure of the concrete before the connector can reach its full strength.

Strain gauges placed on connectors revealed that the upper section was subjected to bending moments and tensile axial forces [Machida (1992a)]. Also shown was the fact that the connector was subjected to shear at lower loading conditions. As the loads increased the flexural deformations become dominant and the lower section of the connector is subjected to large bending moments. This is partly due to the tensile plate around the shear connector being

subjected to forces from the compressive strut. This possibly causing the stress concentrations found at the base of the connector.

An investigation of the shear strength of the bars used in Bi-Steel was conducted by Moy (1998a and 1998b) where the effect of different plate thickness (5 – 12mm) on the shear strength of the connectors was studied. No analytical work is presented. It was found that the thickest plate (12mm) caused the behaviour to change from ductile to brittle since the connector to plate connection failed suddenly. This was concluded to be the upper bound for the shear strength of the bars with a lowest tested value of 458Nmm^{-2}or 225kN per weld. Moy (1998a) concluded that the concrete strength had no effect on the shear resistance of the Bi-Steel bars. However, this was contradicted by a later publication [Moy (1998b)]. This latter publication extended the initial work by testing similar specimens with more instrumentation, in order to determine the behaviour at the bar to plate connection. It was found that the shear strength of the bars was significantly lower than previous testing (approximately 80%) and was contributed to a lower concrete strength (approximately 90%). No direct comparison of shear strength to concrete strength was made.

The behaviour of the connector to plate connection changed in all other plate thickness (5 – 10mm) where the connector caused increasing deformations of the plate with decreasing plate thickness. In some cases, the plate began to tear, initiating from the weld affected zone. None of the brittle behaviour was evident in any of these tests. When the plate thickness is small (5mm), the connector bends as if simply supported at its ends due to a plastic hinge forming in the steel plate. However, when the plate thickness increases to

8mm, it is able to provide restraint at the end of the connector and, hence, negative bending moments occur. It was concluded that the behaviour of the connector was analogous to a beam on an elastic foundation.

In all of the data presented by Moy (1998a) there was little difference in the performance of the specimens having plate thickness of 5mm to 10mm. A comparison is made of bar shear strength to the plate thickness in which there is a slight increase in strength for an increase in plate thickness. However, the values presented for shear strength were taken as the lowest recorded for a particular plate thickness although there was some variation in them.

Another characteristic of the longitudinal shear forces is that of slip between the concrete and steel plates. Slip is generated when the shear connectors deform due to the interface shear forces and is, therefore, dependant on the stiffness of the connector and its connection to the steel plate.

Moy (1998b) also measured slip at the steel to concrete interface, at failure, and was 4.32mm with 5mm plate and 5.32mm with 8mm plate. Slip had reached 1.4mm when brittle failure occurred in specimens with 12mm plates. It was not possible to calculate the degree of connection (the total shear capacity of the connectors divided by the axial capacity of the plate) due to missing dimensions from the papers reviewed.

The effect of additional reinforcement within DSC elements was studied with tie bars acting as shear reinforcement [Nojiri (1986)]. Elements with low levels of reinforcement developed cracks at lower loads than those without although the cracks were more distributed throughout the beam. Failure occurred as the steel plate yielded, followed by tensile failure of the tie bars, and the

development of large deflections. Heavily reinforced samples failed when large flexural cracks had developed and the tensile steel plate started to strain harden. After a certain level of reinforcement the beams reached their flexural capacity.

For the purposes of ductility DSC beams should have additional shear reinforcement to confine concrete, as reinforced concrete beams, particularly if thick plates are used [Nojiri (1986)].

Additional tensile reinforcement in beams increased the flexural capacity and reduced slip at the tension plate interface with the concrete [Edwards (1990)].

It was also found that L-shaped shear connectors may accelerate shear failure although they performed adequately [Machida (1992a)].

1.2.3.3 Fatigue Performance

Roberts and Dogan (1998) investigated the fatigue performance of TRW Nelson shear studs in beam elements and push shear specimens. A comparison is made between each set of results and Eurocode 3 – Design of Steel Structures. It was found that EC3 is generally conservative although the push shear test results were very close to predictions. The beam test results gave shear strengths that were slightly higher, although they compared well with other data presented. The conclusions drawn stated that the design was generally conservative due to assumptions which ignored slip at the steel concrete interface.

Fatigue failure occurred due to cracking of the tension plate stud connectors [Edwards (1990)]. A significant reduction in cycles to failure occurred due to an increased loading range.

Improvement in the fatigue performance of studs could be achieved by implementing the following.

- Increase the diameter particularly at its base and hence reduce the stresses,
- Use a welding procedure that minimises heat input. Friction welding is particularly good and,
- Use low carbon content steel and hence improve the materials resistance to fatigue. Cold forging could also be used to improve strength and enhance grain structure.

1.2.3.4 Construction Methods

It would be difficult to identify and replace poor quality concrete within a DSC element. A high level of quality control needs to be maintained if this situation is to be avoided. Non-destructive testing including ultra-sonic methods are able to detect voids but their extent may not be fully determined. A slight separation can show up the same as a large void in the same area.

In Arctic conditions there could be a temperature difference of 70°C across the sandwich element. The concrete at the steel interface will be close to the interior or exterior temperatures resulting in the temperature gradient across the concrete. Any remaining water in the concrete unable to escape due to the steel skins would migrate to the cold areas and could form ice. The expansion could cause de-bonding of the steel and concrete or lamination of the concrete, which could be prevented by closer spacing of the studs.

Connection of the studs to the parent material should not take place if the parent material is at or below 0°C (manufacturers requirement). This should not provide a problem if construction takes place in a warmer climate if the structure is eventually destined for Arctic waters.

Connections between fabricated panels were also considered [Steel Construction Institute (1994)]. Panel to panel butt joints would be made using a bent steel strip. This would project from the edge of a panel with a slight taper inward to ease slotting together of the panels. It would also provide a backing for welding of the joint. For 'T' and 'X' connections there were several alternatives:

- Plated construction where the joint is fabricated into the panels,
- Hot rolled sections such as 'H' sections. The DSC panels can be welded to the flange outstand or the flange at the web location and,
- Heavier gauge plate could be used locally to distribute loads with reduced local stress.
- Any combination of the above.

The Steel Construction Institute (1994) investigated the effects of lightweight aggregate concrete and a target concrete density of less than 2000 kgm^{-3} was set. This could easily be reached through the use of various commercially available lightweight aggregates, which allow a density as low as 1200 kgm^{-3} to be produced. This density had little effect on the shear stud capacity as it was still possible to achieve the same strength of concrete.

However, the use of lightweight concrete in DSC elements is no longer being considered since it has been shown that it is not necessary to use it to make Bi-Steel a commercially viable product.

1.2.3.5 Economics

Very little information is available regarding the economic viability of DSC. The only current commercial viability investigation is that carried out within SCI (1994). As previously mentioned, Bi-Steel was found to be a cheaper solution than steel or reinforced concrete alternatives in the construction of a FPSO.

1.2.4 Loading

The purpose of this section is to identify the most likely types of loading that structures using DSC in their construction would be subjected to. This information together with that of existing research will show any areas that are deficient in information.

It is important to identify the correct hazards and hence loads that a particular structure will be expected to carry. Without this information the design would be incomplete and could be inadequate during both construction and operation. The impact of structural failure at any point in time would be felt in both financial and human terms. Hence the information regarding load conditions should be established at the outset of a project.

The type of hazard that any structure may be subjected to is dependent upon the location and application to which it has been applied. This means that each and every structure needs to be assessed individually taking into account factors such as environmental conditions (e.g. the weather), ground conditions, usage of the structure and surrounding dangers. This latter point is particularly valid in the case of offshore structures where the possibility of collisions from ships cannot be ignored.

Since it has been shown that the possible application of DSC in the offshore structures market is significant then this will provide the main focus of this section, although others will be mentioned.

1.2.4.1 Offshore Structures

Offshore structures can be subjected to some of the most extreme loading conditions for any structure. The loads created by waves can be large in magnitude and their repeated nature subjects a structure to extreme fatigue forces. The accidental impact of a supply vessel or a passing ship can have serious consequences. From these few examples it can be seen that offshore structures are subjected to loads that are slow or rapid, periodic or occasional and small or large in magnitude. These loads can be sourced from hazards that can basically be divided into two categories, either operational or accidental.

It can be considered that operational loads are those that can be expected to occur on a regular or continuous basis. They can be caused by crane lifts, drilling operations, helicopter landings, supply vessel impacts (slow speed or drift), sea ice ("bergy-bits"), sea currents and waves and are often smaller in magnitude and gradually applied. Some operational loads however, are of significant magnitude such as those imposed by sea ice, which can be as large as 2.8 – 6.7 GN [Bass (1985)].

Norwegian offshore fixed installations should be designed to withstand a collision from a 5000 tonne displacement vessel travelling at 0.5 ms^{-1} [DNV (1981a)]. Added mass should be included at 10% and 40% for head-on and broadside collisions respectively.

Accidental loads are those that occur randomly or have such a small probability of occurrence that their effects are generally checked for as opposed to designed against. This is due to the nature of such events having significant

effects on the structure. Examples of such hazards are the one in one hundred year storm or a collision from a passing ship. This type of loading is allowed to cause significant structural damage provided that the global stability remains intact. The reason for this is that to resist such forces with little damage would have massive structural and hence economic consequences.

Typical examples of accidental loads on offshore structures are caused by collisions by passing ships or ice bergs, dropped objects, emergency helicopter landings, explosions and storm waves. However, the largest cause of accidents offshore that jeopardise the safety of a structure are collisions between vessels and platforms [A.S. Veritec (1995)].

The differences in the vessel size and their velocity and, hence the impact energy in a collision between a ship and an offshore platform vary considerably. This is due to the arbitrary nature in which the platform is positioned and hence the possibility of a collision occurring from a variety of different vessels. A location in the middle of the North Sea, for example, is more vulnerable to a high-speed collision from a passing ship than one just off the Norwegian coast. This location dependability is given in most design references. For example, platforms operating in the North Sea have a minimum requirement to resist an impact from a 5000 tonne vessel with a velocity of 2 ms^{-1} [DNV (1981a)]. Similarly, in designing a protection system around a man-made island on the Trans-Tokyo Bay Highway [Litton (1993)] analyses of impacts of 1900 MJ were carried out, equivalent to a 130,000 tonne semi-laden vessel travelling at 5ms^{-1}. This is obviously far in excess of any

stated minimum requirements, but the location of the structure meant that it was extremely vulnerable to ship impacts.

Sorensen (1976), stated that ship collisions be taken as time varying forces, with a duration of between two and four seconds. It was concluded that it was reasonable to perform static analyses for a given load at any point in the time history provided that the impact duration is greater than the natural period of the structure.

Collisions between icebergs and offshore structures can involve large forces and sometimes infringe on the overall stability of the structure. In one such case, the peak impact force was of the order of 5000 MN and the duration of the impact was 0.95 seconds. Comparing the initial energy with that of Litton (1993) shows that this is a very large impact, being over 80% of that caused by the 130,000 GT tanker previously mentioned. Other analyses showed that these impacts can give rise to extremely large pressures of up to 15 MPa on localised areas or 2.5 MPa over large surface areas [Ellis (1993)]. This obviously depends on the size of the structure, its mooring and the size of the impacting ice. In considering iceberg impacts, the hydrodynamic effects must be accounted for as they can be as large as 30 percent depending upon the ratio of the size of structure to that of the iceberg [Isaacson (1988)].

In the case of floating structures such as FPSO's and FSU's then the danger of an impact from a large iceberg can be removed by having fast disconnect and reconnect facilities [Swamidas (1985a)].

1.2.4.2 Other Hazards

In submerged tube tunnel construction the tunnel is placed on a prepared bed or slight channel on the river bed leaving the upper part exposed. This leaves it vulnerable to collisions from ships using the river channel.

1.3 Conclusions

It has been shown that existing research is not entirely conclusive about the mechanisms that act within DSC beams. It will, therefore, be necessary to observe the failure of any tested elements closely in order to establish the mechanism of failure. Machida (1992a) also drew similar conclusions regarding ultimate load behaviour.

The shear connectors that have been used, almost exclusively, were headed studs. These have been of similar thickness to the steel plates. The exception to this has been individual studies on the various alternatives, which have been previously mentioned.

Test specimens have been narrow with one or two rows of bars along the longitudinal axis of the beam. At the start of this project some concern was shown over the realistic representation of the tests since they might have insufficient containment of the concrete.

Sorensen (1976) stated that it is possible to use static analyses in the assessment of offshore impacts. This greatly reduces the complexity of any test procedure.

DSC can be a competitive alternative to traditional forms of construction in the offshore structures industry. Although simple comparisons of the cost per unit weight of different construction methods does not show DSC to be competitive, it can be financially beneficial when used for an entire structure [SCI (1994)].

The main reasons for DSC not being in use was shown to be a lack of awareness, fragmented research and complications in the construction

process. Therefore, if a design guide was published for a product that simplified the construction process and improved construction time, a marketing opportunity would exist, particularly for offshore and submerged tube tunnels.

Chapter 2 Analytical Solutions

2.1 Introduction

The purpose of the analytical solutions developed is to provide validation of the experimental work carried out in the laboratory. The end result is to be able to predict the performance of Bi-Steel panel elements with respect to load, deflections, post yield capacity and local buckling failure. It will also allow tensile and compressive stresses within the steel plates and compressive stresses in the concrete to be predicted.

The development of the analytical solutions has been broken down into four sections:

1. "Bending Moments", which will locate the position of the neutral axis and will determine the moment capacity of the panels,
2. "Elastic Deformations" to find the magnitude of full composite and shear deflections that occur within the elastic region,
3. "Post Yield Deformations" which predict the gain in strength with additional deflections as the section undergoes plastic deformation and,
4. "Local Buckling" failure which considers the onset of ultimate failure, as the compression plate buckles between adjacent rows of shear connectors.

These four sections give sufficient information to plot the load deflection curve for Bi-Steel panels. Once the load deflection behaviour has been found, part of the

theory can be re-arranged to determine the stresses within the steel plates. This is considered in "Plate Stresses".

2.2 Bending Strength

2.2.1 Neutral Axis Location

It is assumed that in calculating the position of the neutral axis of a double skin composite panel the concrete acting in tension has no strength. This is consistent with the cracked theories of reinforced concrete.

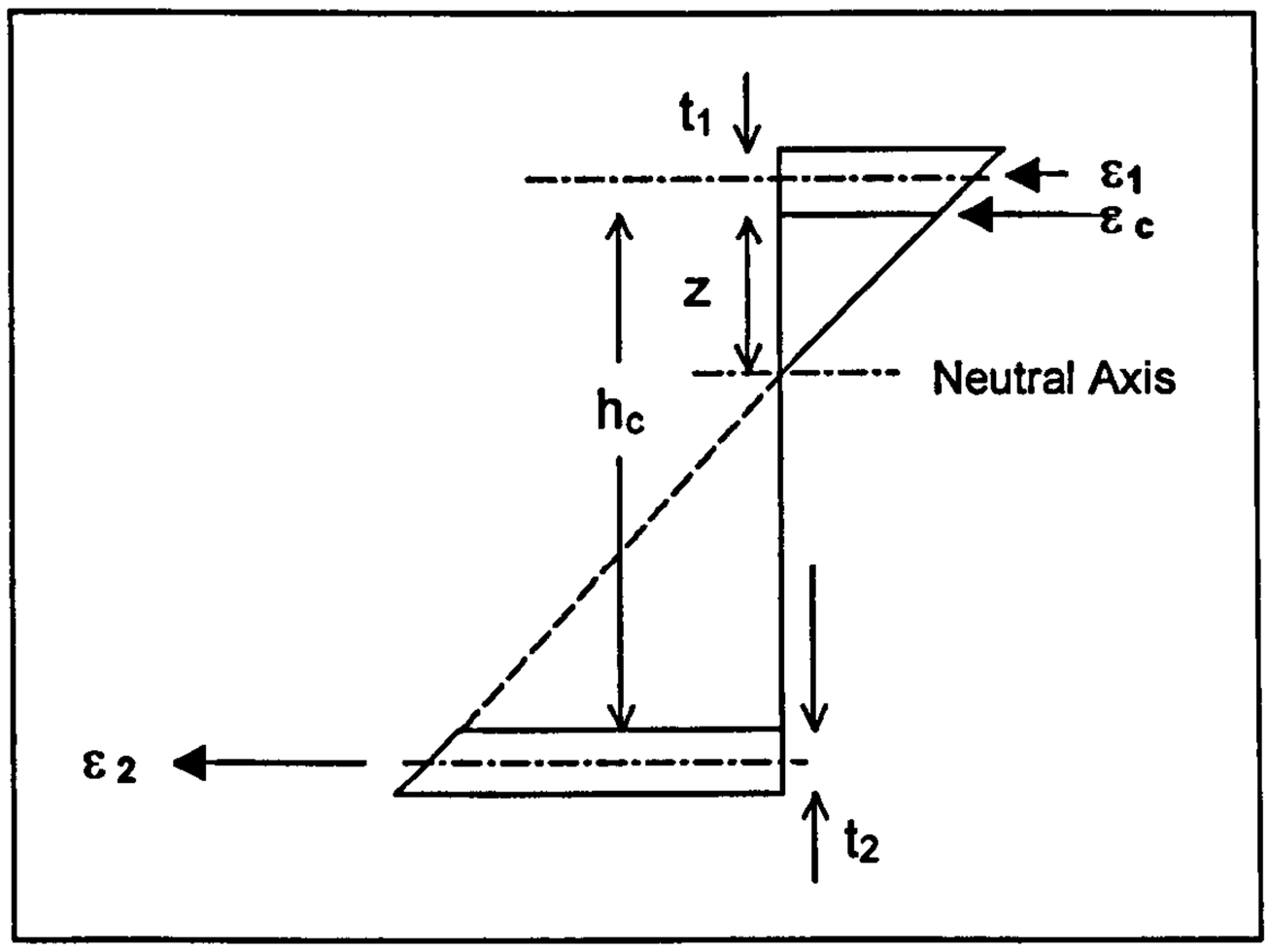

Figure 2.1. Strain distribution through double skin composite panel.

By the geometry represented by Figure 2.1 it is possible to define the steel plate strains, ε_1 and ε_2 in terms of the concrete strain, ε_c.

$$\varepsilon_1 = \frac{\left(z + {}^{t_1}\!/_{2}\right)}{z}\varepsilon_c$$

Equation 2.1

$$\varepsilon_2 = \frac{\left(h_c - z + {}^{t_2}\!/_{2}\right)}{z}\varepsilon_c$$

Equation 2.2

This theory ignores the bending stiffness of the plates about their own axes. The error in doing so is less than 1% provided that d/t >5.77 [Allen (1969)] where:

$$d = h_c + \frac{t_1 + t_2}{2}$$ **Equation 2.3**

The stress in each of the steel plates can be calculated and is equal to Young's Modulus multiplied by the strains in Equation 2.1 and Equation 2.2:

$$f_1 = E_s \varepsilon_1 = m E_c \varepsilon_1$$ **Equation 2.4**

$$f_c = E_c \varepsilon_c$$ **Equation 2.5**

$$f_2 = E_s \varepsilon_2 = m E_c \varepsilon_2$$ **Equation 2.6**

where $m = {E_s}/{E_c}$, is called the modular ratio.

For a balanced section there must be equilibrium between tensile and compressive forces:

$$F_c + F_1 = F_2$$ **Equation 2.7**

where $F = Af$, therefore:

$$\frac{1}{2} A_c f_c + A_1 f_1 = A_2 f_2$$ **Equation 2.8**

Substituting Equation 2.1 to Equation 2.6 into Equation 2.8:

$$\frac{1}{2} A_c E_c \varepsilon_c + A_1 m E_c \frac{\left(z + {t_1}/{2}\right)}{z} \varepsilon_c = A_2 m E_c \frac{\left(h_c - z + {t_2}/{2}\right)}{z} \varepsilon_c$$ **Equation 2.9**

and substituting for A_c, A_1 and A_2 gives:

$$\frac{1}{2}bzE_c\varepsilon_c + bt_1mE_c\frac{\left(z+{}^{t_1}\!/_2\right)}{z}.\varepsilon_c = bt_2mE_c\frac{\left(h_c-z+{}^{t_2}\!/_2\right)}{z}.\varepsilon_c$$

Equation 2.10

Re-arranging and solving for z:

$$z = -m(t_1+t_2)+[m.(t_1+t_2)^2 - m(t_1^2 - 2t_ch_c + t_2^2)]^{\frac{1}{2}}$$

Equation 2.11

This is the neutral axis depth, during elastic deformation, from the underside of the compressive steel plate in terms of plate thickness, steel/concrete modular ratio and concrete depth.

2.2.2 Moment of Resistance

The moment of resistance of a DSC element can be determined by taking moments about the action of the concrete compressive force, F_{cu}, as shown in Figure 2.2.

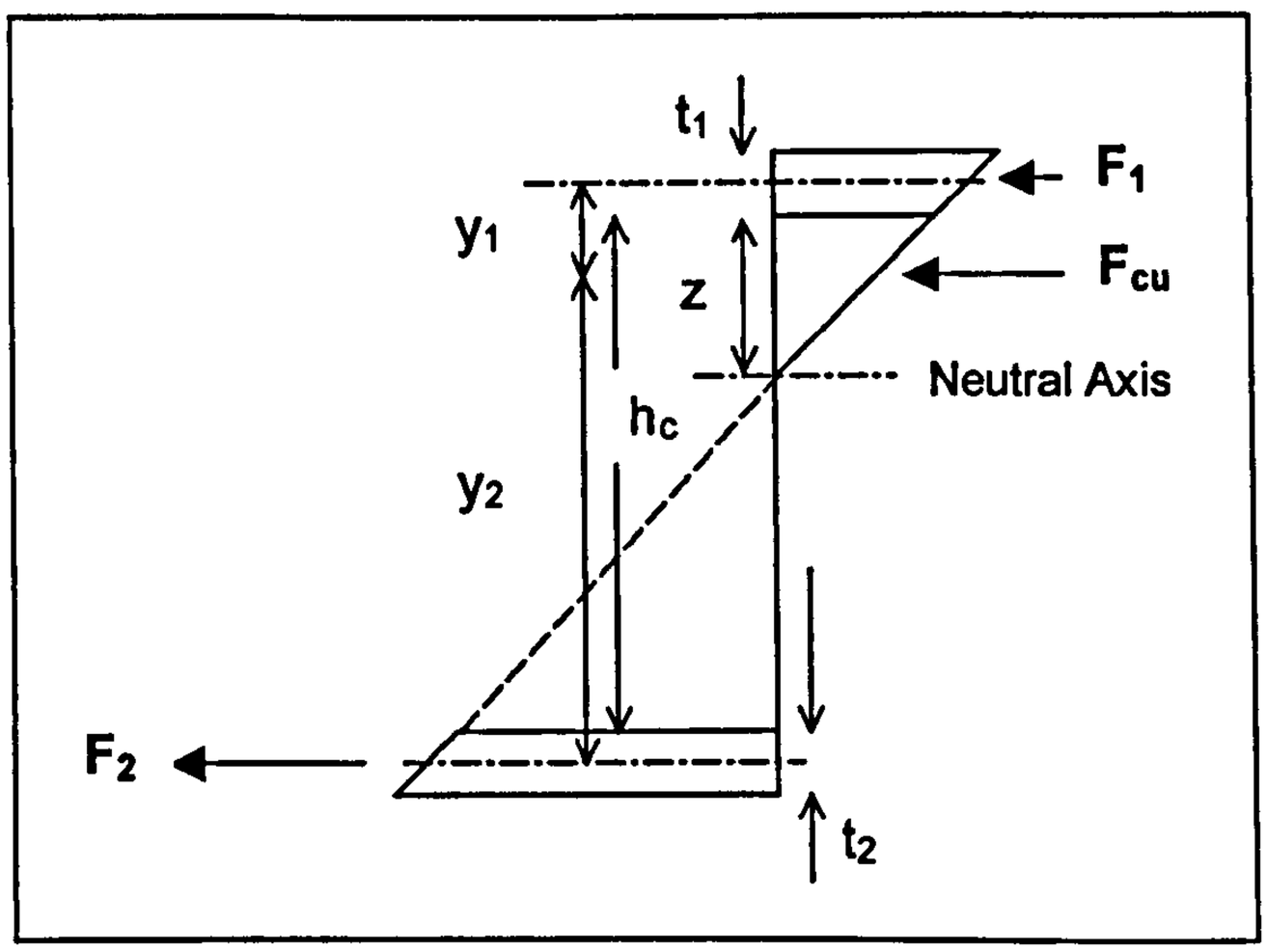

Figure 2.2. Force distribution through double skin composite panel.

$$M = F_1y_1 + F_2y_2$$

Equation 2.12

where:

$$F_1 = f_1 b t_1$$

$$F_2 = f_2 b t_2$$

$$y_1 = \frac{z}{3} + \frac{t_1}{2}$$

$$y_2 = h_c - \frac{z}{3} + \frac{t_2}{2}$$

Therefore:

$$M = f_1 b t_1 \left(\frac{z}{3} + \frac{t_1}{2} \right) + f_2 b t_2 \left(h_c - \frac{z}{3} + \frac{t_2}{2} \right) \qquad \textbf{Equation 2.13}$$

Double skin composites behave similarly to an under-reinforced concrete beam.

That is, at the limit, yield of the tension steel occurs before crushing of the concrete. This is due to the sufficient available compressive capacity in the top steel alone to balance the tension forces. At the elastic limit, therefore, the stress in the tension plate is equal to the yield stress i.e. $f_2 = f_y$, and since the position of the neutral axis is known it is possible to calculate the stress in the compression plate, f_1, in terms of f_2.

$$f_1 = f_2 \frac{z + {}^{t_1}/_{2}}{h_c - z + {}^{t_2}/_{2}} \qquad \textbf{Equation 2.14}$$

Substituting Equation 2.14 into Equation 2.13, the moment of resistance, M becomes:

Equation 2.15

$$M = f_y b t_1 \left(\frac{z}{3} + \frac{t_1}{2}\right) \frac{z + {}^{t_1}/_2}{h_c - z + {}^{t_2}/_2} + f_y b t_2 \left(h_c - \frac{z}{3} + \frac{t_2}{2}\right)$$

Hence as yield of the tension steel occurs, $f_c < f_{cu}$ and increasing moments are carried by an upward movement of the neutral axis. The total compression force remains constant. This type of structural mechanism is accompanied by cracking of the concrete, which is usually extensive, with wide cracks appearing in the latter stages before collapse. At yield, as the neutral axis begins to rise, the observed cracking of the concrete will continue to rise towards the compression steel plate. The moment capacity of the panel is reached when the neutral axis moves up to the lower surface of the compression plate (i.e. $z = 0$) and the stress in the tension plate is at the yield stress. By taking moments about the compression steel plate, the ultimate moment of resistance is, therefore:

Equation 2.16

$$M_y = f_y b t_2 \left(\frac{t_1}{2} + h_c + \frac{t_2}{2}\right)$$

In the case of the experimental work which has been undertaken for this thesis where the steel plates are of equal strength and thickness (i.e. $t_1 = t_2$), the ultimate moment of resistance becomes:

Equation 2.17

$$M_y = f_y b t (h_c + t)$$

The moment of resistance is, therefore, equivalent to the tensile strength of one of the steel plates multiplied by d, the distance between the centroids of the two plates.

2.3 Elastic Deformations

The performance of a DSC panel can be divided into two distinct parts which can be calculated separately, and then superimposed upon each other. These two areas of consideration are represented by Figure 2.3 and are:

1. Full Composite Deflections and,
2. Shear Deflections.

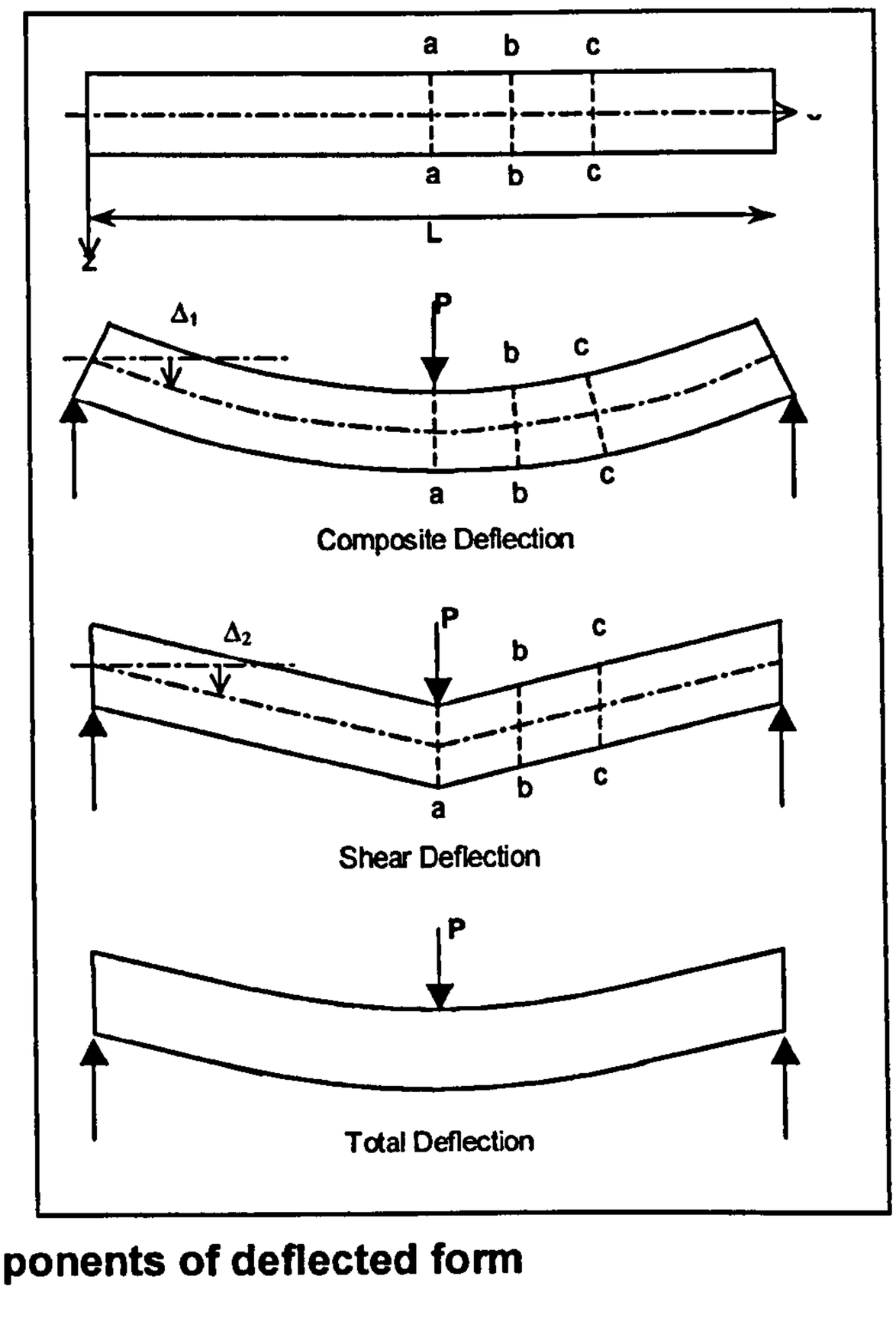

Figure 2.3. Components of deflected form

If a composite element has final deflections that were equal to the composite deflections then it would be acting as a true composite, where the core has infinite shear stiffness. If the core is not stiff then deflections occur due to shear strains

within it [Allen (1969)]. If the shear deflections are taken by themselves, the initially plane sections remain vertical, unlike plane bending when plane sections remain perpendicular to the longitudinal axis. The shear deflection then has to be superimposed with the composite deflection to give the total or actual deflection.

2.3.1 Full Composite Deflections

This theory is developed by assuming that the section remains fully composite. Thus, there is no slip between the steel plates and concrete core or that there is no shear deformation of the core. The theory assumes that the curvature is related to the moments induced in the panel and, therefore can only be used up to the elastic limit. It also assumes that plane sections remain plane, that is, sections that are perpendicular to the longitudinal axis remain so when the panel bends.

From Figure 2.2, taking moments about the action of the concrete compressive force F_{cu} gives:

$$M = F_1 y_1 + F_2 y_2 \qquad \textbf{Equation 2.18}$$

Assuming the section to develop full elastic strength then:

$$F_1 = \kappa\left(z + \frac{t_1}{2}\right) E_s A_1 \qquad \textbf{Equation 2.19}$$

$$F_2 = \kappa\left(h_c - z + \frac{t_2}{2}\right) E_s A_2 \qquad \textbf{Equation 2.20}$$

$$y_1 = \frac{z}{3} + \frac{t_1}{2} \qquad \textbf{Equation 2.21}$$

$$y_2 = h_c - \frac{z}{3} + \frac{t_2}{2}$$ Equation 2.22

Therefore

$$M = \kappa E_s \left[\left(z + \frac{t_1}{2} \right) A_1 y_1 + \left(h_c - z + \frac{t_2}{2} \right) A_2 y_2 \right]$$ Equation 2.23

Approximating κ with $-\frac{d^2\Delta_1}{dx^2}$ (Positive moment gives negative curvature i.e. sagging)

$$\frac{d^2\Delta_1}{dx^2} = -\frac{M}{\mathrm{K}}$$ Equation 2.24

where $\mathrm{K} = E_s \left[\left(z + \frac{t_1}{2} \right) A_1 y_1 + \left(h_c - z + \frac{t_2}{2} \right) A_2 y_2 \right]$, the bending rigidity of the panel.

The double integral of Equation 2.24 will reveal the general solution for the vertical deflection at any point in the beam. For a particular solution, an expression for the bending moments in the panel is required. In the case of the tests described in this thesis, which were all simply supported in three point bending, the particular solution becomes:

$$\frac{d^2\Delta_1}{dx^2} = -\frac{Px}{2\mathrm{K}}$$ Equation 2.25

$$\frac{d\Delta_1}{dx} = -\frac{Px^2}{4\mathrm{K}} + C_1$$ Equation 2.26

$$\Delta_1 = -\frac{Px^3}{12\mathrm{K}} + C_1 x + C_2$$ Equation 2.27

The boundary conditions are defined at two points. At the support the vertical displacement is zero (Condition 1) and at the mid-span the gradient is zero (Condition 2).

$$\text{At } x = 0, \Delta_1 = 0 \qquad \textbf{Condition 1}$$

$$\text{At } x = \frac{L}{2}, \frac{d\Delta_1}{dx} = 0 \qquad \textbf{Condition 2}$$

By substituting Condition 1 into Equation 2.27 gives $C_2 = 0$ and,

Condition 2 into Equation 2.26 gives $C_1 = \frac{PL^2}{16K}$.

Substituting for C_1 and C_2 into Equation 2.27 gives an expression for the full composite deflections of the panels.

$$\Delta_1 = -\frac{Px^3}{12K} + \frac{PL^2}{16K}x \qquad \textbf{Equation 2.28}$$

At mid-span where $x = \frac{L}{2}$

$$\Delta_1 = -\frac{PL^3}{48K} \qquad \textbf{Equation 2.29}$$

where the negative sign indicates a downward deflection.

2.3.2 Shear Deflections

The full composite deflections calculated in the previous section can only predict the performance of double skin composites if there is no shear deformation of the section. If shear strains occur then the effect is to increase the overall deflections. The full composite deflections are, therefore, a lower bound solution.

The shear deflection of composite or sandwich elements has been sufficiently developed by the aerospace industry. The need for lighter and stronger materials for use in high technology fields such as fighter aircraft has been the main driving force behind this. It is necessary to progress through the development of the shear deflections beginning with composite elements where the modulus of elasticity of the core is small with respect to that of the faces. Allowances can then be made when the modulus of elasticity of the core is *not* small with respect to that of the faces [Allen (1969)].

The determination of the shear modulus of Bi-Steel panels will be carried out when the underlying theory has been presented.

The shear deflection, Δ_2, of a simply supported element in three point bending is given by Equation 2.30 [Allen (1969)].

$$\Delta_2 = \frac{VL}{4AG} \qquad \textbf{Equation 2.30}$$

where $A = \frac{bd^2}{h_c}$,

b is the width of the panel,

d is the depth between the centroids of the steel plates,

h_c is the depth of concrete and,

G is the shear modulus of the core (assumes the core to obey plane strain, i.e. $\sigma_x = \sigma_y = \tau_{xy}=0$)

When the modulus of elasticity of the core becomes significant in comparison to that of the faces then the shear strains and stresses are no longer constant throughout the depth of the core. It is still assumed that there are no shear strains in the faces. However, it is still possible to relate the effective shear modulus (G') to the shear modulus (G) by [Hetenyi]:

$$G' = \frac{G}{1 + \frac{E_c}{6E_s}\frac{h_c^2}{t(h_c + t)}}$$

Equation 2.31

Equation 2.30 can still be used by substituting G' for G, therefore:

$$\Delta_2 = \frac{VL}{4AG'}$$

Equation 2.32

2.3.2.1 Determination of shear modulus

In order to be able to use the theory presented above, it is necessary to know the shear modulus of the core (G'). Figure 2.4 shows how the panel might deform due to shear forces.

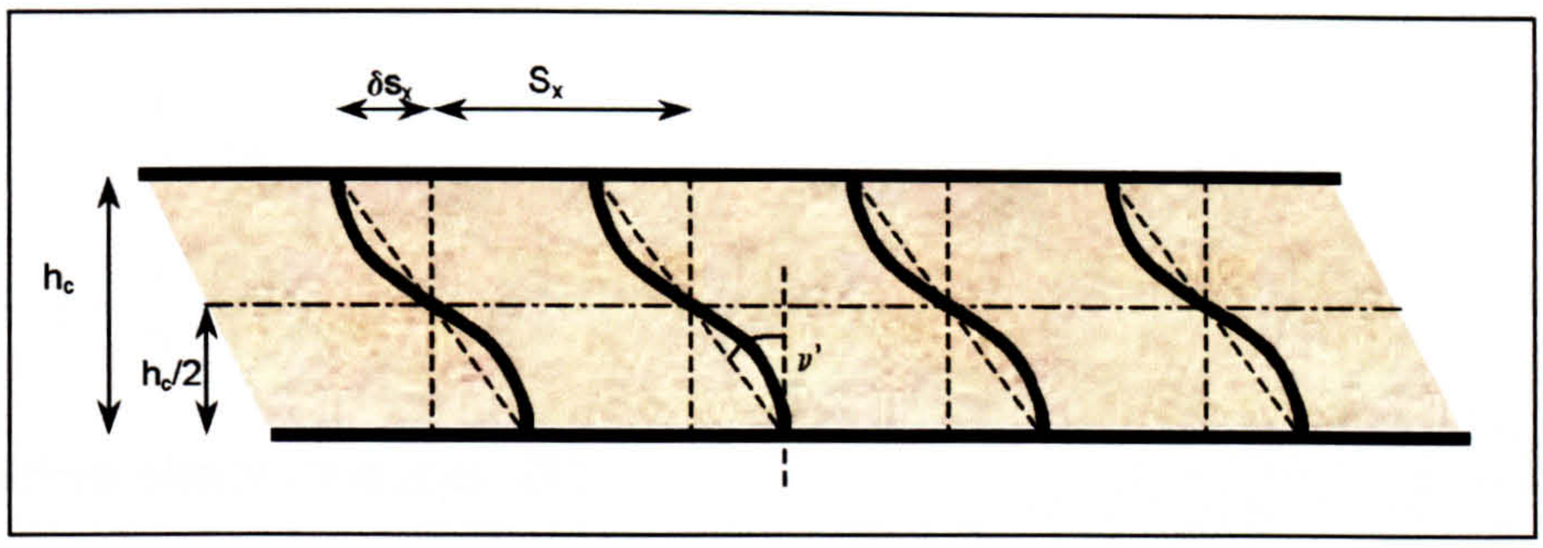

Figure 2.4. Shear deformation of Bi-Steel panel

As there is no bending of the panel, or concrete subject to tension, the "neutral axis" is along the panel centre line. If the panel is split along this axis, as shown in Figure 2.5, it can be seen that displacement of the mid-point of the shear connector could be represented by that of a cantilever resting on a concrete foundation, as given in Equation 2.33 [Allen (1969)].

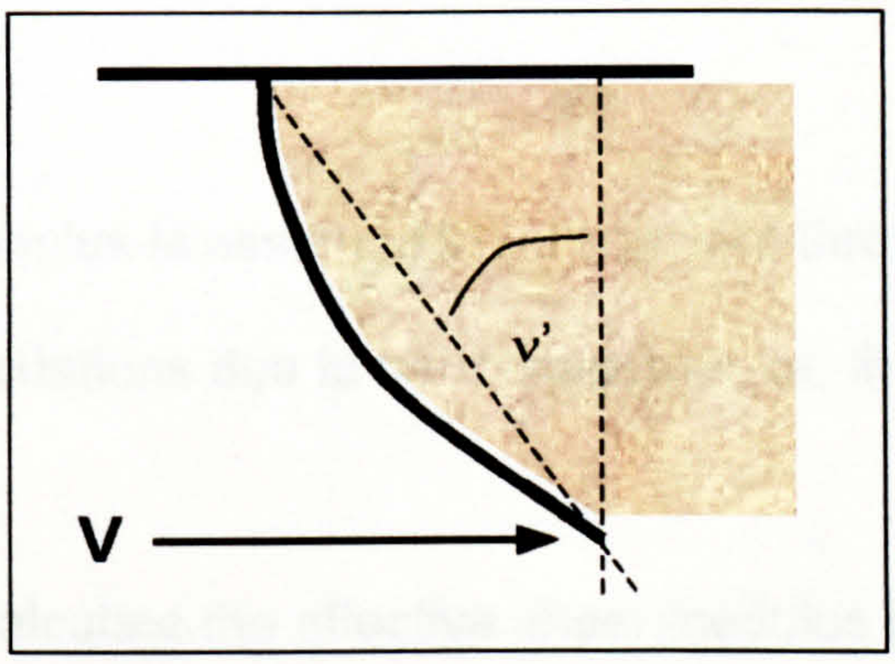

Figure 2.5. Cantilever beam on foundation analogy

$$\delta s_x = \frac{V\lambda}{k}\frac{\sinh 2\lambda l - \sin 2\lambda l}{\cosh^2 \lambda l + \cos^2 \lambda l} \qquad \textbf{Equation 2.33}$$

where: V is the shear force acting on a single bar

k (Nmm^{-3}) is the modulus of the foundation

$$\lambda = \sqrt[4]{\frac{k}{4EI}}$$

$$l = \frac{h_c}{2}$$

The effective shear modulus, *G'*:

$$G' = \frac{\tau}{\upsilon'}$$

Equation 2.34

where: $$\tau = \frac{P}{A_s} = \frac{Px10^6}{2bn_1(h_c + t_1 + t_2)}$$

n_1 is the number of shear connectors in the longitudinal directionin the shear span being considered,

$$\upsilon' = \tan^{-1} \frac{\delta s_x}{h_c/2}$$

The effective shear modulus is assumed to be constant throughout the panel, that is, there are no local variations due to bar connectors, or, the effect is evenly distributed.

In order to be able to calculate the effective shear modulus it is necessary to know the modulus of the foundation, k, of the concrete. However, there is no theoretical way to determine this material property, hence it would be necessary to carry out laboratory tests either on small samples or it could be found from beam tests provided the composite and total deflection was known.

2.4 Post Yield Deformations

2.4.1 Moment of Resistance

It was noticed whilst carrying out a review of previous published information that there may be a gain in the strength of a DSC panel once it past yield. It is the purpose of this section to develop an analytical solution for this effect.

A typical response of a steel tensile coupon is shown in Figure 2.6 (50mm gauge length). For design purposes an elastic, perfectly plastic solution is often used, which assumes that there is no gain in strength after yield has occurred. This is rarely actually found in test data as shown by Figure 2.6.

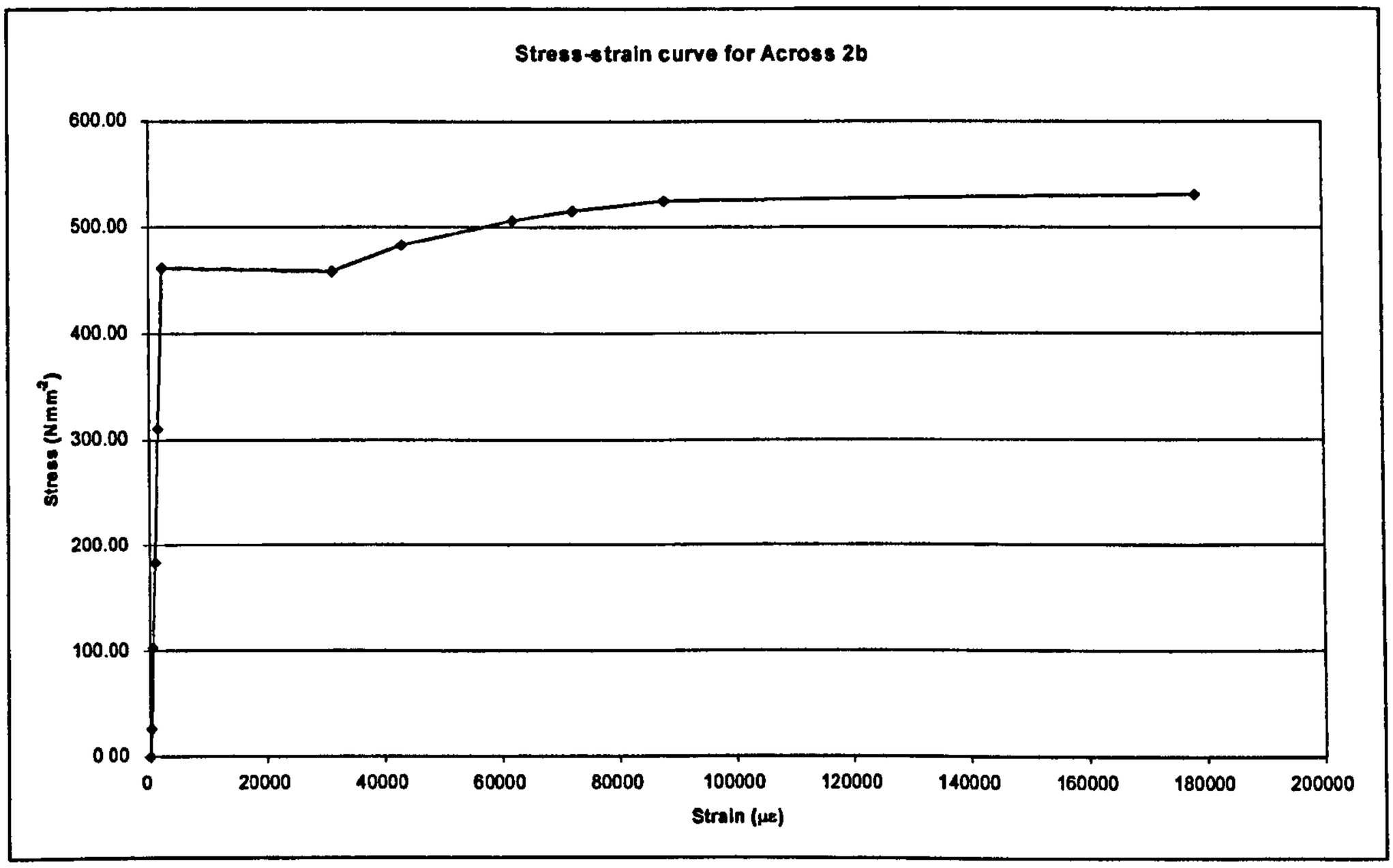

Figure 2.6. Typical response of tensile coupon from Series 1 tests.

Figure 2.6 shows that the elastic, perfectly plastic assumption is valid for strains, in this case, up to 32000με. The plateau is caused by the spread of the yield point

throughout the specimen but does not always occur due to residual stresses in the steel after it has been cold worked.

If large strains are to be considered, then there is a gain in the strength of steel, which is caused by strain hardening. The ultimate tensile strength is approached when the curve of applied load (and engineering stress) flattens and then decreases as necking of the specimen begins. The applied load is then suddenly lost as the specimen fails. The post yield region of the curve has previously been studied and can be well represented by Equation 2.35 (Dowling).

$$\sigma = H\varepsilon^n \qquad \textbf{Equation 2.35}$$

where H is the strength coefficient and,

n is the strain-hardening exponent.

The factors H and n are determined by curve fitting to the post yield region of the stress strain curve in Figure 2.6.

It is now possible to determine the stress at any strain level. Therefore, the post-yield moment capacity of a DSC element can be found by substituting Equation 2.35 into Equation 2.17.

$$M_{py} = H\varepsilon_2^n A_2 (h_c + t) \qquad \textbf{Equation 2.36}$$

2.4.2 Post Yield Deflections

It is necessary to relate the strains in the tension plate to the deflection of the panel at mid-span. In the elastic region of deflections, there is a linear relation between deflection and strain. This relation continues after yield has occurred. However, there is a change in gradient in the post yield region that is

characterised by the strain-hardening exponent. That is, the gradient post yield of a deflection strain relationship is equal to that of the elastic region multiplied by the strain-hardening exponent (Figure 2.7).

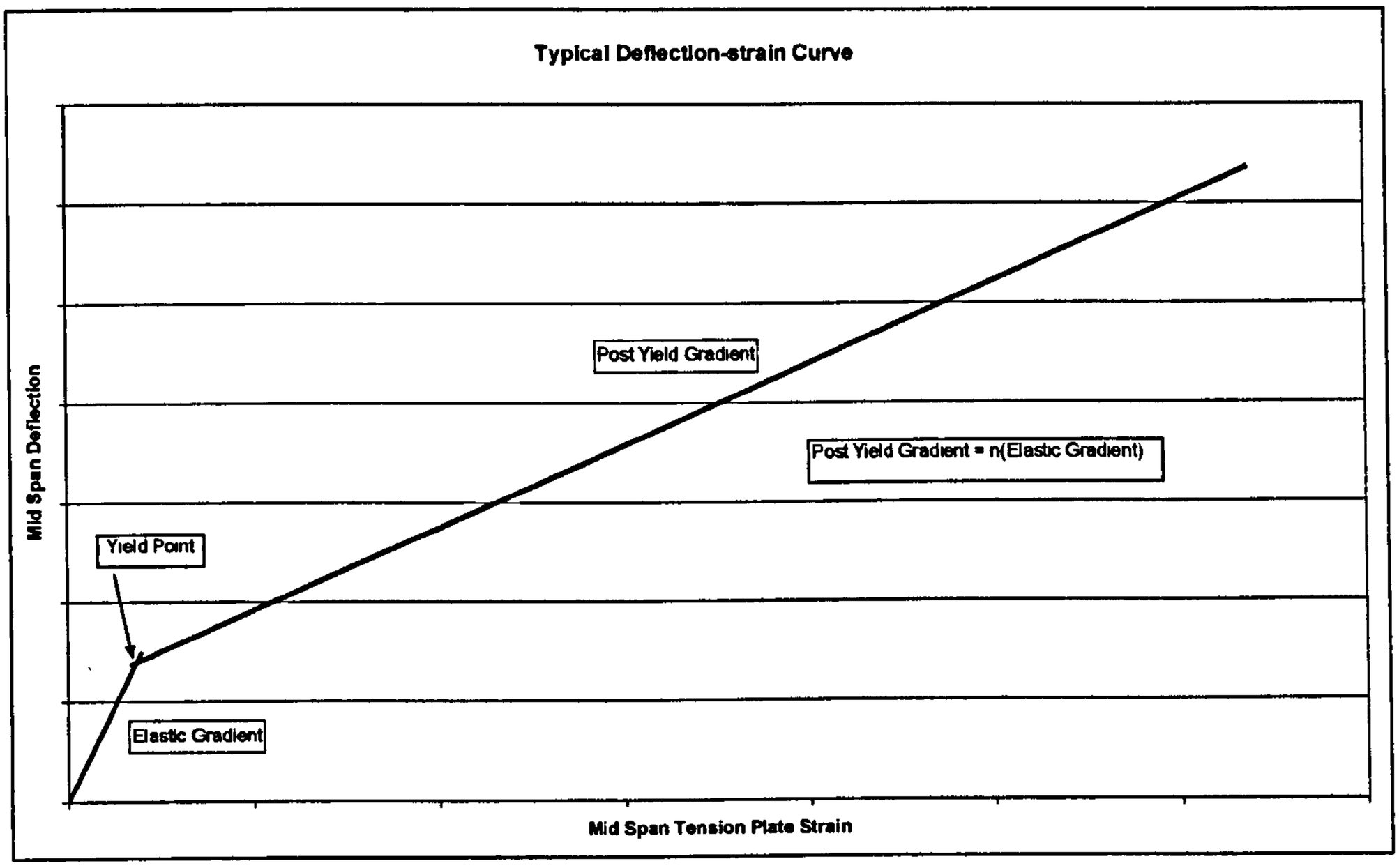

Figure 2.7. Typical Deflection Strain Relationship

The discontinuity between the elastic and plastic parts of Figure 2.7 is caused by strain hardening of the steel. The elastic gradient can be calculated from the elastic total deflection and strain (calculated from yield stress and Young's Modulus) at yield. The post yield gradient can then be calculated by multiplying the elastic gradient by the strain-hardening exponent. The intercept of the post yield line with the deflection axis is found by equating the elastic and post yield curves at the yield point.

The shear deflections do not affect the relationship because:

1. They do not affect the strains in the plates and,

2. They are linear throughout the whole range of total deflections.

2.5 *Local Buckling*

One possible failure mechanism of the Bi-Steel panels is local buckling of the compression plate between adjacent rows of connectors. Presented here is a simple Euler analysis of the problem. As presented and justified in Chapter 4, this gives close comparison to actual data

The axial compressive load, as determined by Euler, at which a pin ended strut will buckle is given by:

$$P_E = \frac{\pi^2 EI}{l^2}$$ **Equation 2.37**

This solution is often used for struts, which are not pin ended by substituting an effective length [Coates (1997)]. Typical examples are shown in Figure 2.8.

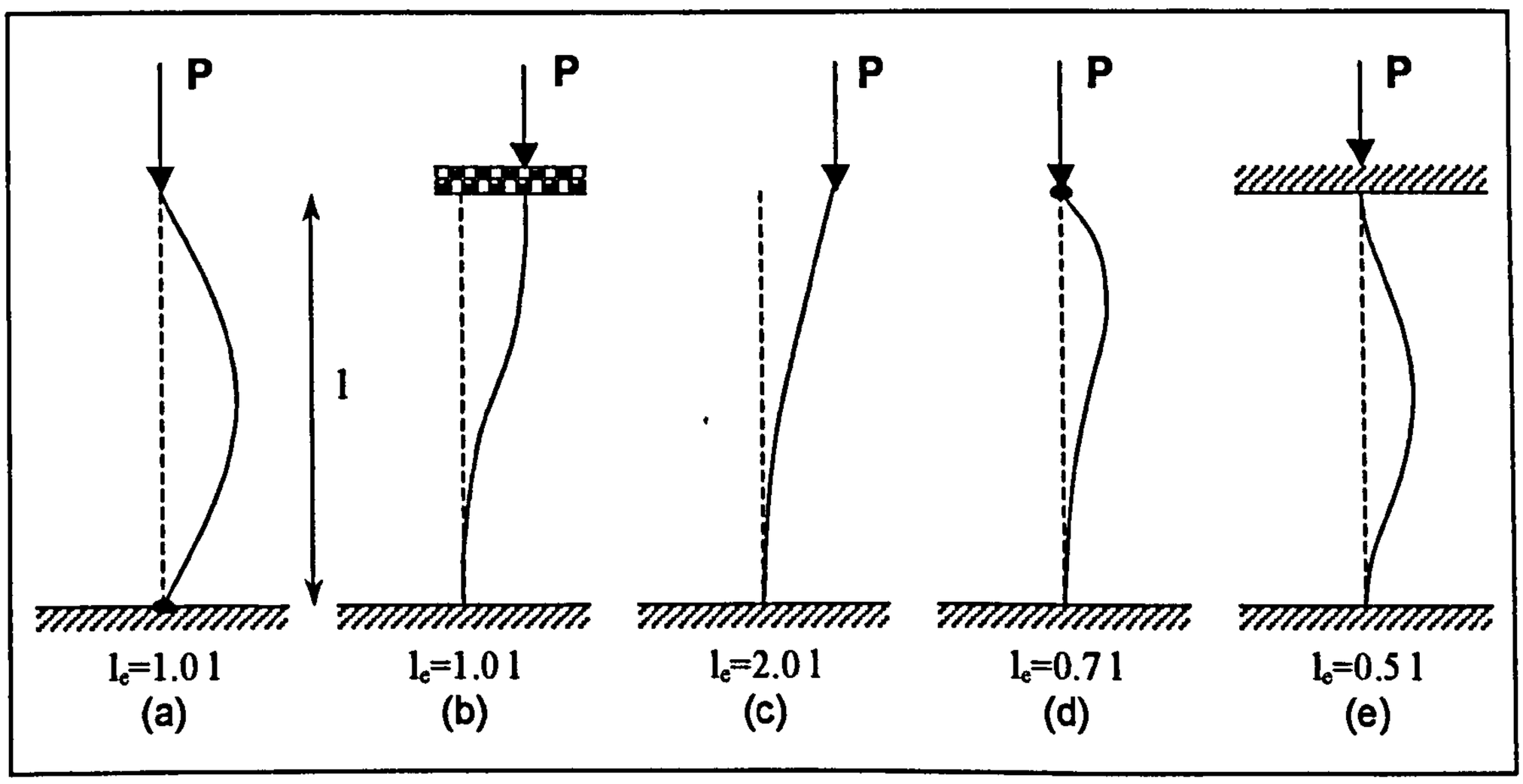

Figure 2.8. Effective lengths for different end conditions

For a cantilever beam with two fixed ends as found in the compression plate between adjacent connectors, the Euler buckling load is, therefore:

$$P_E = \frac{\pi^2 EI}{(0.5l)^2}$$ **Equation 2.38**

However, this assumes that the ends are perfectly fixed, a fact that rarely occurs. It is recommended to steel designers using BS5900 that a factor of 0.7 be used for columns where both ends are fixed and restrained from horizontal movement. This, therefore, gives an Euler buckling load for practical struts with both ends fixed of:

$$P_E = \frac{\pi^2 EI}{(0.7l)^2}$$ **Equation 2.39**

2.6 Plate Stresses

2.6.1 Longitudinal Stresses

From previous research, it is known that the yield of a DSC panel with equal plate thickness is governed by the yield of the tension plate [Hassinen (1989) and Narayanan (1997)]. Therefore, the stress in the tension plate at yield is equal to the yield strength, f_y.

$$f_2 = f_y \qquad \textbf{Equation 2.40}$$

The stress in the compression plate can be determined, by geometric relations, from that of the tension plate and knowing the position of the neutral axis (Figure 2.2). Yield of the DSC panel occurs when the neutral axis has moved to the compression plate, as previously explained, to achieve the maximum lever arm. However, in order to calculate compression plate stress the elastic position of the neutral axis is used. This is because the stress in the compression plate remains unchanged whilst the tension plate undergoes yield although the panel has not quite reached the maximum strength. The following equation provides an expression for the compressive stresses in the plate.

$$f_1 = f_y \frac{y_1}{y_2} \qquad \textbf{Equation 2.41}$$

$$f_1 = f_y \frac{\left(z + {}^{t_1}\!/_{2}\right)}{\left(h_c - z + {}^{t_2}\!/_{2}\right)}$$

2.6.2 Transverse Stresses

It is proposed that the tests in this research are to be carried out on wide beam elements and, therefore, the longitudinal strains may be influenced by strains in the transverse direction even though the tests are to be loaded two dimensionally.

It is assumed, in the transverse direction, that:

1. at the centre the strain is zero and,
2. at the edge the stress is zero.

The longitudinal and transverse components of strain in the tension plate, ε_2 and ε_{2t} respectively, are given by (Hooke's Law):

Equations 2.42

$$\varepsilon_2 = \frac{\sigma_2}{E} - \upsilon\frac{\sigma_{2t}}{E}$$

$$\varepsilon_{2t} = \frac{\sigma_{2t}}{E} - \upsilon\frac{\sigma_2}{E}$$

At the centre using assumption 1 ($\varepsilon_{2t}=0$) and substituting into Equations 2.42b then the stress in the transverse direction becomes $\sigma_{2t} = \upsilon\sigma_2$. Substituting this into Equations 2.42a gives:

Equation 2.43

$$\varepsilon_{2c} = \frac{\sigma_2}{E} - \upsilon^2\frac{\sigma_2}{E}$$

$$\varepsilon_{2c} = \frac{\sigma_2}{E}\left(1 - \upsilon^2\right)$$

Similarly using assumption 2 and Equations 2.42 it is possible to derive the longitudinal strain at the edge of the plate, ε_{2e}.

Equation 2.44

$$\varepsilon_{2e} = \frac{\sigma_2}{E}$$

By substituting for σ_2 from Equation 2.44 into Equation 2.43 the longitudinal strain at the centreline in terms of that at the edge is, therefore:

$$\varepsilon_{2c} = \left(1 - \upsilon^2\right)\varepsilon_{2e} \qquad \textbf{Equation 2.45}$$

2.7 Conclusions

Analytical solutions have been presented that enable the full load deflection curve to be calculated, provided ultimate failure by local buckling occurs.

Existing methods of determining the shear capacity are used and have been presented in Chapter 1.

DSC elements with equal plate thickness will behave as under-reinforced, reinforced concrete beams. This is important in practical applications since it provides warning of failure. The yield of the steel plate is accompanied by large deformations along with extensive cracking of the concrete core, which was highly visible during the experimental programme.

Also presented are the stresses in the steel plates and include a correction for wide beams.

Chapter 3 Experimental Investigations

3.1 Introduction

The experimental investigations detailed within are split into a number of 'Test Series', each of which was chosen to study specific parameters. The purpose of investigation for each series of tests was first determined, after which the panels were fabricated, tested in the laboratory and analysed before proceeding with the next series. The reasoning behind the choices, the testing of the panels and the results from the tests is given in this Chapter. Table 3.1 gives a summary of major dimensions of the test panels.

Series Name	Panel Name	Span L (mm)	Width b (mm)	Plate Thickness t (mm)	Concrete Depth h_c (mm)	End Plates
Series 1	Citv1	3400	1000	10	200	Yes
	City2	3400	1000	10	200	No
	Stud2	3400	1000	10	200	No
	Stud2b	3400	1000	10	200	No
Series 2 (Part I)	Citv3	2600	600	12	200	Yes
	City4a	2600	600	10	200	Yes
	City4b	2600	600	10	200	Yes
	City4c	2600	600	10	200	Yes
	City5	2600	600	8	200	Yes
	City6	2600	600	8	200	Yes
	City7	2600	600	8	200	Yes
	City8	2600	600	8	200	Yes
	City9	2600	600	8	200	Yes
Series 2 (Part II)	Citv4d	2600	600	10	200	Yes
	City6b	2600	600	8	200	Yes
	City10	2600	600	8	200	Yes

Table 3.1. Summary of Test Panel Structural Parameters

3.2 Materials Testing

3.2.1 Introduction

In order to determine the strength of materials used (steel plate and concrete) tests were conducted on specimens that were taken from the same batches as those used to construct the double skin composite test panels.

3.2.2 Steel Tensile Tests

Steel tensile coupons nominally measuring 6 x 6mm (section) by 50mm (gauge length) were tested in a Lloyd Instruments tensile test machine to establish the steel tensile yield strength and ultimate yield strength.

The post yield strength coefficient, *H*, and strain-hardening exponent, *n*, were also determined from the tensile tests. These were found by curve fitting to the curved post yield region only and were only carried out for the first test series. Where available, coupons were taken from material supplied from the same batch. If no material was supplied then the coupons were cut from an unstressed region of the panels once the load test had been completed.

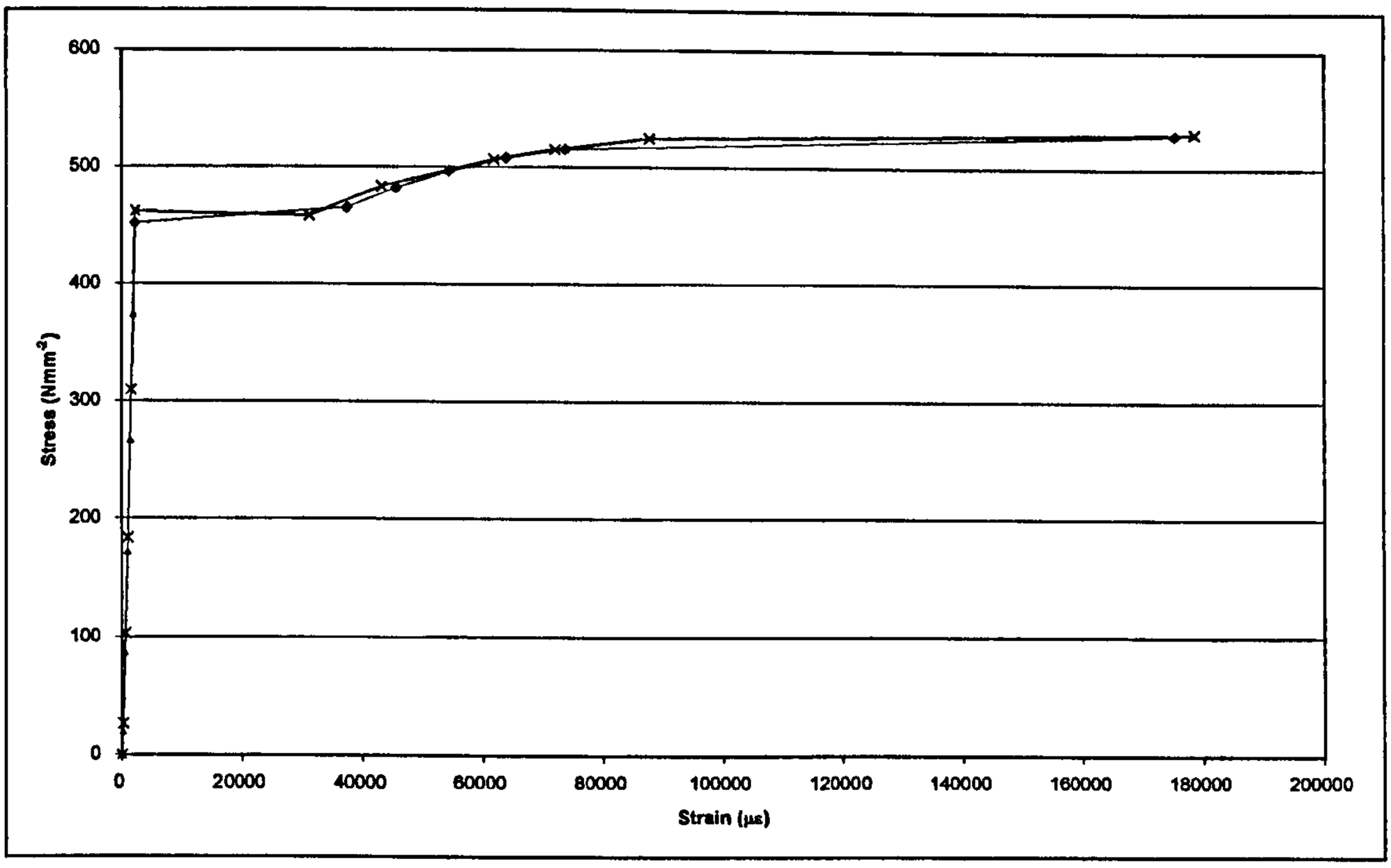

Figure 3.1 Steel tensile test results for Series 1 specimens.

3.2.3 Concrete Cube Tests

Compression tests were carried out on 100mm concrete cubes cast at the same time as the panels and then cured under water. Cube tests were conducted, initially, at regular intervals and then on the same day as panel tests. Figure 3.2 shows the progression of concrete strength with age for the three batches used for Series 1, Series 2 (part I) and Series 2 (part II).

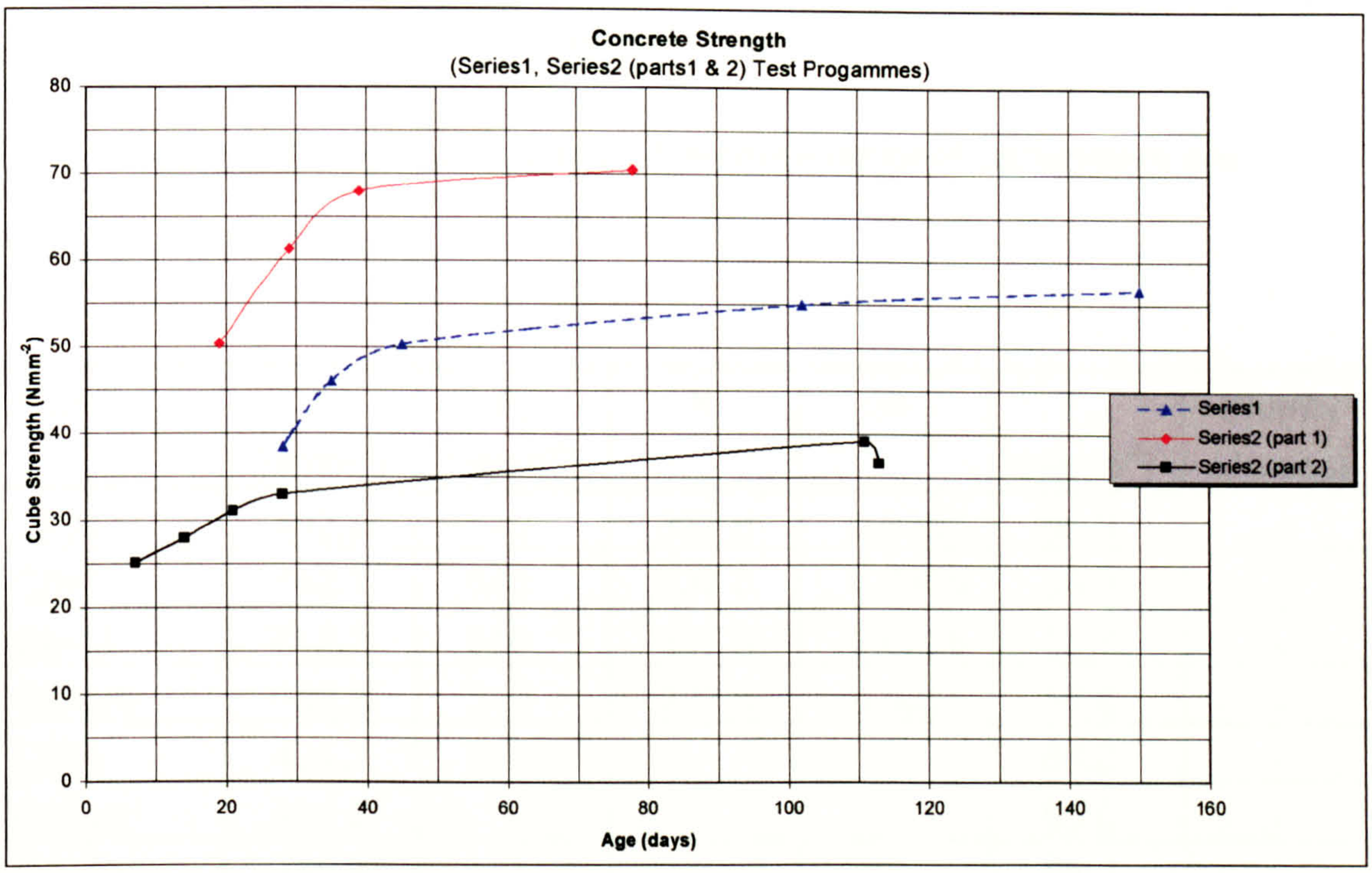

Figure 3.2 Concrete cube strength.

3.2.4 Charpy Tests

After testing the City6 specimen, concern was shown over the fracture strength of the plate used in its construction due to the relatively low strain required to cause fracture. Using 10 x 7.5 x 50mm specimens, a comparison of the plate used in City6 with that of City5 showed it to have approximately 60 percent of the fracture strength. However, these values achieved are greater than the minimum requirement of 27 Joules from a larger 10 x 10mm specimen (BS4360).

Since the fracture strength of the steel plate used in City6 is lower than that of City5, much lower strains were required to reach the fracture strength of the steel hence, failure occurred sooner.

3.2.5 Results of Materials Testing

The results for all tests conducted to determine material parameters are contained within Table 3.2.

Panel	f_y (Nmm^{-2})	F_u (Nmm^{-2})	K	n	F_{cu} (Nmm^{-2})	Charpy (Joules)
Citv1	452.2	540	337.6	0.0355	55.0	-
City2	452.2	540	337.6	0.0355	56.0	-
Stud2	452.2	540	337.6	0.0355	53.3	-
Stud2b	452.2	540	337.6	0.0355	58.0	-
City3	431.2	546	-	-	65.2	-
City4a	381.2	-	-	-	50.0	-
City4b	430.6	-	-	-	55.6	-
City4c	430.6	-	-	-	70.4	-
City4d	397.3	547	-	-	39.0	-
City5	432	-	-	-	57.8	77.4
City6	339.7	-	-	-	61.2	45.5
City6b	404.4	555	-	-	39.1	-
City7	432	-	-	-	63.0	77.4
City8	432	-	-	-	64.5	77.4
City9	432	-	-	-	64.9	77.4
City10	418	547	-	-	39.3	-

Table 3.2. Material Test Results.

3.3 Experimental Equipment

The equipment used throughout the testing of the different series of Bi-Steel panels changed slightly as improvements were made to the system. These were generally carried out in order to improve the test procedure. A description of the final set up is given (Plate 3.1 and Figure 3.3).

Plate 3.1. Test Rig with 1000kN Actuator

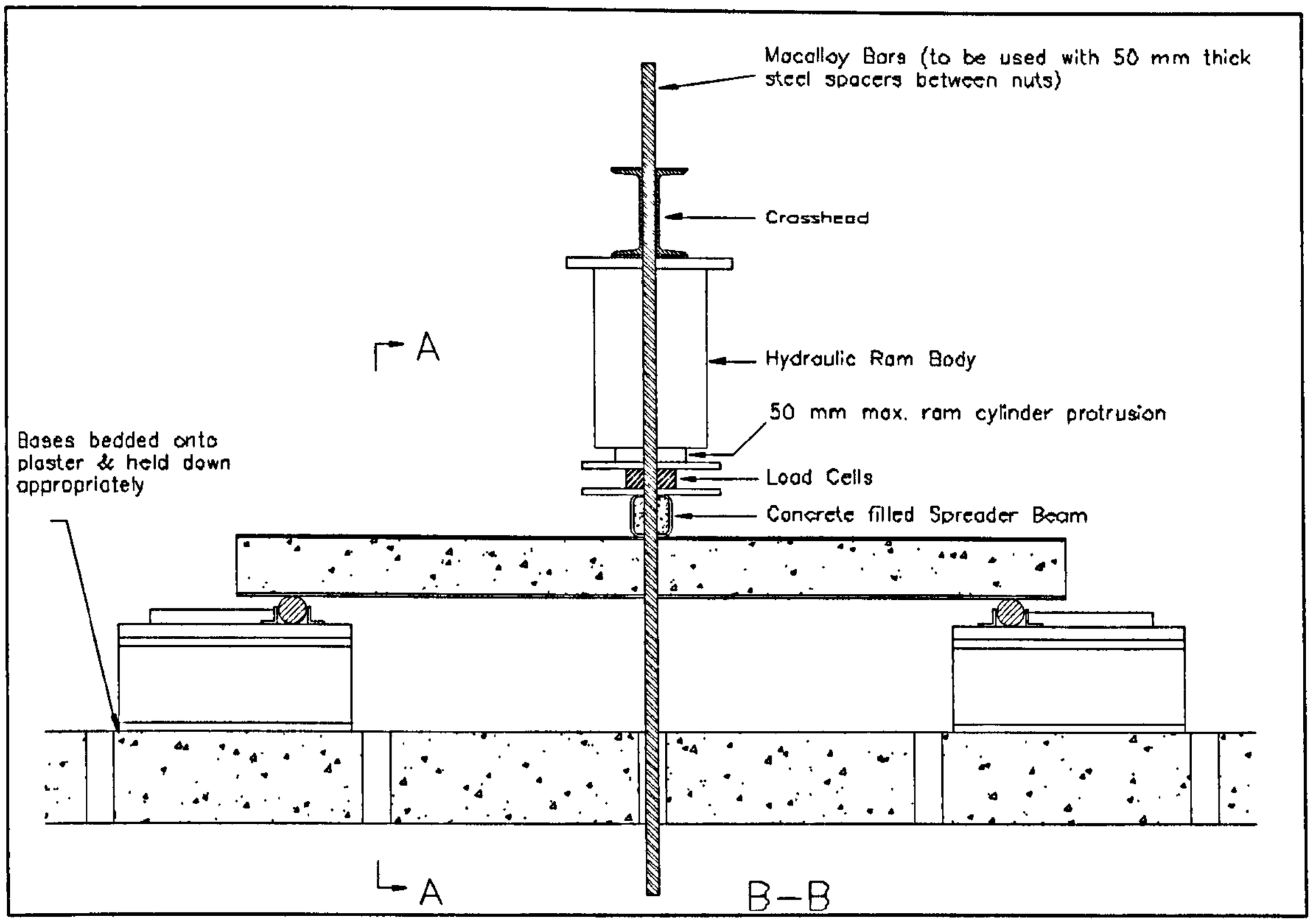

Figure 3.3. Typical test equipment set-up.

Each panel was positioned on two roller supports mounted to the top of suitably large steel sections (bases). The rollers were restrained horizontally through the use of angle sections bolted, either side of the roller, to the bases. Although this induces thrust reactions in the panel, particularly at larger deflections, it was not thought to be significant in the performance of the test. For City1 with a yield tensile stress of 452Nmm^{-2} and a coefficient of friction of 0.5 (assumed), the frictional force is 5% of the tensile force in the plate. Without the restraints, there was a concern for safety from the roller being forced out from under the panel.

Load was applied by the use of hydraulic equipment. Initially hand operated pumps and jacks were used, then electrical pumps and finally a complete computer controlled system built by Dartec was used. This final system comprised of a single 1000kN double acting actuator capable of applying load

in tension or compression. Oil was supplied by an electrical powered hydraulic pump and controlled by a remote panel system where an internal LVDT and a load cell provide the feedback from the actuator.

The laboratory at City University has a large concrete strong floor, which is capable of reacting very large loads through a matrix of holes spaced at 1.0 by 0.8 metres. This removes the need for heavy, self-reacting test equipment.

Load was transferred from the actuator, out through a steel crosshead to two Macalloy bars, each of 100 Tonne capacity. These pass through and were bolted either side of the strong floor.

On the underside of the actuator was bolted a 100mm wide, concrete filled section that spreads the load evenly over the width of the panel. This removed any unwanted three-dimensional effects from the system.

3.4 Test Procedure

Once a panel was positioned in the test equipment the strain gauges are connected to the data logger and the LVDT's positioned. A small load was then applied and released which served to bed in the panel and equipment should they not quite be perfectly seated. It also allows checks for any hydraulic leaks or loose electrical connections.

A set of zero readings was then taken and load applied in approximately 15 percent increments up to yield load, each time recording a data set after the situation becomes stable. The test then continues under deflection control with readings taken every 5 to 10 mm, depending on the expected final deflection.

At each increment, as well as recording data, a visual inspection was made of the panel where any concrete cracks were marked and photographs taken as necessary.

As the test progresses it was closely watched for signs of damage and ultimate failure. As failure becomes imminent, and not always predictable, data recordings are made more often in order to capture data at failure. The video was also zoomed in on the suspected failure zone. After failure occurs the panel was held in position as final observations are made, particularly regarding the failure mechanism.

The load was then released with any recordings taken at the final zero point.

The panel was then removed from the equipment and stored for possible future reference.

3.5 Series 1 Panel Tests

3.5.1 Aims

The initial purpose of the Series 1 tests was to provide a comparison of the performance of Bi-Steel and studded DSC panels. The studded panels would allow comparison with existing data and design guides [SCI-P-131]. Of particular interest was the load - deflection behaviour, rotation capacity and the internal distribution of forces.

3.5.2 Constraints and Parameters

For a number of reasons testing was to be carried out on full size specimens. Firstly, to avoid any scaling characteristics and secondly, due to the manufacturing process, only one panel depth was currently available. The depth of panel was specifically chosen by a market research study on the possible uses of Bi-Steel.

Previous testing in this field has been on narrow beam type elements with a maximum of three rows of connectors across the width. It was thought that this may not provide sufficient containment of the concrete so an additional two rows were added. As the minimum connector spacing is 200 mm due to the manufacturing process, this gave a panel width of 1000 mm.

The span of the test panels was chosen to ensure a bending failure instead of shear failure. Reinforced concrete literature suggests that for a bending failure then the span to depth ratio should be greater than 12. Also required was the provision of sufficient shear strength by including a certain number of connectors, their combined shear strength equal to the tensile strength of the

steel plate. A span of 3400 mm was chosen which gives substantial allowance for bending failure and enough space to include the required number of connectors. Overall length was 4000 mm which allowed for overhang at the supports. For the studded panels the constraints were not as tight, and the connectors could be welded closer together. This also allowed smaller diameter studs to be used hence keeping costs to a minimum. The shear capacity of all the panels was identical.

Previous testing has always shown that slip occurs at the steel - concrete interface at the end of the specimens [Hordyk (1994); Wright (1991); Oduyemi (1989); Steel Construction Institute (1997)]. In order to simulate the continuity of a structure a 20mm steel plate was welded on each end of one of each type of panel.

This implied that the test series contained four panels, two Bi-Steel and two studded with one of each having welded end plates. The two Bi-Steel panels were the first prototype units to be available for test.

3.5.3 Instrumentation

Figure 3.4 and Figure 3.5 respectively show the positions of strain gauges for the Bi-Steel and studded panels used in Series 1 tests. A line of five pairs of strain gauges was placed centrally on the longitudinal axis of the beams with each pair of gauges placed centrally between adjacent shear connectors. For each pair of gauges, one is placed either side of the steel plate (internal and external). This arrangement eliminates any local bending effects that the connectors may have on the strain gauge readings by:

1. Minimising any local effects by placing the gauges midway between adjacent connectors and,
2. Removing any local effects by averaging the readings from each pair of gauges.

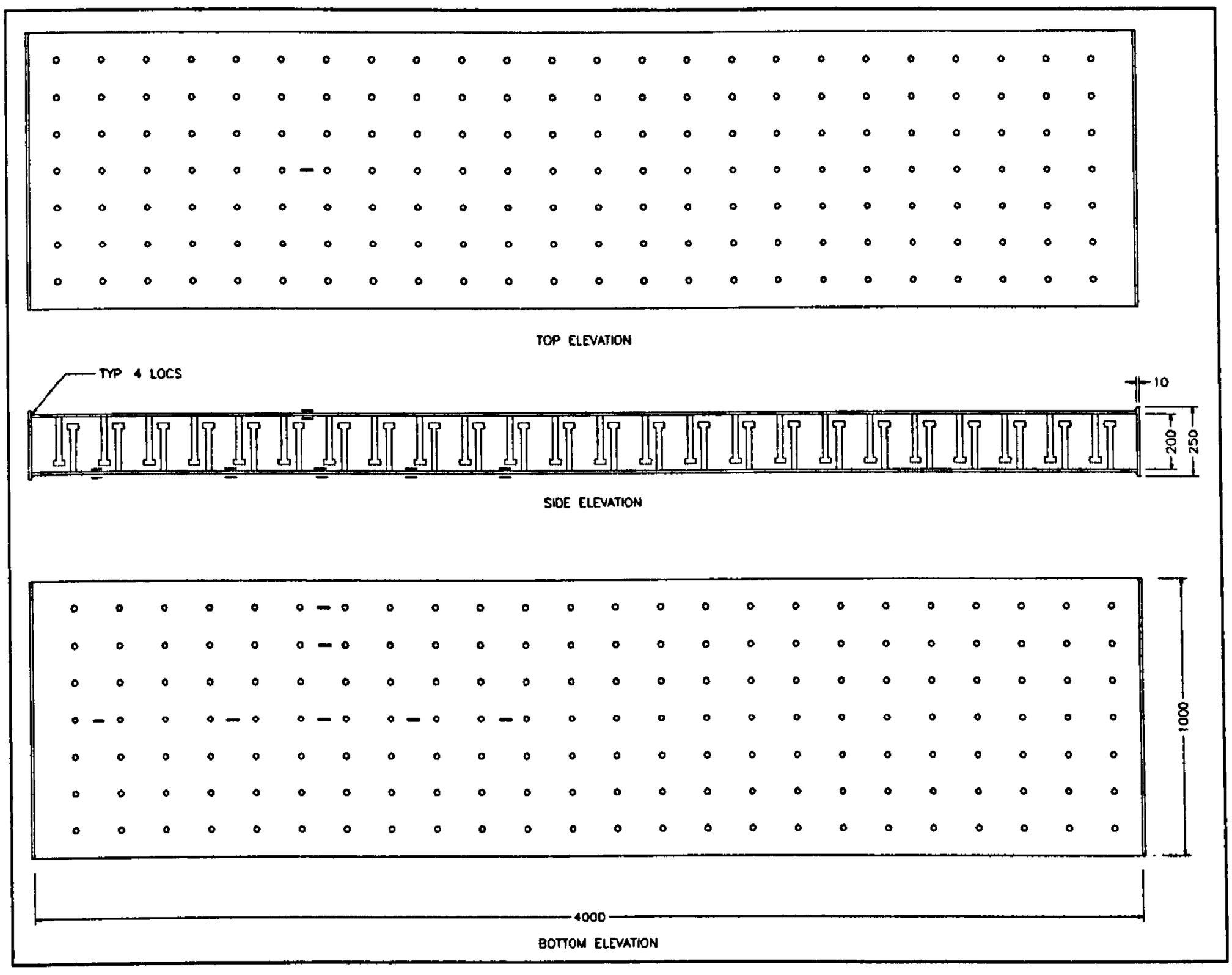

Figure 3.4 Series 1 Studded Panel Tests (Stud2 and Stud2b).

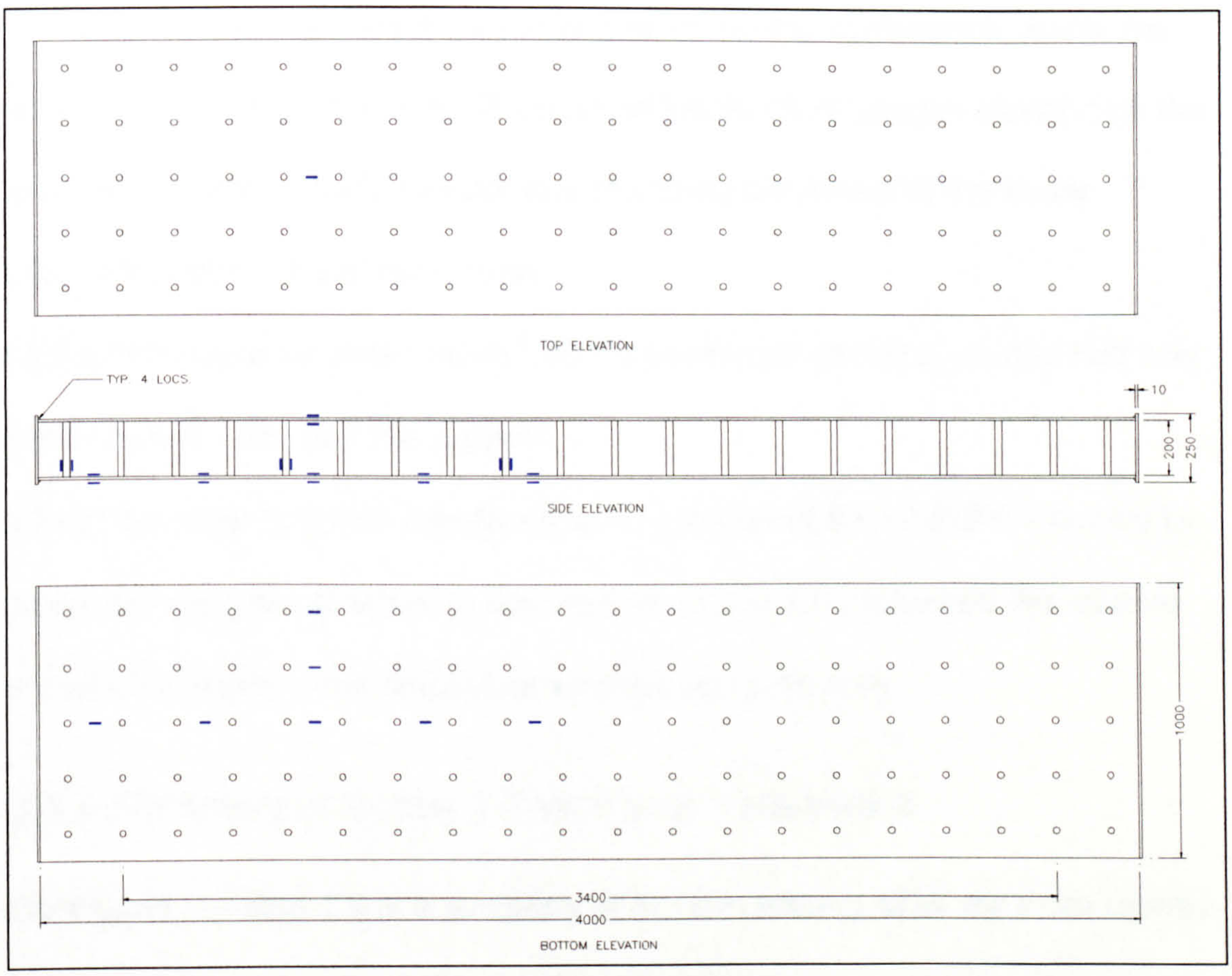

Figure 3.5 Series 1 Bi-Steel Test Panels (City1 and City2).

A line of three pairs of gauges (which includes one of the longitudinal pairs of gauges) were placed on the transverse axis away from any support or loading positions (approximately half way between a support and mid-span. These monitor any changing effects due to the proximity of the edge of the beam. The actual location chosen is such that the transverse section occurs near to the same point in both the DSC and Bi-Steel beams, for easy comparison.

To monitor the section of the beam and to determine the location of the neutral axis, another pair of strain gauges is placed on the top steel plate. These are to be used in conjunction with one of the longitudinal pairs of gauges on the tension plate and two embedded concrete strain gauges placed 25 mm from the steel surface.

Three pairs of gauges were also to be placed on the connectors, which are adjacent to the first, third and fifth pairs of longitudinal gauges situated on the lower steel plate. These monitor any changing behaviour of the shear connectors throughout the section.

Deflections were recorded using LVDT's positioned at mid span and half way between mid span and the support.

Slip at the steel concrete interfaces was recorded at the end of the panels by using dial gauges, attached to the steel plates, which measured the relative movement between the steel plate and the concrete core.

3.5.4 Summary of Series 1 Test Panel Parameters

Contained in Table 3.3 is a summary of the parameters of all the tests carried out on double skin composite panels in Series 1.

Series Name	Panel Name	Span	Width	Plate Thickness	Concrete Depth	Stud or Bar spacing / plate thickness Ratio
		L	b	t	h_c	s/t
Series 1	City1	3400	1000	10	200	20
	City2	3400	1000	10	200	20
	Stud2	3400	1000	10	200	20
	Stud2b	3400	1000	10	200	20

Table 3.3. Series 1 test panel dimensions

3.5.5 Results

Throughout the testing of both types of double skin composite panel it was possible to identify a general pattern of behaviour for each type and to identify similarities between them. For this reason, general descriptions of panel behaviour are given first which include typical crack patterns, pre- and post yield, load - deflection behaviour and failure mechanisms. These are then followed by detailed descriptions of the individual panel tests where details specific to each test are given.

During the initial stages of applying the load the panel exhibited no signs of distress and no visible cracking occurred until approximately 15% of the yield load had been applied. When cracking commenced it did so from the tension plate interface at the locations of the near mid-span shear connectors. The cracks move vertically indicating bending of the panels. As loading continues the cracks begin to propagate towards the load point, i.e. mid-span at the compression plate interface. They also increase in width at the tension plate interface.

All of the cracking is accompanied by sounds, usually small in magnitude and regular. Occasionally a sudden noise occurs although none indicated a loss of load carrying capacity or produced any visible changes as they probably occurred within the panel.

As load is applied throughout the elastic region, the neutral axis remains stable, and is indicated by plots of steel section strains at various load levels (Figure 3.6, also Figures C.13 – C.16 in Appendix C).

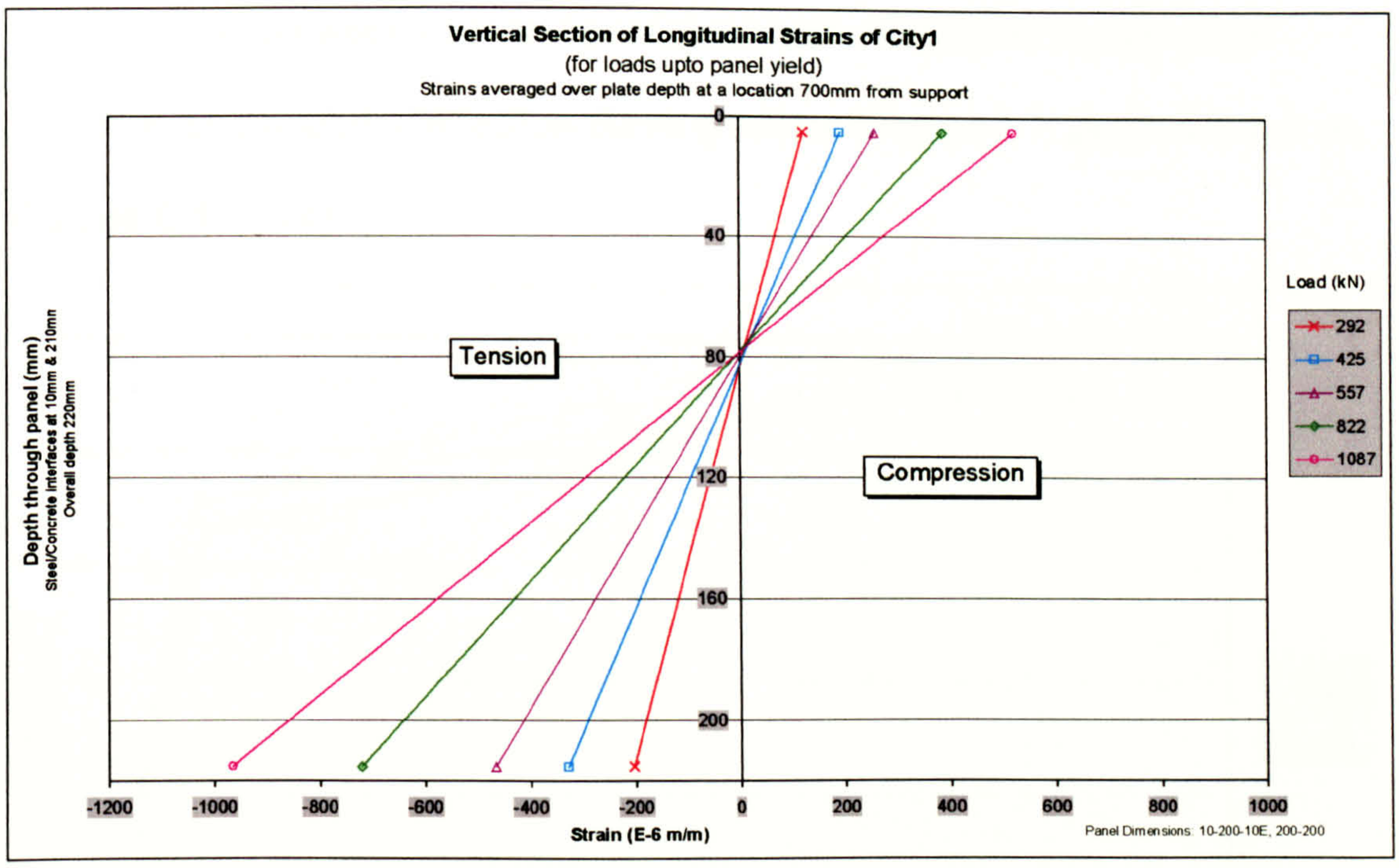

Figure 3.6. Section of strains.

Once 80% of the yield load has been reached the cracks have almost fully developed in terms of length, increasing in width as more load is applied. It is quite obvious by this point that there is a reduction in the width of the tension plate due to the effects of Poisson's ratio.

The transition between pre- and post yield is characterised by a gradual reduction of the load –deflection curve gradient (Figure 3.7, printed larger as Figures C.1 – C.4).

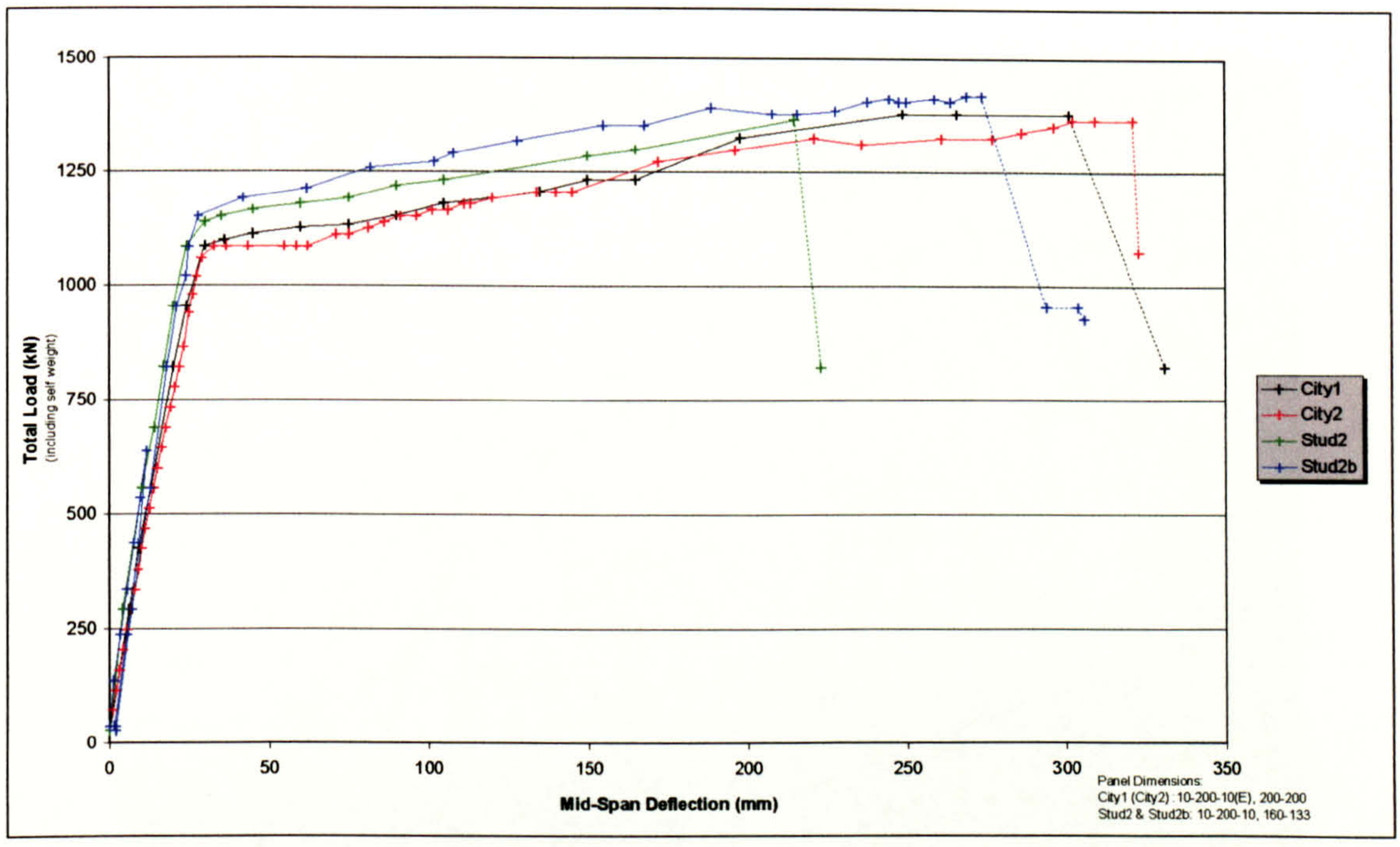

Figure 3.7. Load deflection curves for Series1.

This is due to the gradual movement of the yield point through the depth of the panel. It is initiated as the outermost surface of the tension plate reaches the yield stress and finishes when the innermost surface achieves the same stress. As the neutral axis has moved to the compression plate, the concrete below must be in tension and it is assumed that it does not posses any strength. This is proven by the extent of cracking, which by this point has reached the compression plate.

In general the post yield load – deflection behaviour shows an increase in the load carrying capacity with increased deflection as the tension plate material undergoes strain hardening (Figure 3.7). The increase in load carrying capacity becomes very small as the deflections increase, by failure the curve

has become almost flat. At some point in this region there is a local failure, described in detail in each of the later test descriptions.

3.5.5.1 City1

Plate 3.2. City1 crack patterns.

The testing of City1 proceeded as generally described above. There was generally a linear elastic increase in load in the elastic region, which maximised at 1087kN centrally applied load, equivalent to 924kNm. Failure occurred by local buckling of the compression plate adjacent to mid span. From this point the load carrying capacity was reduced gradually. The region of concrete below the buckle was slightly crushed, some of which fell to the floor.

Throughout the test there was no apparent separation of the compression plate from the concrete (until buckling occurred) or longitudinal slip at either steel - concrete interface. This was to be expected as end plates had been welded to the panel to simulate structural continuity.

3.5.5.2 City2

The testing of City2 proceeded as described above for City1. Again failure occurred by local buckling followed by a gradual loss of load.

Again, no separation or slip occurred. This was not expected as all previous testing on DSC beams had encountered slip, and no end plates were welded to prevent it.

3.5.5.3 Stud2

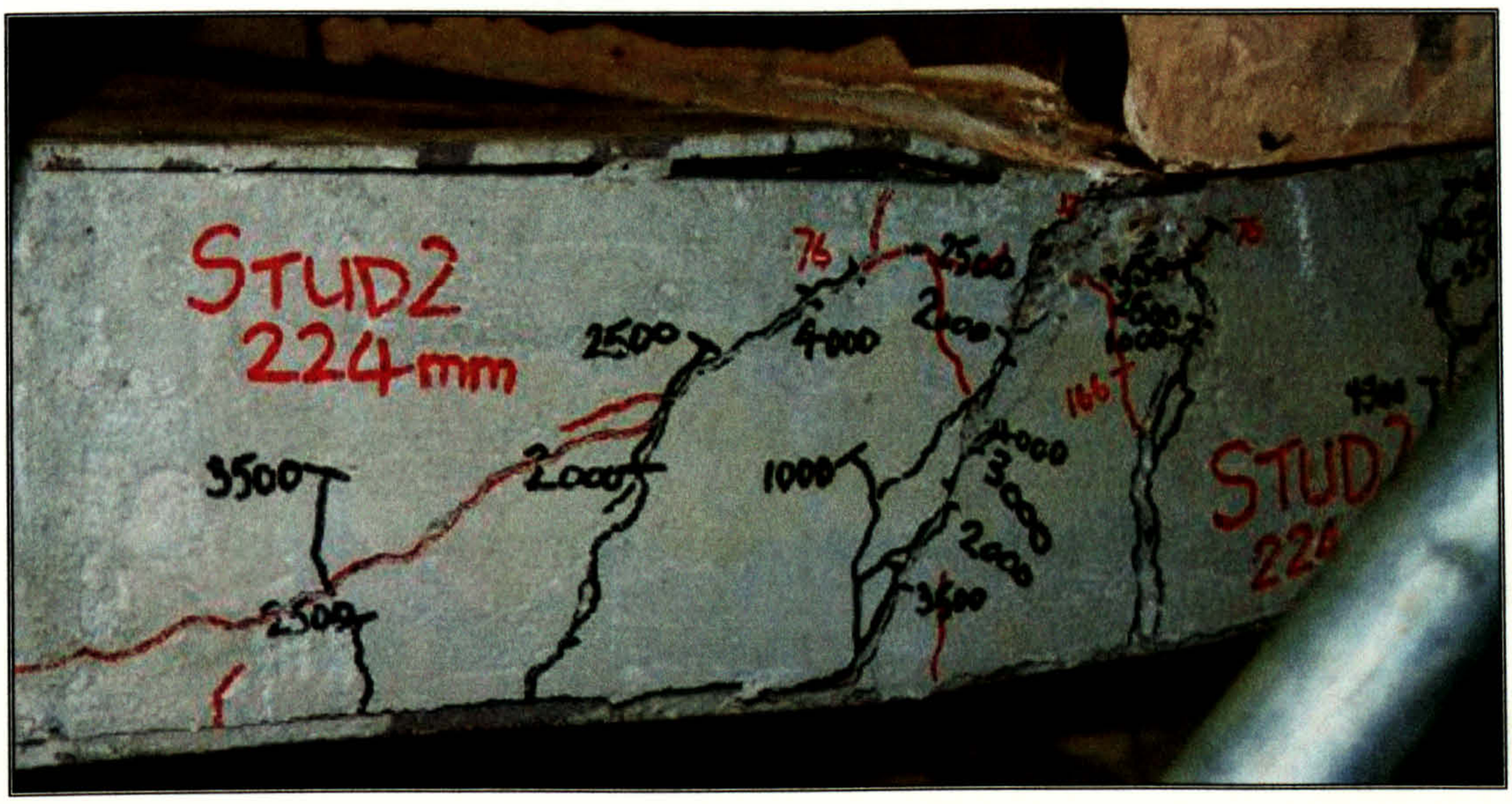

Plate 3.3. Stud2 crack patterns.

The first studded panel to be tested in this series performed very similarly to the Bi-Steel panels of City1 and City2. Cracks propagated from locations where connectors were welded to the steel plate, as previous research has found. Failure occurred when the second row of studs began to pull out of the concrete causing the compression plate to buckle.

Similarly to the Bi-Steel panels, there was no apparent separation or slip at the steel - concrete interfaces.

3.5.5.4 Stud2b

Plate 3.4. Stud2b crack patterns.

After testing the first three panels in this series it was decided to change the parameters of the test for remaining studded panel. The end plates were cut off what was to be Stud1 to make it identical to Stud2, hence its name was changed to Stud2b. The purpose of this test was to cycle the panel over a large load range to try to induce slip at the steel - concrete interface. Approximately 500 cycles between 1% and 54% of the yield load were carried out on this panel with very little change to the initial static load conditions occurring. Ten cycles between zero and 83% were then carried out with some creep of mid span deflection occurring at the end of each cycle. No slip at the concrete interface occurred throughout the whole of this testing.

At this point a regular test to failure was carried out. Failure occurred similarly to Stud2 with the second row of connectors, from mid-span, pulling out from the concrete. This time however, the connector lying on the centreline of the panel remained embedded in the concrete.

3.5.6 Summary of Series 1 Tests

By comparing the load deflection curves (Figure 3.7), after testing the first three panels in this series it was evident that the end plates made no effect on the strength (expected) or stiffness (not expected). This meant that for this size of panel there was no additional stiffness to be gained from the continuity of a structure as a whole.

Also not expected was the lack of slip at the steel - concrete interfaces as has been described in previous research. This may be due to the considerable shear resistance of these panels, sufficient to allow the full tensile strength of the steel to develop.

Figure 3.8 and Figures C.5 – C.8 in Appendix C show the variation of strain along the length of the panel during elastic loading. It can be seen that the variation is approximately linear, from zero at the support to a maximum at mid-span, as would be expected from theory for a beam in three point bending.

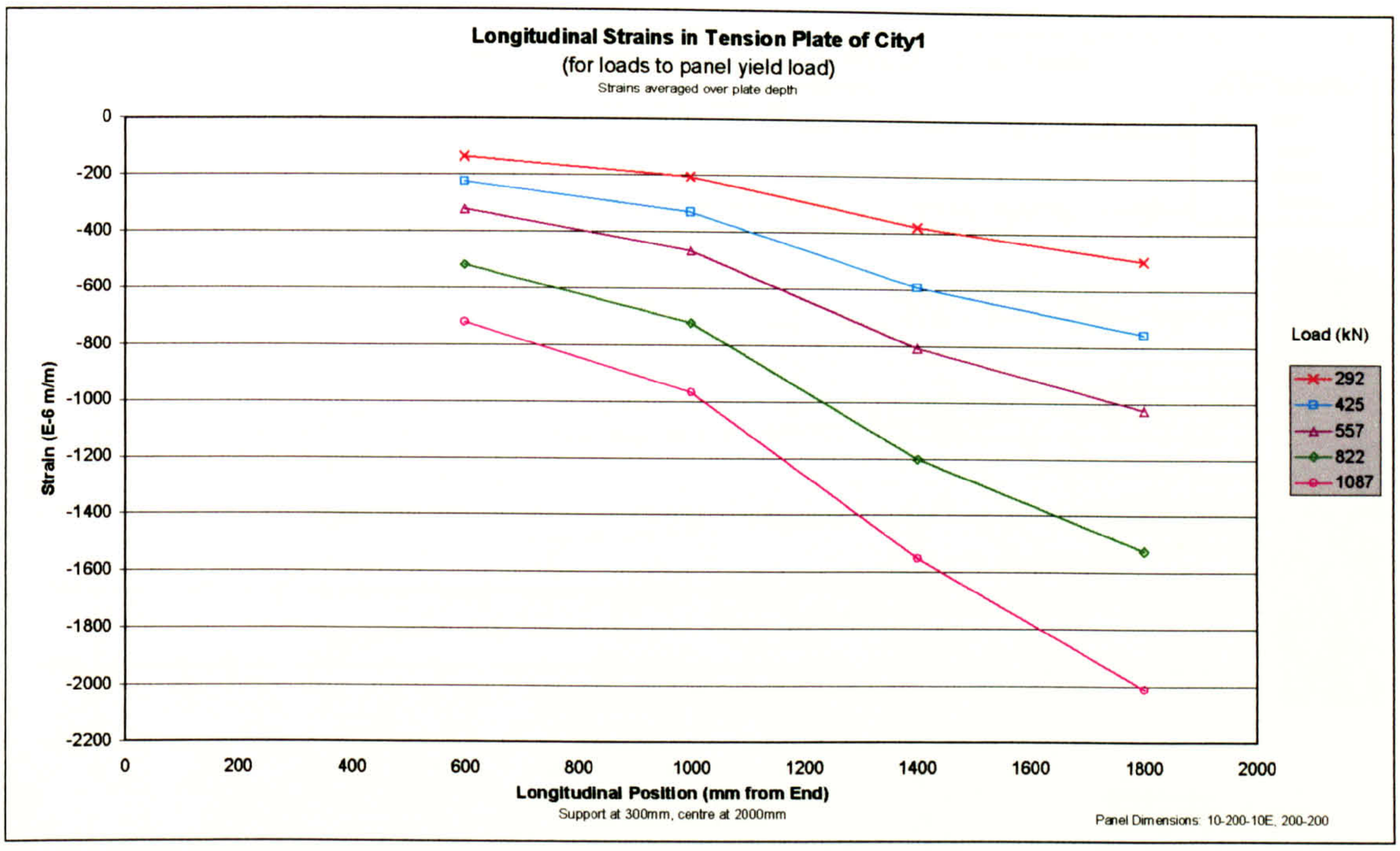

Figure 3.8. Longitudinal strains typical of Appendix C.

Figure 3.9 and Figures C.9 – C.12 in Appendix C show the variation in the longitudinal strains over the width of each of the panels. They show that there is a slight increase in strain from the centre of the panel to its outer edge. This is due to the effects of the Poisson ratio as the tension plate is being stretched. As presented by Equation 2.45 in Chapter 2, the outer strain value is theoretically greater than that at the centreline. In the case of steel with a Poisson's ratio of 0.3, this factor is equal to 0.09.

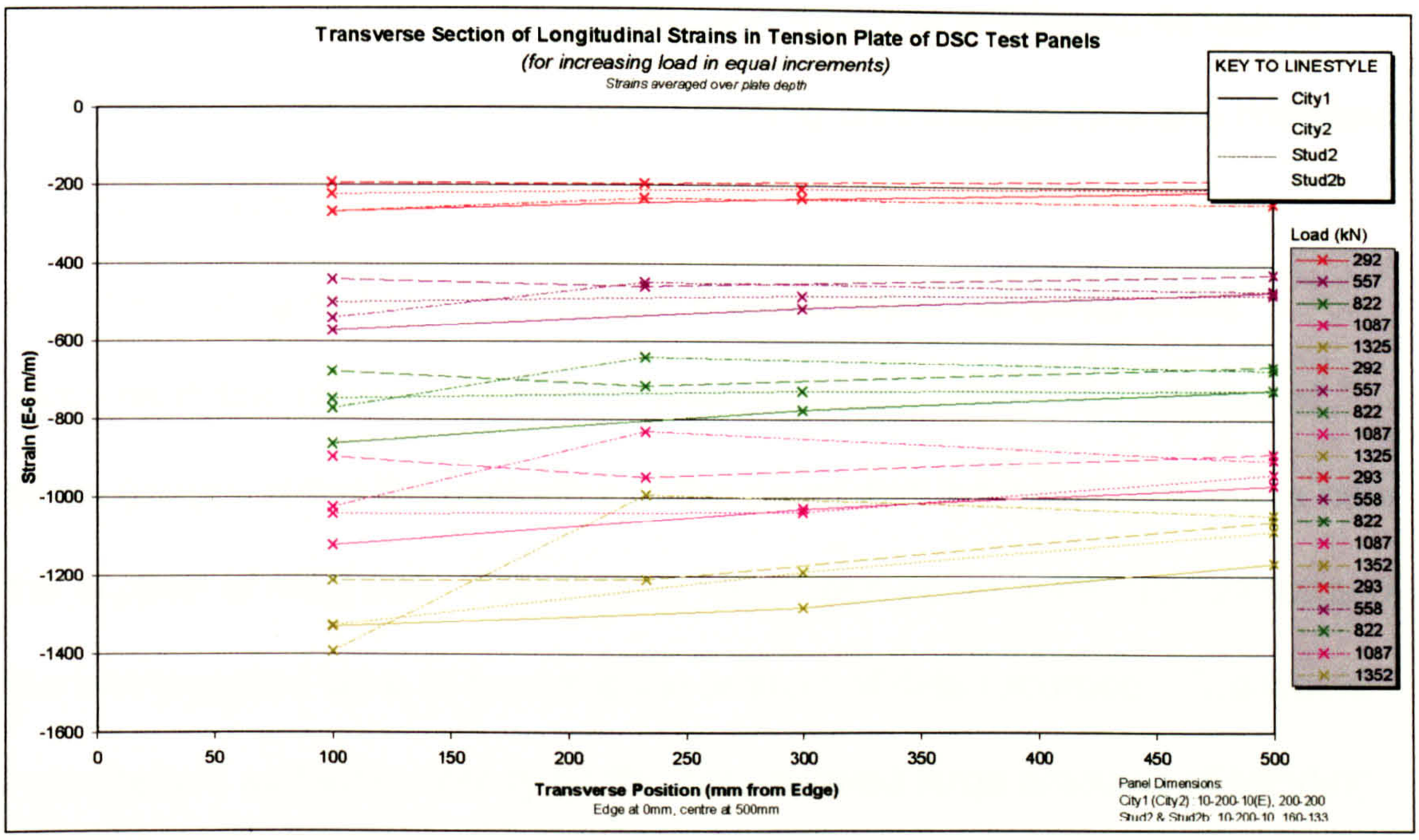

Figure 3.9. Tranverse variation of longitudinal strains (Appendix C).

Strains at a vertical section within the panel represented in Figure 3.6 and Figures C.13 – C.16 in Appendix C show that during elastic loading the neutral axis remains stable.

The relative performance of studded and Bi-Steel double skin composite panels show that there is little difference between them provided the panel remains intact. The major advancement of Bi-Steel over traditional studded methods of construction is in its ability to remain intact due to a welded connection between both faces of the panel. In normal expected use there is not much of a structural advantage, except simplicity of detailing. However, should a structure ever be subjected to considerably local deformation then it has been shown that Bi-Steel can remain intact and in doing so absorb considerable energy.

Bi-Steel is also superior in the construction methods employed, its lack of dependence on additional form work meaning construction time and complexity is greatly reduced.

After the testing had been completed, it was evident that some of the instrumentation choices could have been improved upon. The number of strain gauges along the centreline of the panel was too many, with those near the support of least use. These could have been put to better use on some of the instrumented bars, to increase the amount of data recorded. This would have helped as those already on the bars showed large amounts of bending. More gauges here would help determine the distribution of these bending forces throughout the shear connector. The embedded concrete strain gauges gave erratic information and so were not used in the analysis. It is thought that the method of fixing the gauge was insufficient to restrain it whilst the concrete was poured.

However, the instrumentation used to determine the strain profiles across the tensile plate and through the depth of the section was sufficient.

3.6 Series 2 Bi-Steel Test Panels

This series of tests has been based on the results from Series 1 tests to follow the Bi-Steel route of further investigation. Series 2 tests are split into two parts (I and II). They both investigate the same areas of interest but were carried out after each other as the performance of some areas after testing Part I were able to be clarified by Part II tests.

3.6.1 Aims

The investigation of large rotational capacities of Double Skin Composite panels required further tests to be carried out. It was seen from Series 1 tests that the final collapse of the panel is governed by the buckling of the compression plate, which occurred between adjacent columns of bars near mid-span.

The comparison between panels produced using stud connectors and Bi-Steel has shown that Bi-Steel panels have considerable advantages over studded panels. Also, the results from the Bi-Steel panels have been comparable, i.e. similar, to each other. Results from the studded panels show less conformity. Hence it appears natural to follow the 'Bi-Steel' route.

As the buckling of the compression plate appears to control the point of collapse the next series of tests should focus on the parameter that affects the buckling of the plate. This is governed by the proportion between the buckling length of plate to its thickness, namely the bar spacing to plate thickness ratio (s/t). The effect of concrete strength was also to be studied as the connectors bear onto it as the plate buckles.

3.6.2 Constraints and Parameters

This series of panels are to be 3000 x 600 mm with a span of 2600 mm. This gives a shear span/effective depth ratio of over 12 for all proposed plate thickness, the ratio suggested by reinforced concrete literature above which a bending failure will occur. The width of the panel is sufficient to provide 3 rows of bars at 200 mm between rows. It is thought unnecessary to provide more than this as previous results indicated that there is no change to the strains across the panel other than those that can be calculated due to the effect of Poisson's Ratio. Any fewer than three rows of bars may provide inadequate confinement to the concrete.

The range of bar spacing/plate thickness ratios to be tested includes the minimum constructed of s/t = 16.67 to a value of s/t = 45 (50 for Part 2 tests). This slightly exceeds the maximum suggested by composite construction guides (e.g. EC4) of s/t = 40. In order to achieve this the design of the connector arrangement was made asymmetric. One half of the panel was standardised throughout the series and was not instrumented. In the other half, the required spacing was fitted next to mid span with as many bars as possible fitted into the remaining space. This arrangement gave the benefit of knowing where the panel was going to fail hence reducing strain gauge requirements.

In the size of panel used is was not as possible to provide adequate shear connection using solely bar connectors due to insufficient space in which to fit them. The amount of connection, as a percentage, is the ratio of the amount of shear connection provided to that required to resist the full tensile capacity of

the compression plate. In order to ensure that the bars do not first fail in shear along the steel - concrete interface 10mm thick plates were welded across the ends of the panels and stud connectors were welded to the compression plate. These provide the remaining shear connection and hence allow the full strength of the panel to be studied. In the un-instrumented half of the panel the additional studs were welded in the location where a buckle might be expected to occur. This further ensured that the buckle would not form in this location. In the instrumented half of the panel the studs were placed well away from instrumentation to avoid unwanted influences. Table 3.4 gives a summary of the amount of connection provided by the Bi-Steel bars together with any additional studs that were required.

Panel Name	Bars (No.)	Plate Thickness (mm)	Connection (%)	Additional studs (No.)
City3	21	12	65.7	15
City4a,b,c,d	21	10	78.8	9
City5	21	8	98.5	3
City6,6b	18	8	84.4	6
City7	18	8	84.4	6
City8	18	8	84.4	6
City9	18	8	84.4	6
City10	18	8	84.4	6

Table 3.4. Percentage shear connection of Series2 test panels.

Contained in Table 3.5 is a summary of the parameters for all Series2 test panels.

Series Name	Panel Name	Span	Width	Plate Thickness	Concrete Depth	Bar spacing / plate thickness Ratio
		L	b	t	h_c	s/t
Series 2	City3	2600	600	12	200	16.67
(Part 1)	City4a	2600	600	10	200	20
	City4b	2600	600	10	200	20
	City4c	2600	600	10	200	20
	City5	2600	600	8	200	25
	City6	2600	600	8	200	30
	City7	2600	600	8	200	35
	City8	2600	600	8	200	40
	City9	2600	600	8	200	45
Series 2	City4d	2600	600	10	200	20
(Part 2)	City6b	2600	600	8	200	30
	City10	2600	600	8	200	50

Table 3.5. Series 2 test panel dimensions.

3.6.3 Instrumentation

As it was the intention to study the area around where the buckle forms at final collapse, the instrumentation was confined to this area (Figure 3.10). It was also confined to the centreline of the panel as any three-dimensional effects in the tests can be accounted for.

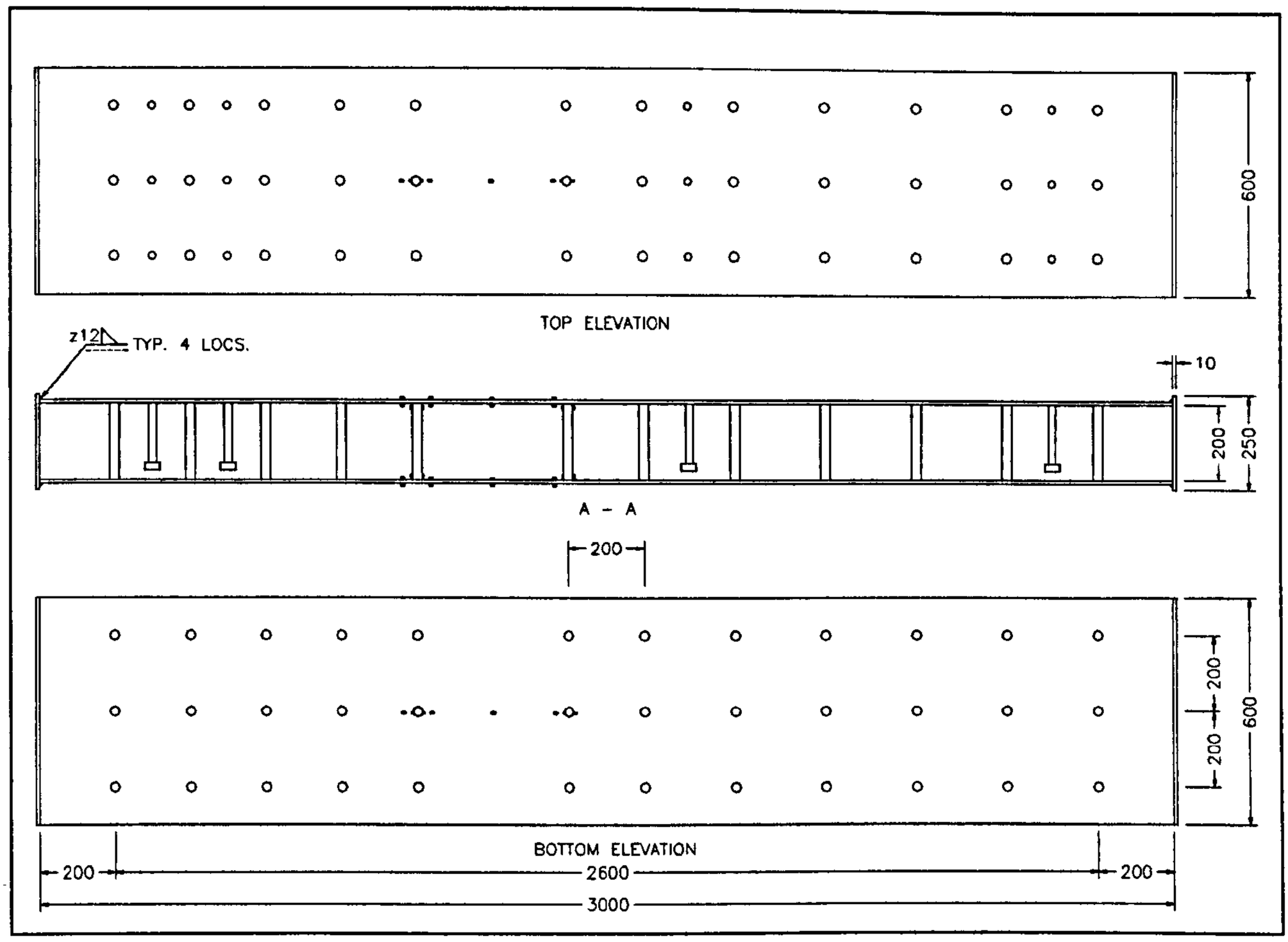

Figure 3.10 Series 2 (part 1) Test Panel General Layout.

Experience showed that the strain gauges only provided information to a point as strains, especially at mid-span were very large. Small transducers were therefore positioned to provide back-up information should the gauge fail or de-bond.

Information obtained from the bars in Series 1 was limited as only strains at the bottom of three bars were obtained. In order to provide better understanding of the behaviour of the interior of the panels the two bars either side of the buckle location were instrumented for Series 2 tests. This was done using two strain gauge pairs per connector, one pair placed 15 mm above each of the two steel plates.

The compression plate is strain gauged to obtain information, particularly when the plate begins to buckle, with a view to future predictions.

By placing gauges at two longitudinal positions it is possible to determine the interface shear forces by calculating the difference in stress at each location, assuming an elastic strain distribution. These can then be used to determine whether or not the design process is efficient regarding the number of connectors required.

For the tests carried out in Part 2 of this series the strain gauge layout was changed (Figure 3.11).

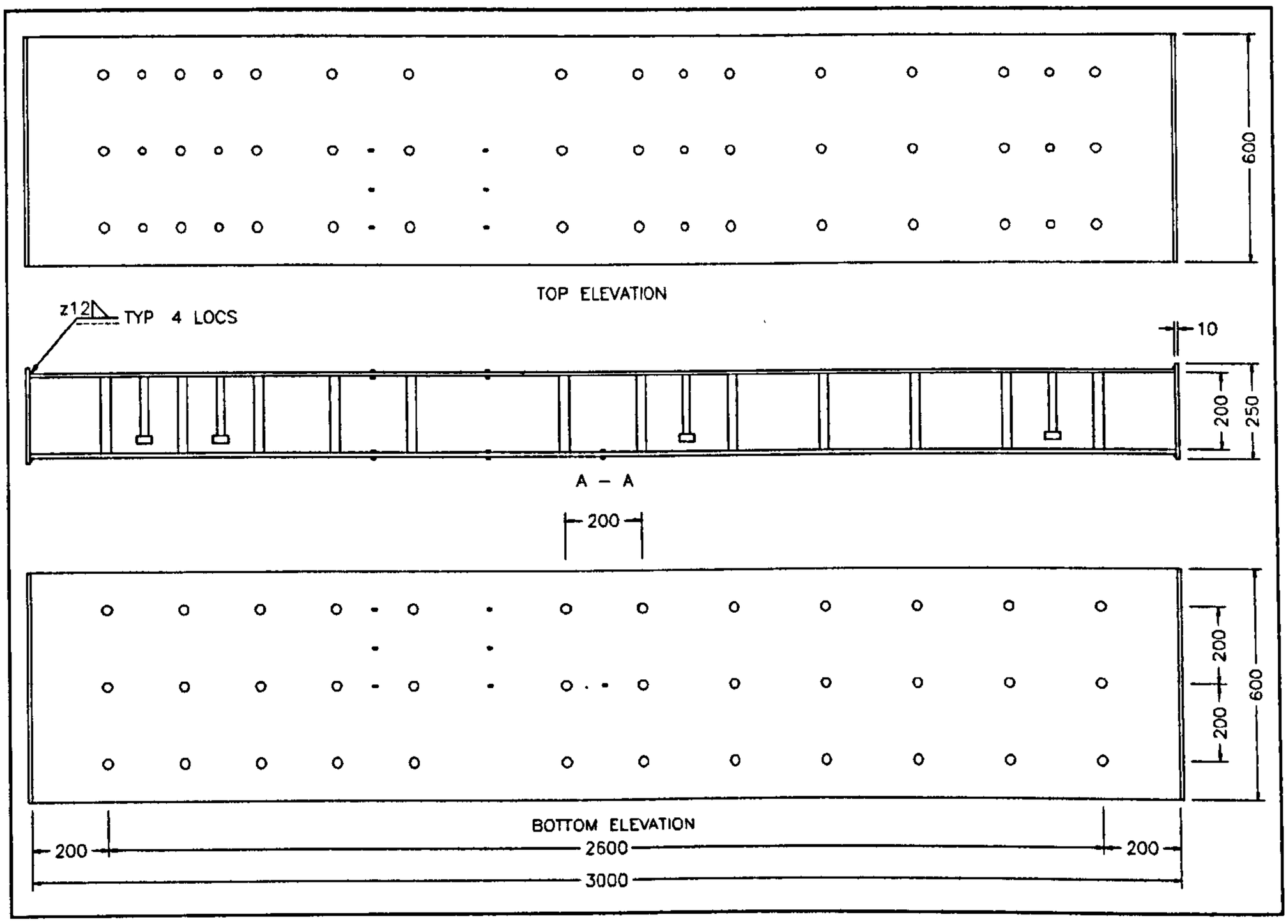

Figure 3.11 Series 2 (part 2) strain gauge layout.

Pairs of gauges were positioned on the tension and compression plate at the location of buckling and between the next rows of connectors. These were positioned along the centreline of the panel and then repeated twice across the width of the panel to provide back up should any gauges fail. This also allows for interface shear forces to be calculated.

In order to map the surface profile of the compression plate, a new technique of using digital photogrammetry was used. This involves the use of specialist PC based software controlling a number of CCD cameras to record the same image from a number of different locations, similar to co-ordination by surveying. By having fixed points within the image it is possible to record the movement of any other points within that image. By using four cameras at a range of approximately 2m it was possible to achieve three-dimensional co-ordinates of reflective targets to an accuracy of less than 0.1mm.

Plate 3.5 Overall set up using CCD cameras.

The system requires the specimen to be targeted using small circular reflective targets that are affixed to the specimen at numerous locations. The only limitations on the number of targets used are spacing (for clarity of image) and the time that is required for processing data, which is recorded during the experiment.

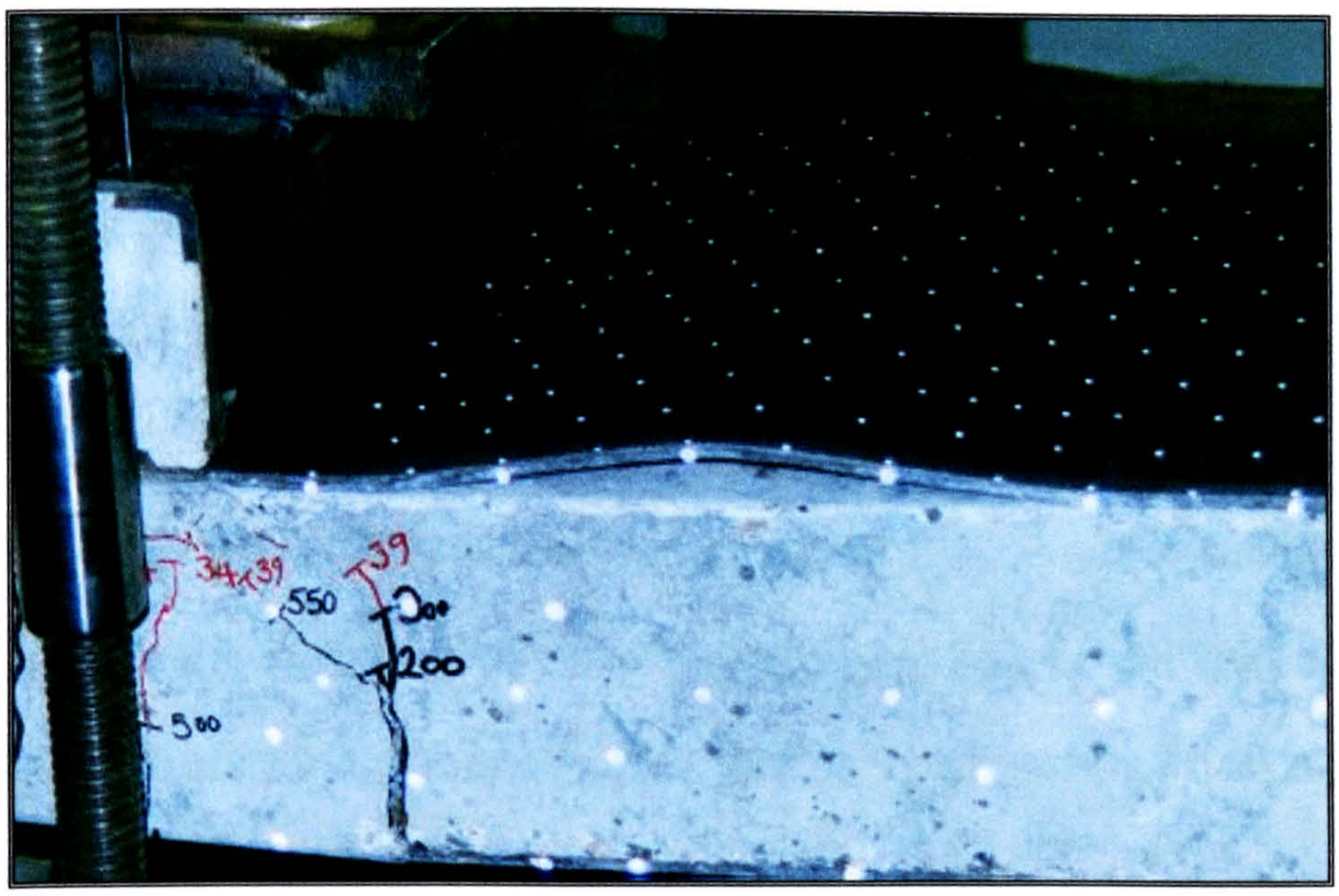

Plate 3.6 VMS targeting system.

3.6.4 Results

Similarly to Series 1 tests it was possible to identify a general pattern of behaviour whilst carrying out Series 2 tests. Again, this included typical crack patterns, the pre- and post yield load deflection behaviour and in most instances within Series 2 tests, the failure mechanisms. A general description of panel behaviour is again given followed by descriptions of the individual panel tests. Results in the form of charts plotted from measured data are given in Appendix D.

Crack propagation throughout the panel tests was as identified in Series 1 tests. That is, cracks propagate from the tension plate and progress towards the load point. Occasionally, a sudden loud noise occurs although most did not indicate a loss of load carrying capacity or produced any visible changes as they probably occurred from within the panel. However, there were exceptions, details of which are given later.

As load is applied throughout the elastic region the neutral axis again remains stable, as indicated by Figure 3.12 and Figures D.13 – D.24 in Appendix D.

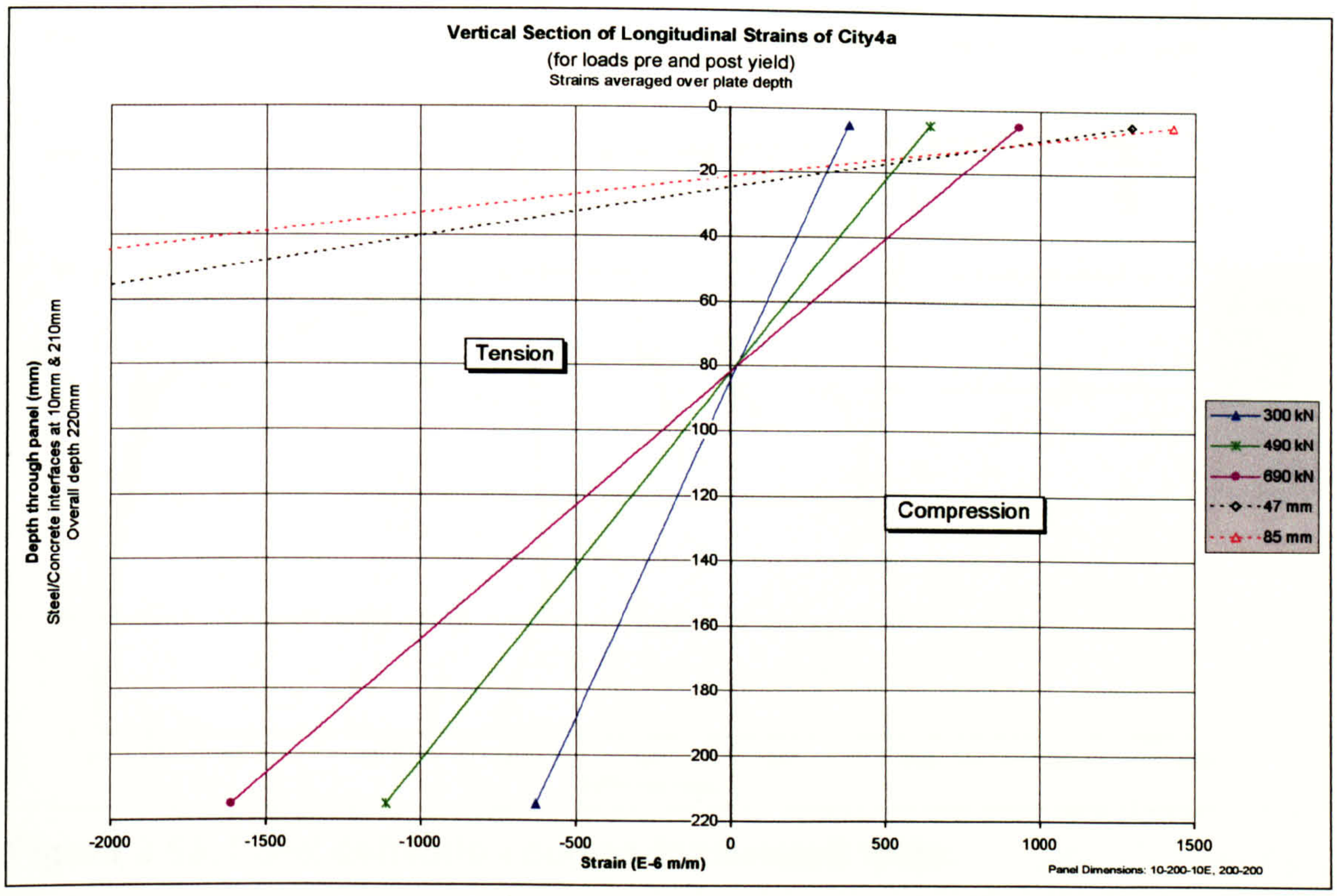

Figure 3.12 Section of Longitudinal Strains typical of Appendix D.

Once yield of the tension plate has commenced, the neutral axis then moves upwards as tension plate strains increase together with simultaneous and slight increases in the compression plate strains, Figure 3.12.

The transition between pre- and post yield is characterised by a gradual reduction of the load –deflection curve gradient (Figure 3.13 and Figures D.1 – D.11 in Appendix D).

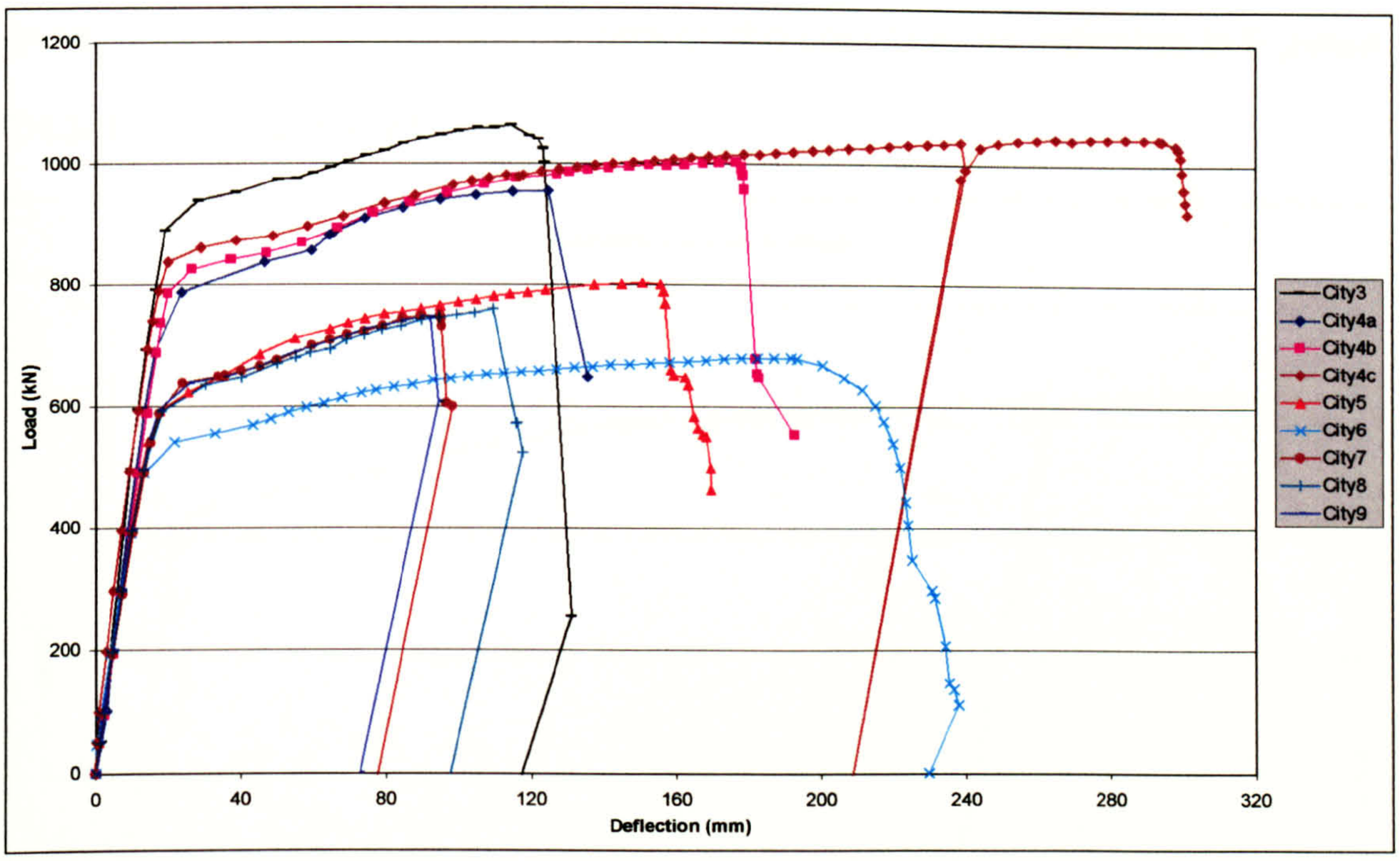

Figure 3.13. Load deflection curves for Series2 tests.

During these tests, it was possible to see some possible effects of concrete strength as the transition between elastic and plastic behaviour, on some of the panels (Part II tests), appeared more gradual than others. The concrete strength for Part II tests is significantly smaller than that used for Part I (Figure 3.2).

In general, the post yield load - deflection behaviour of the Bi-Steel panels shows identical characteristics to those achieved from a tensile test of the same steel from which the tension plate is made. In the tension tests, there is an increase in the load carrying capacity with increased deflection as the material undergoes strain hardening. Further investigations are carried out later, in order to determine whether this causes the increase in strength of the DSC panels.

Initially there is a small section of the curve that flattens indicating increased deflection with little or no increase in load (Figure 3.14). This indicates the

movement of the neutral axis up through the concrete, as indicated in Figures D13- D24 in Appendix D.

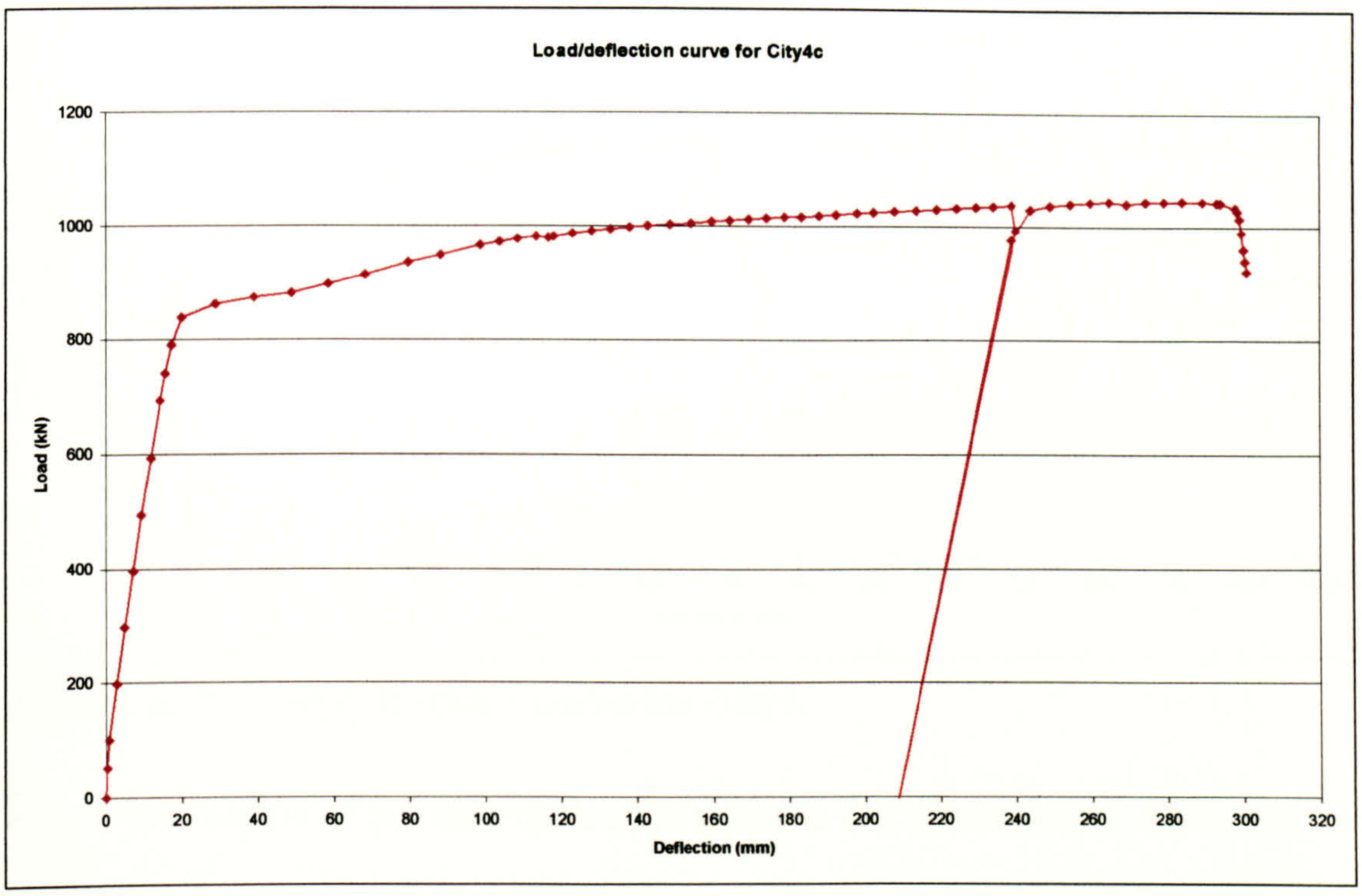

Figure 3.14 Load deflection curve for City4c.

This is due to the lower yield, which is typical of low carbon steels as used for Bi-Steel construction. In some cases it does not occur which is due to the steel not being annealed during the manufacturing process (Figure 3.15). Annealing is a heat treatment process that removes residual stress, from with the steel, that occurs during rolling and welding. The removal of the residual stresses allows the steel to deform plastically without any increase in the load.

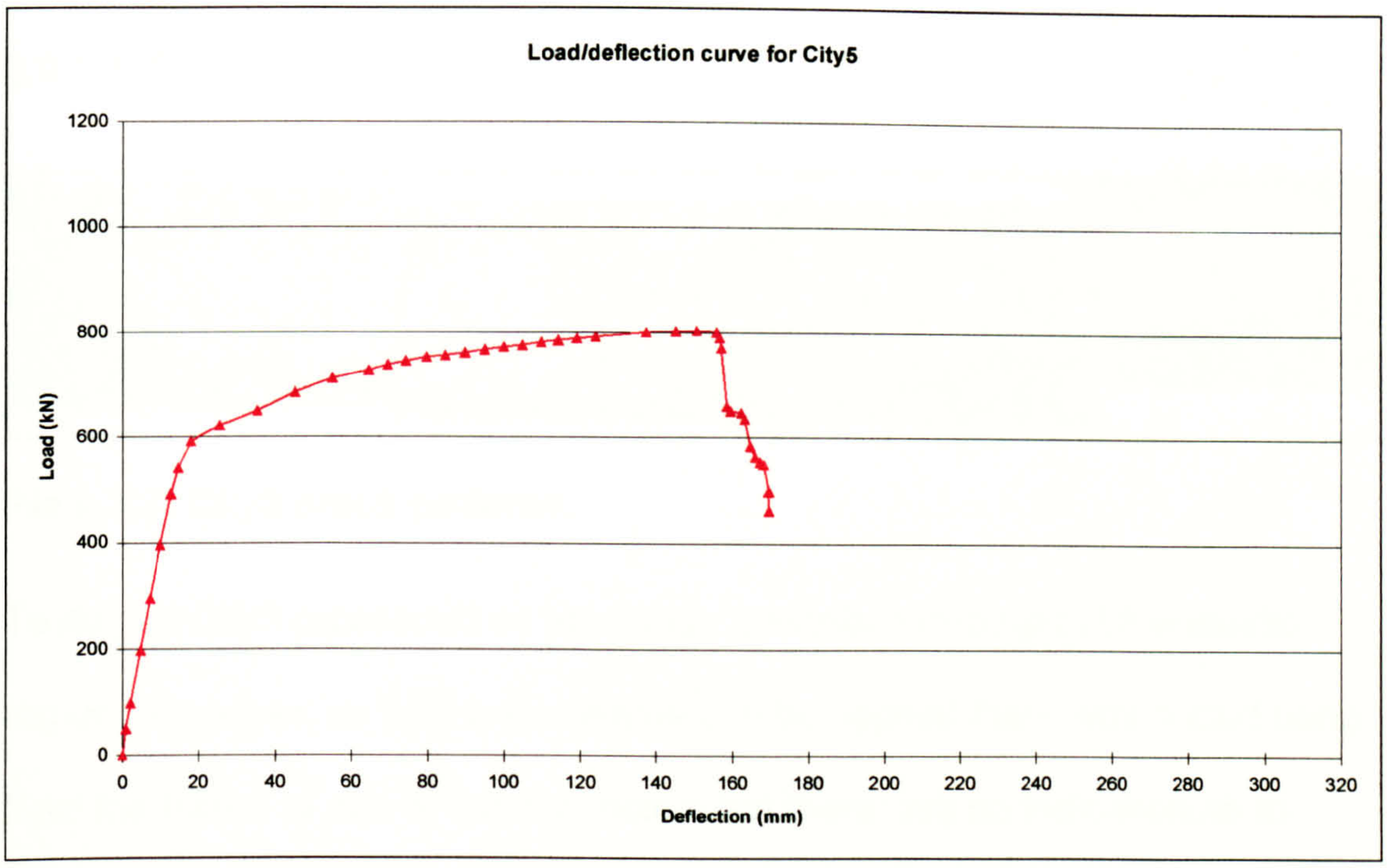

Figure 3.15 Load deflection curve for City5.

The upper bound of the load deflection curve is the same as that achieved from the moment carrying capacity of the steel section alone when using the ultimate tensile strength of the steel plate. Premature panel failure may however occur due to a local failure of one of the following:

1. The shear connector in tension,
2. The weld between the connector and plate,
3. Local buckling of the compression plate.

If any of these occur then the ultimate strength of the panel may not be reached.

Due to longitudinal shear deformation of the panels the connectors inside are subjected to bending. This creates considerable moments at the plate connection and is characterised at large deformations by dimples appearing at the point of connection. This generally occurs on the tension plate near mid-span and only at very large deflections.

3.6.4.1 City3

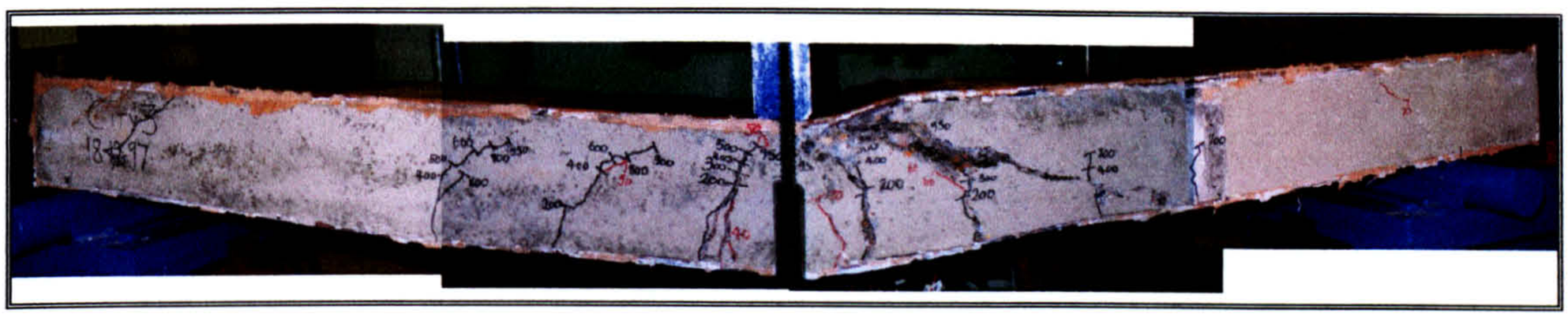

Plate 3.7. City3 crack patterns.

Testing of City3 proceeded as previously described throughout the elastic region. However, as load was continued to be applied there was a loud bang from the failure of one of the connectors but there was no indication as to which one. This was gradually followed by a shear crack developing from near mid-span compression plate and extending downwards towards the support roller (RHS of Plate 3.7). As this crack grew in width and length there was a continuous low level noise indicating cracking within the panel. There was then a sudden shear collapse of the panel as the remaining connectors, in the second row from mid span, failed. This was the only panel to fail in this manner and was also the only one to use 12mm plates.

Removing concrete manually from the side of the panel revealed the weld to have failed at the surface of the plate, the bar and plate remaining intact (Plate 3.8).

Plate 3.8. City3 failure at shear connector bar.

3.6.4.2 City4a

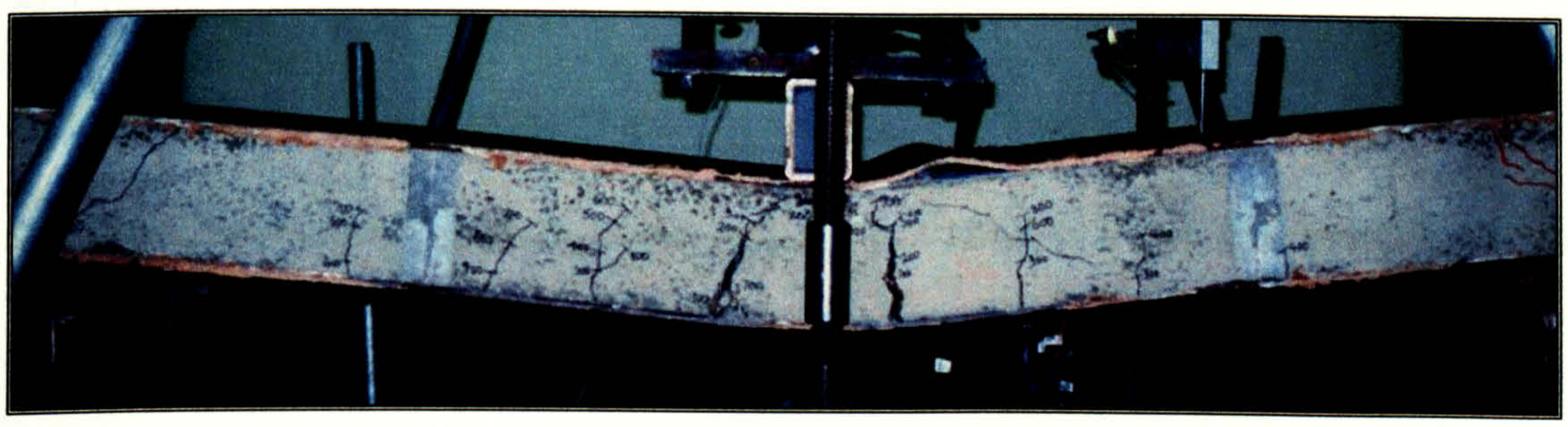

Plate 3.9. City4a crack patterns.

Cracks were first seen at 200 kN, approximately 25 % of the yield load. These continued to grow, along with some additional cracks until 600 kN. At 700 kN load a large shear crack appeared at End B. Cracks did not appear at the interface between the steel and concrete until 800 kN (yield load). By this point the cracks at the centre of the panel had opened up to 2.5 mm in width at their base. At approximately 45 mm mid span deflection a large bang occurred although there was no visible change to the panel and no loss of load or increase in deflection. By 120 mm mid span deflection, a failure was expected

due to very large compression strains where the buckle was expected to form.

Failure occurred after 135mm deflection when a buckle occurred gradually.

3.6.4.3 City4b

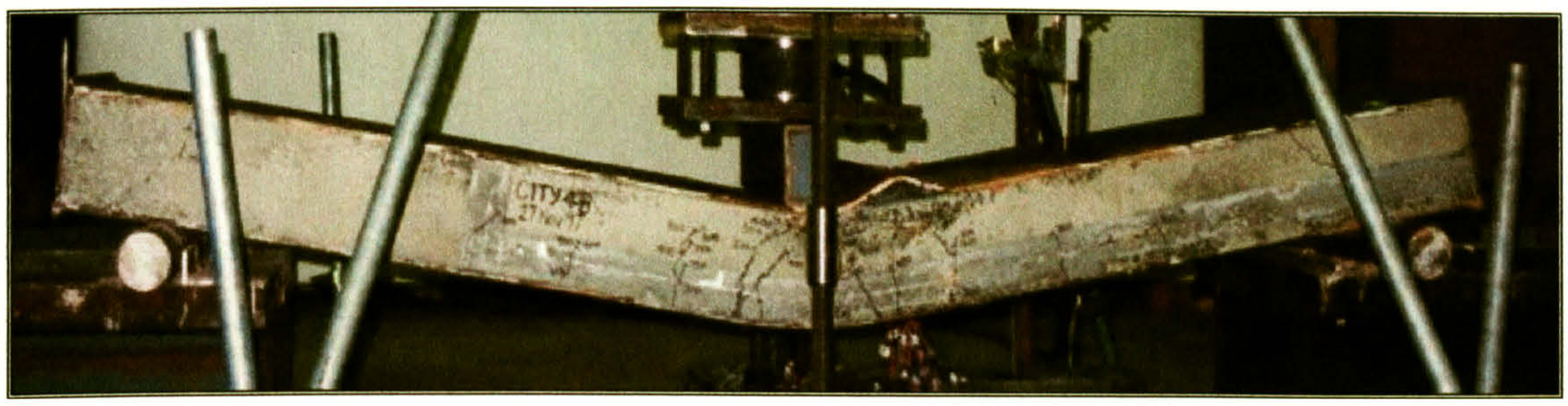

Plate 3.10. City4b crack patterns.

As in City4a, cracks did not appear until 200 kN applied load. Significant crack noises occurred after 200 kN load and interface cracking did not occur until 600 kN.

At failure there was a gradual loss of load as the compression plate began to buckle adjacent to mid span. This rapidly increased with continued deflection and the load settled at approximately 50 % of that before failure.

An immediate observation was that City4b had undergone considerably larger deflections than City4a, by almost 50%, before failure had occurred. The only difference in the panels being the concrete strength.

3.6.4.4 City4c

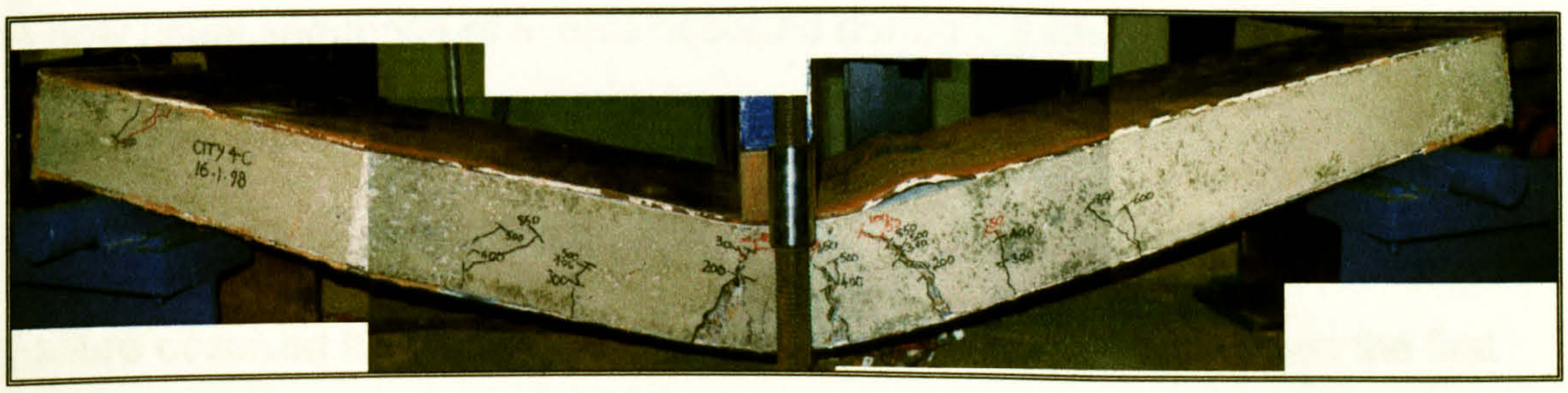

Plate 3.11. City4c crack patterns.

City4c followed a similar route as City4a and City4b. As had occurred with City4b, there was considerable deflection before loss of load, which was even greater than previously experienced. The final deflection before any load was lost was approximately 295 mm, equivalent to 11.3% of span (Plate 3.11).

3.6.4.5 City4d

Test results exhibited the usual characteristics of previous Bi-Steel tests. The region of the load-deflection curve between elastic and post yield appeared to be much more gradual for this test (Figure D.5 in Appendix D). Final failure was initiated by local buckling of the compression plate in the usual position. The deflection at the commencement of loss of load was greater than initially predicted although was within six percent once concrete strength had been measured accurately. The loss of load was gradual and data successfully captured at this point.

3.6.4.6 City5

Plate 3.12. City5 crack patterns.

A now usual sequence of events occurred during the testing of City5. There were some isolated large noises from the panel but there were no simultaneous visible signs or loss of load.

Failure occurred by local buckling of the compression plate between the first and second rows of connectors from mid-span.

3.6.4.7 City6

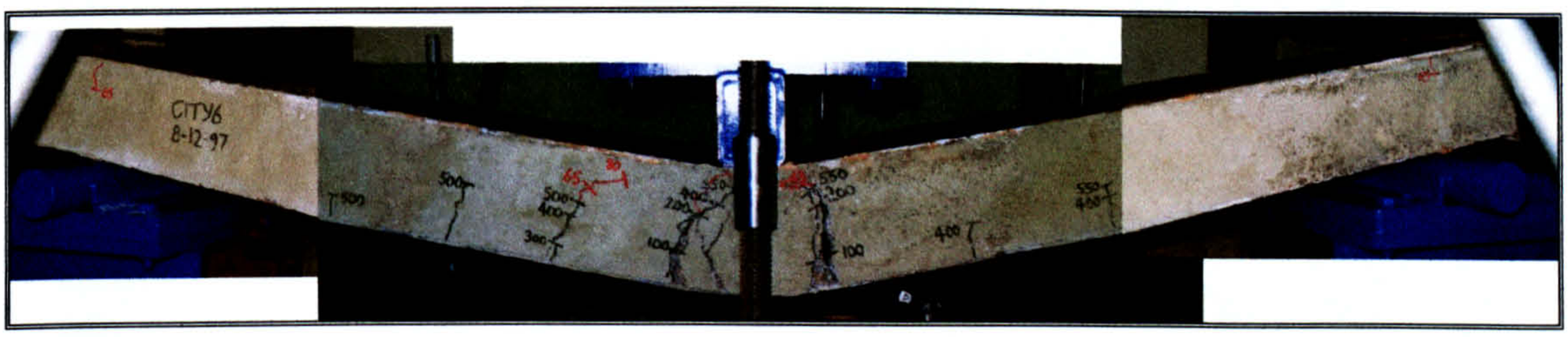

Plate 3.13. City6 crack patterns.

City6 followed the usual pattern up to yield. The load level at yield appeared to be low, but without tensile specimens it was impossible to determine if it this was caused by a lower steel tensile strength. As loading continued through the post yield region it became apparent that the deflections achieved were greater than had been experienced from tests of similar panels. After a mid-span deflection of 210 mm was achieved there was a loud noise from the centre of the panel. This was followed by a loss of load, much more gradual than previously experienced, although no buckling was occurring. It was initially suspected that one or more connectors had failed. Investigating the underside of the panel it became obvious that the reason was due to tensile failure of the steel plate. Further investigations showed that the crack had initiated at the shear connector in the middle of the panel, propagating outwards and almost reaching the edge of the panel.

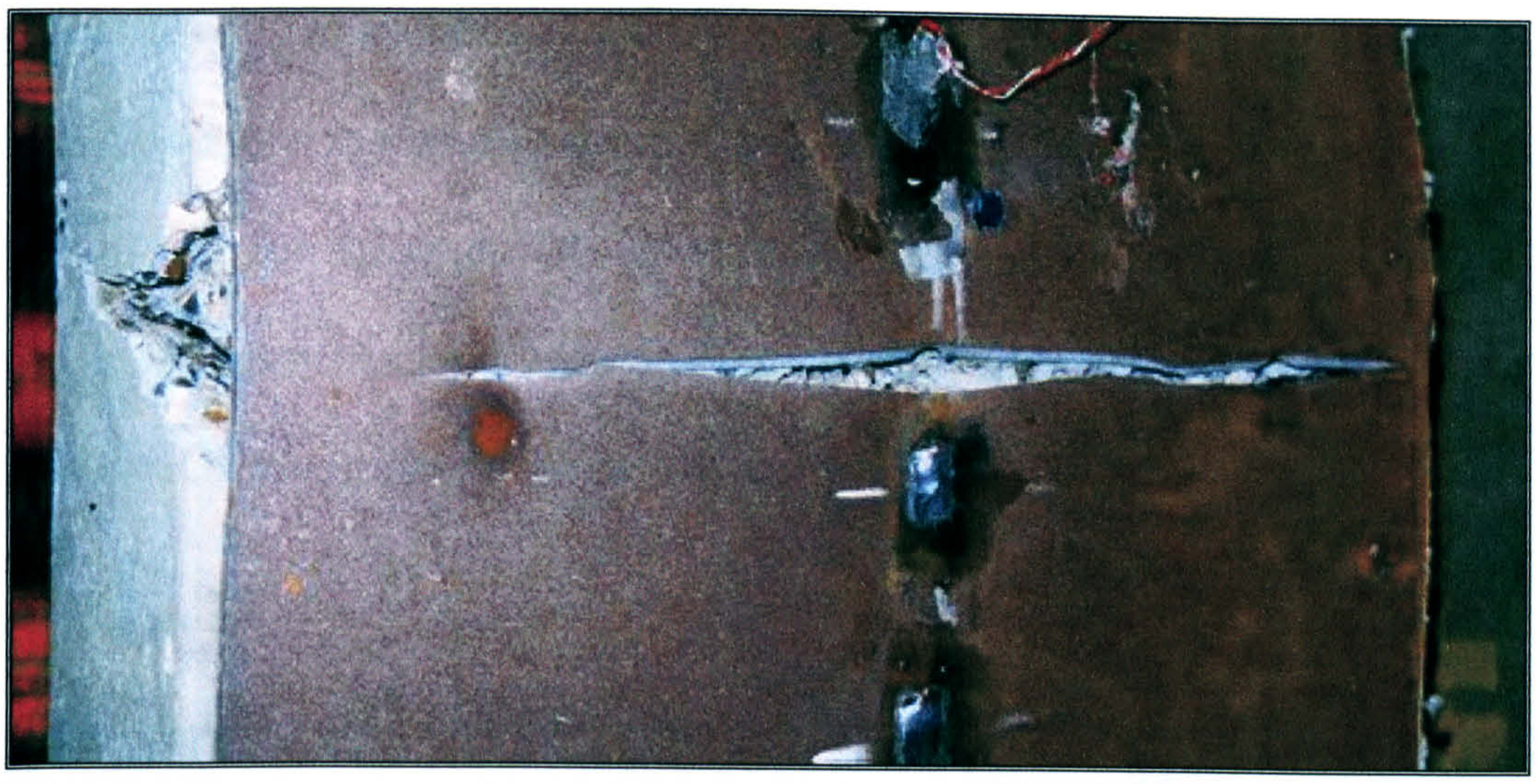

Plate 3.14. City6 tension plate failure.

Specimens were cut from an unstressed region of the tensile steel plate for Charpy tests. The results of these tests indicated that the steel used in City6 required only 60 % of the energy to break as that used in City5. As strains reach considerable size during these tests, particularly at mid-span in the tension plate, they exceeded that capable of being sustained by the steel plate used in the testing of City6.

3.6.4.8 City6b

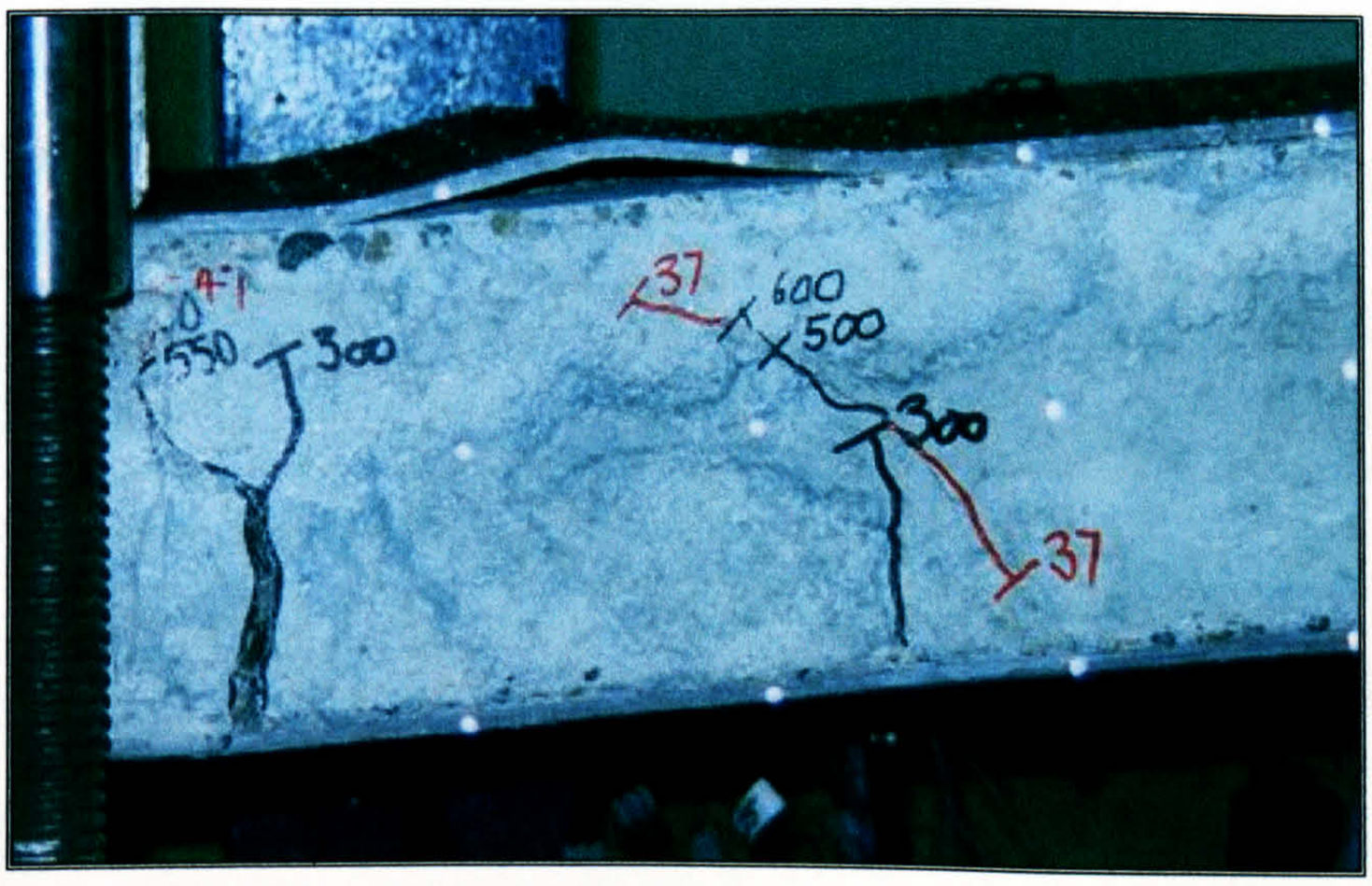

Plate 3.15. City6b crack patterns.

This exhibited typical characteristics throughout the whole of the test with cracks growing in the usual manner. The initial post yield region is extremely flat (Figure D.8 in Appendix D) with considerable increase in strength after this point. Buckling of the compression plate caused failure of the panel at a deflection slightly greater than expected.

3.6.4.9 City7

Plate 3.16. City7 crack patterns.

This was the only test where cracks appeared between adjacent connectors although the usual crack patterns were also seen. At around 300 kN the concrete to steel interface cracked.

Failure was by local buckling of the compression plate where there was a rapid loss of load.

3.6.4.10 City8

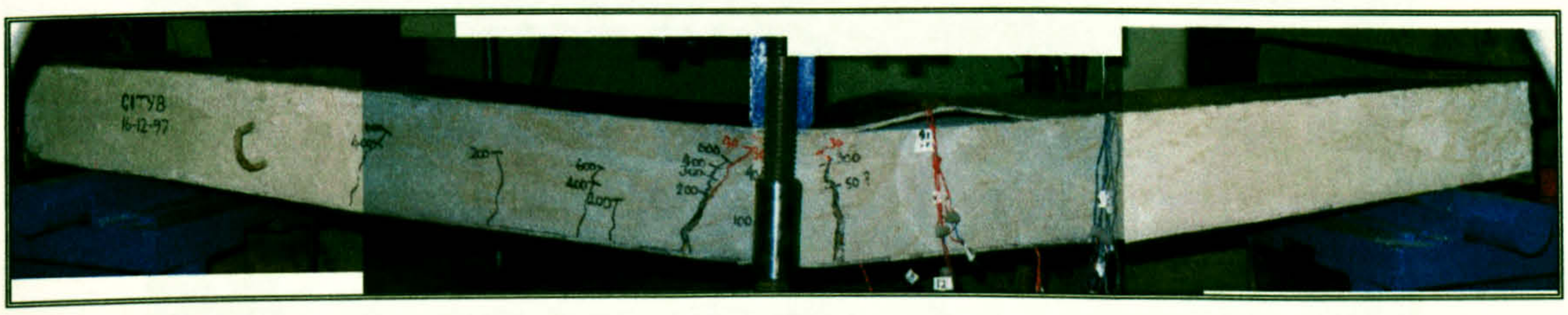

Plate 3.17. City8 crack patterns.

Throughout the whole of the test there was no cracking on the instrumented half (End A) of the panel, except at the first row of connectors where considerable rotation takes place (Plate 3.17).

Failure occurred quite suddenly as the compression plate buckled between the first and second rows of connectors from mid span.

3.6.4.11 City9

Plate 3.18. City9 crack patterns.

Throughout the whole of the test there was no cracking on the instrumented half (End A – RHS of Plate 3.18) of the panel, except as previously described in the City8 test.

Failure occurred quite suddenly as the compression plate buckled the first and second rows of connectors from mid span.

3.6.4.12 City10

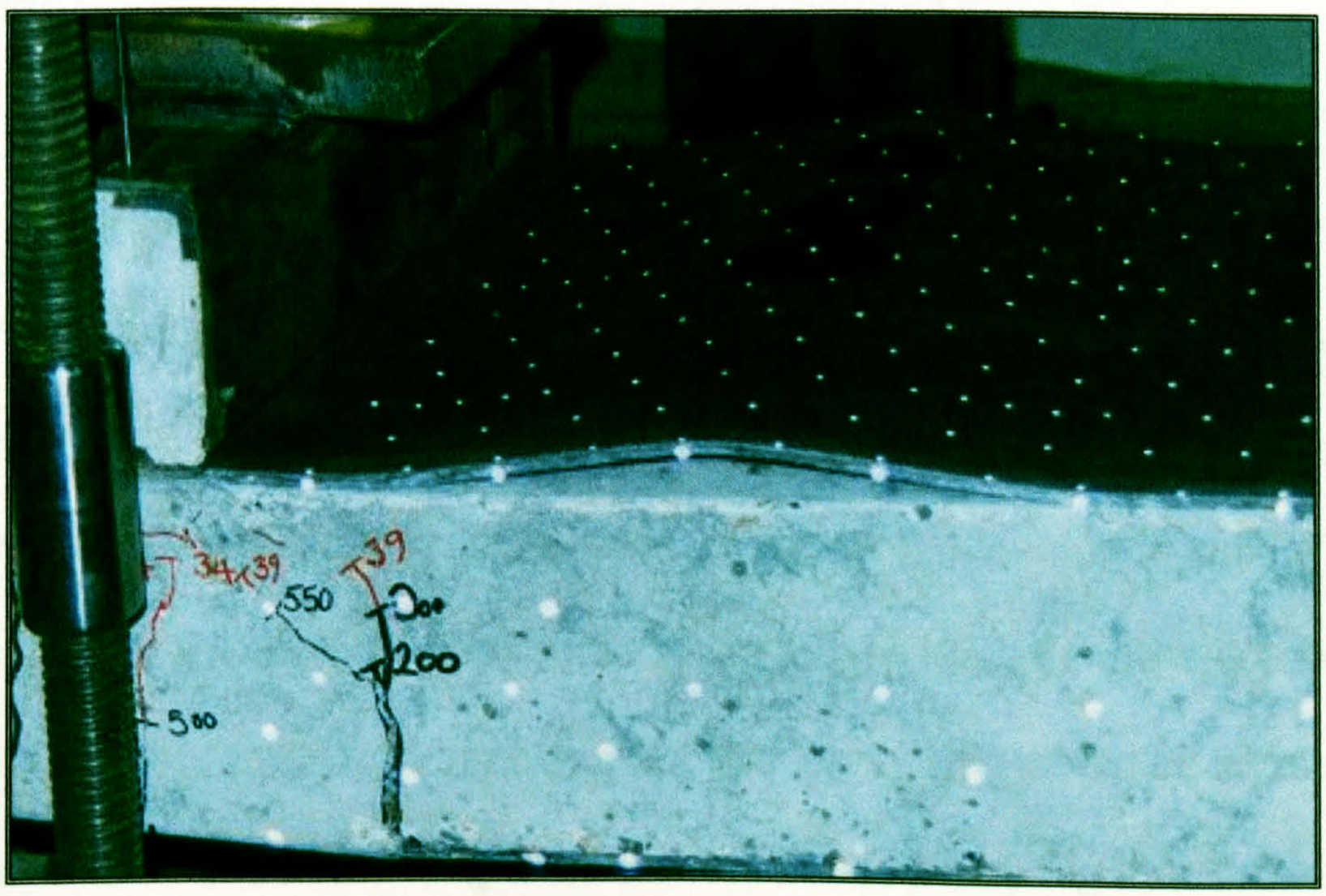

Plate 3.19. City10 crack patterns and VMS reflective targets.

The final test in Series 2 progressed with no problem. Whilst waiting for the final deflection increment to settle there was a sudden failure by buckling of the compression plate. Plate 3.19 shows that, like City9, there is no cracking of the concrete other than adjacent to mid-span.

3.6.5 Summary of Series 2 Testing

From the tests of City8, City9 and City10 it was observed that no cracking has appeared on the panel. Hence for bar spacing to plate thickness (s/t) ratios greater than 40 no cracking appears to form. This is of great importance for serviceability limits that define structural performance for a long service life.

By comparing the results from City4a, City4b and City4c (Figure 3.13) it is immediately noticeable that the strength of the concrete effects the point at which failure by local buckling occurs, since this was the only variable in these tests. The deflection at failure is increased as the strength of the concrete is increased.

The neutral axis remains stable (Figures D.1 – D.11 in Appendix D) during the elastic load region which supports the under-reinforced concrete analogy. The same result was observed in the Series 1 tests.

The shear force acting along the interface can be calculated from the difference in average tension plate strain at two longitudinal locations. Figures D.37 – D.48 in Appendix D show that, during elastic loading, there is a linear increase in shear force for increasing applied load. This would be expected from the linear variation in longitudinal strain indicated by Figures C.5 – C.8 in Appendix C. They also show that as yield of the test panel is reached there is a considerable increase in the shear force at the tension interface. This would

be critical if the degree of connection was insufficient, as it would lead to shear failure of the connector, which is a sudden and explosive event indicated by City3.

Although the failure of City3 occurred suddenly, and was the only specimen to fail in such a manner, it was also the only one to use 12mm steel plate. Failure occurred when the shear connectors failed at the interface with the tension steel plate. This is the same result as achieved by Moy (1998a and 1998b). Figures D.25 – D36 in Appendix D show the tensile stress in the bar located in the third row from mid-span along the centreline of the panel. These generally vary approximately linearly with linear elastic applied load. A comparison between tests using the same structural arrangement but different plate thickness (Figures D.25, D.26 and D.30) indicate that for increasing plate thickness there is a decrease in the tensile bar stress.

The above point contradicts a theory that Bi-Steel behaves as a truss because for the same structural arrangement, the same distribution of forces would be expected. This would lead to lower plate stresses in the panels with thicker steel plates, but with the same stresses in the shear connectors, since their area remains constant throughout all of the tests.

Figures D.26, D.27 and D.29 show similar relations between applied load and bar stress for City4a, 4b and 4d where the only structural difference is the concrete strength. There is, therefore, no effect on the bar stress due to the change in concrete strength.

3.7 Test Conclusions

Two series of tests have been carried out which show that most of the component stresses or strains vary linearly in the elastic range of applied load. Series 1 proved that Bi-Steel out-performs traditional methods of double skin composite construction in terms of rotation capacity and ease of construction. It also showed that there was no effect from providing end plates even though the amount of shear connection (11.1%), without the end plates is below the 20% which is suggested by Roberts (1996) as being required to resist slip. There was, therefore, no significant slip at the ends of these test specimens. The second test series set out to assess the effects caused by the geometry of the specimens. They demonstrated that the point at which the plate buckles is affected by the bar spacing to plate thickness ratio; Figure 3.16. This figure is a plot of the specimen rotation against s/t.

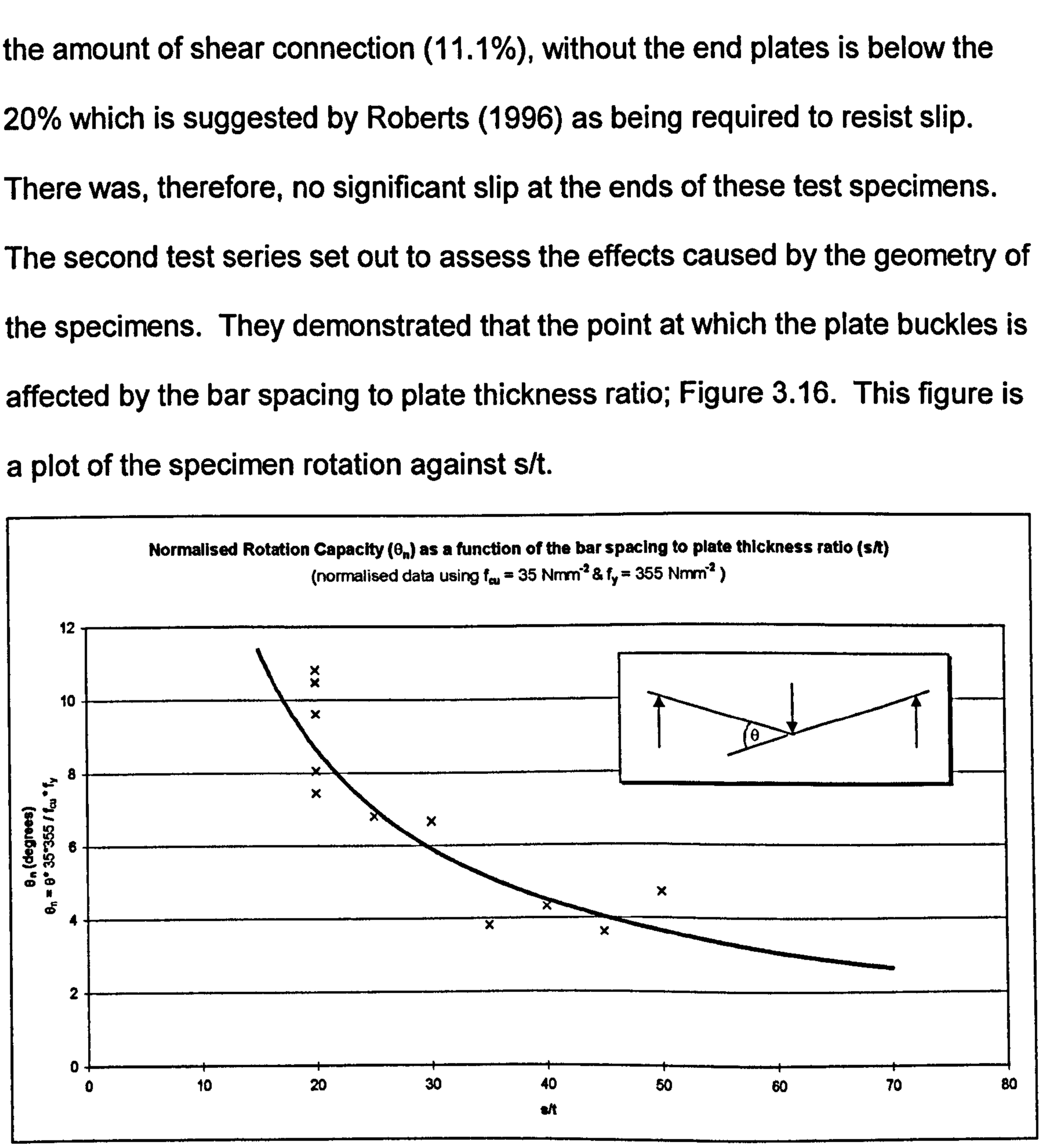

Figure 3.16. Rotation of Bi-Steel panels at buckling.

Comparison of the load deflection curves in Figure 3.13, for the tests of City4a, City4b and City4c show that the concrete strength appears to affect the buckling of the compression plate. As the concrete strength increases, the ultimate failure load and deflection of the panels increases. However, this may be due to the concrete being able to carry a greater portion of the load and hence reduce the steel plate stresses. This would allow further load to be applied before the buckling stresses are reached within the steel hence, apparently increasing the capacity of the panel.

Chapter 4 Comparison of Experimental Data and Analytical Solutions

4.1 Introduction

The test data obtained from the experimental programme has been presented in Chapter 3. An interpretation of these data will enable a comparison to be made between theory and experiment and an explanation of the structural performance of Bi-Steel to be made. This chapter will present these findings and make comparisons with the analytical solutions developed in Chapter 2. The three areas of study that are presented are:

1. A comparison of the types of DSC using overlapping studs and Bi-Steel,
2. Development of overall load deflection characteristics including:
    - Moment of resistance
    - Elastic deflections
    - Post yield deformation
    - Local Buckling of the compression plate and,
3. A consideration of the internal forces including:
    - Longitudinal plate stresses
    - Transverse plate stresses

For the purpose of presentation, example calculations and comparisons will be given for one of the test panels, City1. The parameters are given in Table 4.1.

Description	Symbol	Units	Dimension
Span	L	mm	3400
Width	b	mm	1000
Plate thickness	t	mm	10
Steel yield strength	f_y	Nmm^{-2}	452
Bi-Steel bar spacing-longitudinal	s_1	mm	200
Bi-Steel bar spacing – transverse	s_2	mm	200
Bi-Steel bar diameter	D	mm	25
Bi-Steel bar yield strength	$f_{y(bar)}$	Nmm^{-2}	450
Shear stud spacing-longitudinal	s_1	mm	159
Shear stud spacing – transverse	s_2	mm	133
Shear stud diameter	D	mm	19
Shear stud yield strength	$f_{y(stud)}$	Nmm^{-2}	450
Concrete Depth	h_c	mm	200
Concrete cube strength	f_{cu}	Nmm^{-2}	55

Table 4.1. Parametric information for test panel City1

4.2 Comparison of Studded DSC and Bi-Steel

The first test series consisted of four specimens that would compare the performance of the existing, studded method of constructing DSC elements with that of the new form, Bi-Steel. Two panels of each type were constructed with one of each having welded end plates to simulate continuity. All of the panels used the same batches of steel and concrete, although time between actual tests allowed the concrete to gain in strength.

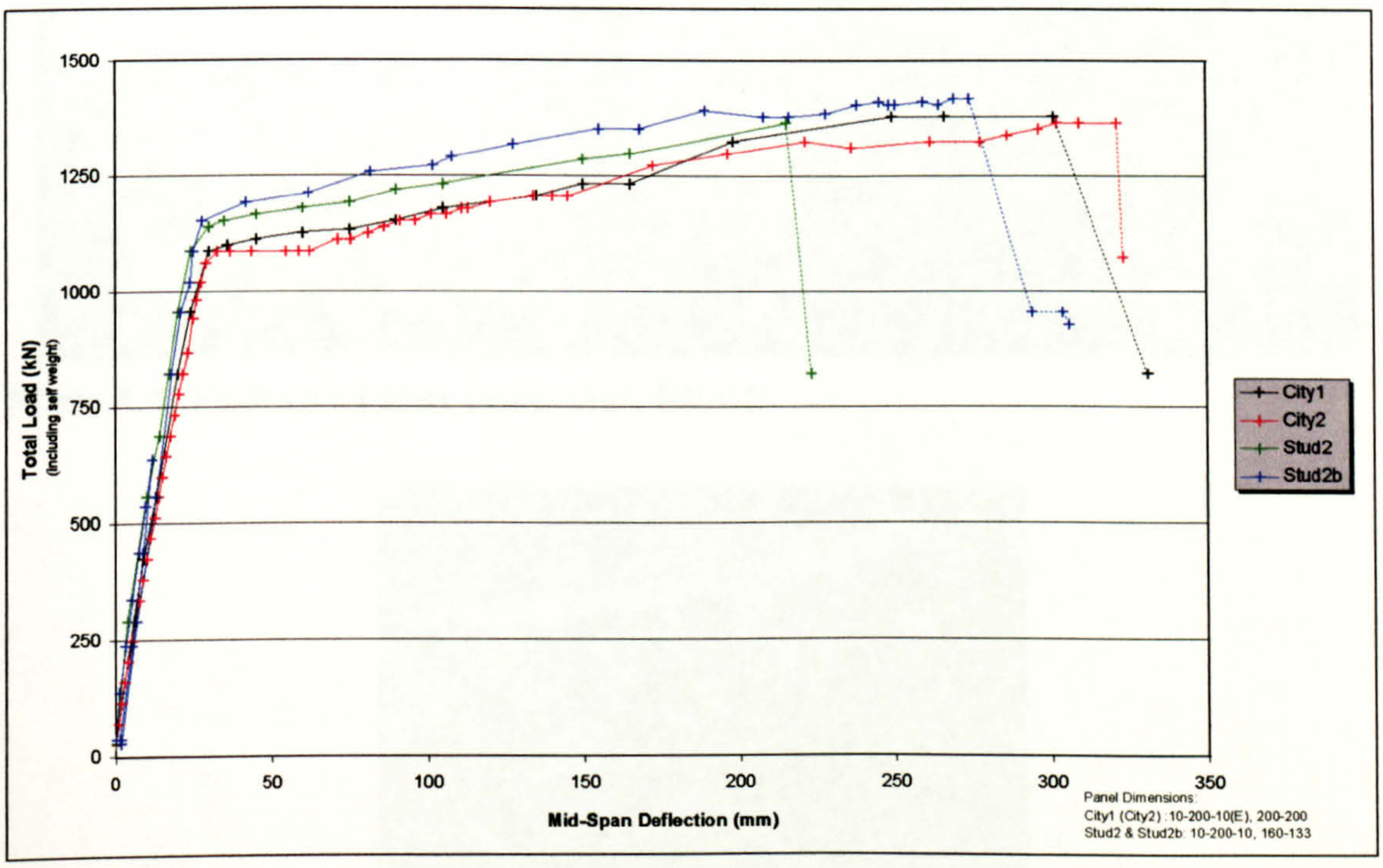

Figure 4.1. Load deflection curves for Series1 test specimens.

Figure 4.1 shows the load deflection curves for all of the tests carried out during Series1. It is immediately apparent that all the specimens have near identical performance for a large portion of their deformation. The slight increase in load capacity of Stud2 and Stud2b is due to the panel being slightly deeper than City1 and City2. A lack of sufficient formwork allowed the opposite faces to move apart when the concrete was placed. The effect of this is to increase the lever arm between the plates giving a greater moment capacity.

Figure 4.1 also shows that the studded panels failed before the Bi-Steel specimens. Stud2 failed when a column of shear studs, which were attached to the compression plate, pulled out of the concrete causing the compression plate to separate from the concrete (Plate 4.1).

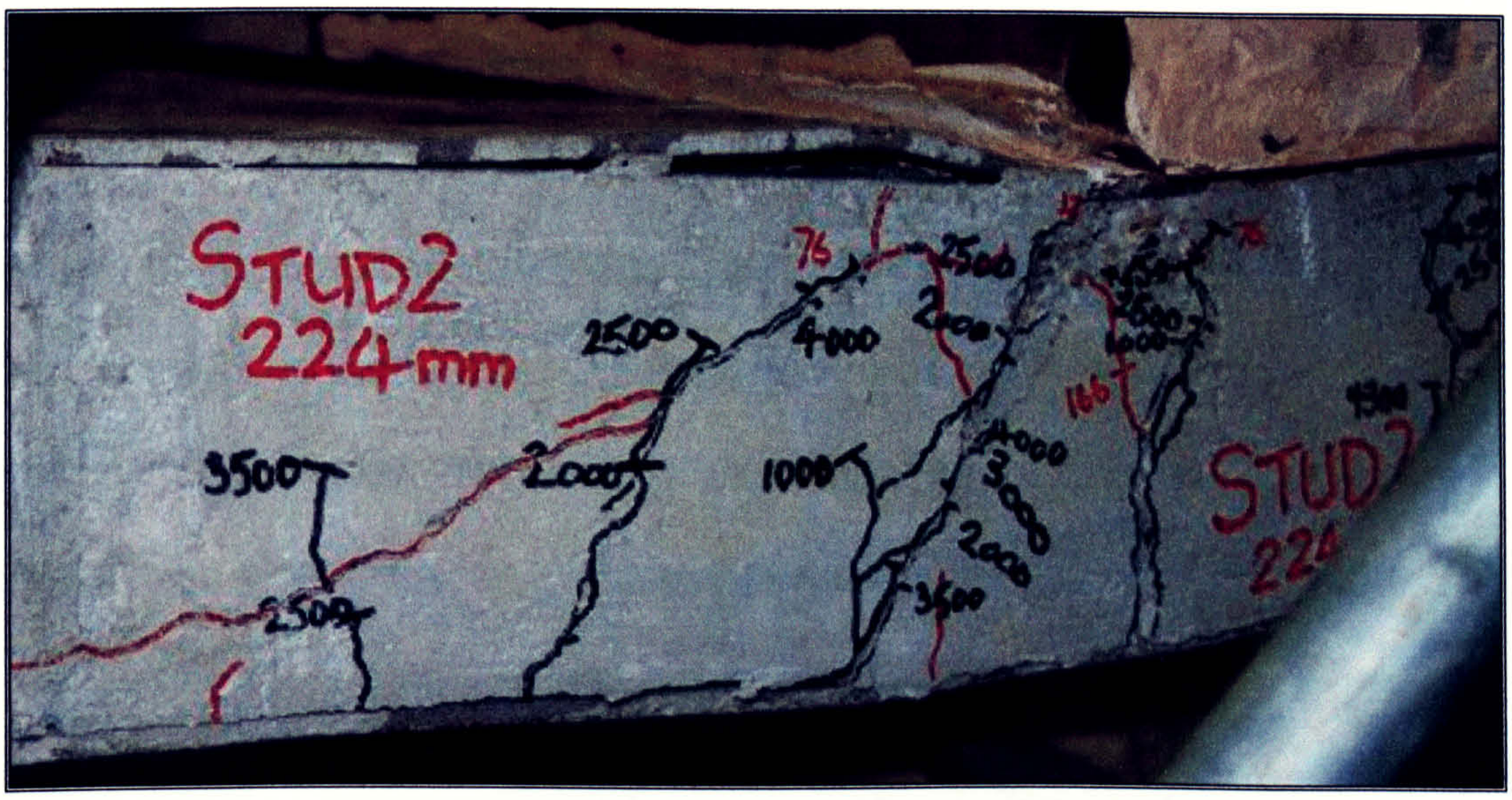

Plate 4.1. Failure of test specimen Stud2

Plate 4.2. Stud pullout of Stud2b

Plate 4.2 shows a near identical failure of Stud2b after the concrete has been removed from the surface to reveal the shear connectors.

The pullout strength of the headed stud is a function of the concrete strength [Narayanan (1997)]. Therefore, the deformation of Stud2b before failure was greater than that of Stud2 (Figure 4.1) since there was an increase in the concrete strength from 53 to 58Nmm^{-2}.

The two Bi-Steel panels, City1 and City2, failed in a different manner as the shear connectors are welded to the plates at both ends, making their 'pullout' strength much greater. These two panels failed by local buckling of the compression plate between two adjacent rows of shear connectors (Plate 4.3).

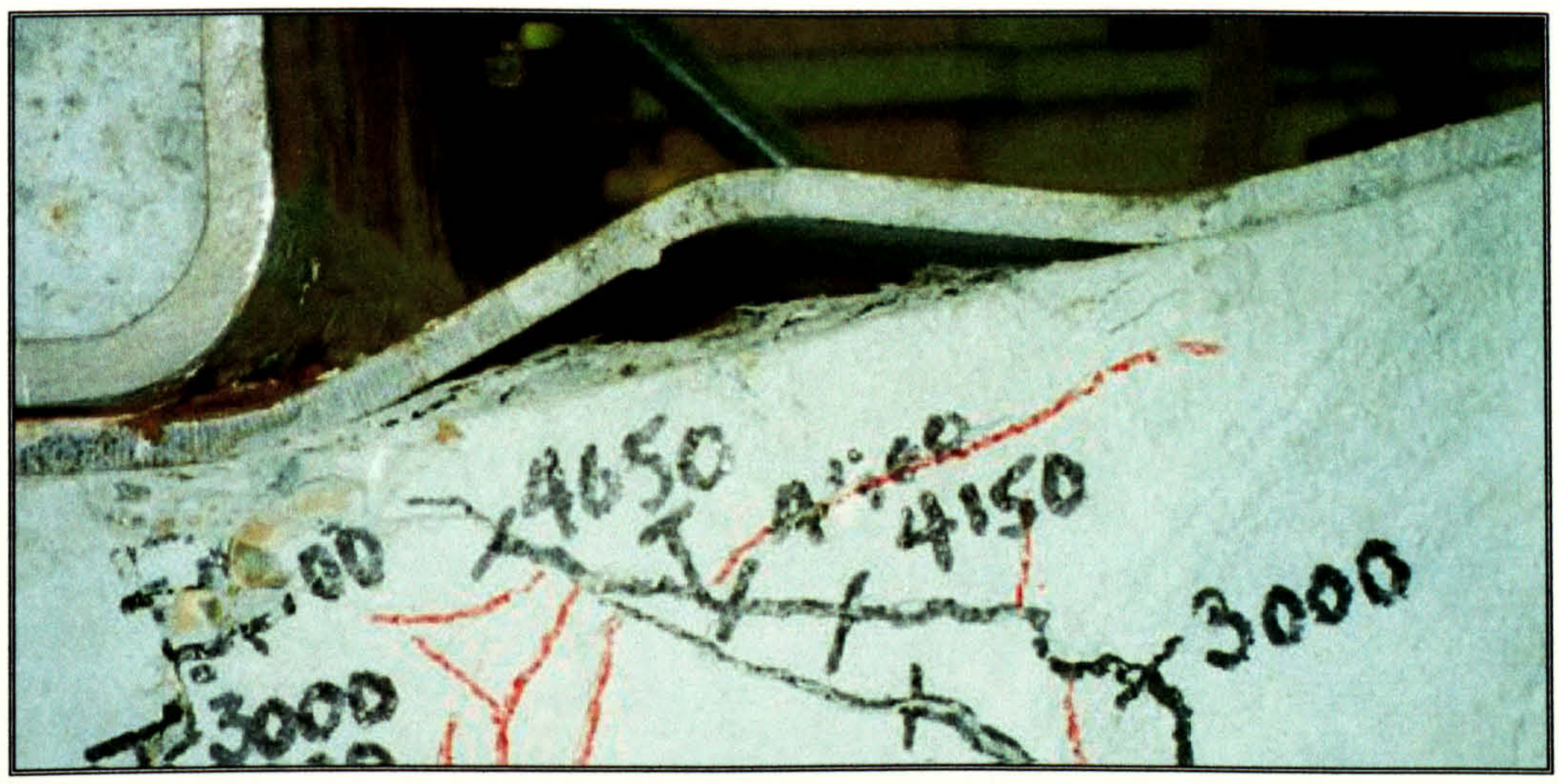

Plate 4.3. Buckling of Compression plate of City1

The load spreader beam in the upper left corner of Plate 4.3 is at a 50mm distance from the row of connectors and has not restricted the formation of the buckle.

The local buckling shown in Plate 4.3 can be achieved in specimens using headed studs provided that the concrete has sufficient strength to resist the pull out forces.

The purpose of using end plates in these specimens was to simulate the effects of structural confinement. By comparing the results of City1 and City2 in Figure 4.1 it can be seen that there has been no apparent loss of stiffness of City2 which did not have the end plates. At yield of City2 the end slips were measured at 0.00mm and 0.18mm at tension and compression plate interfaces, respectively. The small amount of slip recorded at the end of City2 (no end plates) can be considered as having no effect as there was no difference in the performance of the test specimens City1 and City2.

4.3 Development of load deflection characteristics.

Some of the most basic and useful information regarding the behaviour of beams is determined from a load deflection curve, particularly in the elastic region where structural elements are designed to behave in normal use. The key aspects, which may be determined from this curve, are:

1. Moment of resistance and,
2. Elastic deflections due to composite and shear action.

Although not used in normal design, the post yield characteristics are important if consideration needs to be given to accidental loads e.g. offshore collisions. Aspects included here are:

3. Post yield deformation
4. Local Buckling of the compression plate

Local buckling will also need to be considered in elastic design as the connector spacing to plate thickness ratio (s/t) affects the limit at which buckling occurs. This could easily be within the elastic region if s/t is great enough.

4.3.1 Moment of Resistance

From Chapter 2, Equations 2.15 and 2.17 gives the elastic and yielded moments of resistance of a DSC panel, respectively, as:

$$M = f_y b t_1 \left(\frac{z}{3} + \frac{t_1}{2}\right) \frac{z + {}^{t_1}\!/_{2}}{h_c - z + {}^{t_2}\!/_{2}} + f_y b t_2 \left(h_c - \frac{z}{3} + \frac{t_2}{2}\right)$$ **Equation 2.15**

$$M_u = f_y b t (h_c + t)$$ **Equation 2.17**

A comparison of the results of M_u for various plates of different thickness at concrete depths of 200mm with the results from the laboratory tests is given in Figure 4.2.

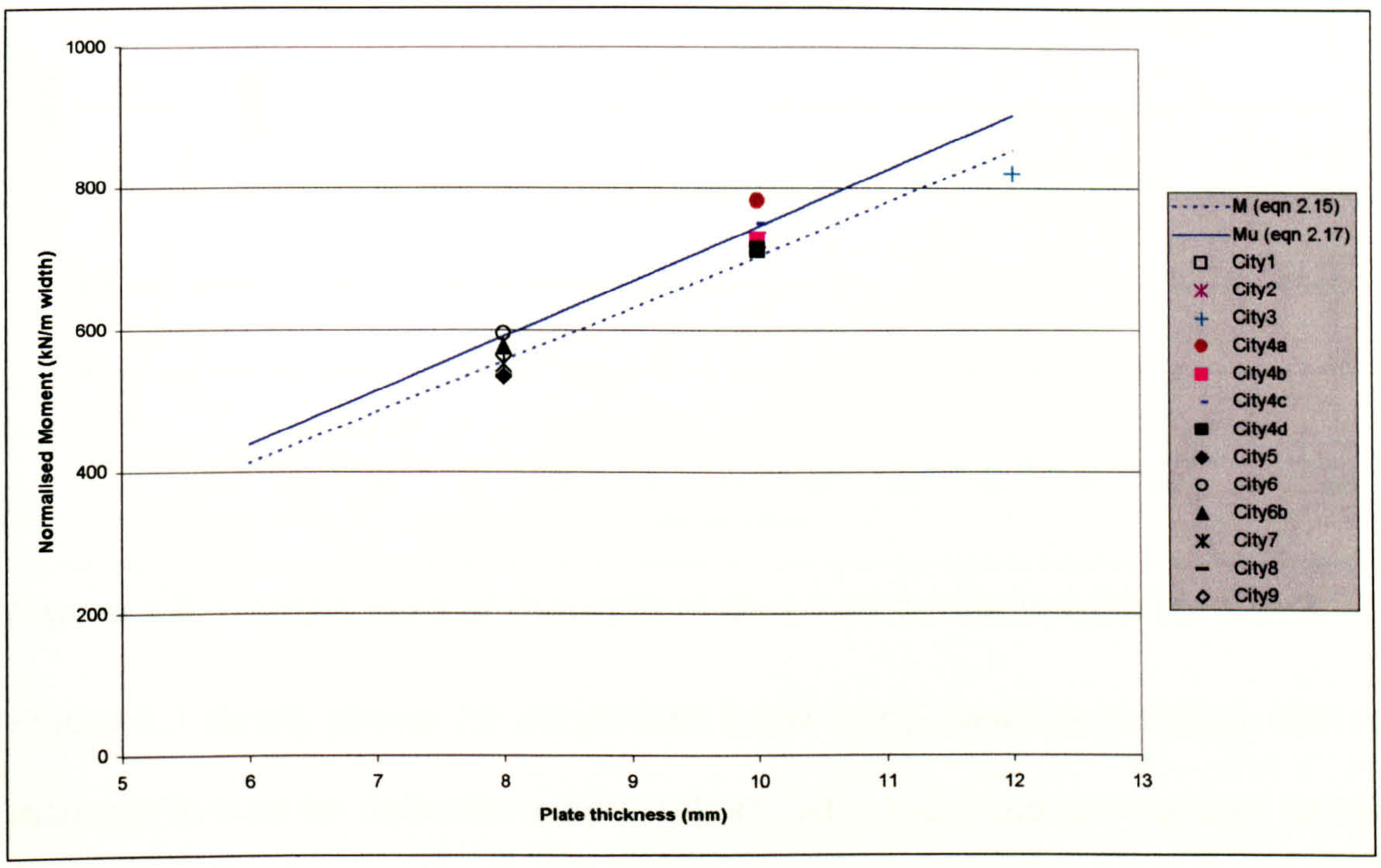

Figure 4.2. Calculated and Measured Moment per Unit Width.

Comparing the results shown in Figure 4.2 gives a standard deviation for the calculated data of 4.25% below the measured data. Since the measured data is a best estimate taken from the load-deflection curves then this result is considered satisfactory. A 4.25% error reading the load deflection curve for City1 would be represented by 44kN (1116kN at yield).

Equation 2.17 gives the same numerical value for Moment of Resistance as Equation 2.15, although it represents a different point on the load deflection curve. From all of the results obtained, the theoretical performance of a DSC panel is given by City2, Figure 4.3.

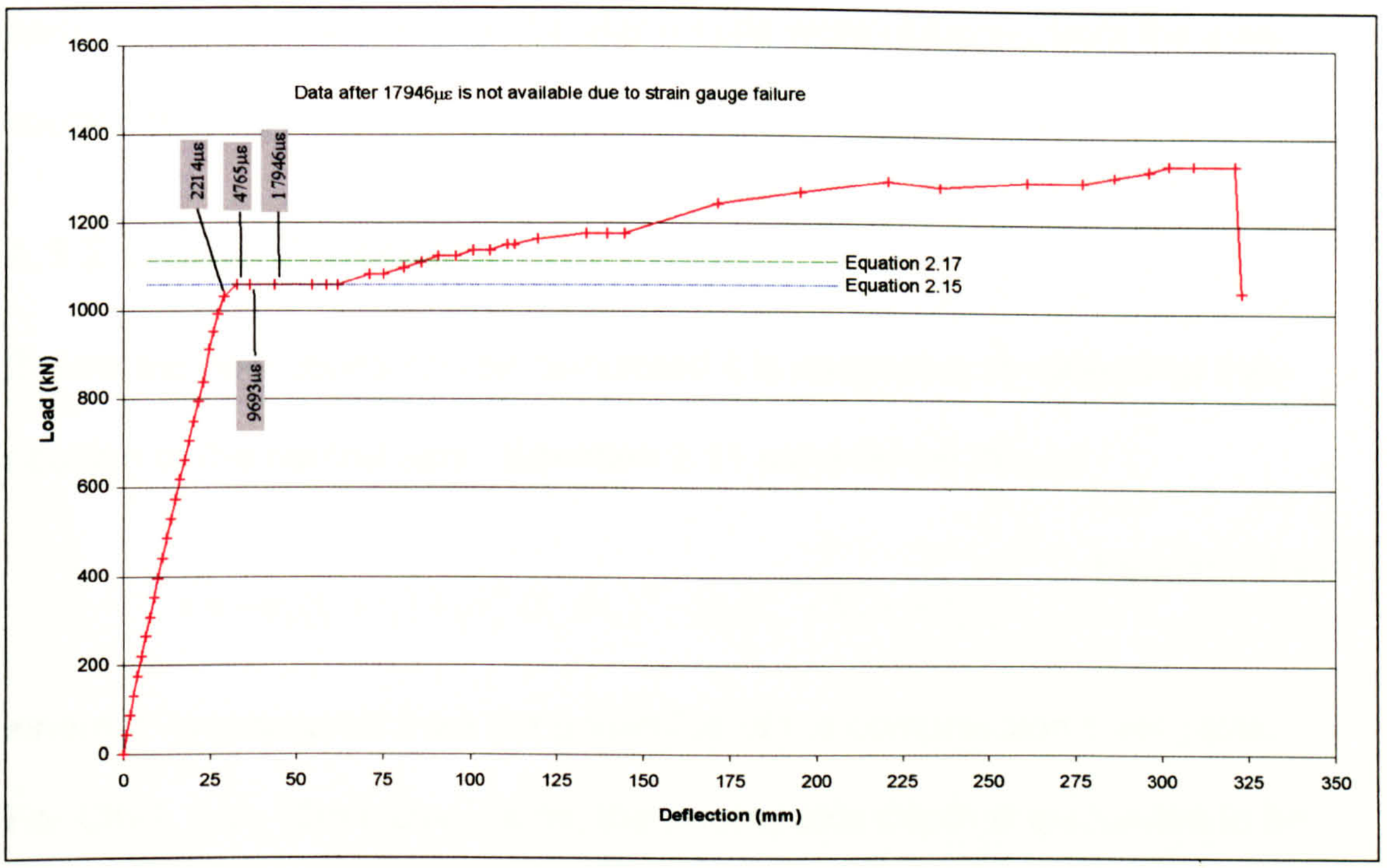

Figure 4.3. Comparison of theoretical data and actual results for City2.

Figure 4.3 clearly shows the elastic limit followed by plastic deformation with no increase in load for deflections up to 60mm. Also indicated are the load levels representing Equations 2.15 and 2.17 and some strain gauge measurements taken at various stages during the test.

The strain measurements indicated in Figure 4.3 show that the tension steel plate does not reach yield until linearity of the load deflection curve ends. The transition from first yield, represented by Equation 2.15, to the commencement of strain hardening, Equation 2.17, is indicated by the plateau in the load deflection curve from 32 to 62mm. During this period, the neutral axis moves upwards through the depth of the concrete, which is confirmed by Figures D16 – D24 in Appendix D.

Some of the load deflection curves do not possess the plateau as found in the results of City2. This is due to residual stresses in the steel plates that had not

been removed by annealing. Similar results were obtained from the steel coupon testing.

4.3.2 Elastic Deflections

Before the deflections can be calculated it is necessary to determine the position of the neutral axis. Equation 2.11 established this as:

$$z = -\alpha_e(t_1 + t_2) + [\alpha_e^2.(t_1 + t_2)^2 - \alpha_e(t_1^2 - 2t_2h_c + t_2^2)]^{\frac{1}{2}}$$ **Equation 2.11**

where 'z' is measured from the underside of the compression steel plate.

For City1, with 10mm steel skins, the neutral axis depth is calculated to be 74.6mm from the underside of the steel plate.

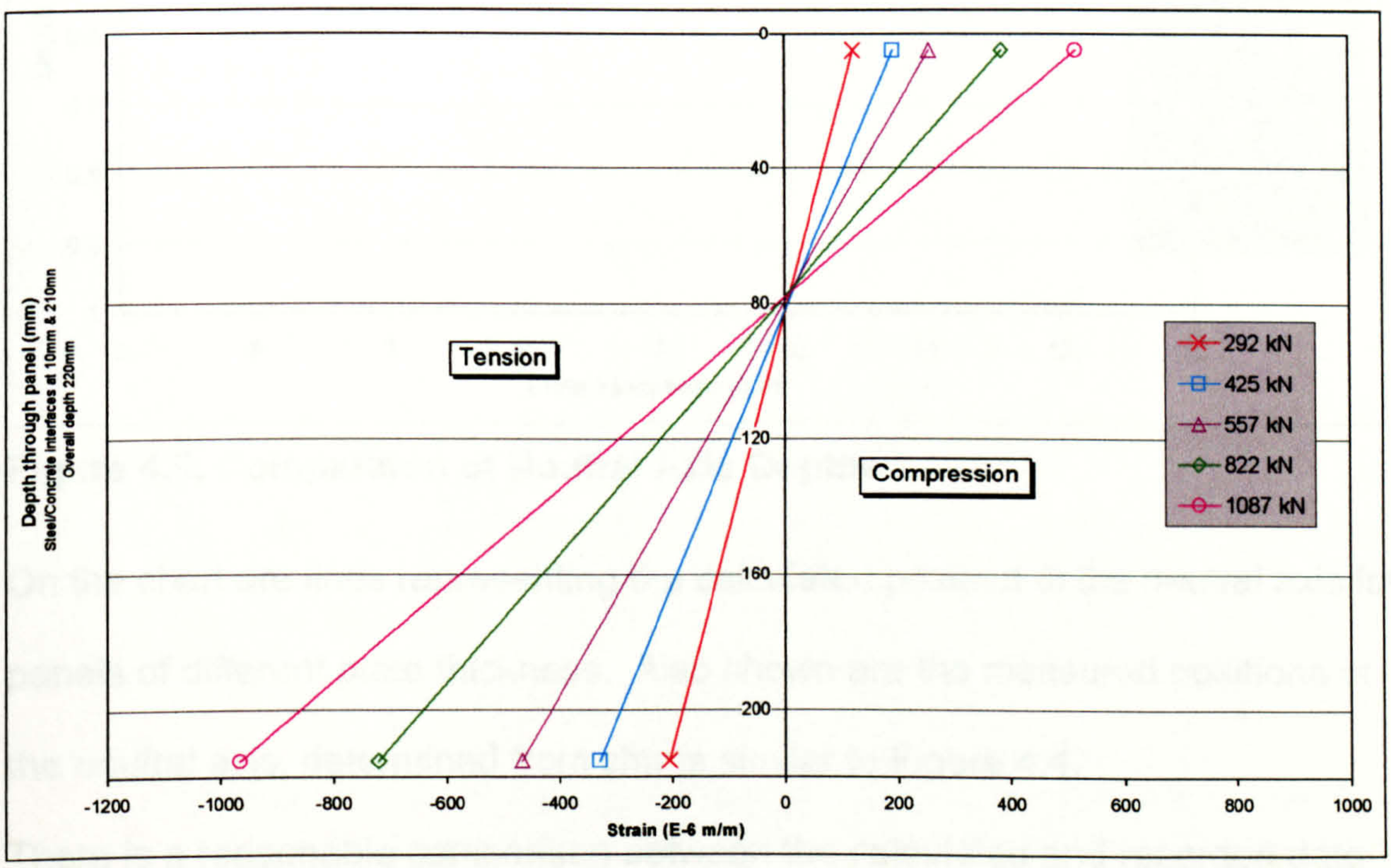

Figure 4.4. Section of strains for City1

Figure 4.4 shows the average steel strains in the top and bottom plates of City1 and an assumed linear distribution between. The point of zero strain indicates the position of the neutral axis at that load level. As all the data in Figure 4.4 was recorded during the elastic region of deformation it shows the location of

the neutral axis to be fairly stable. During the early stages of the test (252kN applied load) the position is approximately 84mm below the upper surface of the panel. The parameter 'z' is therefore approximately 74mm, which is very close to the calculated value. A comparison of the neutral axis depth factor (z/h_c) for all the tests is given in Figure 4.5, together with two theoretical curves representing different modular ratios.

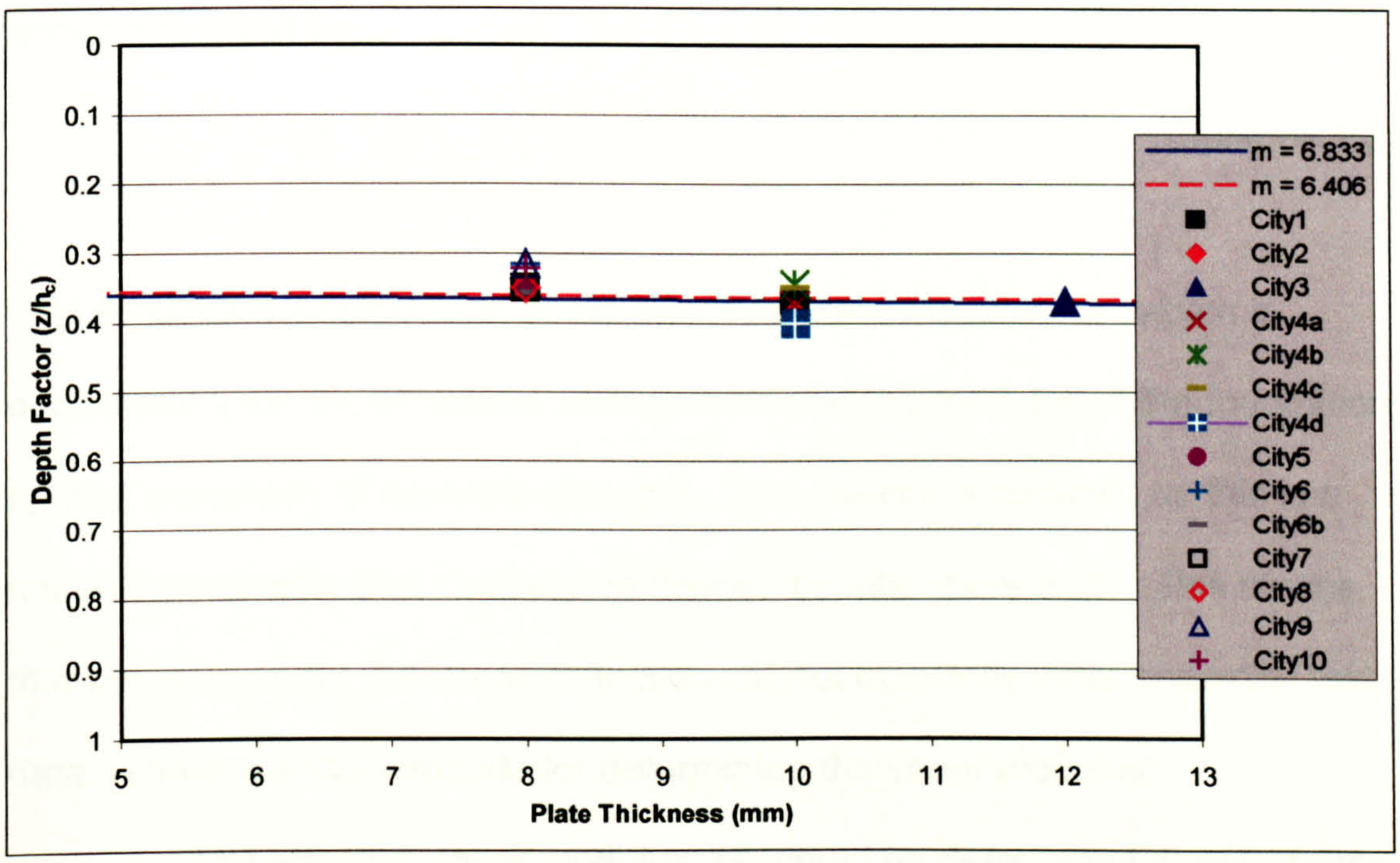

Figure 4.5. Comparison of Neutral Axis Depths

On the chart are lines representing the calculated position of the neutral axis for panels of different plate thickness. Also shown are the measured positions of the neutral axis, determined from charts similar to Figure 4.4.

There is a reasonable comparison between the calculated and recorded data although with a variation of z/h_c by ± 0.05, or ± 5 percent of the concrete depth.

It can also be seen that the variation of the steel plate thickness has little effect on the position of the neutral axis.

The development of the full composite theory presented in Chapter 2 gives the deflection of a DSC beam as:

$$\Delta_1 = -\frac{PL^3}{48K}$$ **Equation 2.29**

where $K = E_s\left[\left(z+\frac{t_1}{2}\right)A_1y_1+\left(h_c-z+\frac{t_2}{2}\right)A_2y_2\right]$

For City1, therefore, the full composite deflection, $\Delta_{1(City1)}$ =17.2mm.

From Chapter 2 the shear deflection for a simply supported beam in three point bending is given by,

$$\Delta_2 = \frac{PL}{4AG'}$$ **Equation 2.32**

This requires the calculation of the effective shear modulus, G', which is dependant upon the structural arrangement and the modulus of the foundation, *k*, itself a property of concrete strength. This creates a problem, as this is a material parameter that can only be defined by laboratory tests. This means that the solution for the shear deflection cannot be wholly independent of test data. There are two methods for determining the shear modulus:

1. The effective shear modulus, G', could be determined directly from the laboratory testing of the DSC test panels. The shear deflection can be deduced by subtracting the composite deflection from the test total defection. This can then be equated to Equation 2.32 and, hence, G' found. This could then be used to determine *k* for use in other calculations.
2. The foundation modulus could be measured directly in an appropriate test. However, this would require a separate series of tests and may not give a true indication of the effective shear

modulus due to differences between the test and what actually occurs within a Bi-Steel panel.

It was decided to use Method 1 to determine the effective shear stiffness of the panels. Although it means the calculations are linked to the tests, it gives a result that can be used with more confidence.

Using the results from City1:

Total deflection, Δ_T, at yield of City1 = 30mm and full composite deflection is 17.2mm which has been previously calculated. Therefore:

$$\Delta_2 = \Delta_T - \Delta_1$$
$$\Delta_2 = 30 - 17.2$$
$$\Delta_2 = 12.6mm$$

By re-arranging Equation 2.32, the effective shear stiffness for City1 is:

$$G' = \frac{PL}{4A\Delta_2}$$
$$G'_{City1} = \frac{1116x10^{-3}x3400x200}{4x1000x210^2x12.6}$$
$$G'_{City1} = 341.5Nmm^{-2}$$

This value will also be the same for any panel where there is a 200 x 200mm spacing of the shear connectors. Hence substituting this into Equation 2.32 for each of the specimens with a 200 x 200mm spacing will give the shear deflections (Table 4.2).

Deflections					
	Measured	Calculated			Error
Panel	Δ_T	Δ_1	Δ_2	Δ_T	%
City1	30	17.1	12.3	29.4	-2.0
City2	30	17.1	12.3	29.4	-2.0
City3	20.5	9.6	13.0	22.6	10.2
City4a	20	8.5	11.1	19.6	-1.8
City4b	21	11	11.7	22.7	8.2
City4c	20	11.3	12.1	23.4	16.9
City4d	19	10.3	11.1	21.4	12.9
City5	19	11.2	8.8	20.0	5.3

Table 4.2. Comparison of Deflections

Table 4.2 shows that there is quite some variation in the results, between –2.0 and +16.9%. The standard deviation of the percentage errors is 7.3%, indicating that the calculated deflections are generally 7.3% too great. Part of the error could be in reading actual values of total deflection from the load deflection curves. Due to the duration of a typical test, continuous data recording would generate too much data, therefore, some interpretation between data points close to yield is required. Due to the changing gradient of the load-deflection curve between two data points, it was not always possible to define a point, which represented the yield point. The best estimates that could be achieved were of the order of ±0.5mm - 1.0mm, which are equivalent to ±2.5% - 5.0% of 20mm total deformation.

4.3.3 Post Yield Deformation

Equation 2.36 determines the post yield moment capacity of a Bi-Steel panel for any strain in the tension steel plate.

$$M_{py} = K\varepsilon_2^n A_2 (h_c + t) \qquad \textbf{Equation 2.36}$$

The relationship between mid-span deflection and strain of a Bi-Steel panel was determined by Figure 2.7 in Chapter 2.

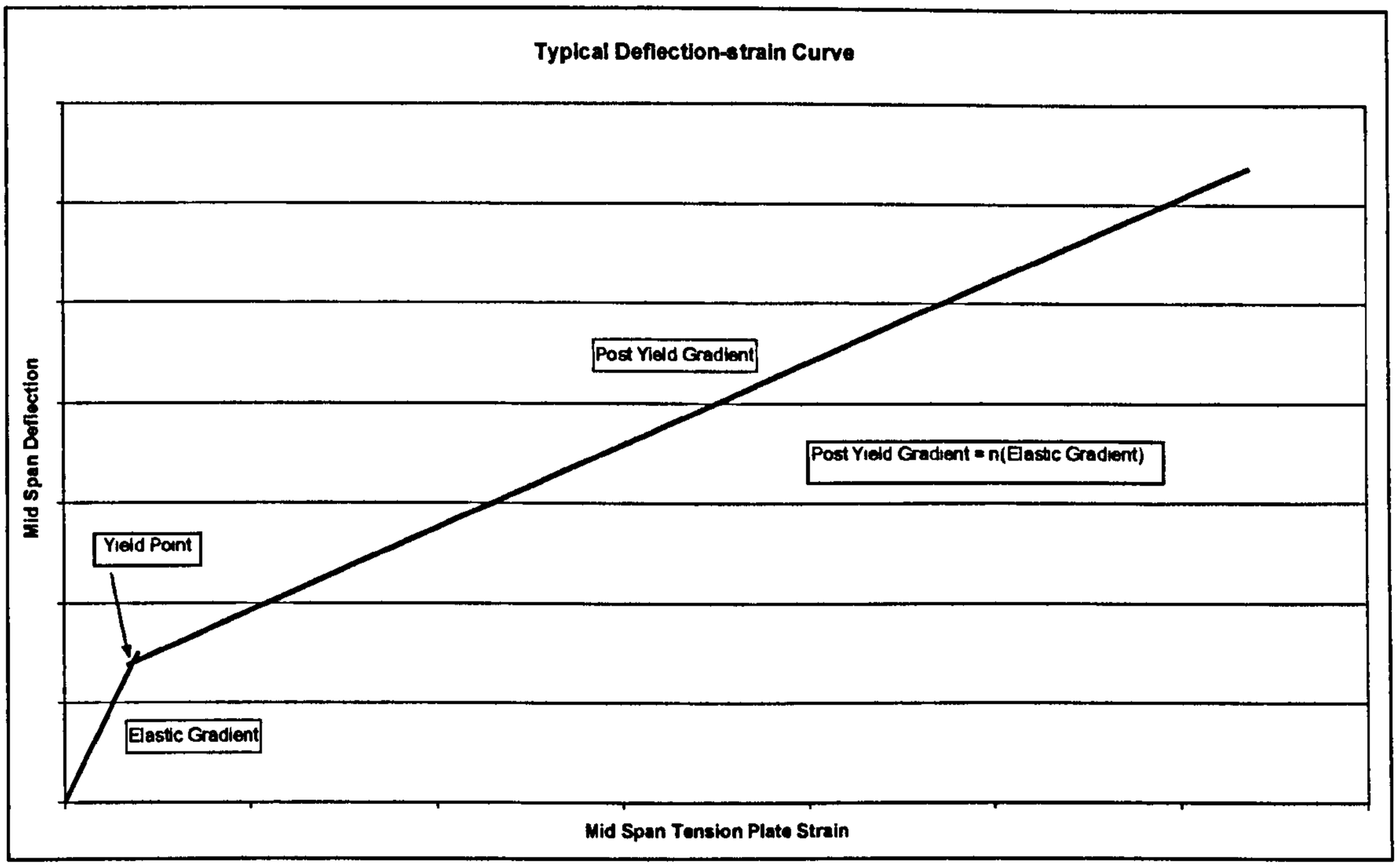

Figure 4.6. Typical Deflection Strain Relationship

By substituting the relevant values for material properties from Table 3.2 for City1 it is possible to determine the load deflection behaviour over a range of strain values (Figure 4.7)

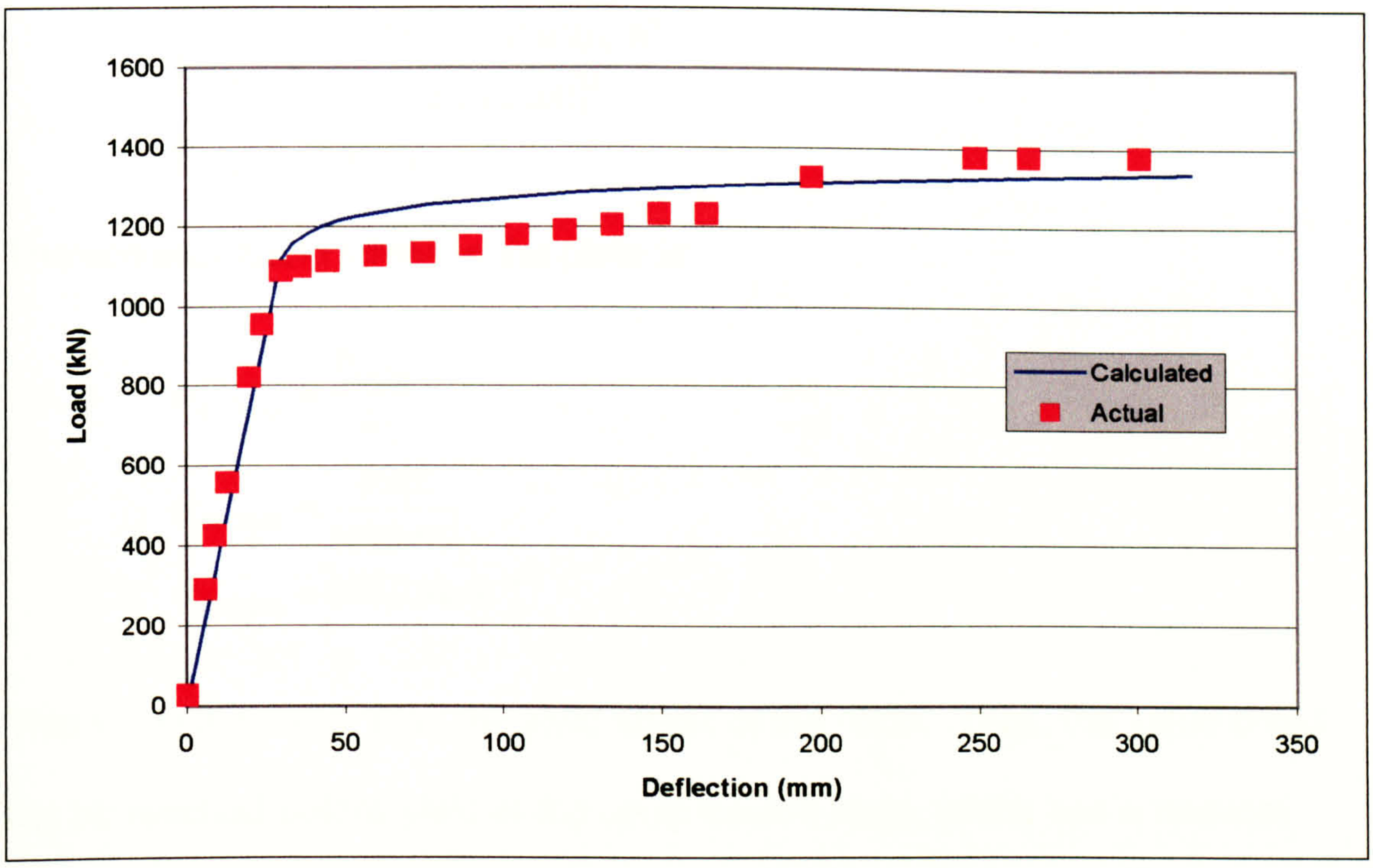

Figure 4.7. Load deflection behaviour for City1.

It can be seen in Figure 4.7 that there is generally good agreement between the calculated and actual values for the load deflection behaviour. In the post yield region there is some discrepancy, which is due to the difference between the actual and assumed plastic behaviour of the steel. However, as the actual behaviour varies and cannot be accurately determined without individual coupon tests, it is not practical to allow for slight variations in different batches of steel.

4.3.4 Local Buckling of Compression Plate

The buckling load for the plate acting between adjacent connectors is given by:

Equation 2.39

$$P_E = \frac{\pi^2 EI}{(0.7L)^2}$$

For City1, this gives a buckling load in the compression plate of:

$$P_{E(City1)} = \frac{\pi^2 x 205000 x 1000 x 10^3}{12x(0.7x200)^2}$$

$$P_{E(City1)} = 8602kN$$

The corresponding stress in the plate is:

$$\sigma_{E(City1)} = \frac{P_{E(City1)}}{bt_1}$$

$$\sigma_{E(City1)} = \frac{8602}{1000x10}$$

$$\sigma_{E(City1)} = 860.2Nmm^{-2}$$

This value is greater than the yield stress of the plate. Thus, the value could not be reached before yield of the compression plate, which has a nominal strength of 355 Nmm^{-2}.

Figure 4.8 shows the theoretical boundary as a stress ratio (i.e. σ_E/f_y) for various ratios of bar spacing to plate thickness, together with the experimental results.

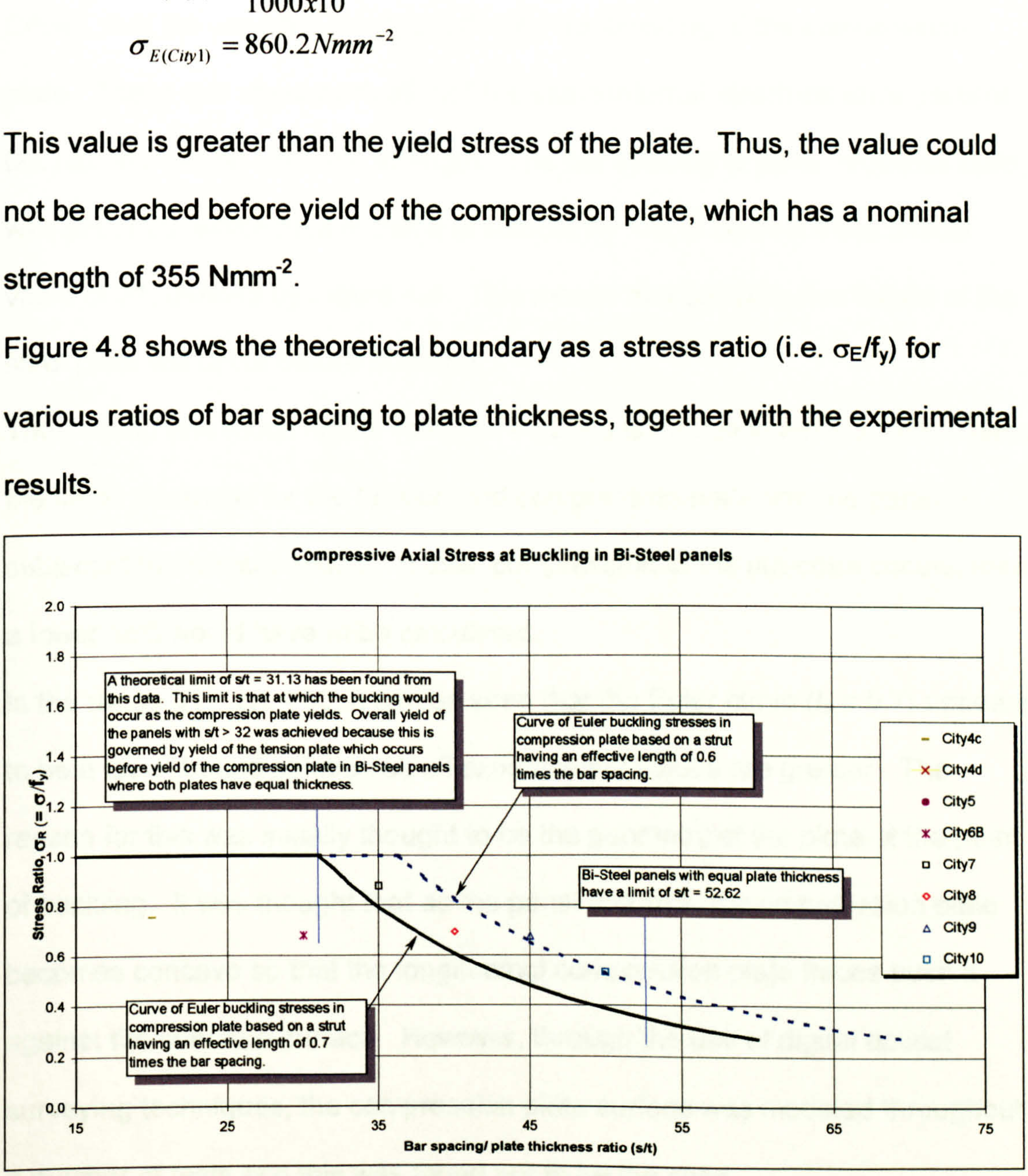

Figure 4.8. Compressive Axial Stress at Buckling in Bi-Steel panels

Shown on Figure 4.8 are two limits for the maximum allowable ratio of s/t for use in design. The first, at s/t = 31.13, is the maximum ratio if the compression plate is to reach yield before any other type of failure (tension plate yield, shear of connectors). This may occur if the compression plate is thinner than the tension plate, which is the case for a more economical structural arrangement.

In the previous chapter it was concluded from tests of City4a, City4b and City4c, that the concrete strength affected the buckling of the compression plate. These test specimens all had the same internal structural arrangement but had increasing concrete strength. The bar spacing to plate thickness ratio was set at 20, which means that it is sufficiently low to be below the critical value of 31, defined by Figure 4.8. This means that compressive failure of the steel plate will occur before buckling.

The second and much higher ratio (s/t = 52.62) is for use when the panels have the same thickness for the tension and compression plate and the panel is subjected to normal bending. If axial compression of the structure occurs, then a lower limit would have to be calculated.

In the range 31 < s/t < 50, it can be seen that the Euler curve (l_e = 0.7) appears to be a lower bound solution as all experimental values are greater. The reason for this was initially thought to be the geometry of the plate at the point of buckling. It was thought that as the panel deforms, the compression plate becomes concave so that the longitudinal compression plate forces push it against the concrete surface. However, through the use of digital optical surveying techniques, the compression plate surface was modeled throughout a number of tests and this was found not to be the case.

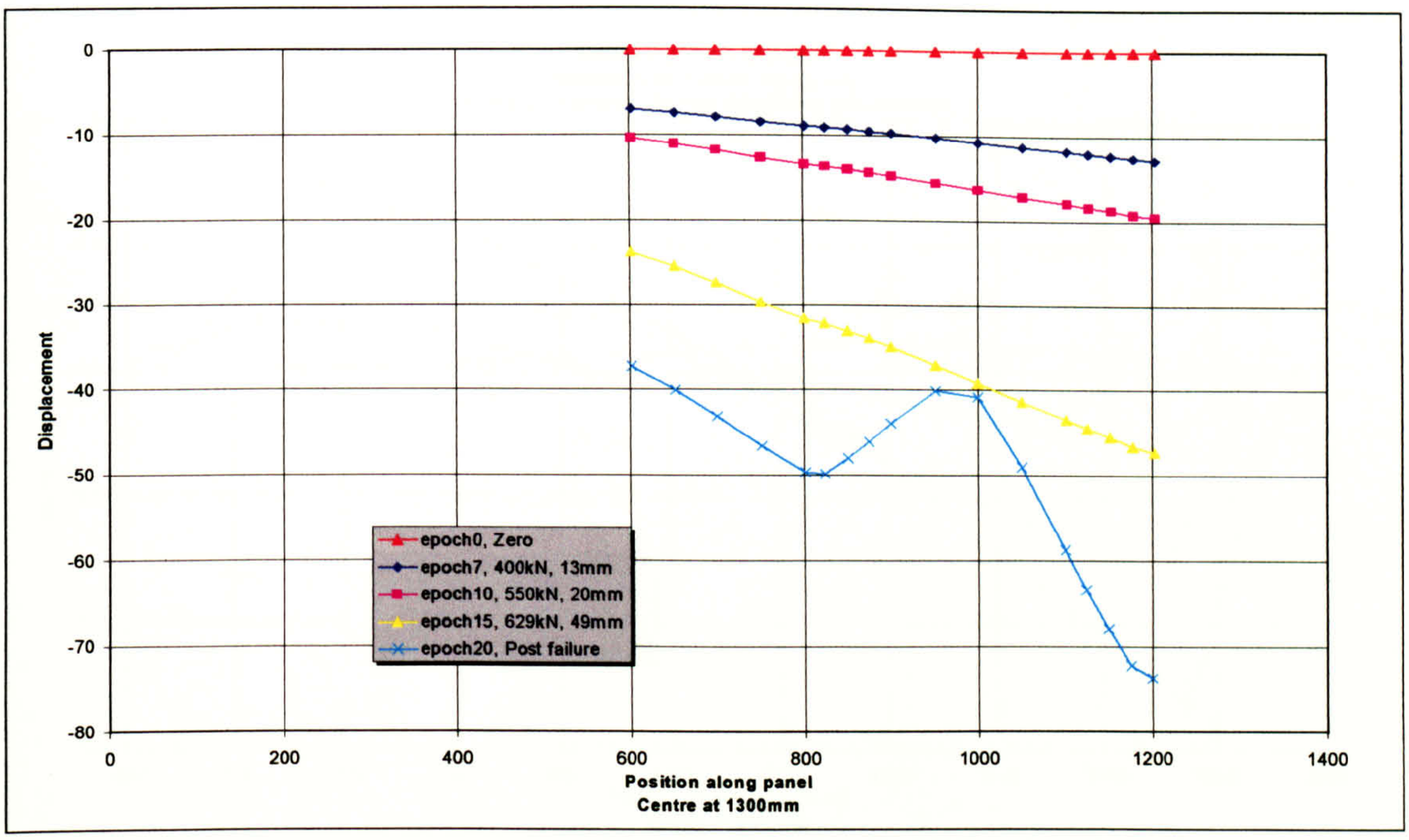

Figure 4.9. Surface profile along centreline of City10.

Figure 4.9 shows that the surface of the plate does not have a concave curvature but has a linear variation of deflection along the length of the panel. This data supports the idea of using an Euler approach to this problem as this theory covers initially straight elements. Furthermore, by looking closely at the variation of the plate profile relative to the connectors, the Euler approach is further validated (Figure 4.10).

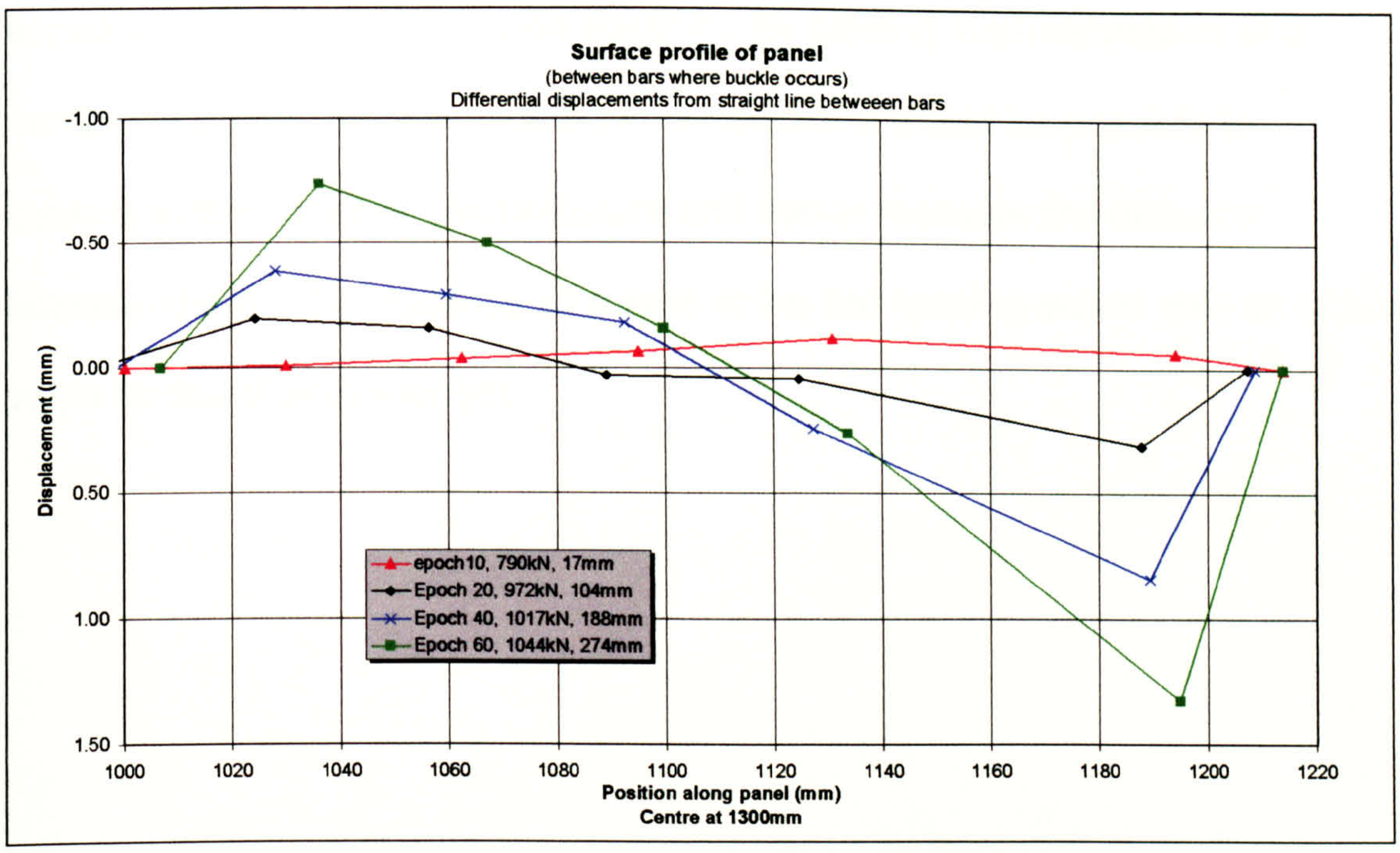

Figure 4.10. Compression Plate Surface Profile for City4c

By removing the global gradient from the deflection data, Figure 4.10 shows that the compression plate forms a wave between the connectors (at 1000 and 1200mm). The displacements indicated are mainly caused by the deformation of the bars that are welded to the compression plate, as the panel deflects. Unfortunately it was not possible to capture data at the start of the buckling as it occurred quite suddenly.

Figure 4.10 shows that the mid-point between the bars (1110mm) remains on a line directly between the tops of the adjacent connectors and, therefore, it would be expected that the first mode of buckling still coincide with the Euler load. At this point the load in the plate is such that, should the plate be given any lateral displacement it will continue to deform without any additional load. One factor, which will influence the accuracy of this approach, which without further investigation is beyond the scope of this thesis, is that of the effective length of the strut. It is expected that the recommendation given by BS5950 of an effective length of 0.7 will be conservative. Substituting a factor of 0.6

appears to give an upper bound solution. By placing instrumentation at a number of points, between a pair of connectors, it would be possible to determine the points of contra-flexure and hence measure the distance between them. This distance as a ratio of the bar spacing would give an actual value for the effective length.

4.4 Internal Forces and Stresses

The stresses in the steel plates of a DSC panel were derived in Chapter 2 and will be compared with actual results.

4.4.1 Longitudinal Plate Stresses

The inline stresses in the steel plates at yield are defined by Chapter 2 as:

$\sigma_2 = f_y$ in the tension plate and, **Equation 2.40**

$$\sigma_1 = f_y \frac{\left(z + {}^{t_1}/_2\right)}{\left(h_c - z + {}^{t_2}/_2\right)} \text{ in the compression plate.} \quad \textbf{Equation 2.41}$$

For City1, the measured value of yield stress of the steel plate, f_y, was 452Nmm^{-2}. Hence, the stress in the tension plate, σ_2 =452Nmm^{-2} and the stress in the compression plate, σ_1 is:

$$\sigma_1 = f_y \frac{\left(z + {}^{t_1}/_2\right)}{\left(h_c - z + {}^{t_2}/_2\right)}$$

$$\sigma_1 = 452 \frac{\left(74.6 + {}^{10}/_2\right)}{\left(200 - 74.6 + {}^{10}/_2\right)}$$

$$\sigma_1 = 275.9 Nmm^{-2}$$

Figure 4.4 shows the distribution of strains through the section of City1 at various load levels. At 1087kN applied load, the strains in City1, at a location 700mm from the support, are 518μs in the compression plate. Assuming an elastic distribution, this is equivalent to 264.9 Nmm^{-2} at mid-span with an applied load of 1116kN. Comparing this value with the calculated stress, the calculated value is approximately 4% greater than the experimental value.

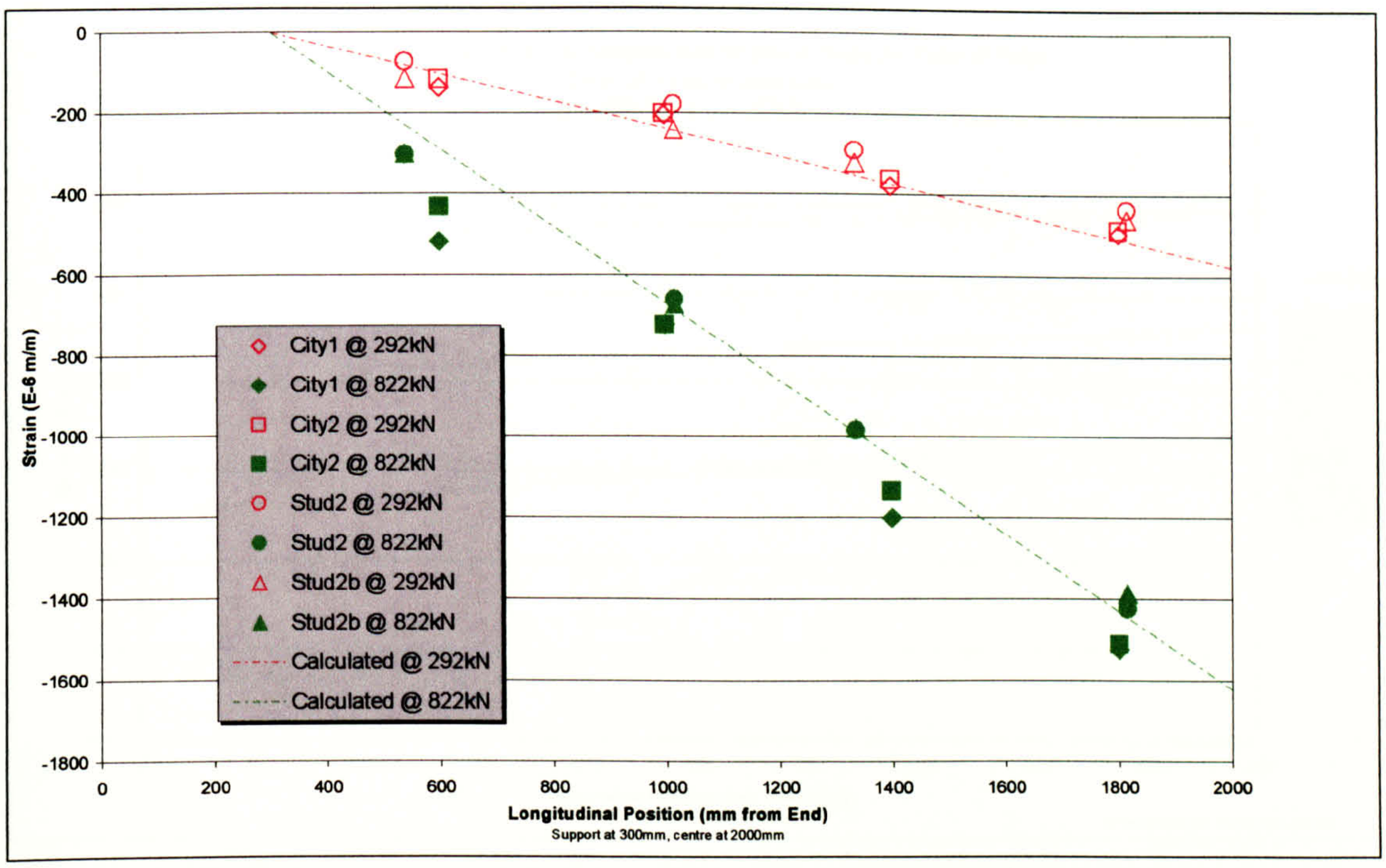

Figure 4.11. Longitudinal variation of strains in tension plate.

Figure 4.11 shows how the longitudinal strains are expected to vary along the length of the panel. The variation is linear since the strains are proportional to stress and hence the applied moment which, for a simply supported beam, vary linearly between the support and mid-span.

4.4.2 Transverse Plate Stresses

The instrumentation of Series 1 panel tests showed that there was an increase in the longitudinal strains from the centre out towards the edge (Figure 4.12). It has been stated in Chapter 2, that this was expected to be the effect of Poisson's ratio.

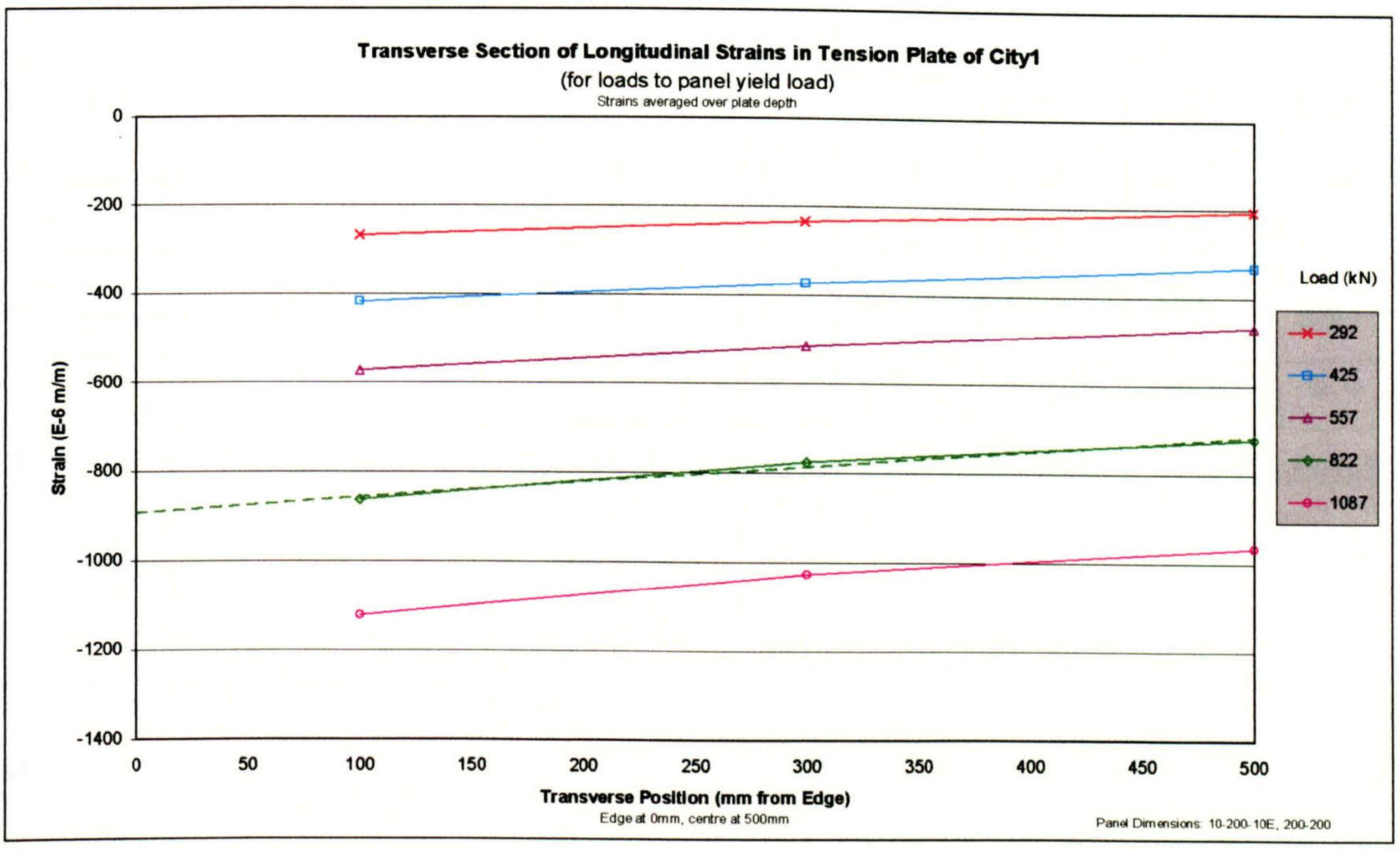

Figure 4.12. Transverse variation of longitudinal strains in City1.

Figure 4.12 shows the typical response of the strain gauges that were positioned on the transverse section of the beam, others can be found in Figures C.9 – C.12 in Appendix C. From Figure 4.12 it can be seen that for City1 at 822kN, the projected edge strain from the data is 892μs. With Poisson's ratio for steel being 0.3 and using Equation 2.45, the centreline strain is calculated to be:

$$\varepsilon_c = \varepsilon_e(1-\upsilon^2) \qquad \textbf{Equation 2.45}$$

$$\varepsilon_c = 892(1-0.3^2)$$

$$\varepsilon_c = 811.7\mu s$$

The measured value at this location is 721.1 μs, which is 88.8% of the value calculated. Similar results are presented in Table 4.3.

	City1				City2			
Load (kN)	**292**	**425**	**557**	**822**	**292**	**425**	**557**	**822**
$\varepsilon_{2e(measured)}$	280	439	600	892	224	368	501	752
$\varepsilon_{2c(measured)}$	205	330	466	721	201	336	475	723
$\varepsilon_{2e(calculated)}$	254	399	546	811	204	335	456	684
% Error	**23.9**	**20.9**	**17.1**	**12.4**	**1.5**	**-0.3**	**-4.0**	**-5.4**

Table 4.3. Transverse variation of measured and calculated longitudinal strains.

The percentage errors given in Table 4.3 shows a considerable variation between specimens but more consistent for each specimen alone. The similar overall performance of these two specimens would indicate that that there may have been some errors for this data. These may be in strain gauge placement, local influence from connectors or other reasons not apparent.

4.4.3 Interface Shear Forces

From the tests conducted within this thesis it is not possible to determine the full shear strength of the connectors as none of the tests failed in longitudinal shear. However, it is possible to examine whether the forces agree with the changes in the longitudinal force in the plate.

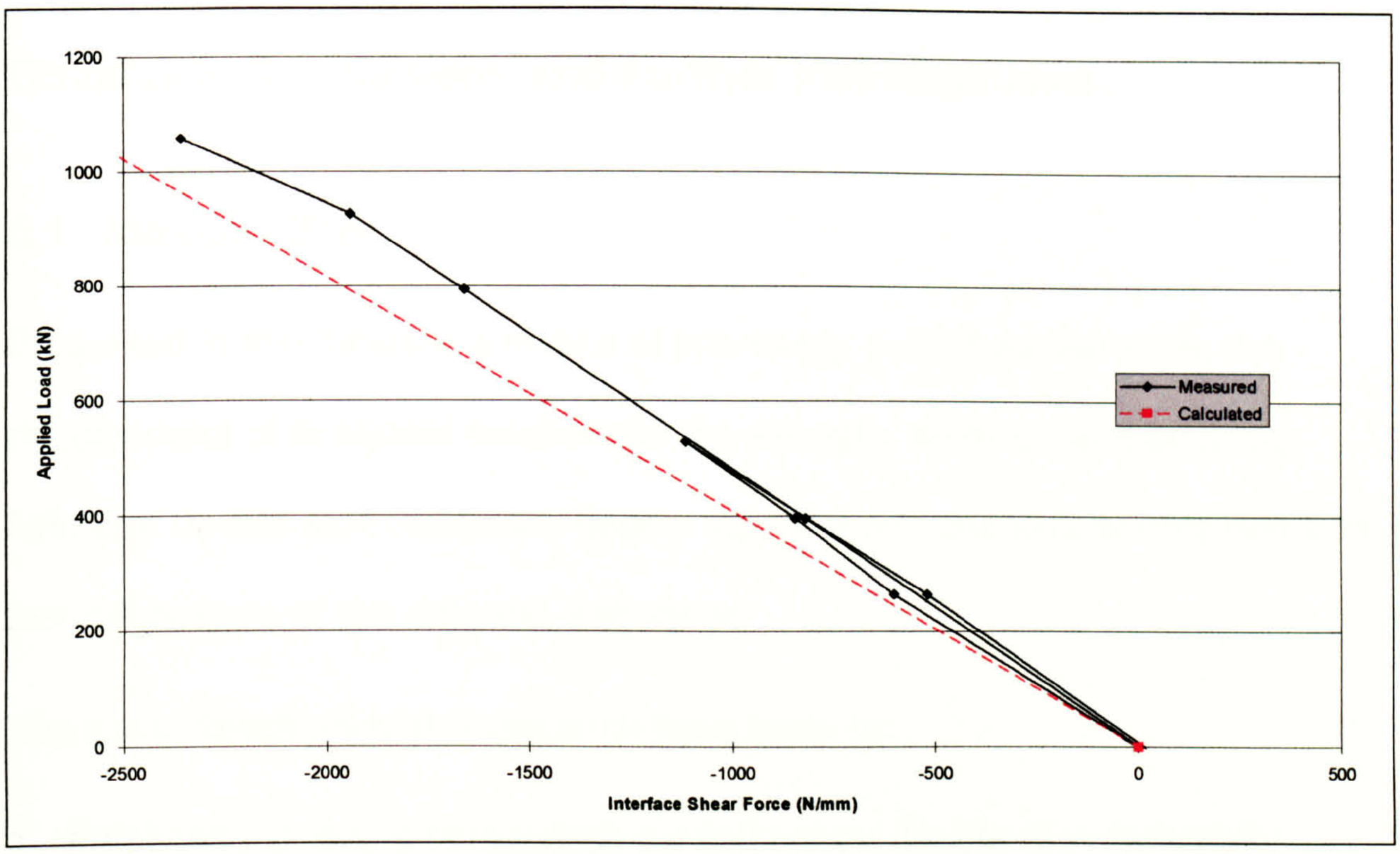

Figure 4.13 Interface shear forces for City1

Figure 4.13 shows the interface shear force in the tension plate of City1. Also indicated are the calculated shear forces, which have been determined in accordance with Chapter 3. It can be seen that the measured values are slightly smaller than calculated, with a 16.7% difference in the gradients.

Chapter 5 Conclusions and Further Investigations

5.1 Introduction

Presented in this thesis is a review of previously published literature, the development of analytical solutions to the strength, stiffness and buckling failure of double skin composite beams together with the results obtained from laboratory tests of two different test series.

The main objectives of this research have been to:

1. Establish the extent of research carried out on double skin composite structures and to extend this to include the possible uses for Bi-Steel,
2. Provide a comparison between existing methods of constructing DSC elements with the new British Steel product, 'Bi-Steel', as well as providing information regarding structural continuity from the use of end plates and,
3. Develop Bi-Steel knowledge in areas of strength, stiffness and local buckling failure of the compression plate.

The first objective was achieved through the study of previously published research, which not only showed the actual investigations but also the context in which it was being conducted. Two series of tests, together with analytical solutions, provided the information to achieve the other objectives.

5.2 Review of Previously Published Research

By studying the previously published research in fields containing composite or sandwich structures it was possible to identify what research had been conducted. It also showed the fields in which double skin composites and, in particular, Bi-Steel might be used.

Considerable research has been conducted on DSC elements using headed shear studs [Hordyk (1990); Machida (1992); Narayanan (1987); Oduyemi (1989) and Wright (1991)], some of which has been used to publish a design guide by the Steel Construction Institute.

Investigation of the possible uses for Bi-Steel has identified two main areas. Offshore floating structures such as FPSO's, FPU's, TLP's and Semi-submersibles can use Bi-Steel for their hull structures. Many of these types of structure use the hull for oil storage and therefore benefit from the double steel skins and the impact resistance of Bi-Steel in the event of an accident.

Submerged tube tunnel construction techniques have been identified by a number of sources [Narayanan (1987)] as being suitable for construction using double skin composites. From this research, The Steel Construction Institute has published a Design Guide. It would be a natural progression for Bi-Steel to take over wherever headed studs were considered for use in double skin composite construction.

5.3 *Analytical Solutions*

Analytical solutions have been developed for the elastic and plastic behaviour of Bi-Steel panels, which allow for shear strains to develop in the concrete core. The solutions have also been extended to include local buckling of the compression plate. The limitations of their use cover basic beam type elements in bending and axial compression has not been allowed for. If axial compression were present in the structural system required it could be allowed for by subtracting it from the allowable stress.

Initially, the solution for the position of the neutral axis from the underside of the compression plate was determined.

$$z = -m(t_1 + t_2) + [m.(t_1 + t_2)^2 - m(t_1^2 - 2t_c h_c + t_2^2)]^{\frac{1}{2}} \qquad \textbf{Equation 2.11}$$

A comparison of the analytical solution and the experimental data (Figure 4.4) show good agreement with each other, but there is some scatter. This is due to the interpretation of Figures B13 – B24, which do not always indicate an exact point for the position of the neutral axis. In such cases, the average value was taken.

Solutions have been developed for the moment of resistance at the elastic and plastic limits. A solution is also derived that defines the point when the neutral axis moves from its elastic position to the bottom of the compression steel plate. This solution for the moment of resistance of a Bi-Steel beam is given by:

$$M_y = f_y bt(h_c + t) \qquad \textbf{Equation 2.17}$$

Figure 4.2 shows that it agrees well with experimental data, the standard deviation of the results being 4.25% below measured data.

The development of elastic theory to estimate specimen deflections has also given good agreement with experimental data. Two solutions have been developed, which calculate the full composite deflection (Δ_1) and shear deflection (Δ_2), respectively. The total deflection is the summation of the two parts.

$$\Delta_1 = -\frac{PL^3}{48K}$$ **Equation 2.29**

$$\Delta_2 = \frac{VL}{4AG'}$$ **Equation 2.32**

However, this has had to rely on determining the shear stiffness of the panels from one of the tests. All of the specimens used for this area of the study have a symmetrical distribution of shear connectors and share the same spacing; they will have, therefore, equal shear stiffness. This has limited this area of study, which is currently being addressed by further testing, of panels with different bar spacing and panel depths, at City University.

Solutions have been developed to enable the shear stiffness to be calculated which are based on a cantilevered, round steel bar supported on a continuous concrete foundation. The shear stiffness is given by Equation 2.34.

$$G' = \frac{\tau}{\upsilon'}$$ **Equation 2.34**

where: $$\tau = \frac{V}{A_s} = \frac{V}{2b(h_c + t_1 + t_2)}$$

$$\upsilon' = \tan^{-1} \frac{\delta s_x}{h_c/2},$$

and $$\delta s_x = \frac{V\lambda}{k} \frac{\sinh 2\lambda l - \sin 2\lambda l}{\cosh^2 \lambda l + \cos^2 \lambda l}$$

However, these solutions depend on a foundation modulus for the concrete, which can only be determined from laboratory measurements.

A solution for the post yield moment of resistance of a double skin composite panel has also been developed. This relates the moment of resistance to the strain in the tension steel plate and the material post yield parameters.

$$M_{py} = K\varepsilon_2^n A_2 (h_c + t)$$ **Equation 2.36**

In order to relate the post yield moment of resistance to the deflection of the panel a further solution was derived to relate the strain to the deflection. The tension plate strain at the elastic limit can be calculated from the moment of resistance, and the deflection at this point can also be calculated. Hence, it is possible to calculate the gradient of the elastic strain-deflection relationship. The post yield strain-deflection gradient is equal to the elastic gradient multiplied by the strain-hardening component, n.

Euler analysis with an effective length of strut equal to 0.7 times the bar spacing has been used to determine the buckling loads within the compression plate.

$$P_E = \frac{\pi^2 EI}{(0.7l)^2}$$ **Equation 2.39**

By re-arranging Equation 2.39, it has been possible to determine the limiting bar spacing to plate thickness ratios. A limit of s/t = 31 has been found, below which compressive yield of the upper plate will occur before the full elastic strength of the panel has been reached. However, most Bi-Steel panels are to be manufactured with equal plate thickness, which mean that there are lower stresses in the compression plate than the tension plate. Therefore, s/t can be increased to 53 and the full elastic strength of the panel can still be achieved.

Equation 2.39 has given reasonable agreement with the data, but does appear to be conservative since it under estimates all the results in the range s/t>31. Below this value, Equation 2.39 can not be used because the bar spacing to plate thickness ratio is small enough to allow the compression plate to reach compressive failure before buckling.

5.4 Experimental Studies

Sixteen tests have been performed on double skin composite wide-beam elements. They have been divided into two test series (Series 1 and Series 2), the second of which has been divided into two parts (Part I and Part II). The two parts of Series 2 tests are dimensionally the same but have different concrete strengths as they were cast at different times.

Series 1 tests compared the existing method of constructing double skin composite elements using overlapping, headed shear studs with Bi-Steel, a new product developed for and by British Steel for commercial use to develop steel as a competitor to concrete. Bi-Steel was in its infancy at the outset of this particular research programme.

Comparisons made between the two types of construction (Figure 3.6) show that there is no difference in the elastic and early plastic deformations and load characteristics. Due to the continuity of the steel structure used in Bi-Steel, it was evident that it could withstand larger deformation before failure. Failure of the two different types of construction was different. The studded specimens failed by studs, attached to the compression plate, pulling out of the concrete whereas the Bi-Steel specimens failed through local buckling of the compression plate.

Series 1 tests also compared panels using end plates in order to simulate structural continuity by confining the concrete longitudinally. It was seen that no benefit came through the use of these plates even though when no plate was present; small amounts of slip were recorded at the tension plate interface but none at the compression plate interface. Measured strains and deflections

of the two types of panel were identical. This is due to sufficient shear connection to resist the interface shear forces.

Series 2 (Part I and II) test panels were used to compare the effects of the bar spacing to plate thickness ratio on the failure by local buckling of the compression plate. They were also used to validate the analytical solutions for the strength and stiffness of Bi-Steel elements.

Comparison of the various load deflection curves showed that as the bar spacing to plate thickness ratio increased, then the onset of local buckling came sooner. The measured strains (Figure 3.12) at the time of buckling also showed that the forces in the compression plate agreed with an Euler analysis.

By comparing the results from City4a, City4b and City4c in Figure 3.12, it is clear that the concrete strength affects local buckling failure. However, this is only true when the bar spacing to plate thickness ratio is sufficiently small, given as s/t = 31 in the analytical solutions. The experimental data confirms this with all tests with s/t below 30 all failing by yield of the compression plate before buckling occurred.

Figure 4.2 and Table 4.2 show that there is good agreement between the comparison of panel strength and stiffness, respectively, with the analytical solutions.

5.5 *Future Research*

One avenue of further investigation is that of panel shear stiffness. This is due to the limited variation of the internal structure of the laboratory tests so far carried out. These panels have equal concrete depth and similar arrangements of the shear connectors. This leads to similar shear stiffness for all of the tests detailed within this research. At the time of writing, this is being partly addressed by further testing at City University by a test series that uses two different concrete depths, larger spans and four point bending. The results of these tests will allow comparison with full composite deflection calculations as well as giving different shear deformations from previous tests. Further work in this area may also be extended to defining the modulus of the foundation for a Bi-Steel bar connector resting on a concrete foundation. This would then allow the shear stiffness, for any internal arrangement, to be calculated.

The buckling investigations detailed in this research programme have been limited to initially flat specimens and have shown that they agree well with Euler theory. Although the deformation at the time of buckling was significant, it was shown not to affect the buckling strength. Above bar spacing to plate thickness ratios of 31, it appears that buckling will occur as a primary failure mechanism. This assumes that there is sufficient shear capacity within the connectors and sufficient tensile capacity within the steel plate. Further studies are to be carried out on specimens with initial curvatures to introduce eccentricity between the forces and the centre of the plate. This eccentricity will induce failure to occur before the Euler buckling load is reached because of the initial shape of the specimen. For this study, it will be necessary to develop further

analytical solutions, as those presented in this thesis are not able to account for the initial shape of the plate. It will be necessary to investigate the use of column buckling theories.

It has been shown that for values of s/t less than 31, the compression plate will yield before local buckling. This assumes a steel nominal yield strength of $355Nmm^{-2}$. It is in this region that further work is required as this research limits itself to failure by local buckling and does not investigate compressive yield or concrete crushing around the shear connectors.

Further buckling investigations could also determine the actual effective length of strut to be used in the Euler analysis, rather than relying on what is probably a conservative estimate taken from BS5950.

To summarise, the investigations detailed in this thesis have given considerable information on the performance of Bi-Steel. It has also shown that there are still areas that require further study. By carrying out this research, a contribution has been made to making double skin composite structures a marketable product by contributing to a design guide to be published by The Steel Construction Institute.

References

Adams, P; Zimmerman, T; MacGregor, J (1987).
Design and behaviour of composite ice-resisting walls.
Conference on Port and Ocean Engineering under Arctic Conditions 1987.

Allen, H.G. (1969). Analysis and Design of Structural Sandwich Panels.
(Pergamon Press, Oxford).

A. S. Veritec (1995). Worldwide Offshore Accident Databank.
Det Norske Veritas Annual Statistic Report.

Bass, D; Gaskill, H; Riggs, N. (1985).
Analysis of Iceberg Impacts with Gravity Base Structures at Hibernia.
International Offshore Mechanics and Arctic Engineering Symposium Volume 2.

BS4360: 1990 & BS EN10 025:1990. Weldable structural steel plate.

Chunqun, J. (1993).
Analysis and Research of Ice Loads Acting on Offshore Structures.
China Ocean Engineering 7 (2): 167 - 176.

Coates, R.C; Coutie, M.G; Kong, F.K (1997) Structural Analysis
(Chapman & Hall, London).

Det Norske Veritas. (1981a).
Design against Accidental Loads.
Det Norske Veritas Recommended Practice RP D204.

Det Norske Veritas. (1981b)
Impact Loads from Boats.
Det Norske Veritas Recommended Practice RP D205.

Dowling, N.E. Mechanical Behaviour of Materials: Engineering methods for deformation, fracture and fatigue.
(Prentice-Hall International Editions, New Jersey).

Ellis, R.M; MacGregor, J.G. (1993).
Tests on Arch-Shaped Ice-Resisting Walls for Offshore Structures.
American Concrete Institute Structural Journal: 42 - 51.

Frieze, P.A; Cho, S-R. (1993).
Impact Damage and Assessment of Offshore Tubulars (OTC 7152).
Offshore Technology Conference: 193-200.

Hassinen, P; Kouhi, J; Zimmerman, T; Stephens, M. (1989).
Static and cyclic load tests of a composite ice-resisting wall.
Research Notes 965 Technical Research Centre of Finland.

Henery, D; Inglis, R.B. (1995).
Prospects and Challenges for the FPSO (OTC 7695).
Offshore Technology Conference: 9-21.

Hetenyi, M. Beams on Elastic Foundations.
(University of Michigan Press).

Hordyk, M; Billington, C.J; Morahan, S.P; Smedley, P.A. (1994).
Steel-Concrete-Steel Sandwich Construction. The Development of Design Guidelines for Marine Structures.
Billington Osborne-Moss Engineering Ltd Internal Report: 150 - 158.

Hughes, J (1995).
Exploration & Production Technology International.

Isaacson, M; Cheung, K.F. (1988)
Influence Of Added Mass On Ice Impacts.
Canadian Journal of Civil Engineering 15: 698 - 708.

Litton, R.W; Puskar, F.J. (1993)
Ship Collision Analysis for the Kawasaki Island Steel Platforms (OTC 7141).
Offshore Technology Conference: 61-72.

Machida, A; Makabe, T; Mutsuyoshi, H; Malek, N. (1992a).
Experimental Study on Mechanical Properties of Steel Concrete Sandwich Beam.
Transactions of the Japan Concrete Institute 14: 475 - 482.

Machida, A; Makabe, T; Mutsuyoshi, H; Malek, N. (1992b).
Mechanical Properties of Steel Concrete Composite Member.
Transactions of the Japan Concrete Institute 14: 469 - 474.

Moy, S.S.J; Xiao, R.Y; Lillestone, D (1998a)
Tests for British Steel on the Shear Strength of Studs used in the Bi-Steel System.
University of Southampton, Department of Civil and Environmental Engineering.

Moy, S.S.J; Lillestone, D (1998b)
Tests for British Steel on the Shear Behaviour of Studs used in the Bi-Steel System.
University of Southampton, Department of Civil and Environmental Engineering.

Narayanan, R; Wright, H.D; Francis, R.W; Evans, H.R (1987)
Double Skin Composite Construction for Submerged Tube Tunnels
Steel Construction Today 1, 185-189.

Narayanan, R; Bowerman, H.G; Naji, F.J; Roberts, T.M; Helou, A.J. (1994).
SCI-P-131: Design Guide for Steel-Concrete-Steel Sandwich Construction.

Volume 1: General Principles and Rules for Basic Elements.
Steel Construction Institute.

Nojiri, Y; Koseki, K; Yoshiki, T; Sawayanagi, M. (1986).
Structural Behaviour and Design Method of Steel/Concrete Composite Ice Walls for Arctic Offshore Structures (OTC 5292).
Offshore Technology Conference: 597-604

Oduyemi, T.O.S; Wright, H.D (1989).
An Experimental Investigation into the Behaviour of Double Skin Sandwich Beams.
Journal of Constructional Steel Research 14: 197-220.

Roberts, T.M; Edwards, D.N; Narayanan, R (1996)
Testing and Analysis of Steel-Concrete-Steel Sandwich Beams
Journal of Constructional Steel Research 3 (38): 257-279.

Roberts, T.M; Dogan, O (1998).
Fatigue of Welded Stud Shear Connectors in Steel-Concrete-Steel Sandwich Beams.
Journal of Constructional Steel Research 3 (45): 301-320.

St. John, J; Minnick, P.V; Sheinberg, R. (1992)
Plastic Design Method for Icebreaker Shell Plating subjected to Measured Ice Loads. SNAME Transactions 100: 117 - 141.

Shukry, M.E.S; Douglas Goode, C (1990)
Punching shear strength of composite construction.
American Concrete Institute Structural Journal 1 (1): 12-22.

Sorensen, K.A. (1976).
Behaviour of Reinforced and Prestressed Concrete Tubes under Static and Impact Loading.
International Conference on the Behaviour of Offshore Structures: 798-813.

Steel Construction Institute (1984).
Double Skin Composite Construction - Phase 1 Report.
Internal Report.

Steel Construction Institute (1994).
Bi-Steel Application Study - Offshore Floating Platforms.
Internal Report.

Swamidas, A.S.J; El-Tahan, H; Arockiasamy, M. (1985a).
Response of Semi-submersible Models to Bergy-Bit Impacts.
POAC 2: 544 - 555.

Swamidas, A.S.J; El-Tahan, H; Arockiasamy, M. (1986).
Structural Integrity of Semi-submersibles and Gravity Platforms to Bergy-

Bit/Iceberg Impact (OTC 5087).
Offshore Technology Conference 1: 39 - 49.

Wright, H.D; Oduyemi, T.O.S; Evans, H.R. (1991a).
The Experimental Behaviour of Double Skin Composite Elements.
Journal of Constructional Steel Research 19: 97 -110.

Wright, H.D; Oduyemi, T.O.S. (1991b).
Partial Interaction Analysis of Double Skin Composite Beams.
Journal of Constructional Steel Research 19: 253 - 283.

www.Bluewater-Offshore.com (1998).

www.energyweb.net/oso/oso0545.htm (1998)

Zahran,M; Kanaya,K et. al. (1994).
Shear Fatigue Behaviour of Steel-Concrete Sandwich Beams without Web Reinforcement.
Transactions of the Japan Concrete Institute 16: 431-438.

Bibliography

Billington Osborne-Moss Engineering Ltd (1992).
Steel-Concrete-Steel sandwich construction. Work Package 04. C554R053-17 Revision 0.
Billington Osborne-Moss Engineering Ltd.

Davies, R.L; Martin, J.G. (1990).
Wave-Impact Loads on Large-Diameter Horizontal Cylinder Placed Above Still Water (OTC 6408).
Offshore Technology Conference: 585-591

Det Norske Veritas (1981c). Guidance - Fixed Offshore Installations - Impact Loads from Boats, Technical Note TN B202.

Ellinas, C.P; Valsgard, S. (1985).
Collisions and Damage of Offshore Structures: A State of the Art.
Fourth International Offshore Mechanics and Arctic Engineering Symposium 2: 475 - 495.

Faulkner, D; Cowling, M.J; Frieze. P.A. Integrity of Offshore Structures (Major Ship Collision Damage to the Prestressed Concrete Towers of Offshore Gravity Structures).

Fjeld, S. (1979).
Offshore Oil Production and Drilling Platforms. Design against Accidental Loads.
Second International Conference on the Behviour of Offshore Structures 2 (75): 391 - 414.

Furnes, O; Amdahl, J. (1980)
Ship Collisions with Offshore Platforms.
Det Norske Veritas. Paper No: 80-P080.

Gerwick, B.C; Berner, D.E. (1991)
Design of Offshore Concrete Structures for Local Loads due to Ice Impact.
Conference on Port and Ocean Engineering under Arctic Conditions 1: 28 - 42.

Gowda, S.S; Hassinen, P; Juntunen, J; Erikoinen, O. (1991).
Static and cyclic tests on composite ice-resisting walls.
Technical Research Centre of Finland: Research Notes 1229.

Hunter, K.C; De Souza, P.M.F.M; Carra, C.J. (1995).
Griffin - A state-of-the-art FPSO and some thoughts on FPSO Trends in Australia (OTC 7699).
Offshore Technology Conference: 59-69.

Johnson, R.C; Benoit, J.R. (1987).
Iceberg Impact Strength (OTC 5599).
Offshore Technology Conference: 417-423.

Jones, G. Analysis of Beams on Elastic Foundations.
(Thomas Telford, London).

Jones, N and Wierzbicki, T. (1983). Structural Crashworthiness and Failure.
(Butterworth Press)

Kennedy, S.J; Roger Cheng, J.J. (1992a).
Behaviour of Transversely Loaded Continuous Steel-Concrete Composite Plates: Experimental Program and Test Results.
Canadian Journal of Civil Engineering 19: 323 - 335.

Kennedy, S.J; Roger Cheng, J.J. (1992b).
Behaviour of Transversely Loaded Continuous Steel-Concrete Composite Plates: Analyses and Design Applications.
Canadian Journal of Civil Engineering 19: 336 - 348.

Koehler, P.E; Jorgensen, L. (1985).
Ship Ice Impact Analysis.
International Offshore Mechanics and Arctic Engineering Symposium Volume 2.

Kong, F.K; Evans, R.H. Reinforced and Prestressed Concrete.
(Chapman & Hall. London)

Kountouris, G. (1990).
Design Charts for Double-Skin Composite Elements.
BSc Dissertation, University of Wales College of Cardiff.

Link, R.A; Elwi, A.E. (1995).
Composite Concrete-Steel Plate Walls: Analysis and Behaviour.
American Society of Civil Engineering Journal of Structural Engineering 121(2): 260 - 271.

Mosley, W.H; Bungey, J.H. Reinforced Concrete Design.
(Macmillan London)

Narayanan,R; Lee,I.L; Roberts,T.M; Evans,H.R; Edwards,D.N; Helou,A.J. (1995).
Studies on Steel-Concrete-Steel Sandwich Construction for Submerged Tube Tunnels. Steel Construction Institute.

Plantema, F.J. Sandwich Construction: The Bending and Buckling of Sandwich Beams, Plates, and Shells
(John Wiley & Sons, Inc. New York)

Ronalds, B.F. (1990).
Vessel Impact Design for Steel Jackets (OTC 6384).
Offshore Technology Conference:339-350.

Sato,K (1992).
Elastic Buckling of Incomplete Composite Plates.
Journal of Engineering Mechanics 118 (1): 1-19.

Smith, C.S; Dow, R.S. (1981).
Residual Strength of Damaged Steel Ships and Offshore Structures.
Journal of Constructional Steel Research 1: 2-15.

Swamidas, A.S.J; El-Tahan, H; Arockiasamy, M. (1985b).
Response of Offshore Structures to Bergy-Bit and Iceberg Impacts.
International Conference on the Behaviour of Offshore Structures: 951 - 961.

United Kingdom Atomic Energy Authority (1987). Design and Assessment of Concrete Structures subjected to Impact, Design Guide DG3, Part 1.

Zhu, L; Faulkner, D. (1994).
Dynamic Inelastic Behaviour of Plates in Minor Ship Collisions.
International Journal of Impact Engineering 15 (2): 165 – 178.

Appendix A Drawings

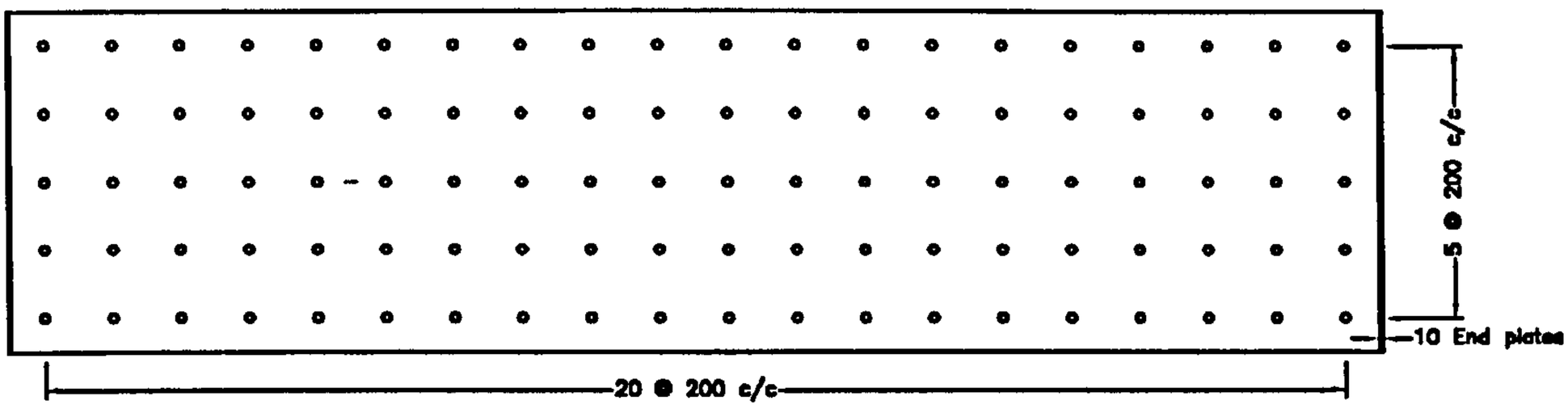

TOP ELEVATION

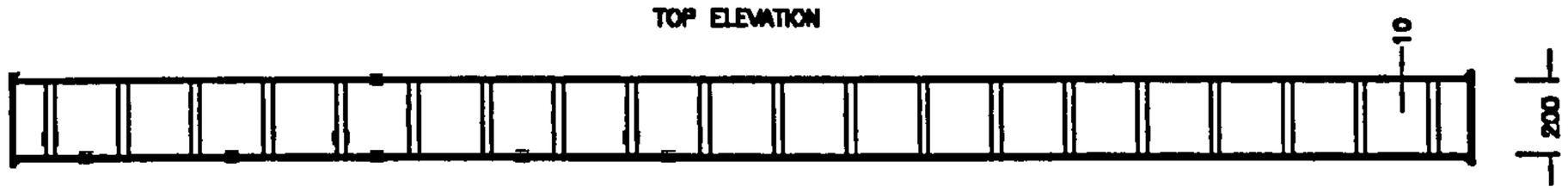

SIDE ELEVATION

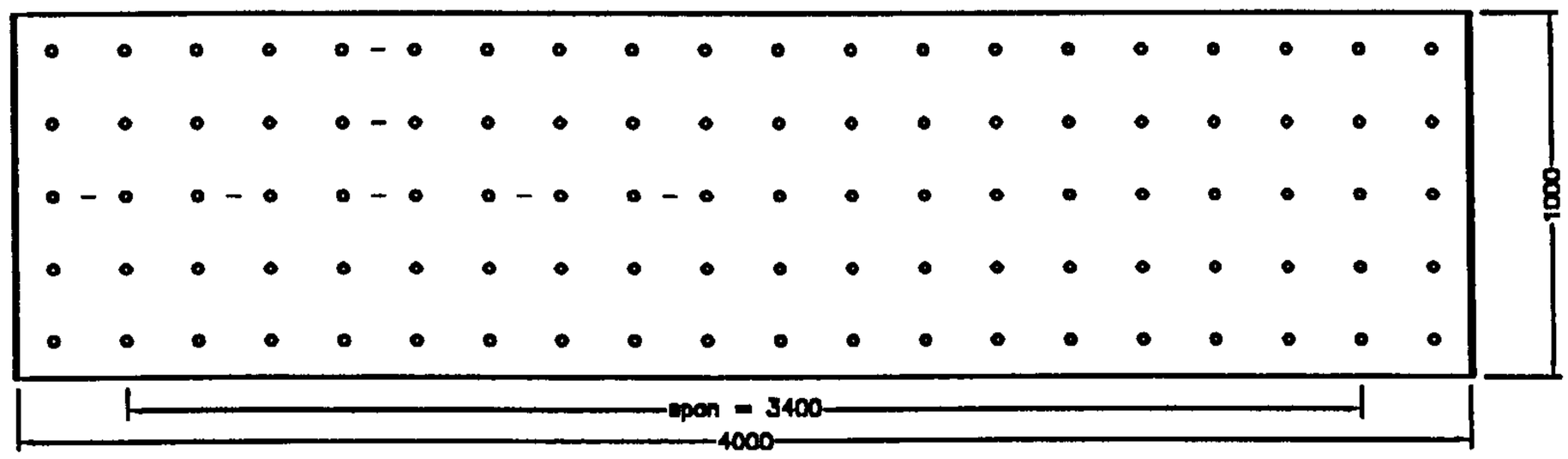

BOTTOM ELEVATION

NOTES:
1. Steel plate is S355JR (Grade 50B).

SERIES 1 TEST PANELS

CITY1

Design By: B.McKinley
Drawn By: B.Mckinley
Date: April 1998

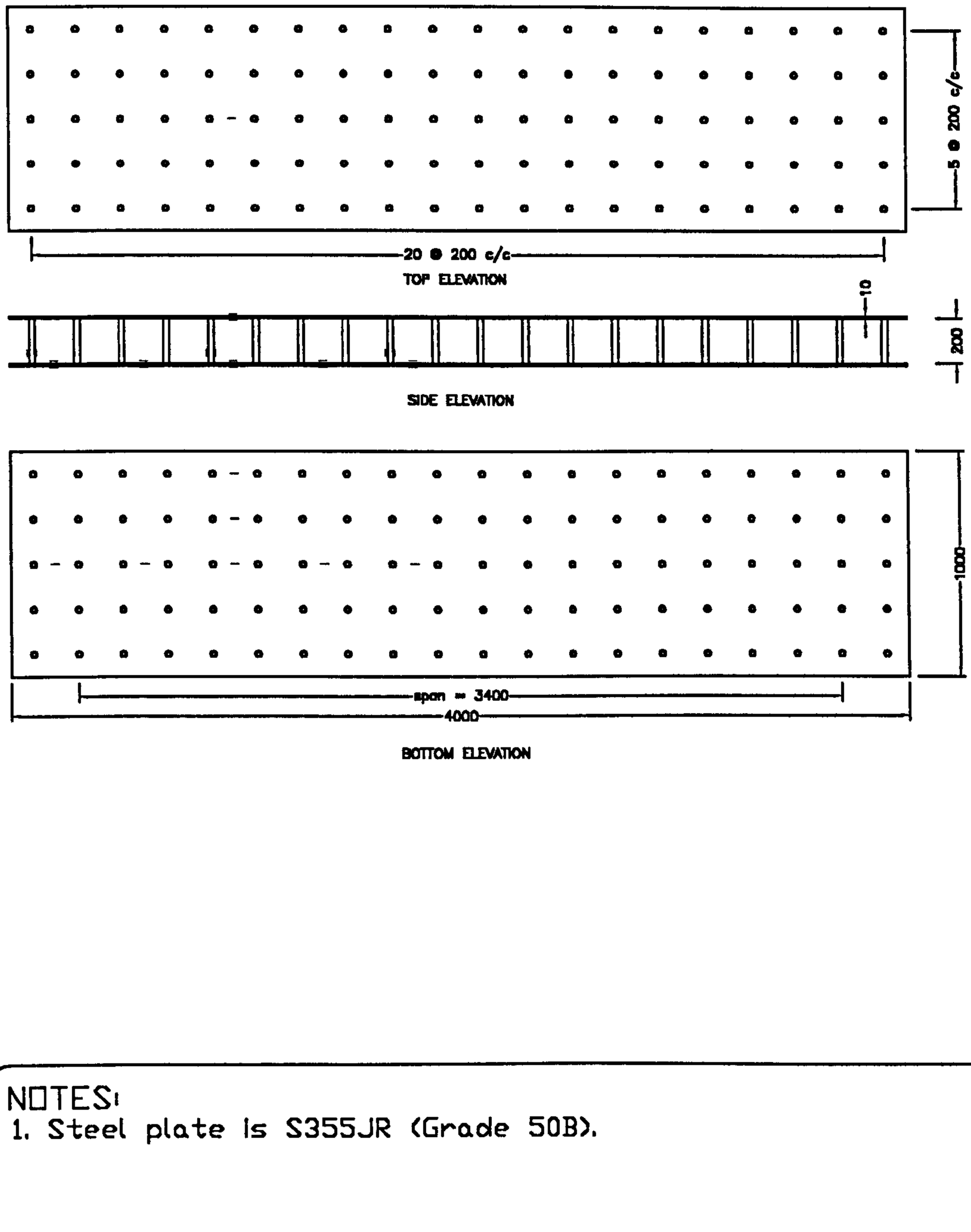

NOTES:
1. Steel plate is S355JR (Grade 50B).

SERIES 1 TEST PANELS

CITY2

Design By: B.McKinley
Drawn By: B.McKinley
Date: April 1998

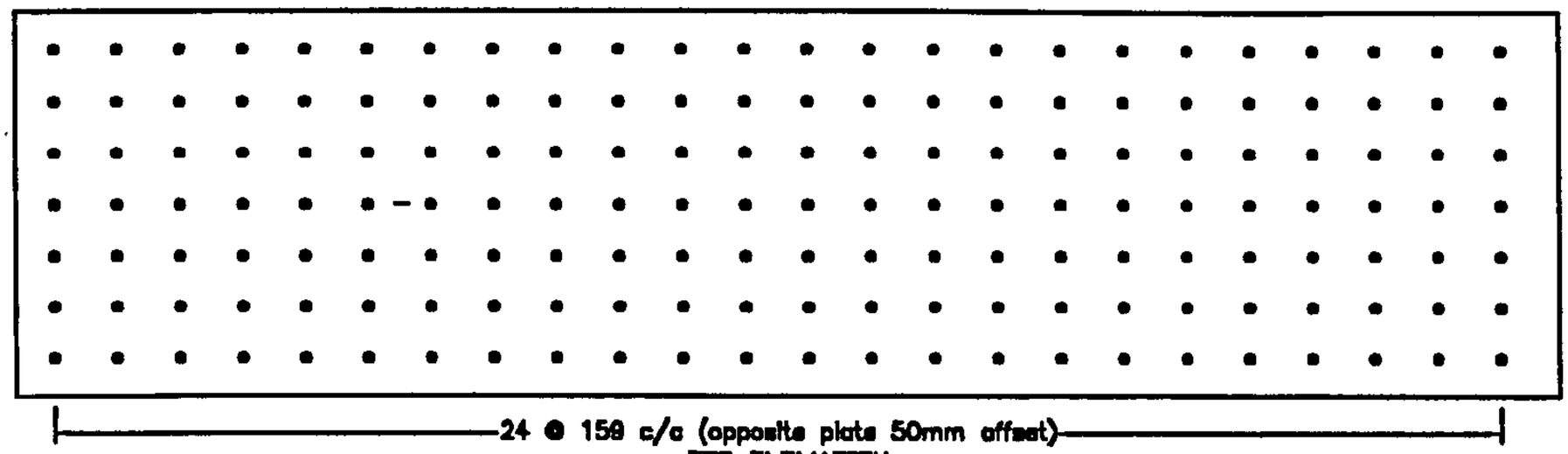

TOP ELEVATION

SIDE ELEVATION

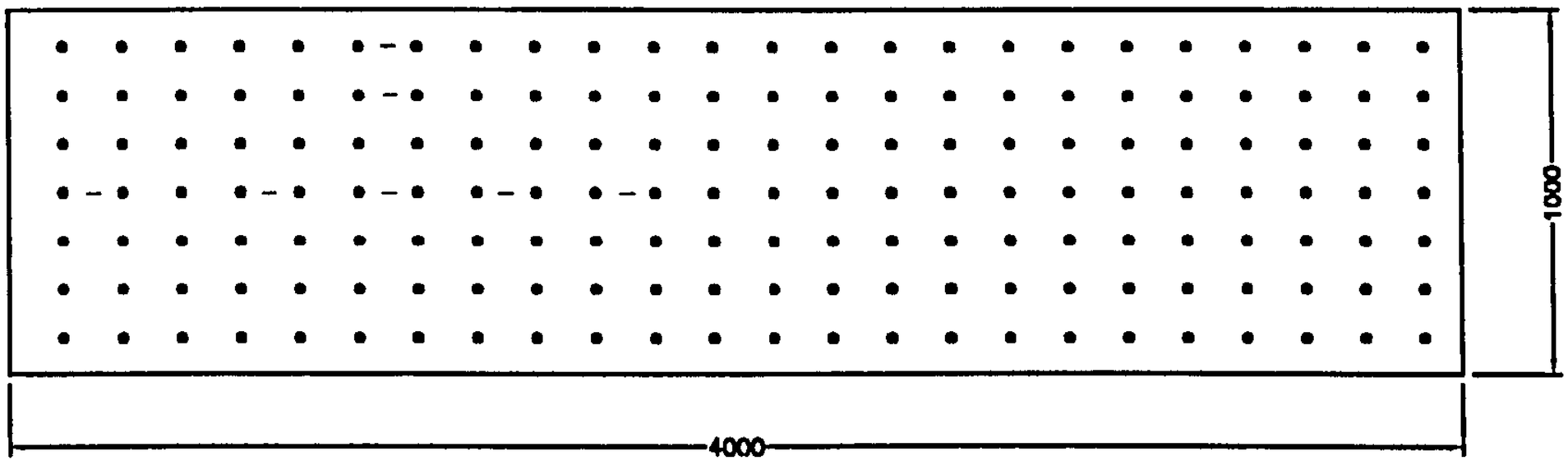

BOTTOM ELEVATION

NOTES:

1. Steel plate is S355JR (Grade 50B).

SERIES 1 TEST PANELS

STUD2

Design By: B.McKinley
Drawn By: B.McKinley
Date: April 1998

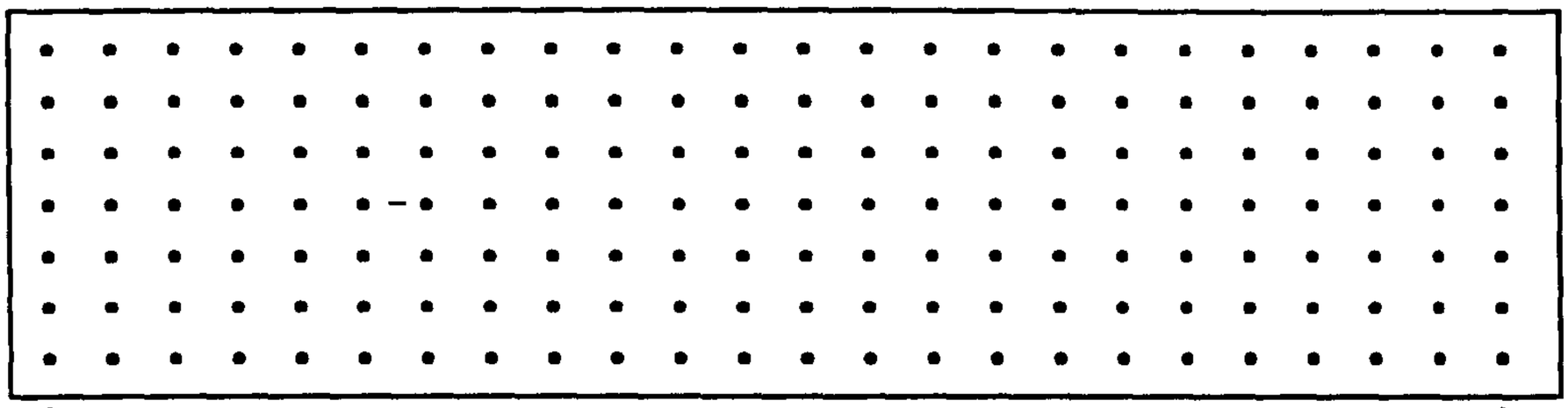

TOP ELEVATION

SIDE ELEVATION

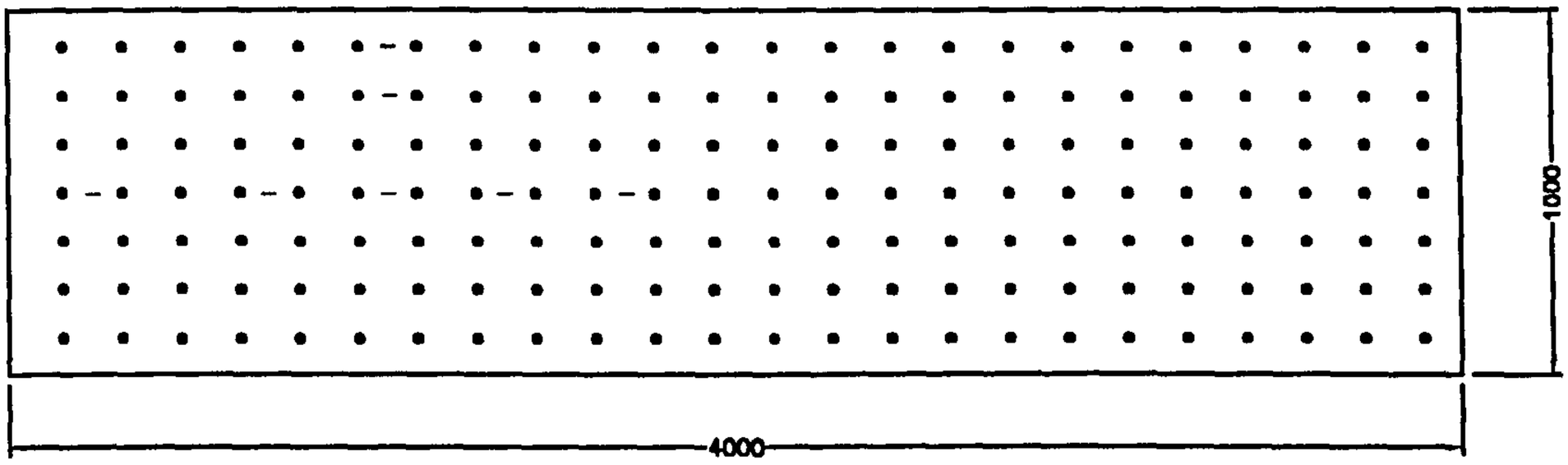

BOTTOM ELEVATION

NOTES:

1. Steel plate is S355JR (Grade 50B).

SERIES 1 TEST PANELS

STUD2b

Design By: B.McKinley
Drawn By: B.McKinley
Date: April 1998

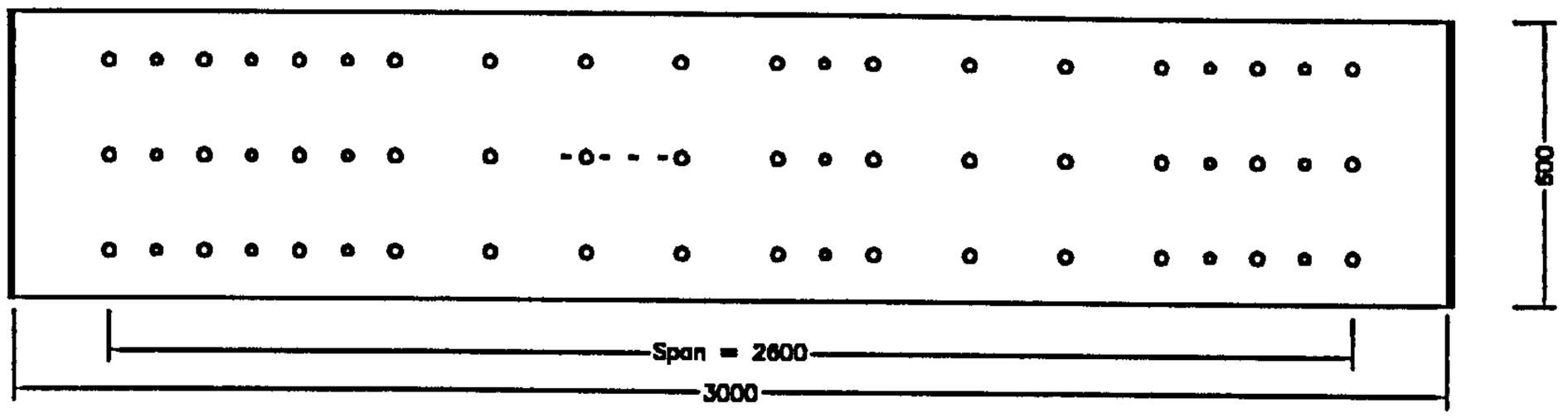

TOP ELEVATION

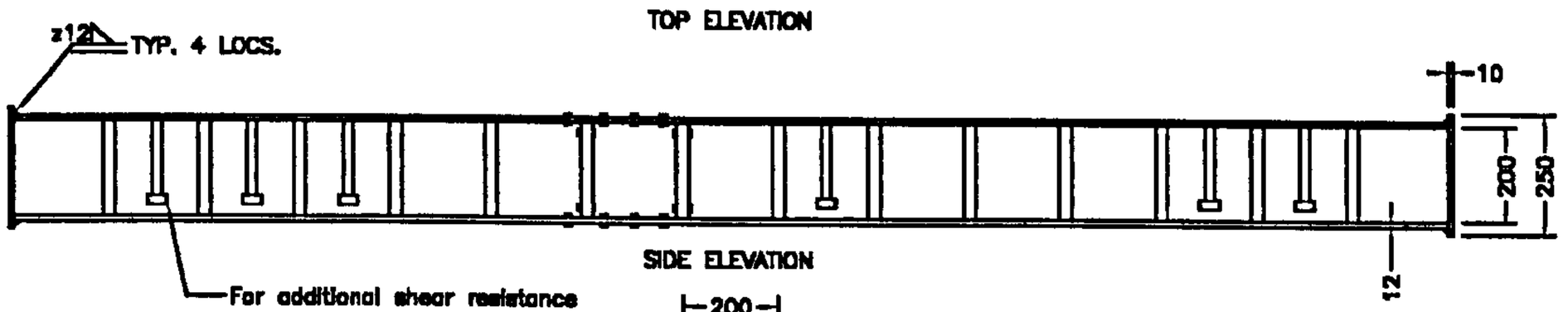

SIDE ELEVATION

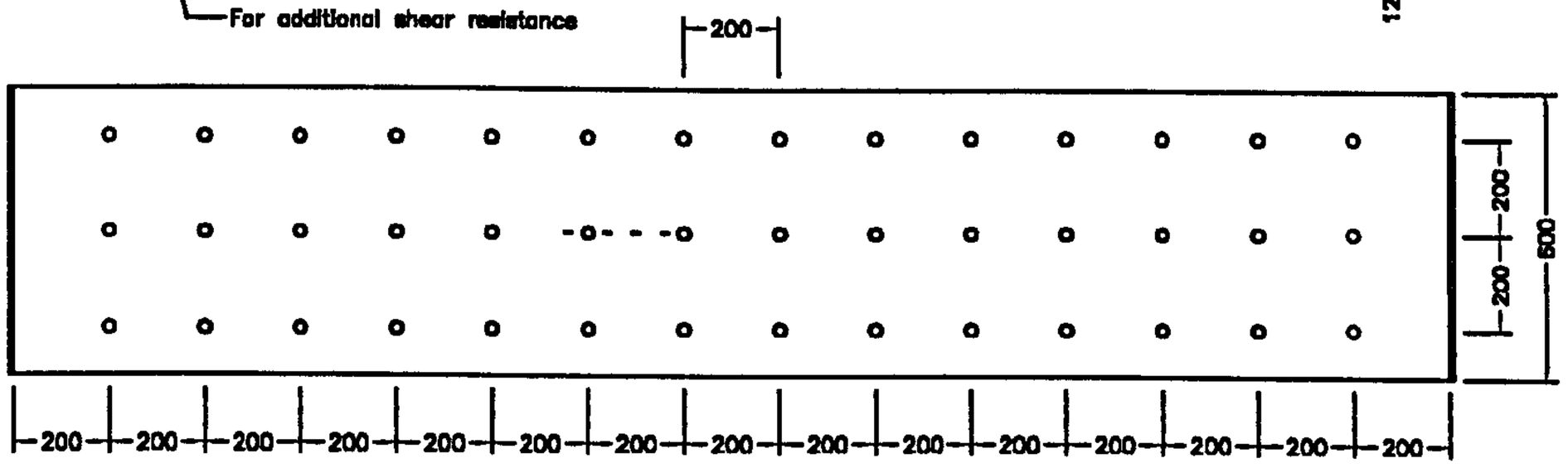

NOTES:

1. Steel plate is S355JR (Grade 50).
2. Strain gauges are located on the steel plates are either mid way between adjacent bars or are 15mm from the bar. Strain gauges located on the bars are 15mm from the surface of the steel plate.

SERIES 2 TEST PANELS

Part 2

City3

Design By: B.McKinley
Drawn By: B.McKinley
Date: July 1997

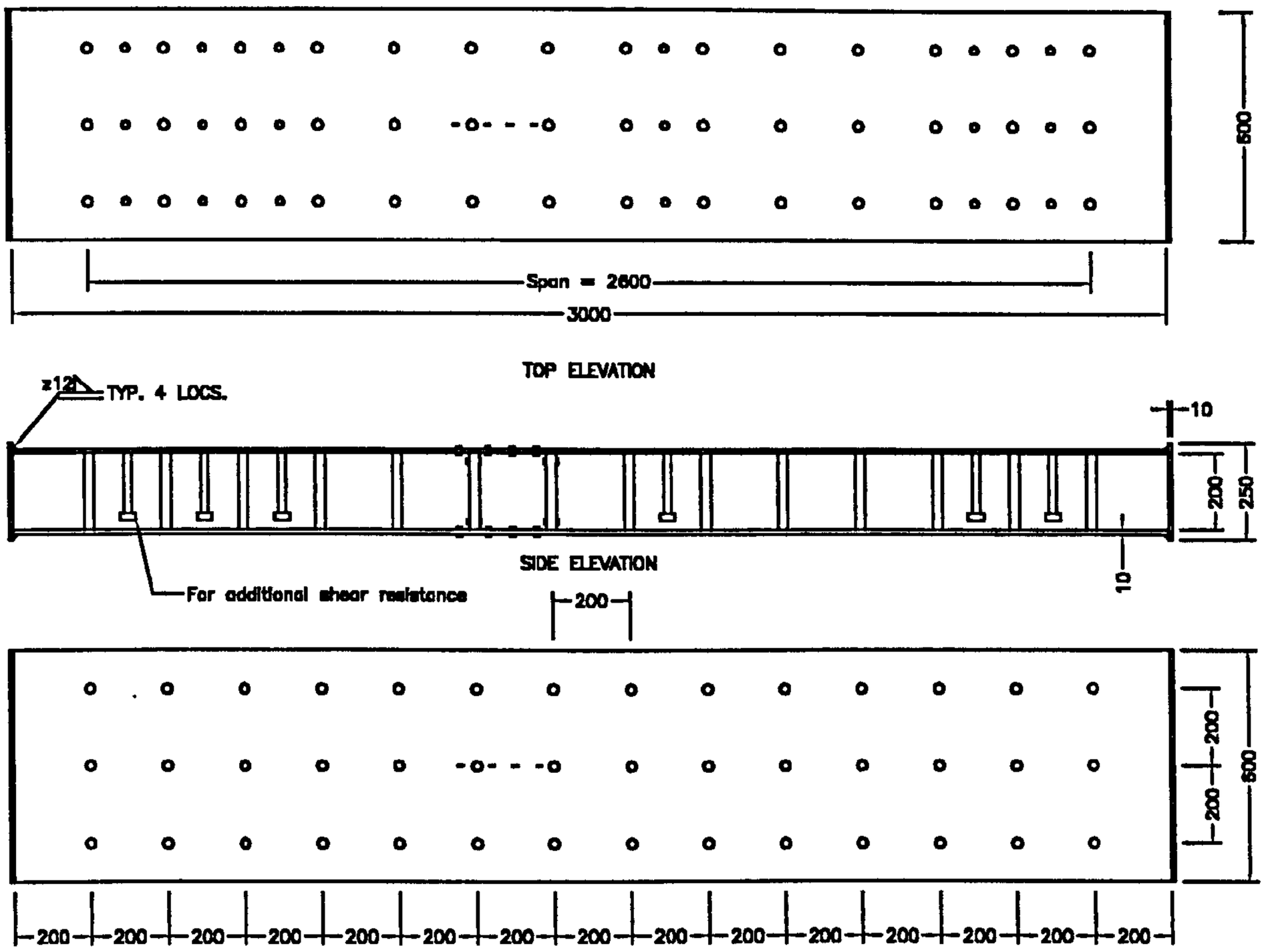

NOTES:

1. Steel plate is S355JR (Grade 50).
2. Strain gauges are located on the steel plates are either mid way between adjacent bars or are 15mm from the bar. Strain gauges located on the bars are 15mm from the surface of the steel plate.

SERIES 2 TEST PANELS

Part 1

City4a

Design By: B.McKinley
Drawn By: B.McKinley
Date: July 1997

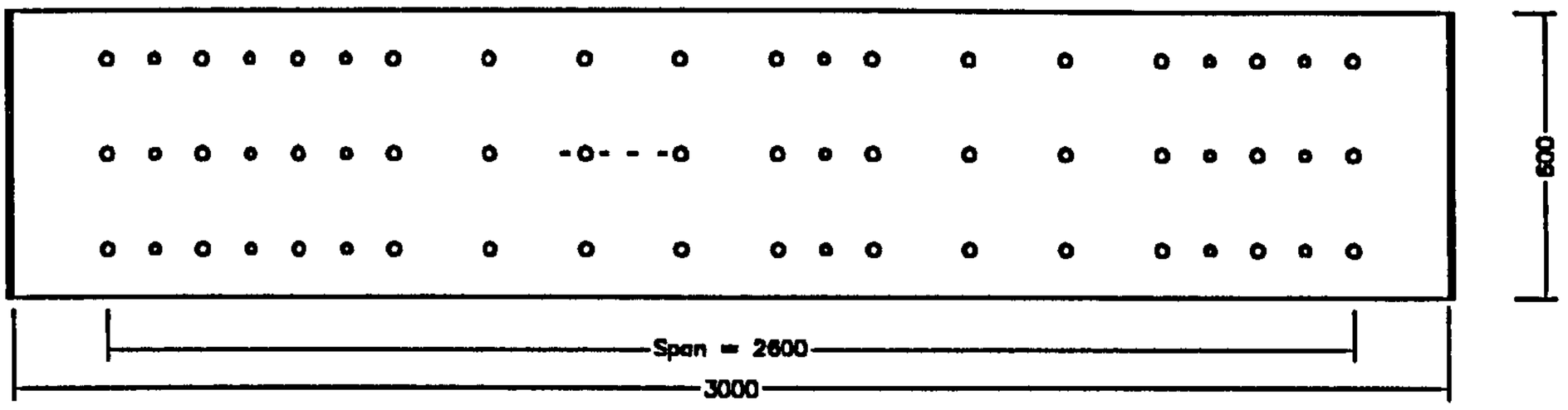

TOP ELEVATION

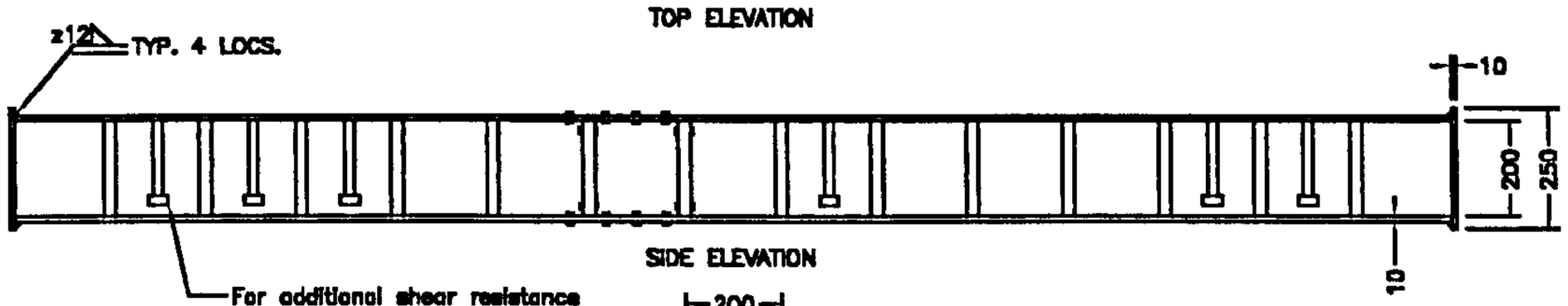

SIDE ELEVATION

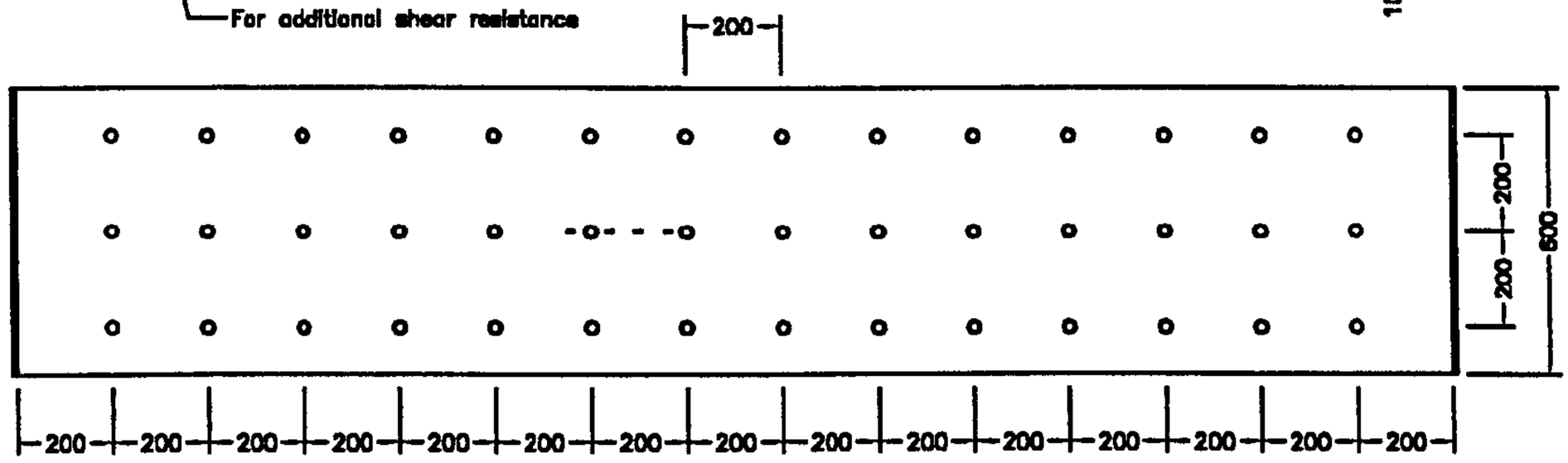

NOTES:

1. Steel plate is S355JR (Grade 50).
2. Strain gauges are located on the steel plates are either mid way between adjacent bars or are 15mm from the bar. Strain gauges located on the bars are 15mm from the surface of the steel plate.

SERIES 2 TEST PANELS

Part 1

City4b

Design By: B.McKinley
Drawn By: B.Mckinley
Date: July 1997

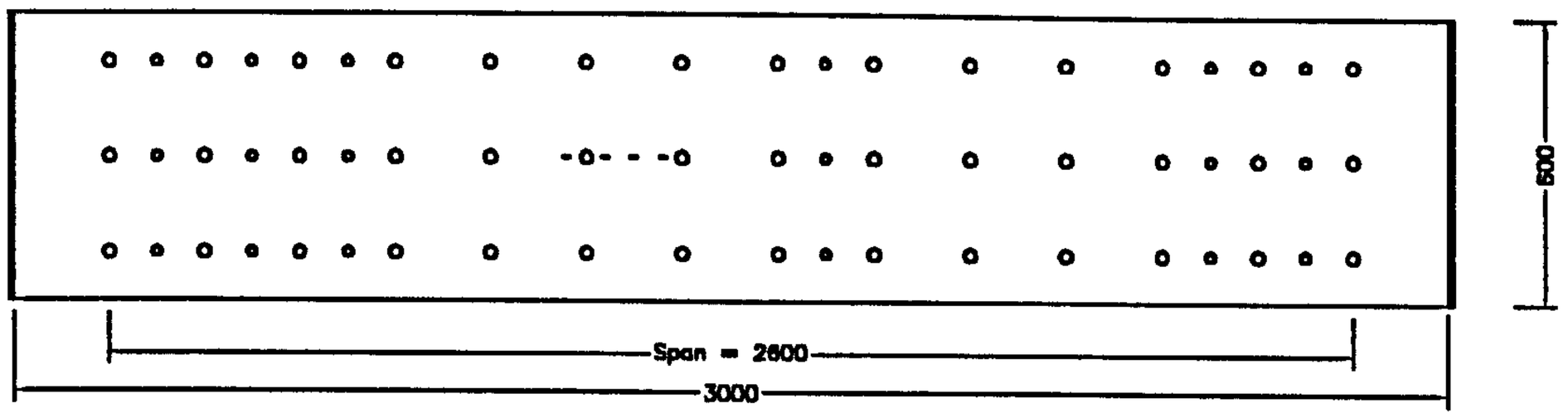

TOP ELEVATION

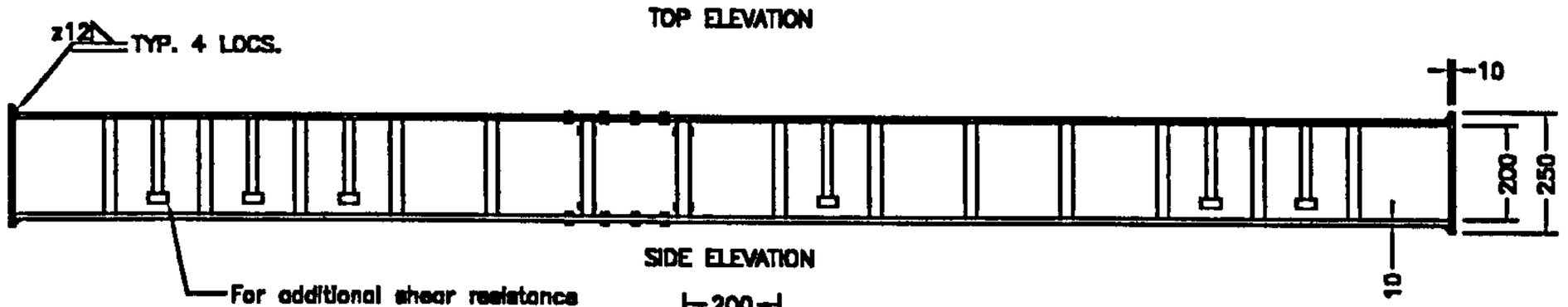

SIDE ELEVATION

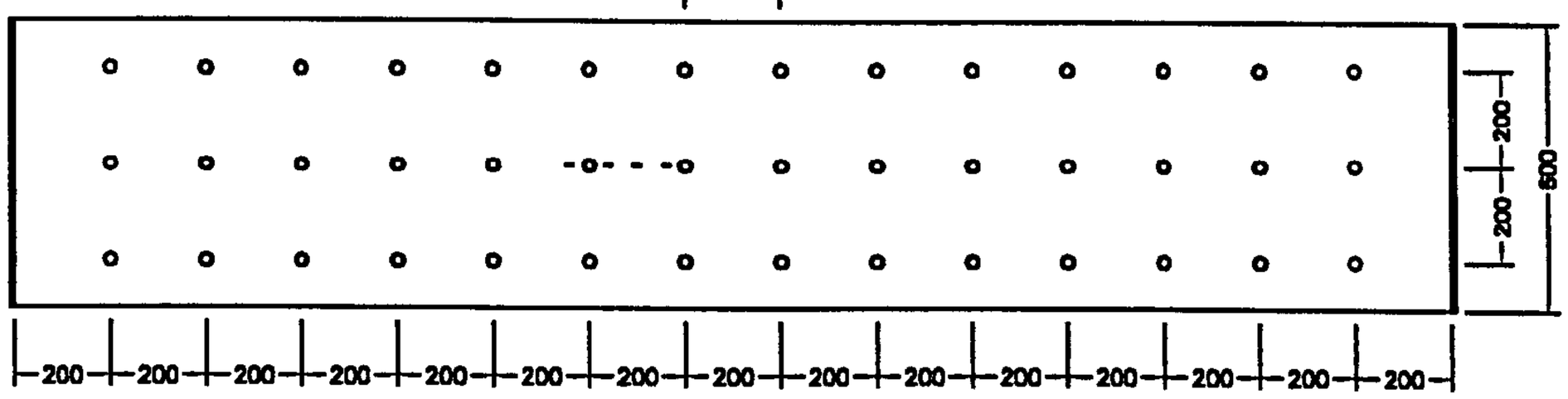

NOTES:

1. Steel plate is S355JR (Grade 50).
2. Strain gauges are located on the steel plates are either mid way between adjacent bars or are 15mm from the bar. Strain gauges located on the bars are 15mm from the surface of the steel plate.

SERIES 2 TEST PANELS
Part 1
City4c

Design By: B.McKinley
Drawn By: B.McKinley
Date: July 1997

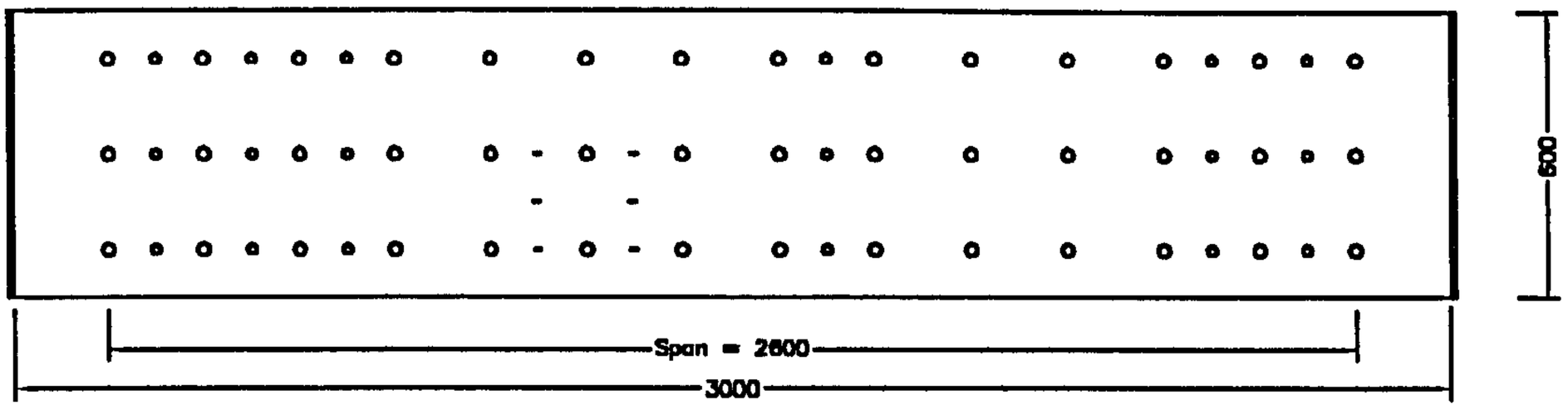

TOP ELEVATION

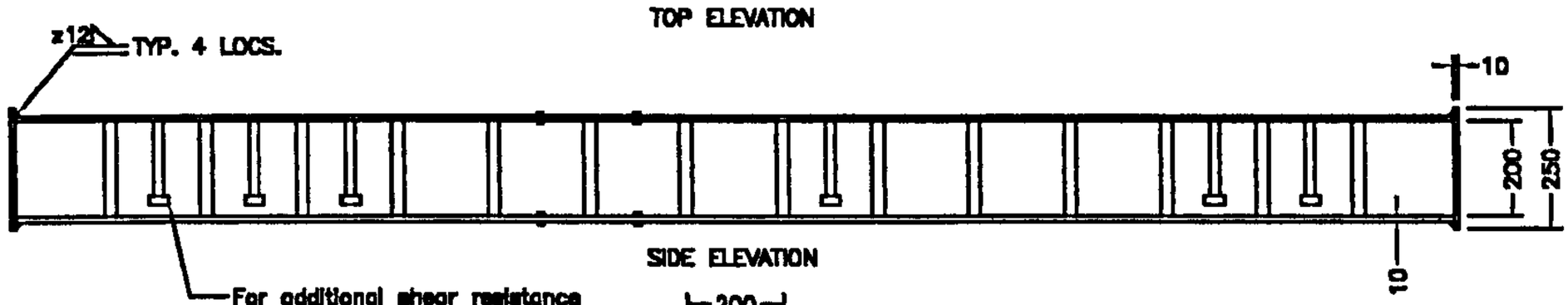

SIDE ELEVATION

NOTES:

1. Steel plate is S355JR (Grade 50).
2. Strain gauges that are located on the steel plates are mid way between adjacent bars.

SERIES 2 TEST PANELS

Part 2

City4d

Design By: B.McKinley
Drawn By: B.McKinley
Date: April 1998

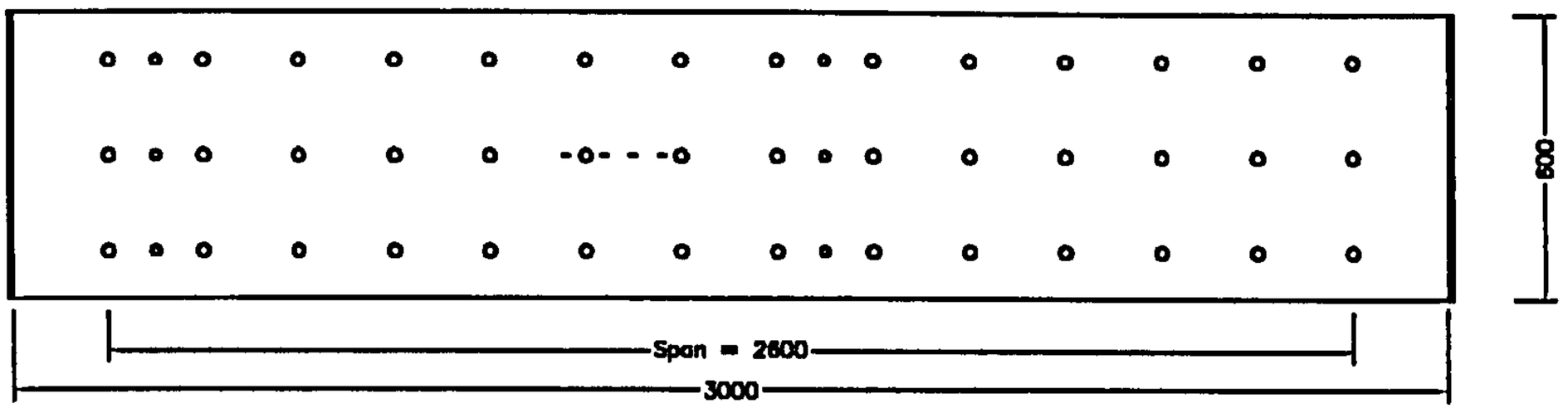

TOP ELEVATION

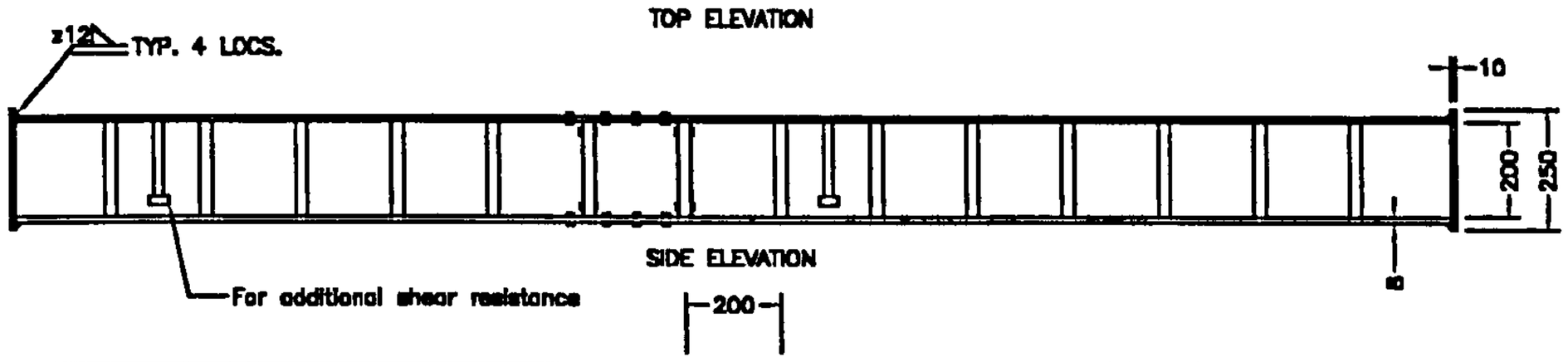

SIDE ELEVATION

NOTES:

1. Steel plate is S355JR (Grade 50).
2. Strain gauges are located on the steel plates are either mid way between adjacent bars or are 15mm from the bar. Strain gauges located on the bars are 15mm from the surface of the steel plate.

SERIES 2 TEST PANELS

Part 1

City5

Design By: B.McKinley
Drawn By: B.McKinley
Date: July 1997

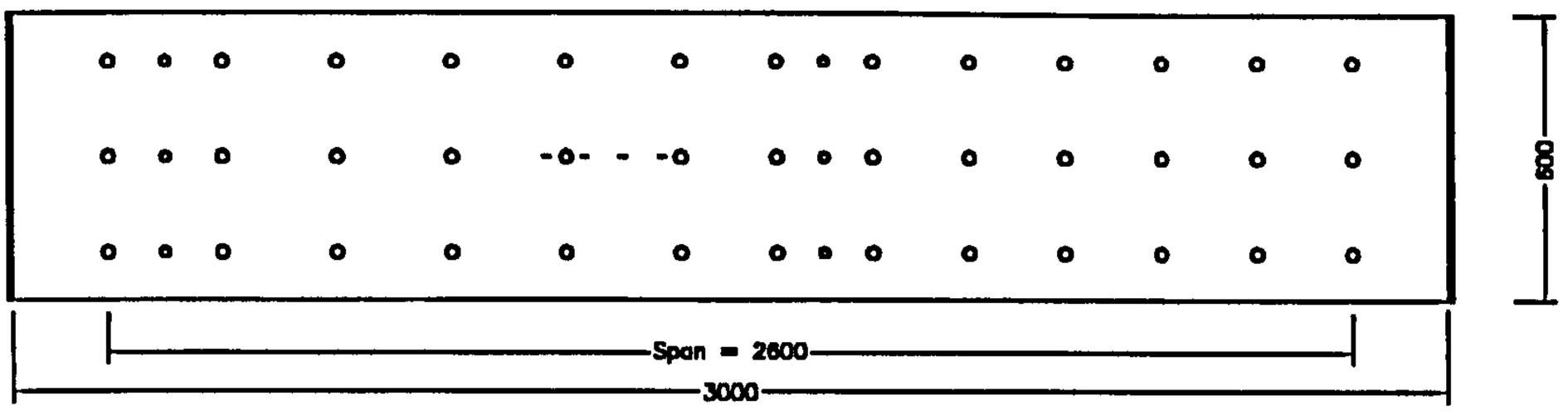

TOP ELEVATION

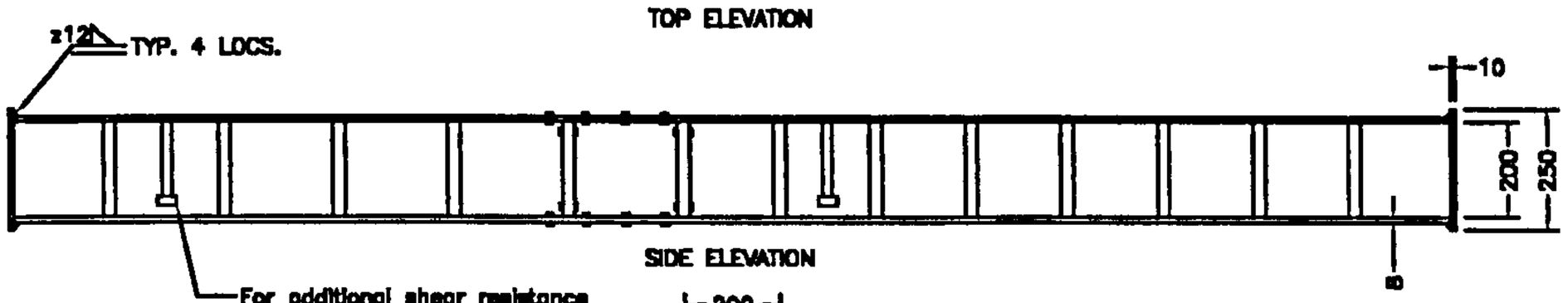

SIDE ELEVATION

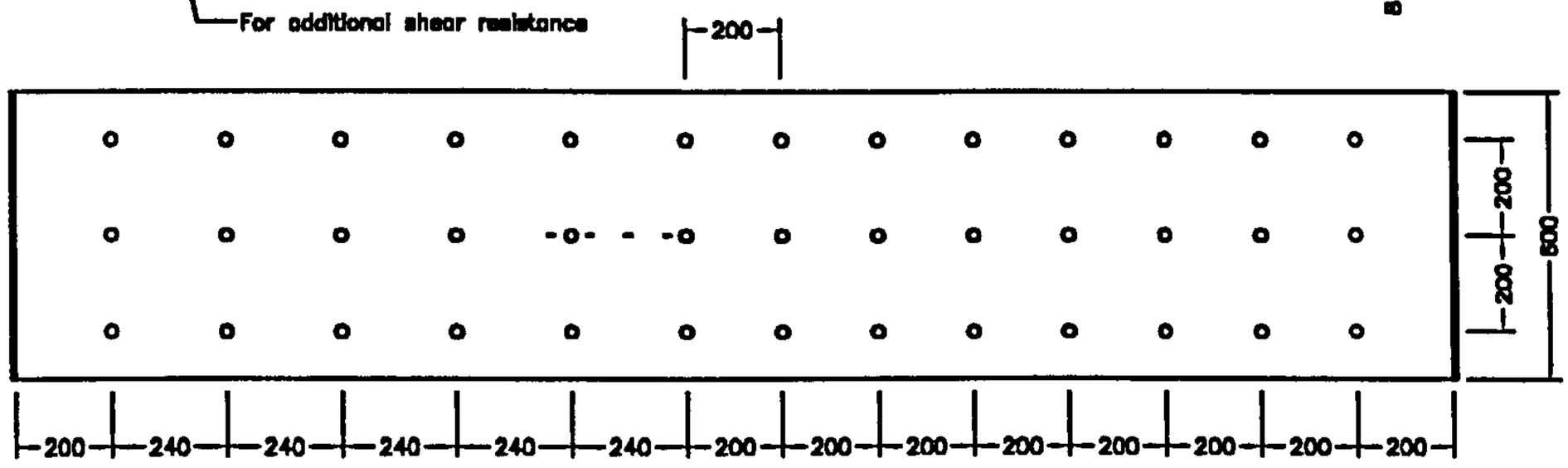

NOTES:

1. Steel plate is S355JR (Grade 50).
2. Strain gauges are located on the steel plates are either mid way between adjacent bars or are 15mm from the bar. Strain gauges located on the bars are 15mm from the surface of the steel plate.

SERIES 2 TEST PANELS

Part 1

City6

Design By: B.McKinley
Drawn By: B.McKinley
Date: July 1997

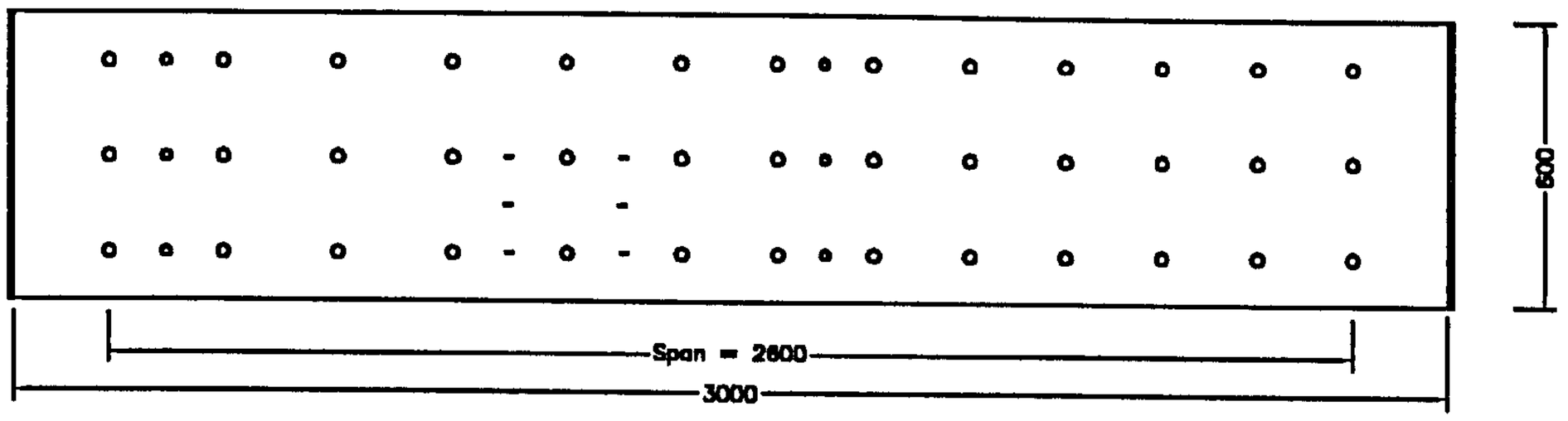

TOP ELEVATION

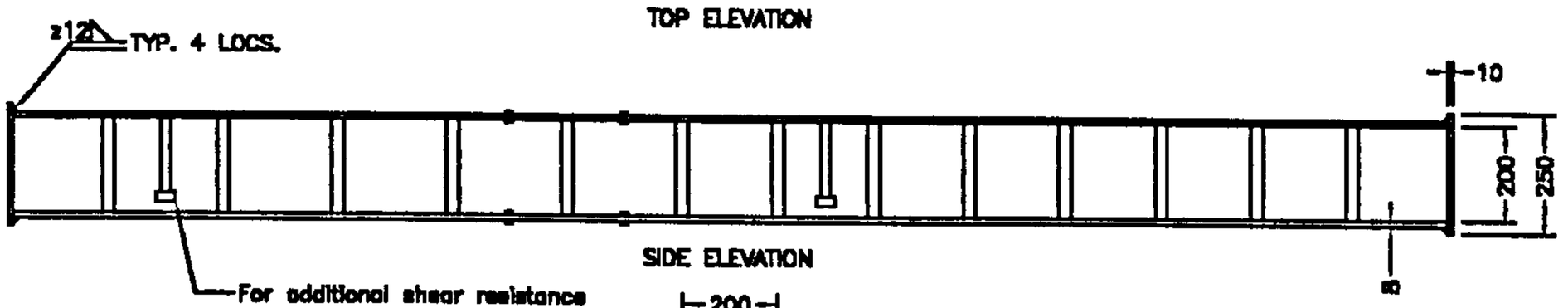

SIDE ELEVATION

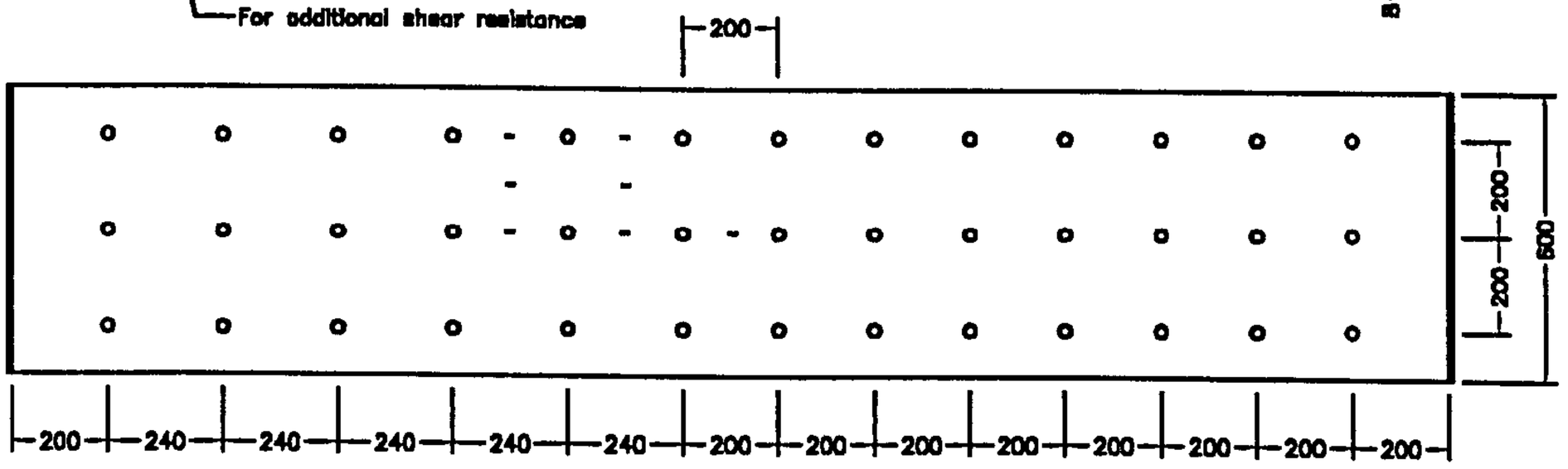

NOTES:

1. Steel plate is S355JR (Grade 50).
2. Strain gauges that are located on the steel plates are mid way between adjacent bars.

SERIES 2 TEST PANELS

Part 2

City6b

Design By: B.McKinley
Drawn By: B.Mckinley
Date: April 1998

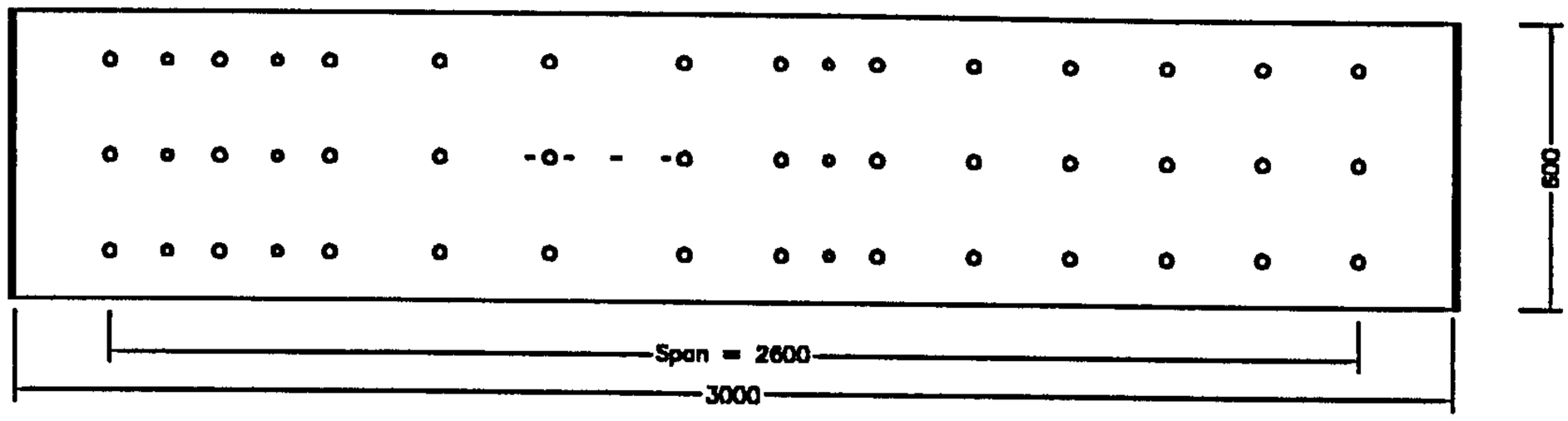

TOP ELEVATION

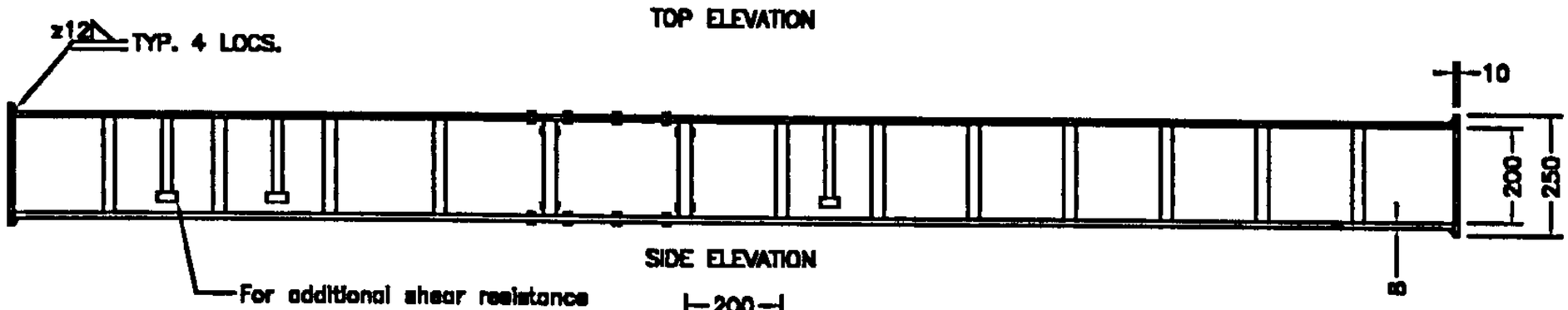

SIDE ELEVATION

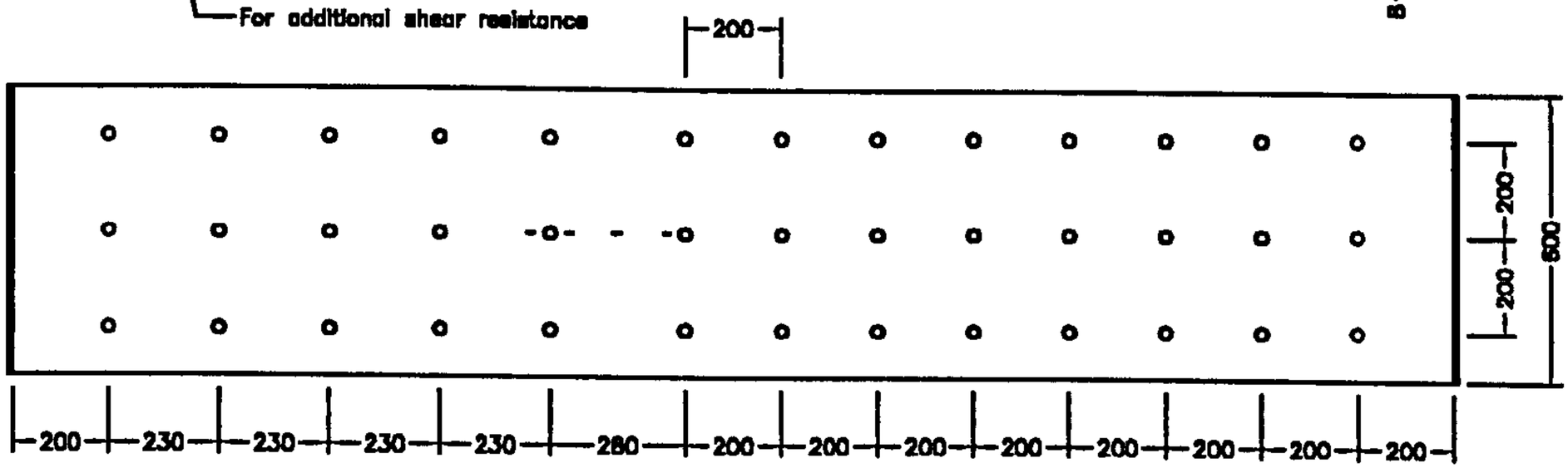

NOTES:

1. Steel plate is S355JR (Grade 50).
2. Strain gauges are located on the steel plates are elther mid way between adjacent bars or are 15mm from the bar. Strain gauges located on the bars are 15mm from the surface of the steel plate.

SERIES 2 TEST PANELS

Part 1

City7

Design By: B.McKinley
Drawn By: B.McKinley
Date: July 1997

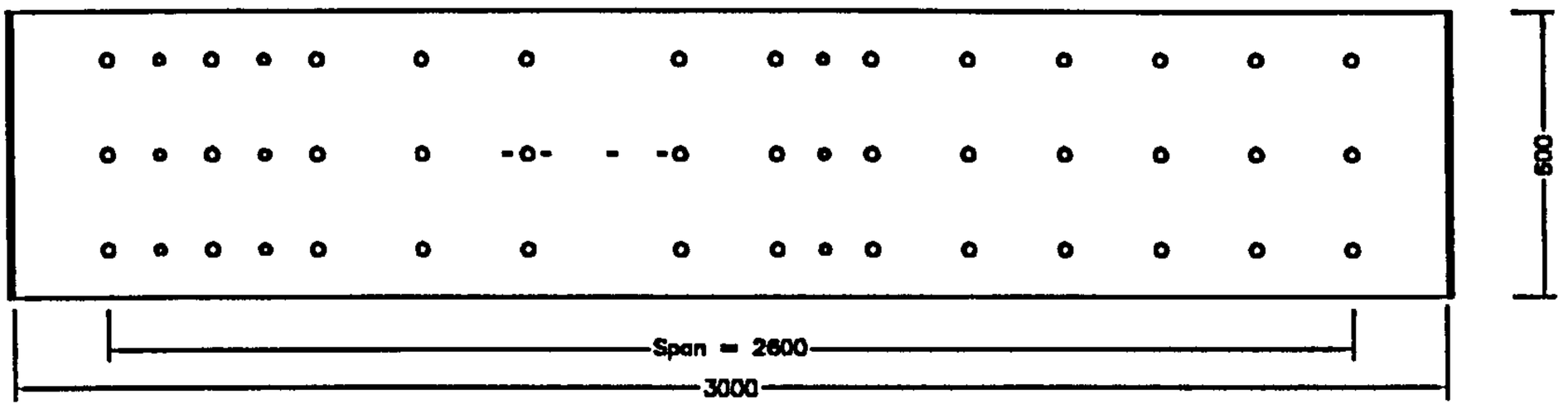

TOP ELEVATION

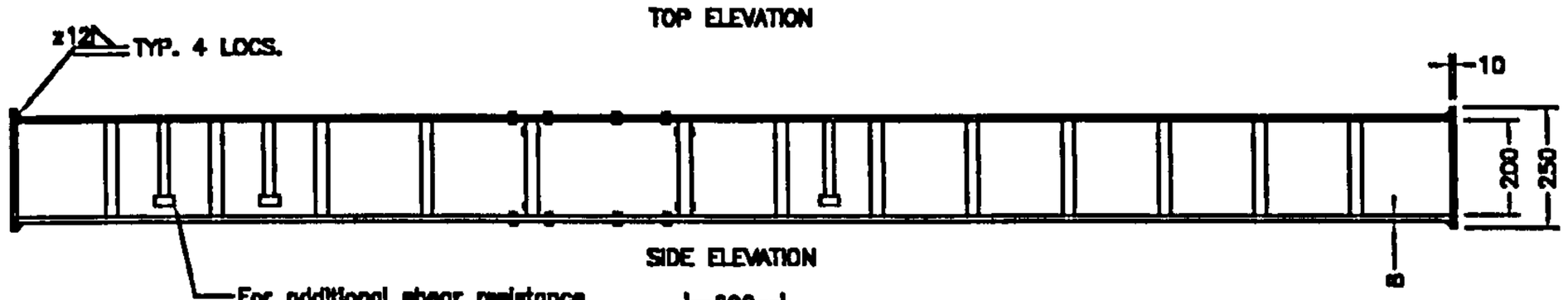

SIDE ELEVATION

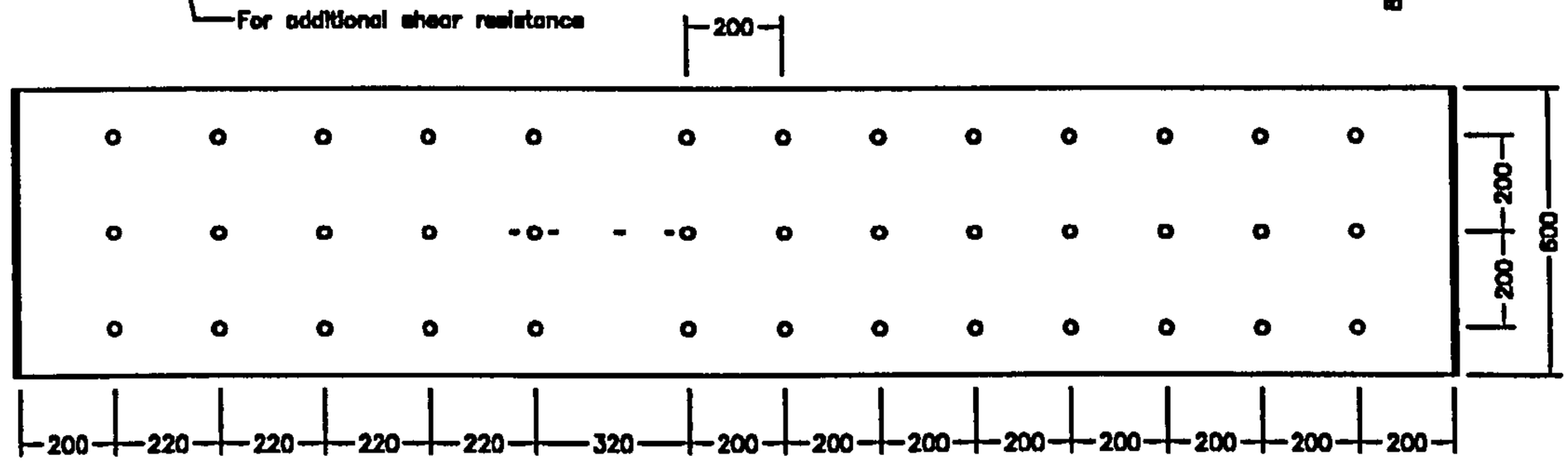

NOTES:

1. Steel plate is S355JR (Grade 50).
2. Strain gauges are located on the steel plates are either mid way between adjacent bars or are 15mm from the bar. Strain gauges located on the bars are 15mm from the surface of the steel plate.

SERIES 2 TEST PANELS

Part 1

City8

Design By: B.McKinley
Drawn By: B.Mckinley
Date: July 1997

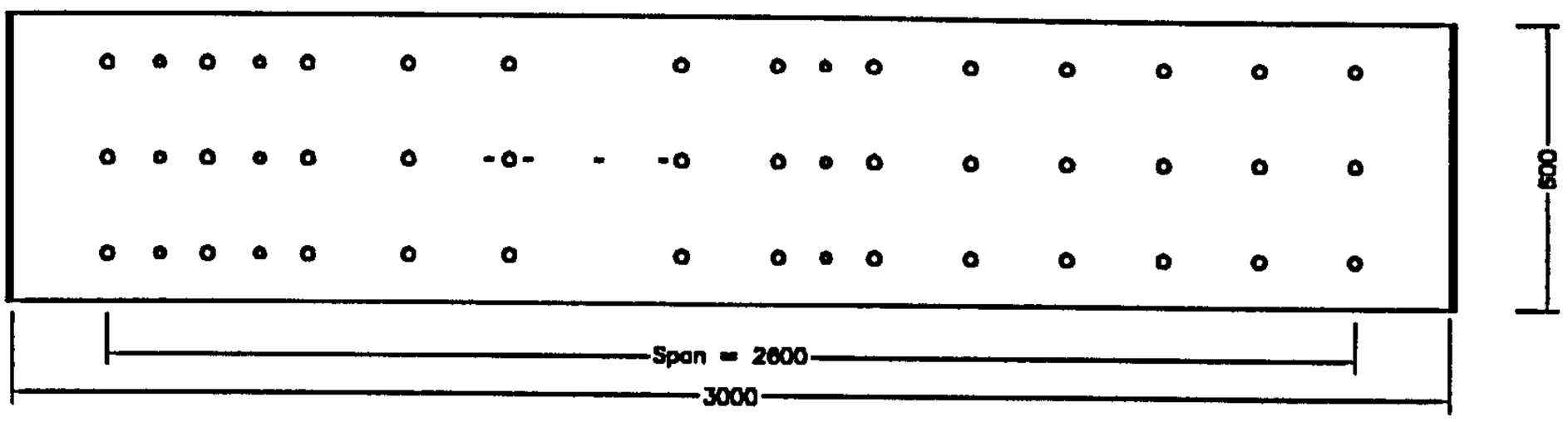

TOP ELEVATION

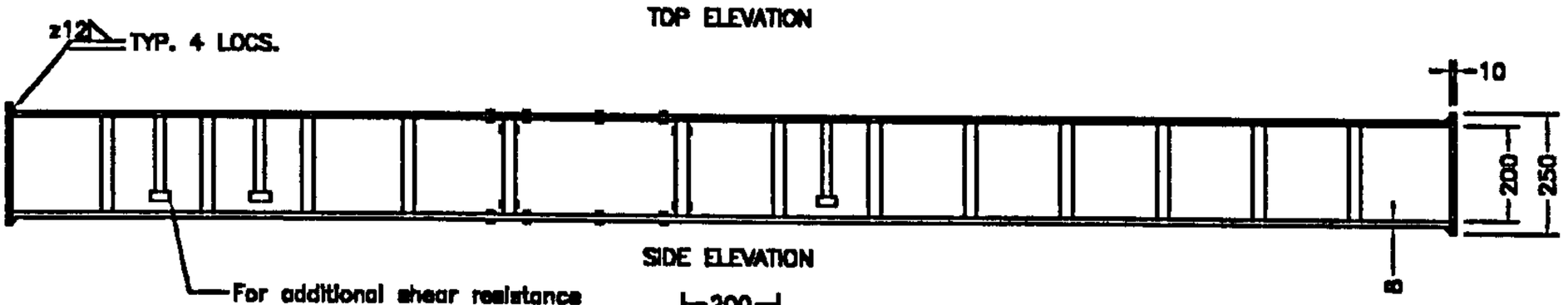

SIDE ELEVATION

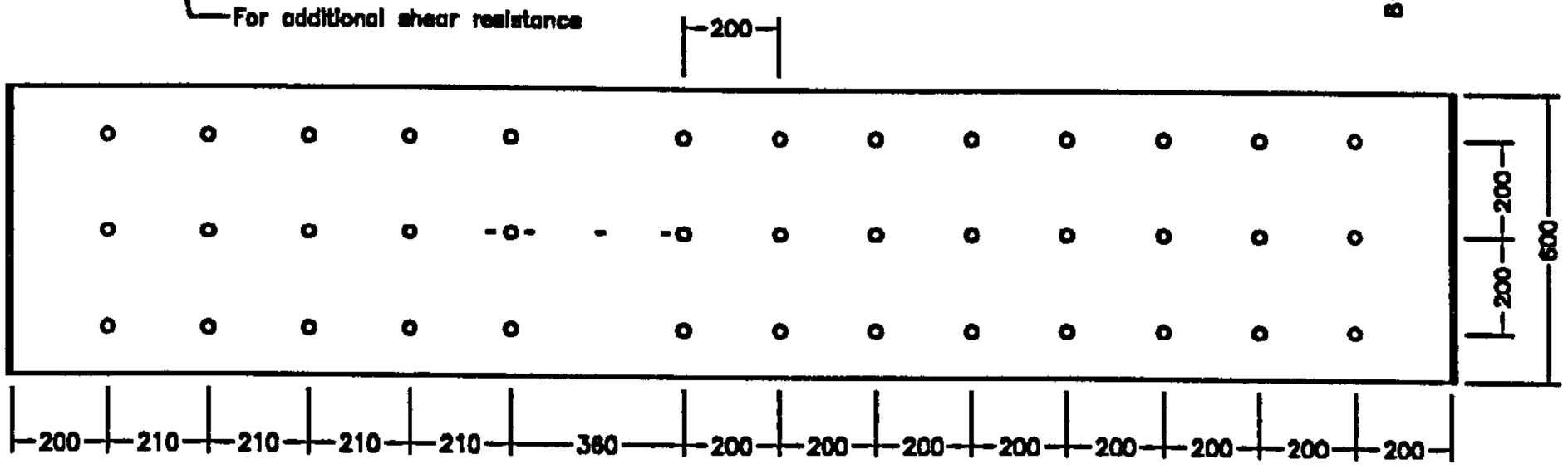

NOTES:

1. Steel plate is S355JR (Grade 50).
2. Strain gauges are located on the steel plates are either mid way between adjacent bars or are 15mm from the bar. Strain gauges located on the bars are 15mm from the surface of the steel plate.

SERIES 2 TEST PANELS

Part 1

City9

Design By: B.McKinley
Drawn By: B.McKinley
Date: July 1997

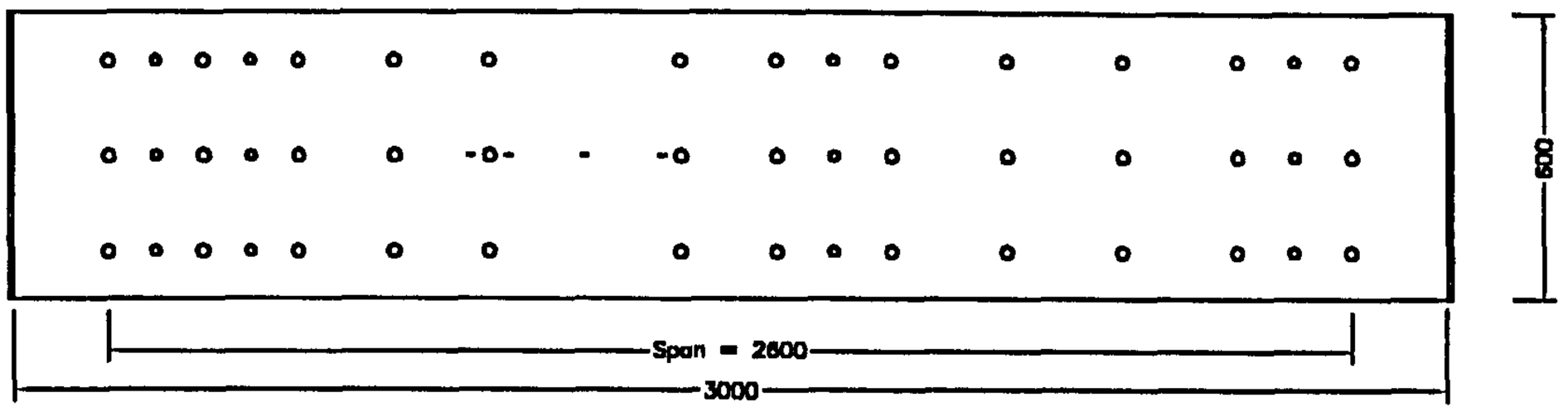

TOP ELEVATION

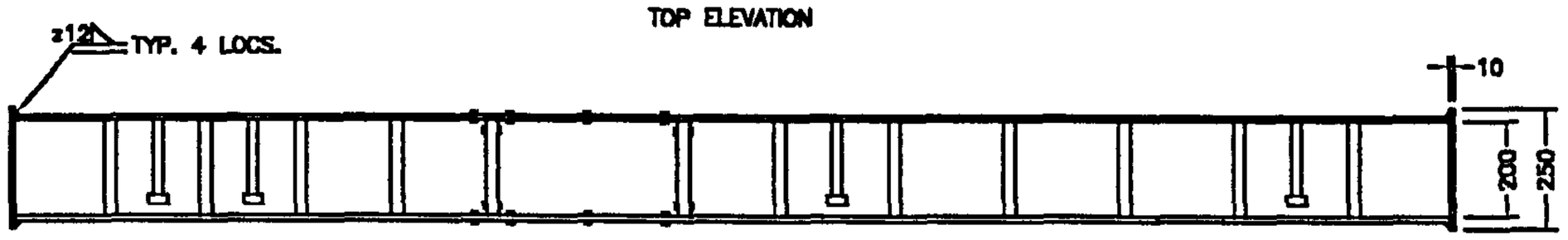

SIDE ELEVATION

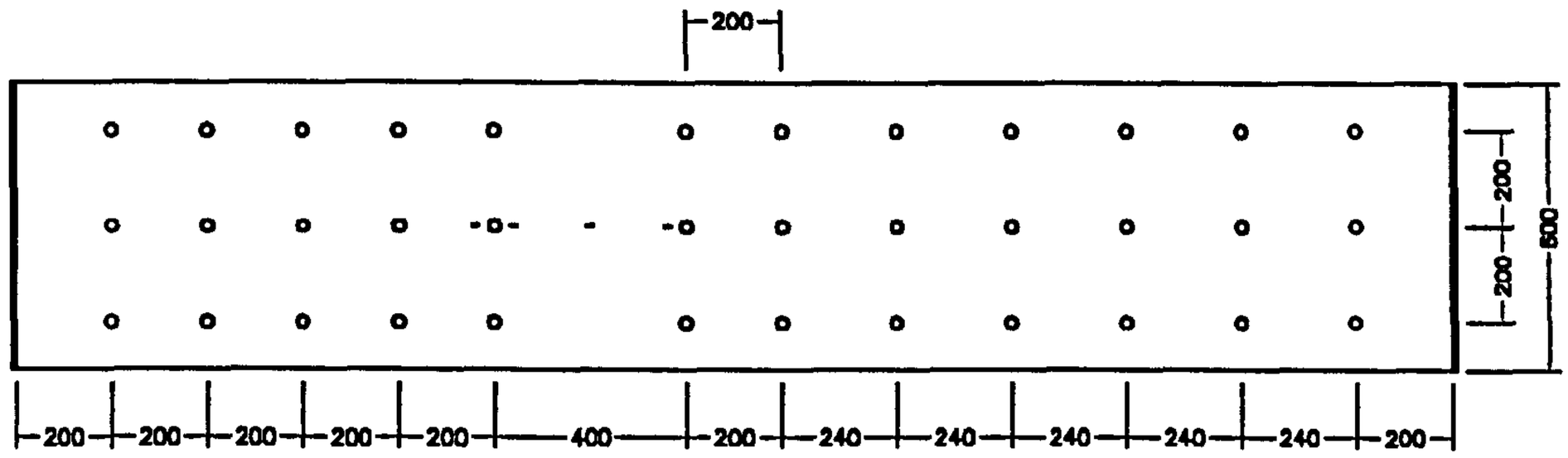

BOTTOM ELEVATION

NOTES:

1. Steel plate is S355JR (Grade 50).

SERIES 2 TEST PANELS

PART 2

CITY10

Design By: B.McKinley
Drawn By: B.Mckinley
Date: April 1998

Appendix B Plates

Plates B1 – City1

Plate B1a. Close-up of failed area showing concrete cracks originating from connector locations. Crack progression is marked in black for load (psi) and red for deflection (mm).

Plate B1b. Close-up of failed area showing local buckling of the compression plate.

Plates B2 – Stud2

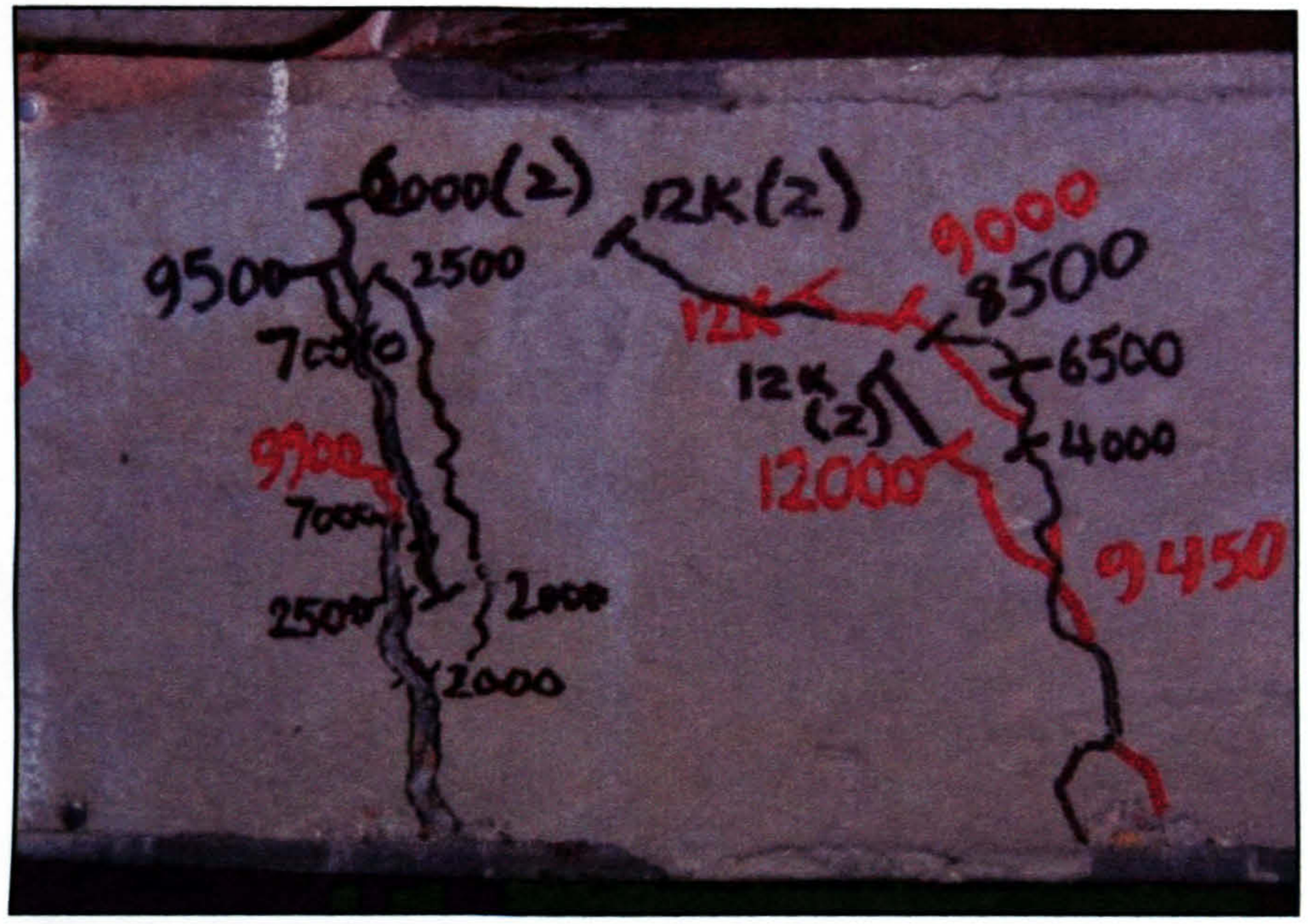

Plate B2a. Close-up of failed area showing concrete cracks originating from connector locations. Crack progression is marked in black for elastic load (psi) and red for plastic load (psi).

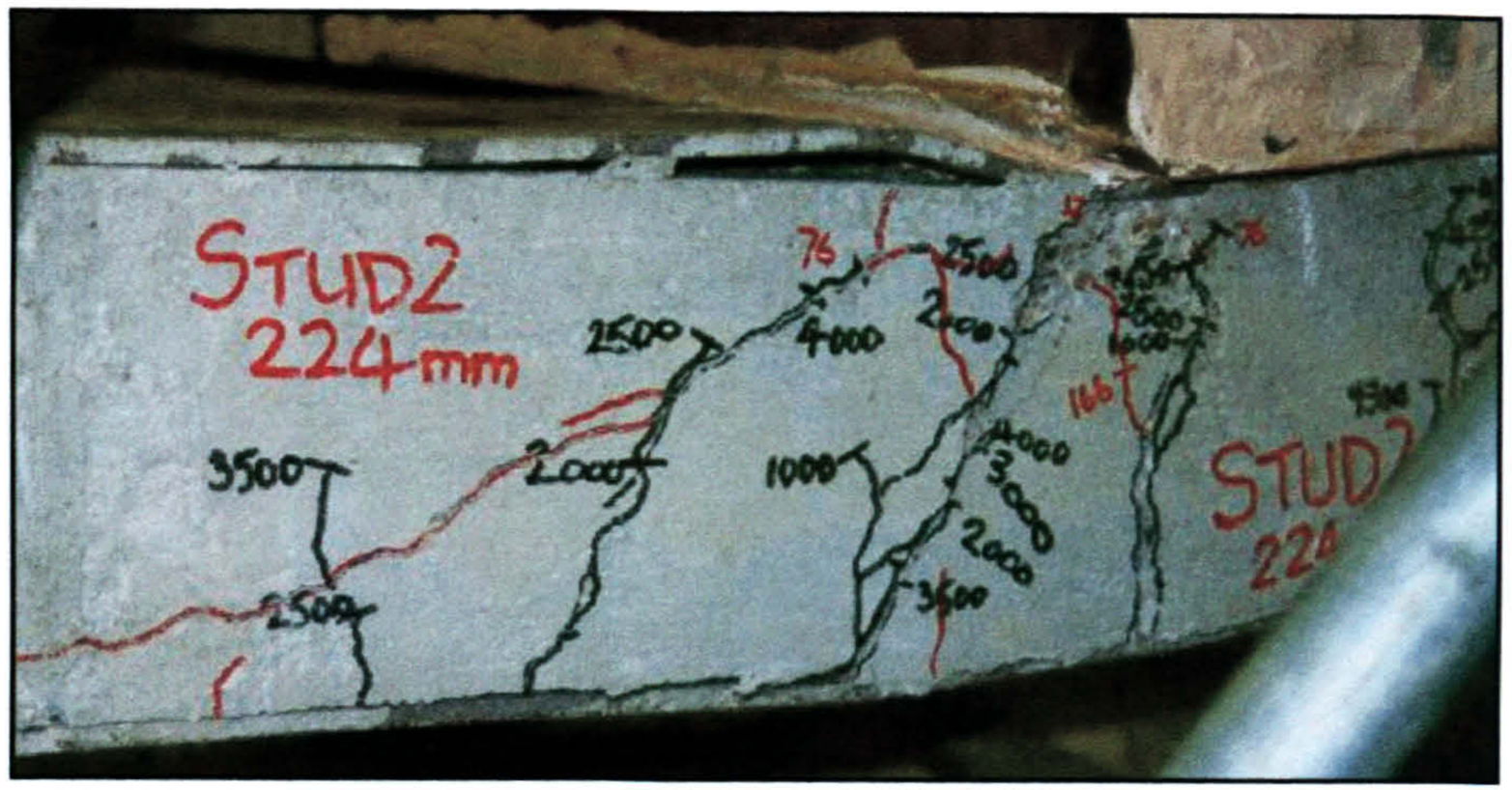

Plate B2b. Close-up of failed area showing buckling of the compression plate caused by stud pull-out.

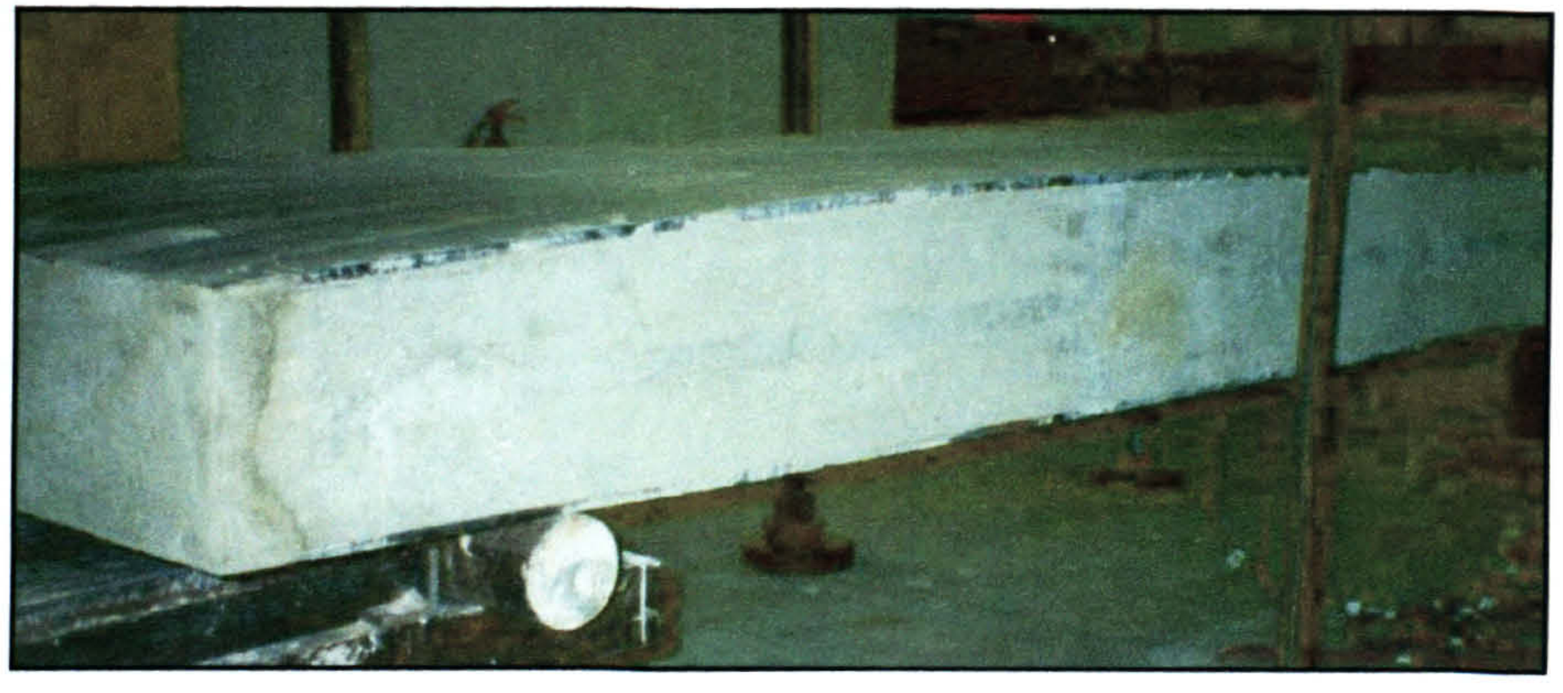

Plate B2c. Bulge in Stud2 caused by inadequate formwork.

Plates B3 – Stud2b

Plate B3b. Close-up of failed area showing buckling of the compression plate caused by stud pull-out.

Plate B3b. Stud pull-out.

Plates B4 – City3

Plate B4a. Overall view of failed specimen

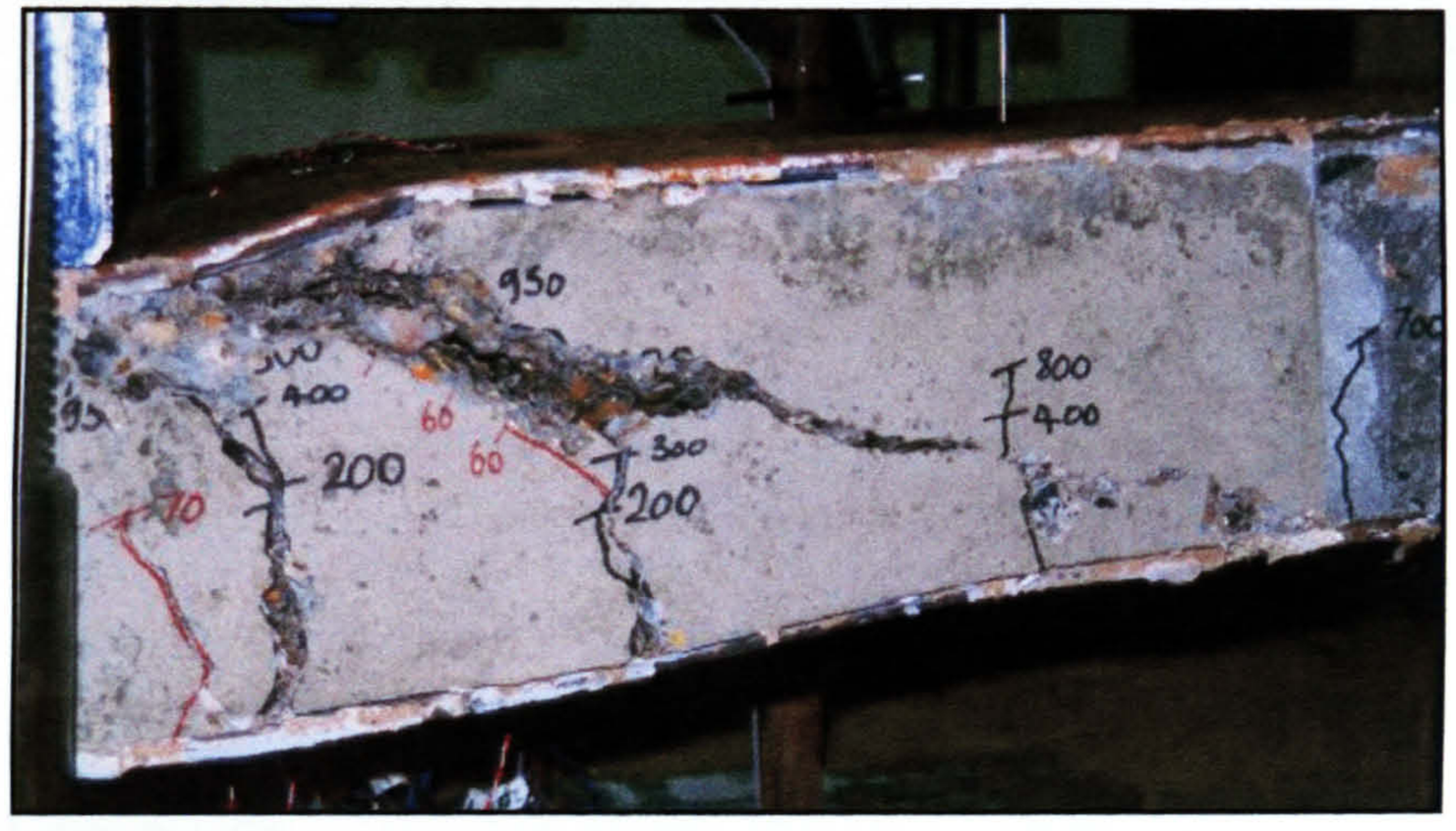

Plate B4b. Close-up of failed area showing concrete cracks originating from connector locations. Crack progression is marked in black for load (kN) and red for deflection (mm).

Plate B4c. Close-up of failed area showing connector weld failure.

Plates B5 – City4a

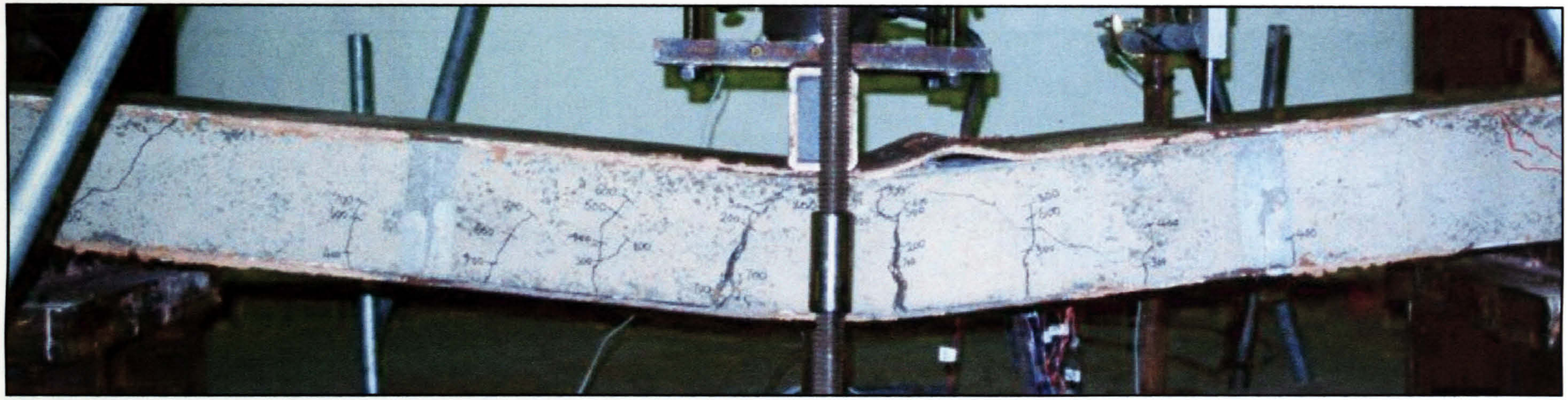

Plate B5a. Overall view of failed specimen

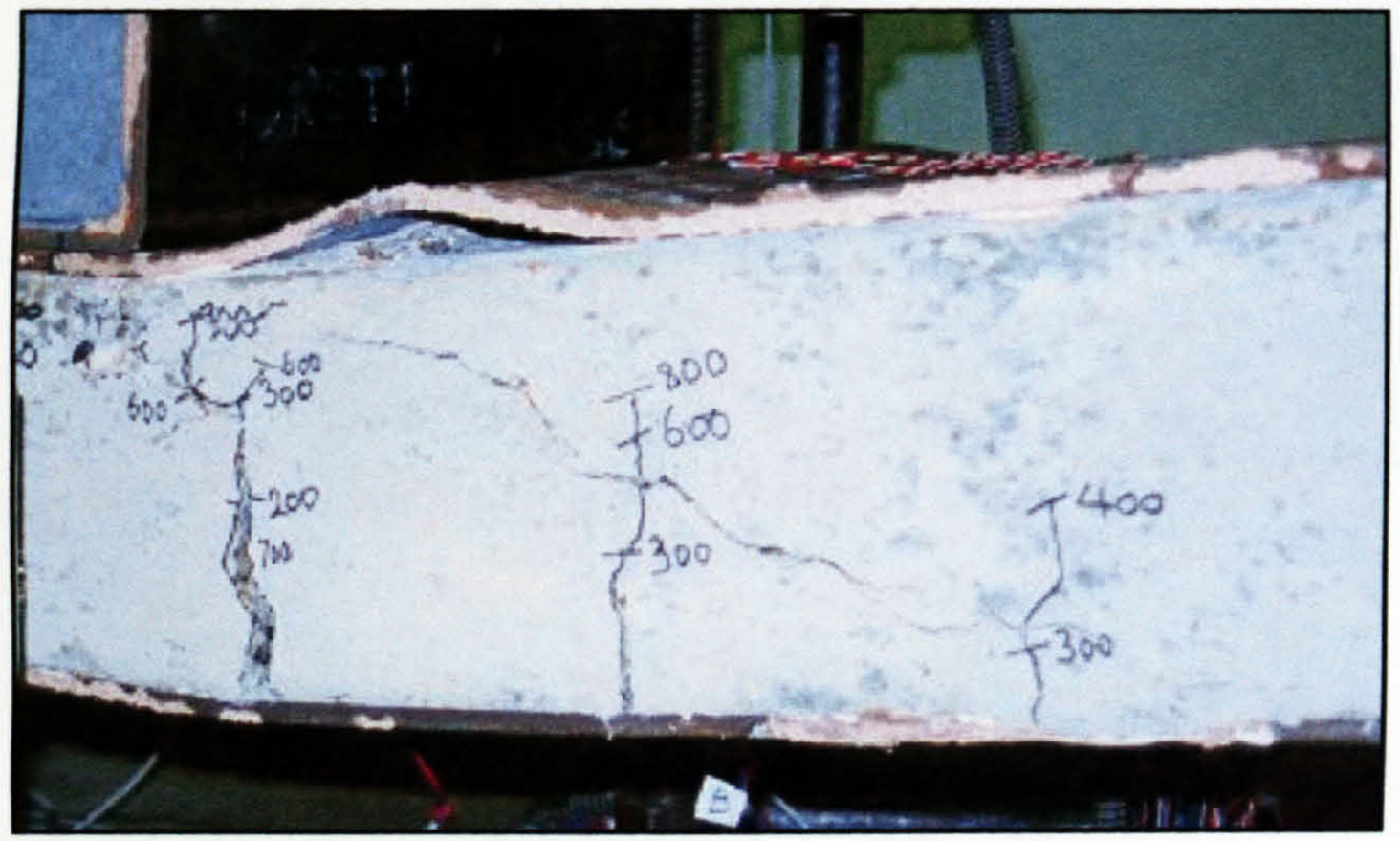

Plate B5b. Close-up of failed area showing concrete cracks originating from connector locations. Crack progression is marked in black for load (kN).

Plates B6 – City4b

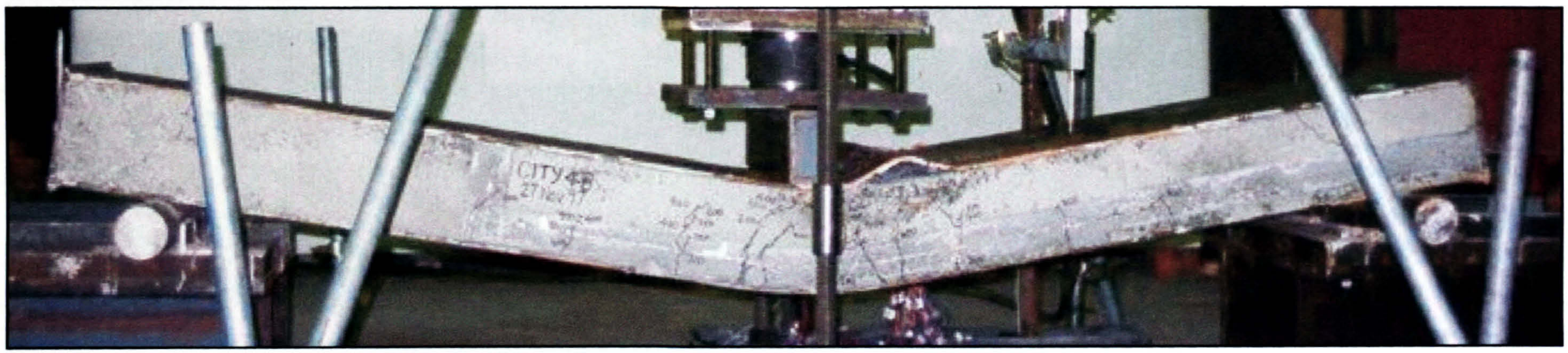

Plate B6a. Overall view of failed specimen

Plates B7 – City4c

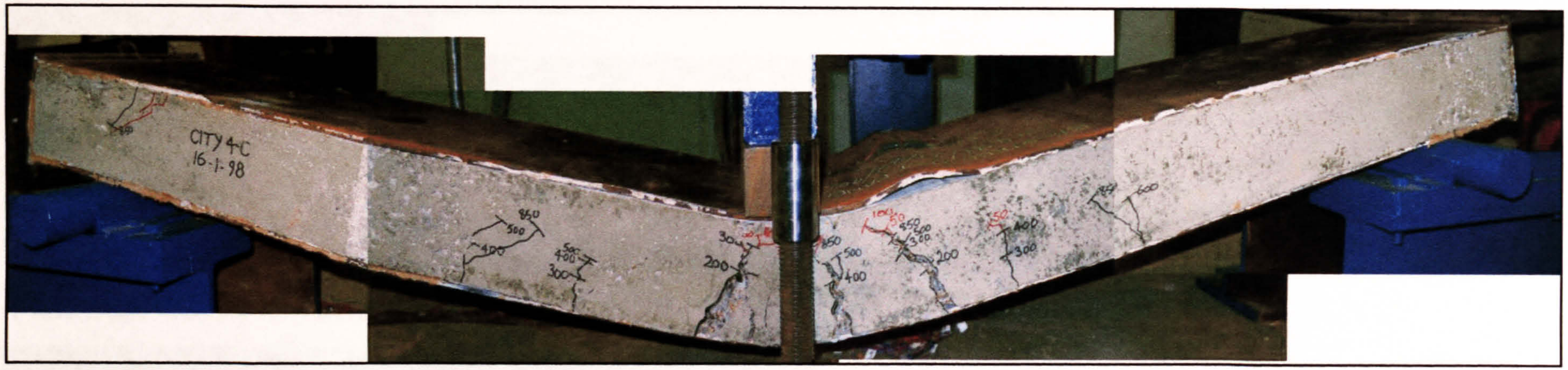

Plate B7a. Overall view of failed specimen

Plate B7b. Close-up of failed area showing concrete cracks originating from connector locations. Crack progression is marked in black for load (kN).

Plates B8 – City5

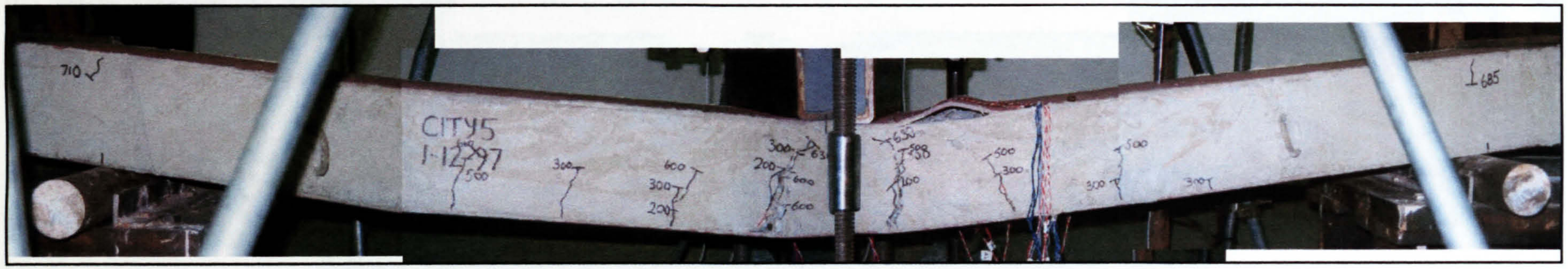

Plate B8a. Overall view of failed specimen

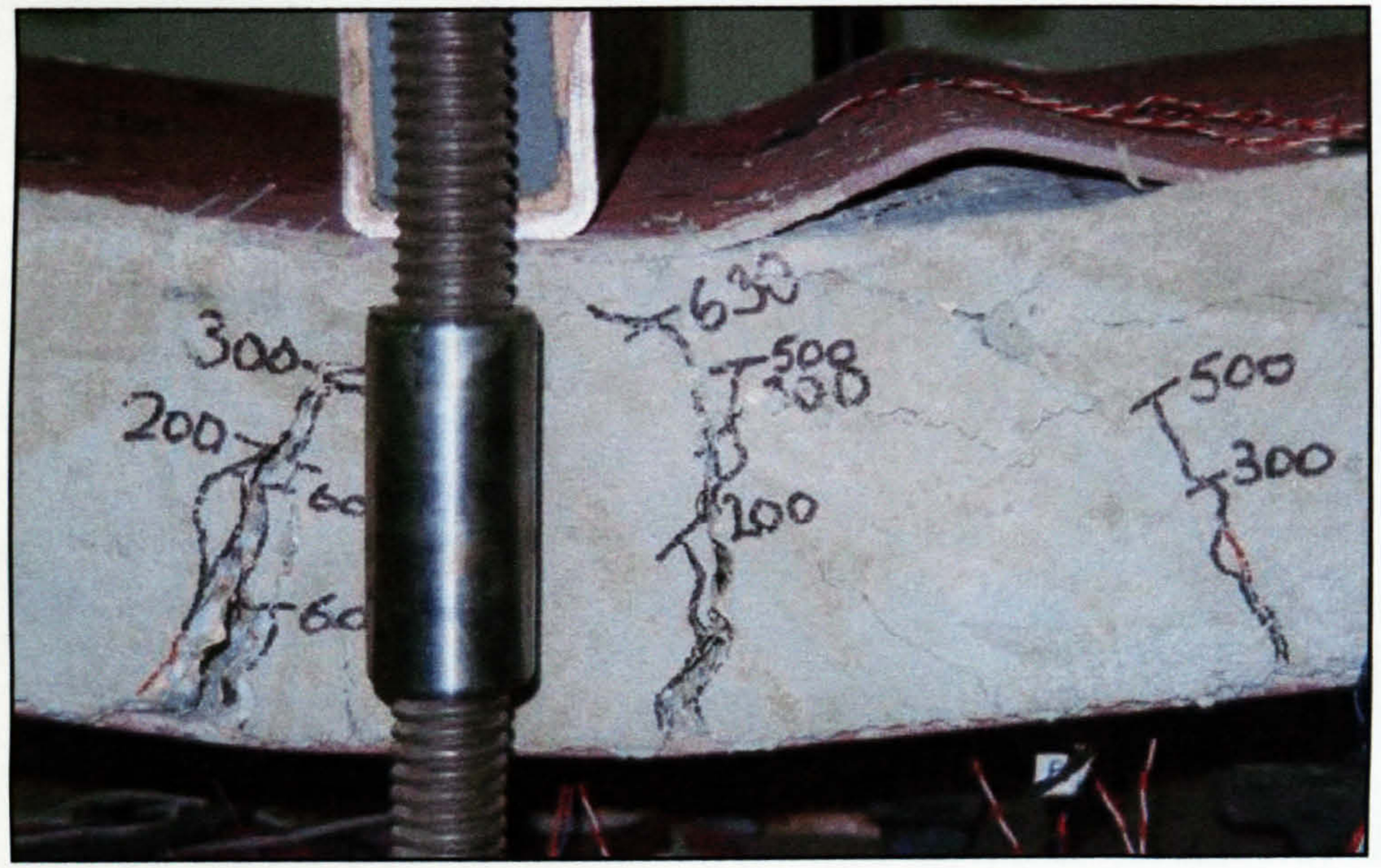

Plate B8b. Close-up of failed area showing concrete cracks originating from connector locations. Crack progression is marked in black for load (kN). Also shown is the buckling of the compression plate with evidence of concrete crushing between the two right-most cracks.

Plates B9 – City6

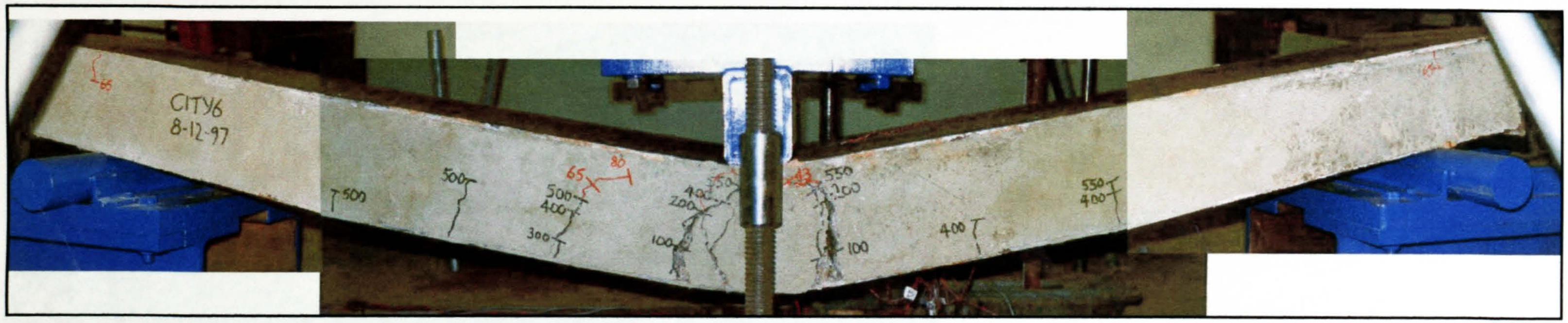

Plate B9a. Overall view of failed specimen

Plate B9b. Close-up of failed area showing tension failure of the lower plate. At the centre of the picture it can be seen that failure has initiated from the weld of the shear connector, indicated by the crescent shape within the crack.

Plates B10 – City6b

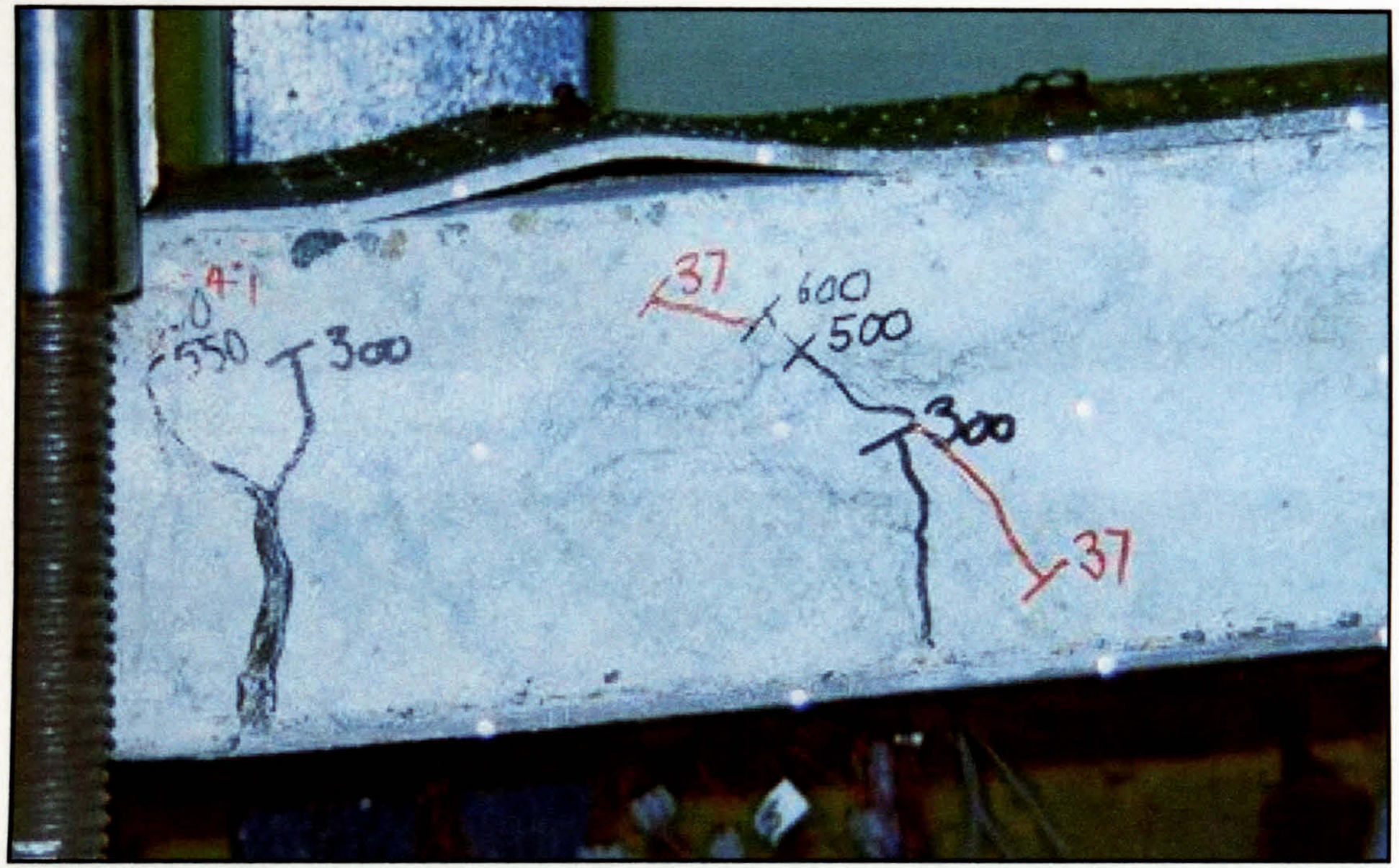

Plate B10a. Close-up of failed area showing concrete cracks originating from connector locations. Also shown is the local buckling of the compression plate.

Plates B11 – City7

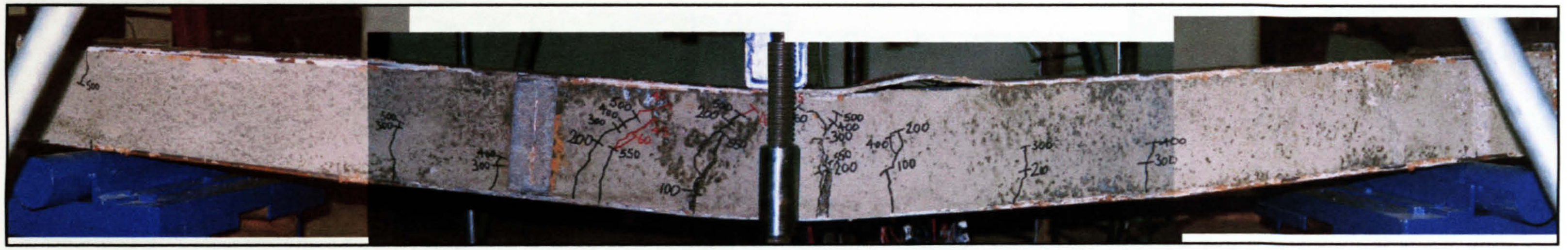

Plate B11a. Overall view of failed specimen

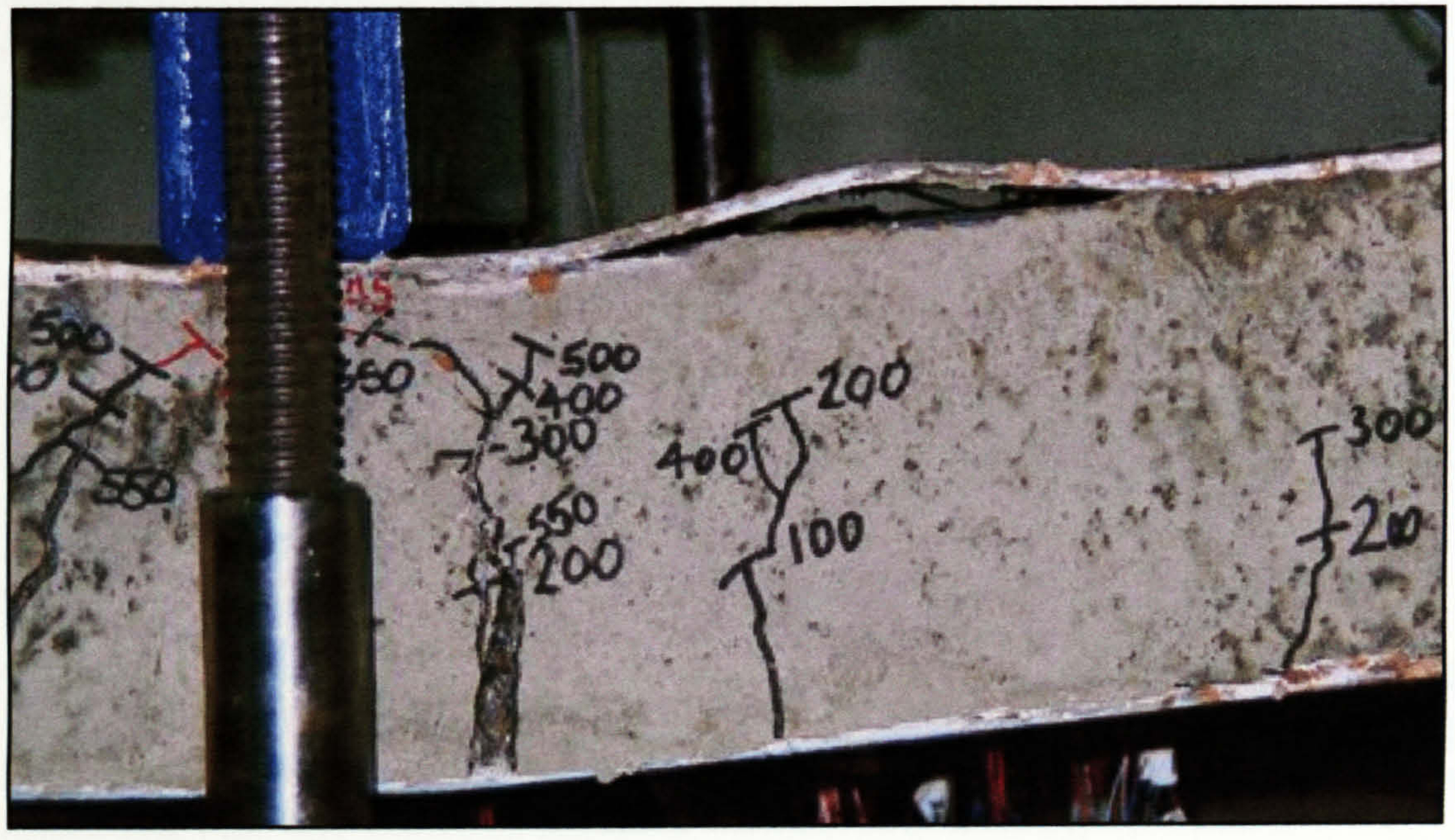

Plate B11b. Close-up of failed area showing concrete cracks originating from connector locations.

Plates B12 – City8

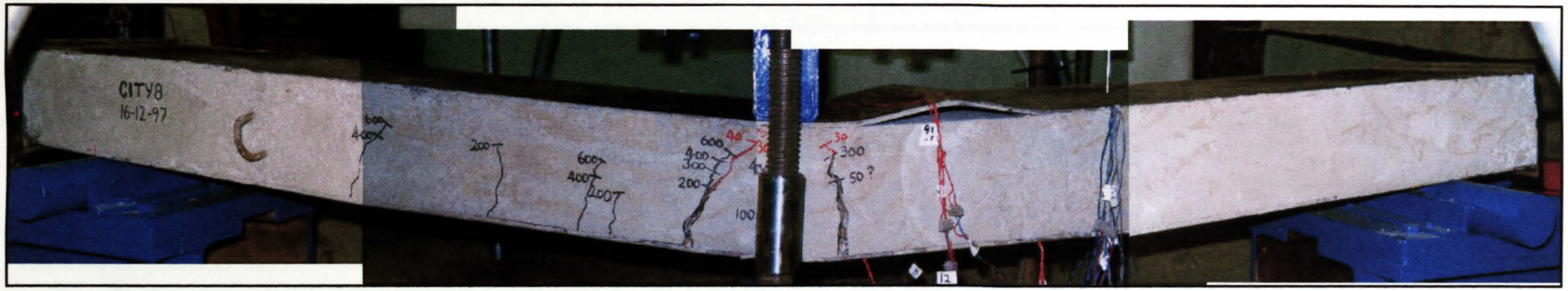

Plate B12a. Overall view of failed specimen

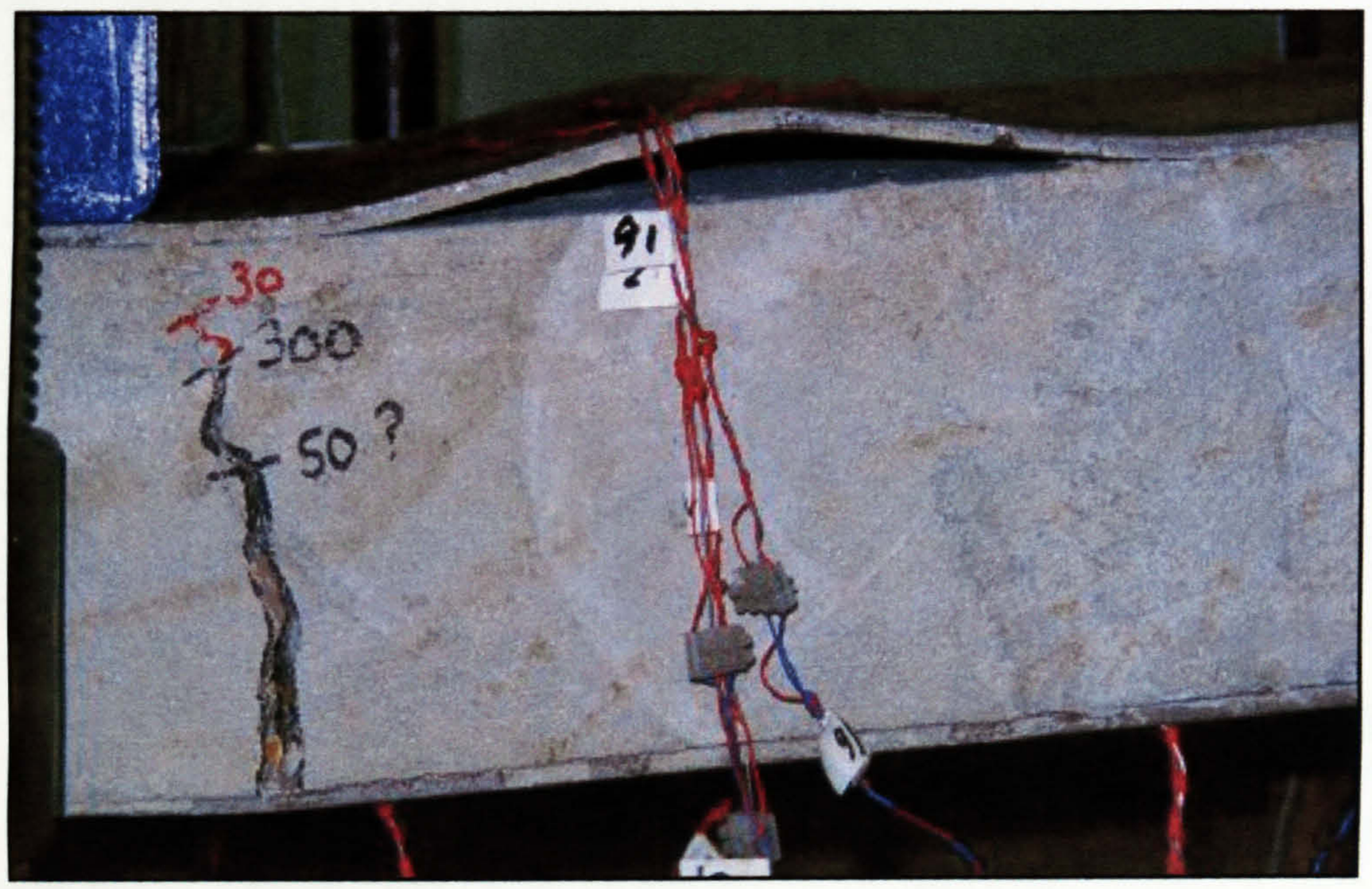

Plate B12b. Close-up of failed area showing local buckling and lack of cracking to the right of the picture, where another shear connector is located.

Plates B13 – City9

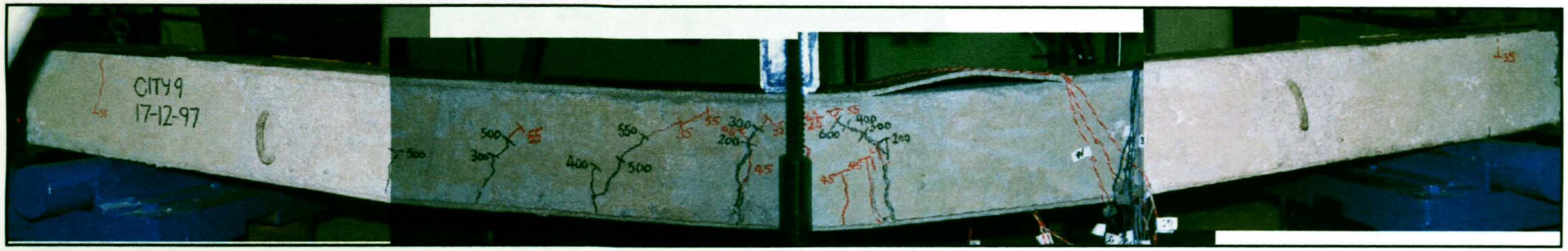

Plate B13a. Overall view of failed specimen

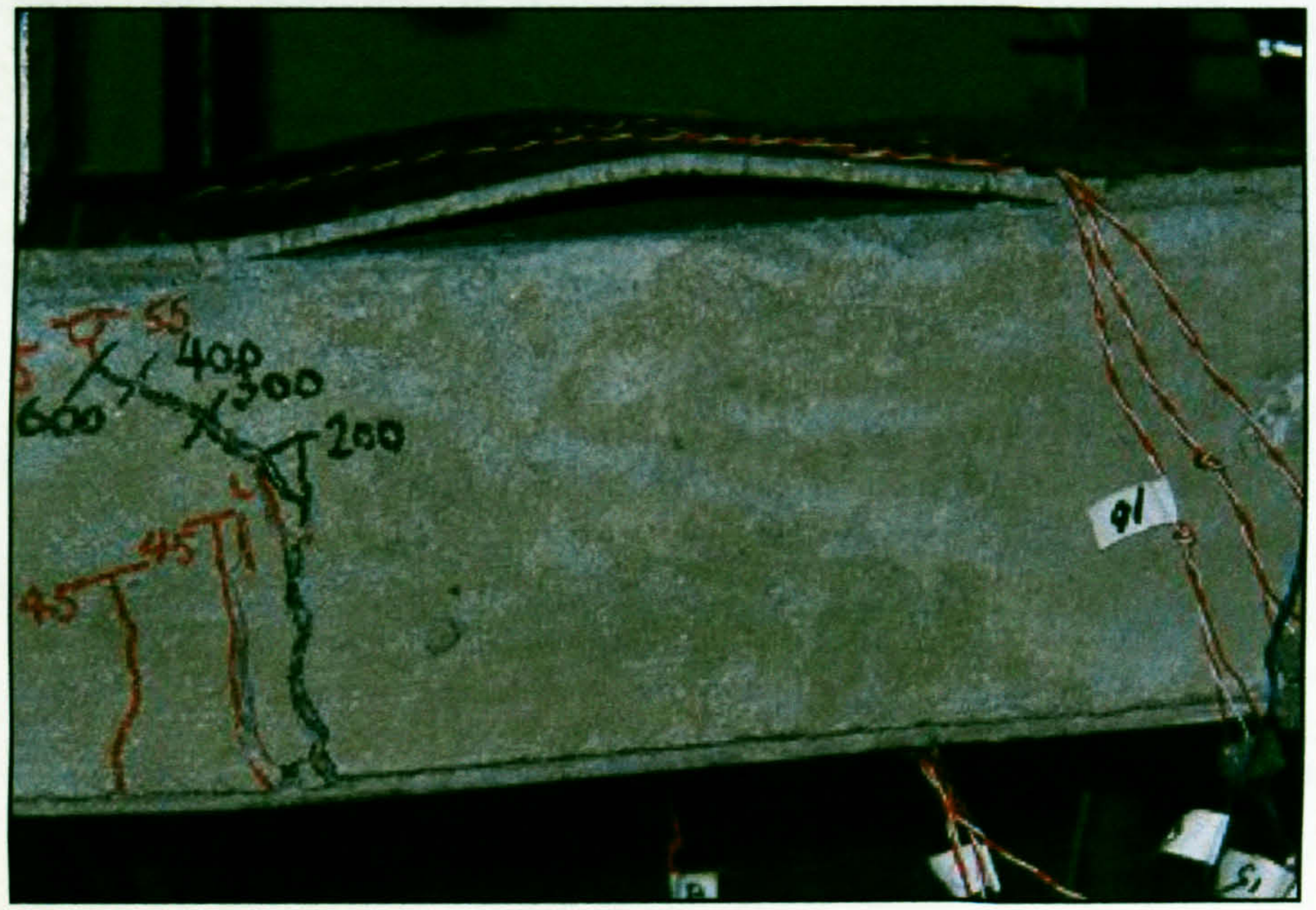

Plate B13b. Close-up of failed area showing local buckling and lack of cracking to the right of the picture, where another shear connector is located.

Plates B14 – City10

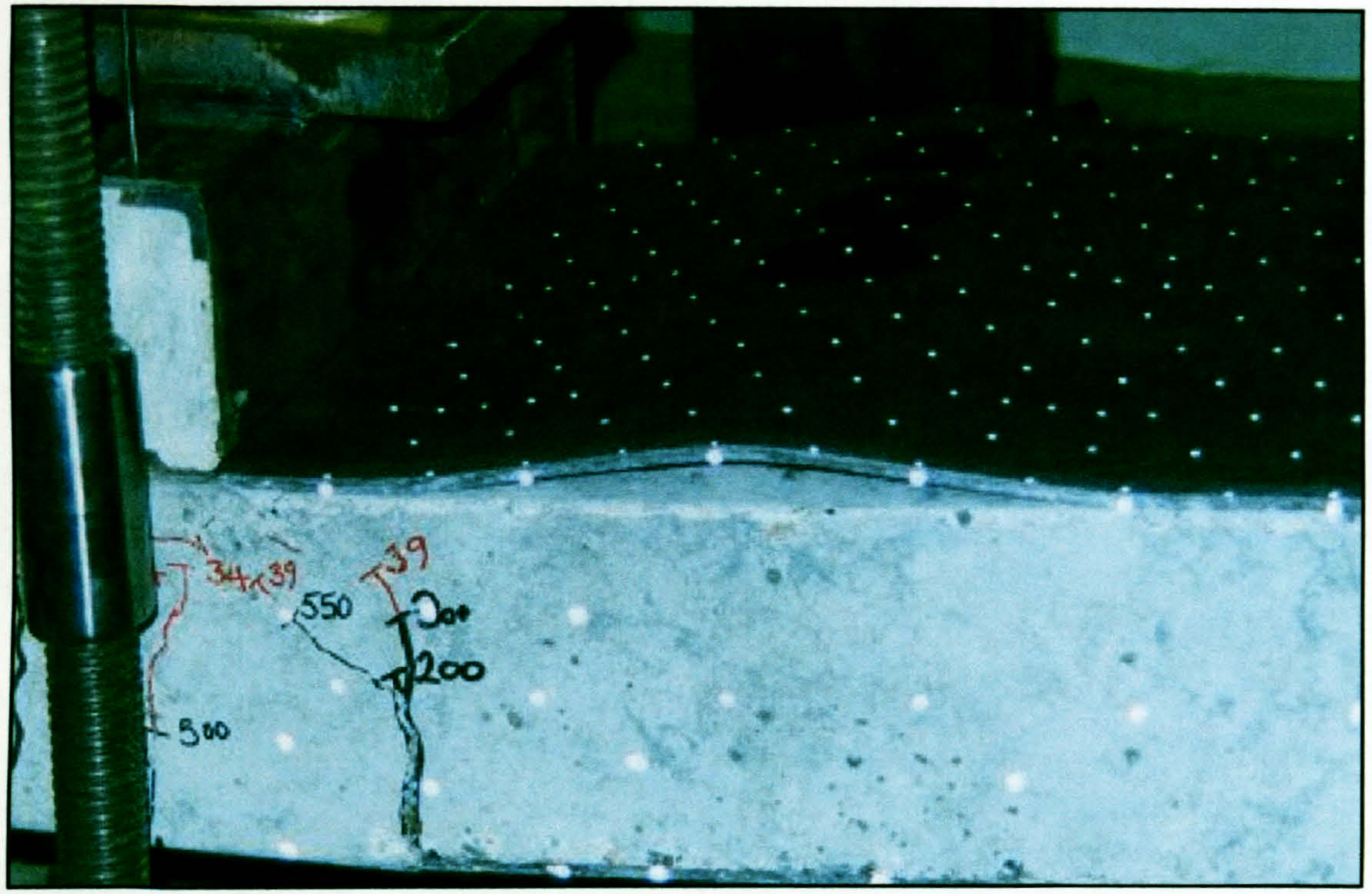

Plate B14a. Close-up of failed area showing local buckling and lack of cracking to the right of the picture, where another shear connector is located.

Appendix C Series 1 Test Results

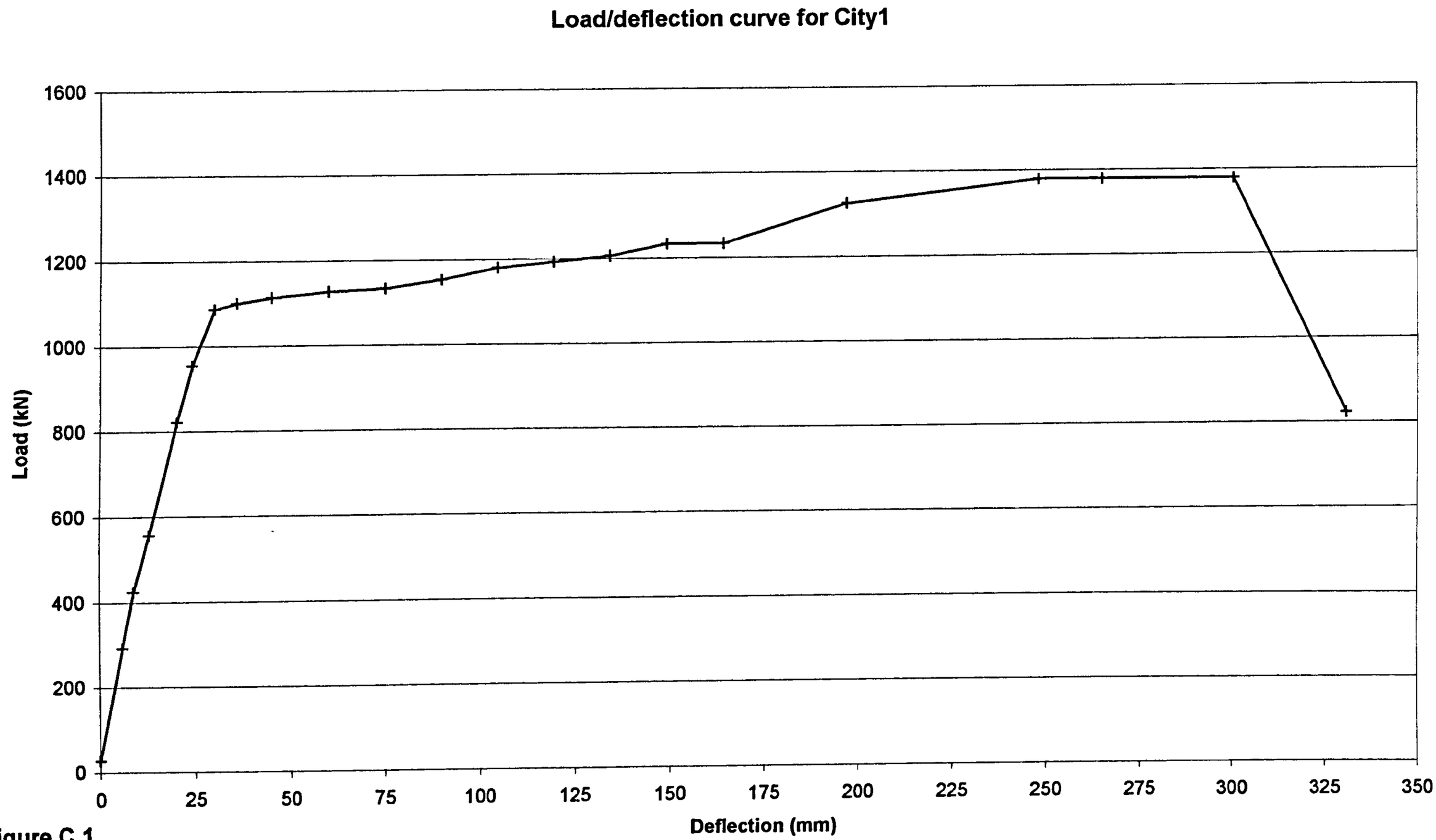
Load/deflection curve for City1
Load (kN)
1600
1400
1200
1000
800
600
400
200
0
0
25
50
75
100
125
150
175
200
225
250
275
300
325
350
Deflection (mm)

Figure C.1

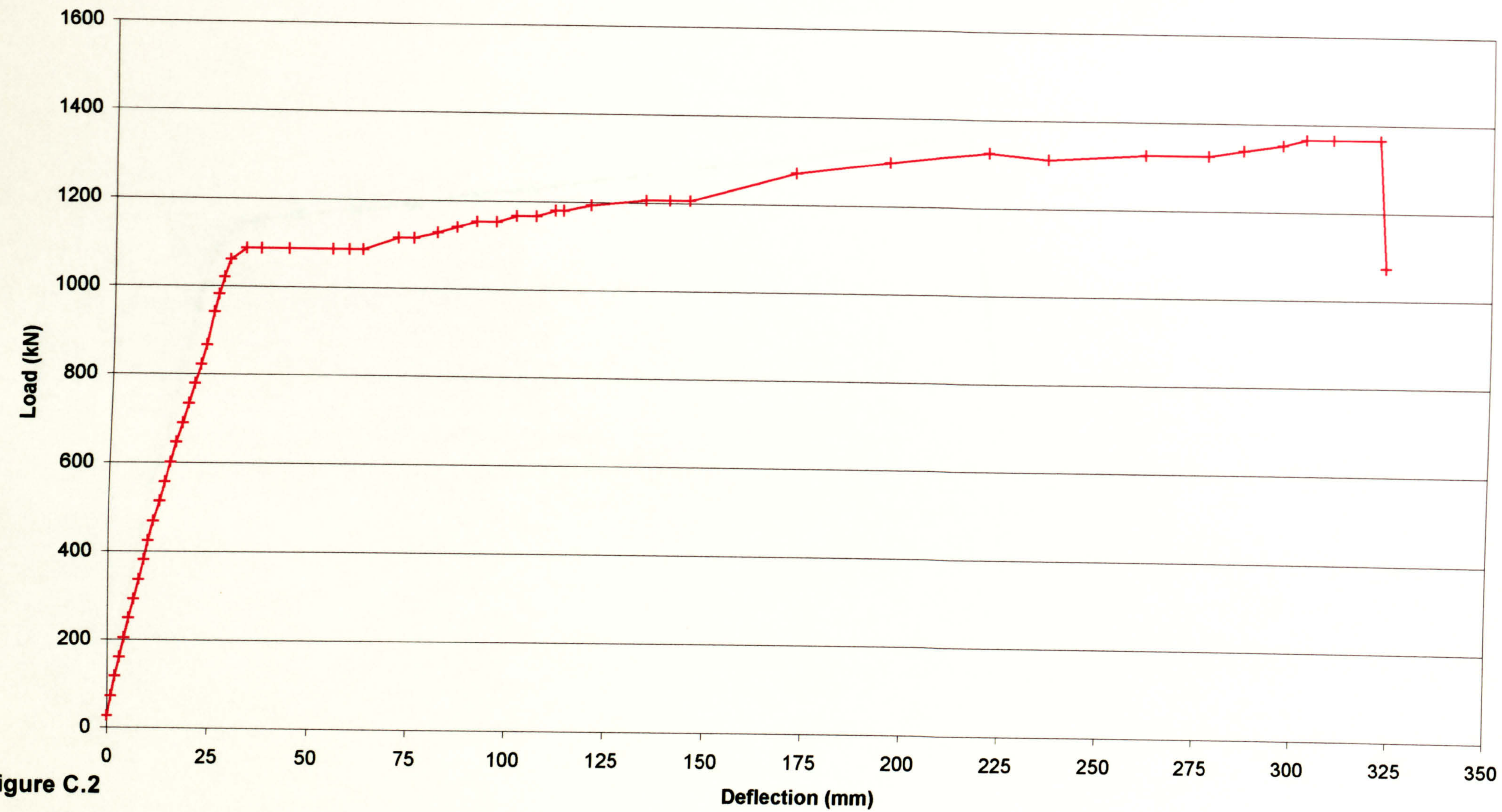
Load/deflection curve for City2
Load (kN)
1600
1400
1200
1000
800
600
400
200
0
0
25
50
75
100
125
150
175
200
225
250
275
300
325
350
Deflection (mm)

Figure C.2

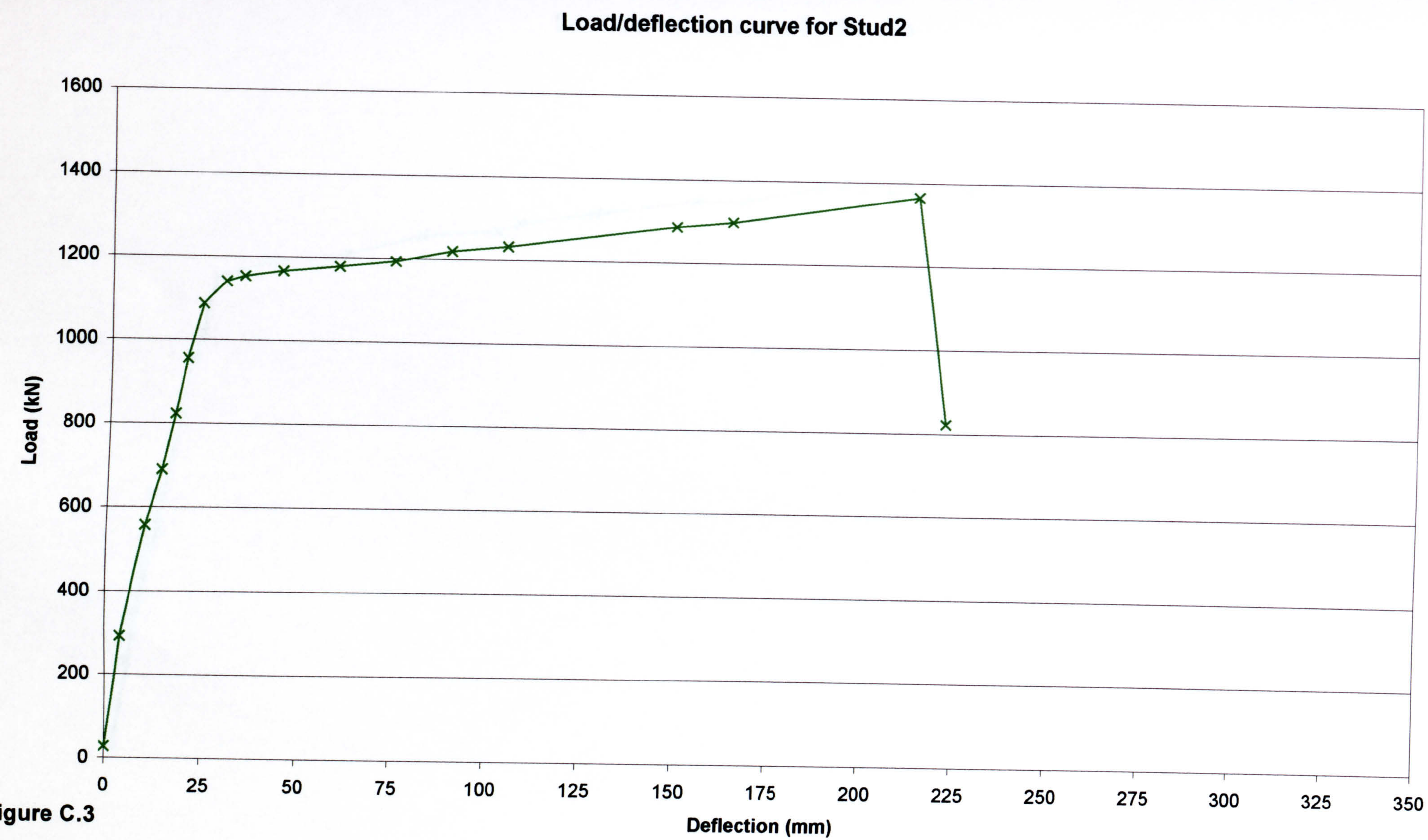
Load/deflection curve for Stud2
Load (kN)
1600
1400
1200
1000
800
600
400
200
0
0
25
50
75
100
125
150
175
200
225
250
275
300
325
350
Deflection (mm)

Figure C.3

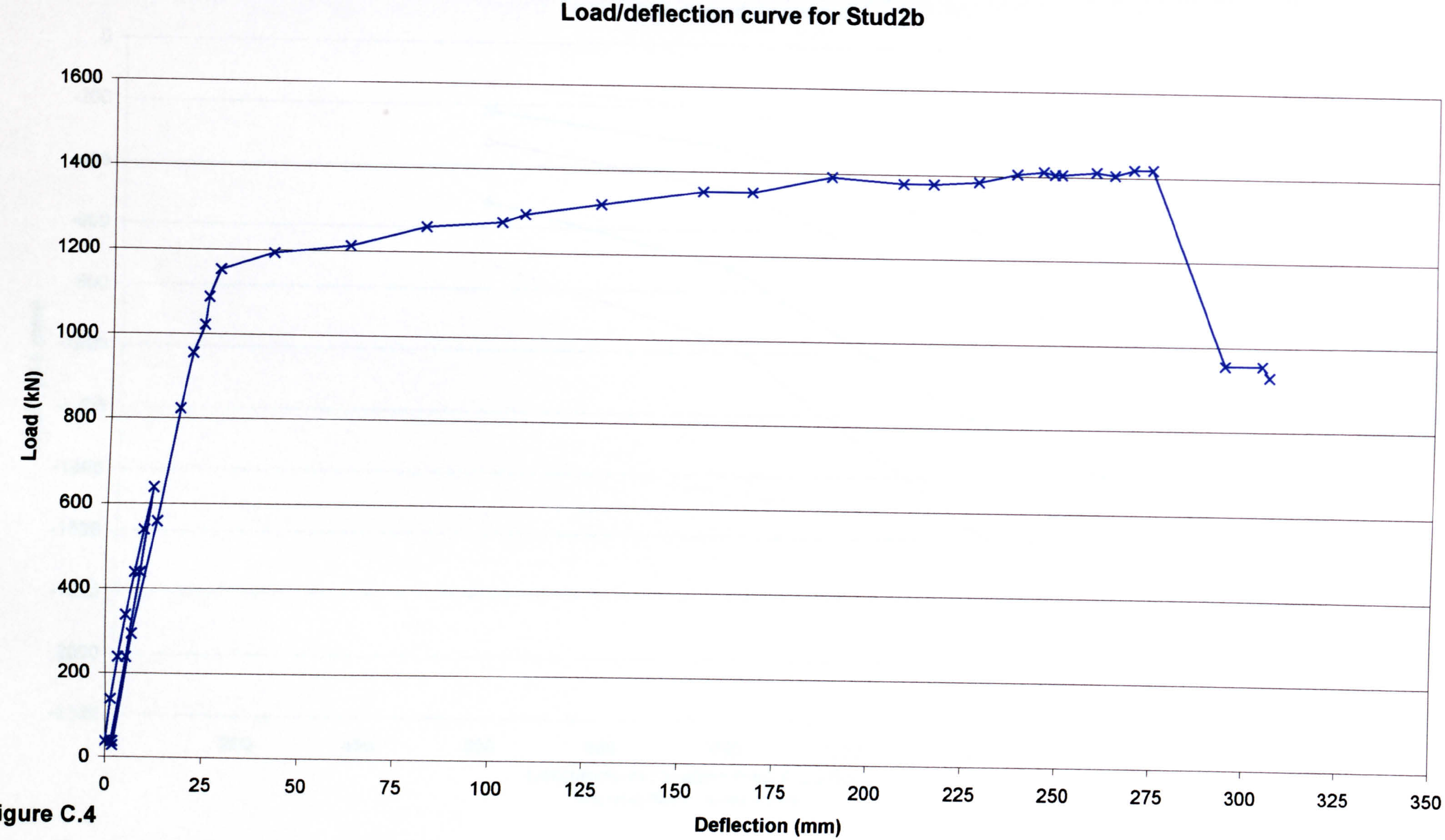
Load/deflection curve for Stud2b
Load (kN)
1600
1400
1200
1000
800
600
400
200
0
0
25
50
75
100
125
150
175
200
225
250
275
300
325
350
Deflection (mm)

Figure C.4

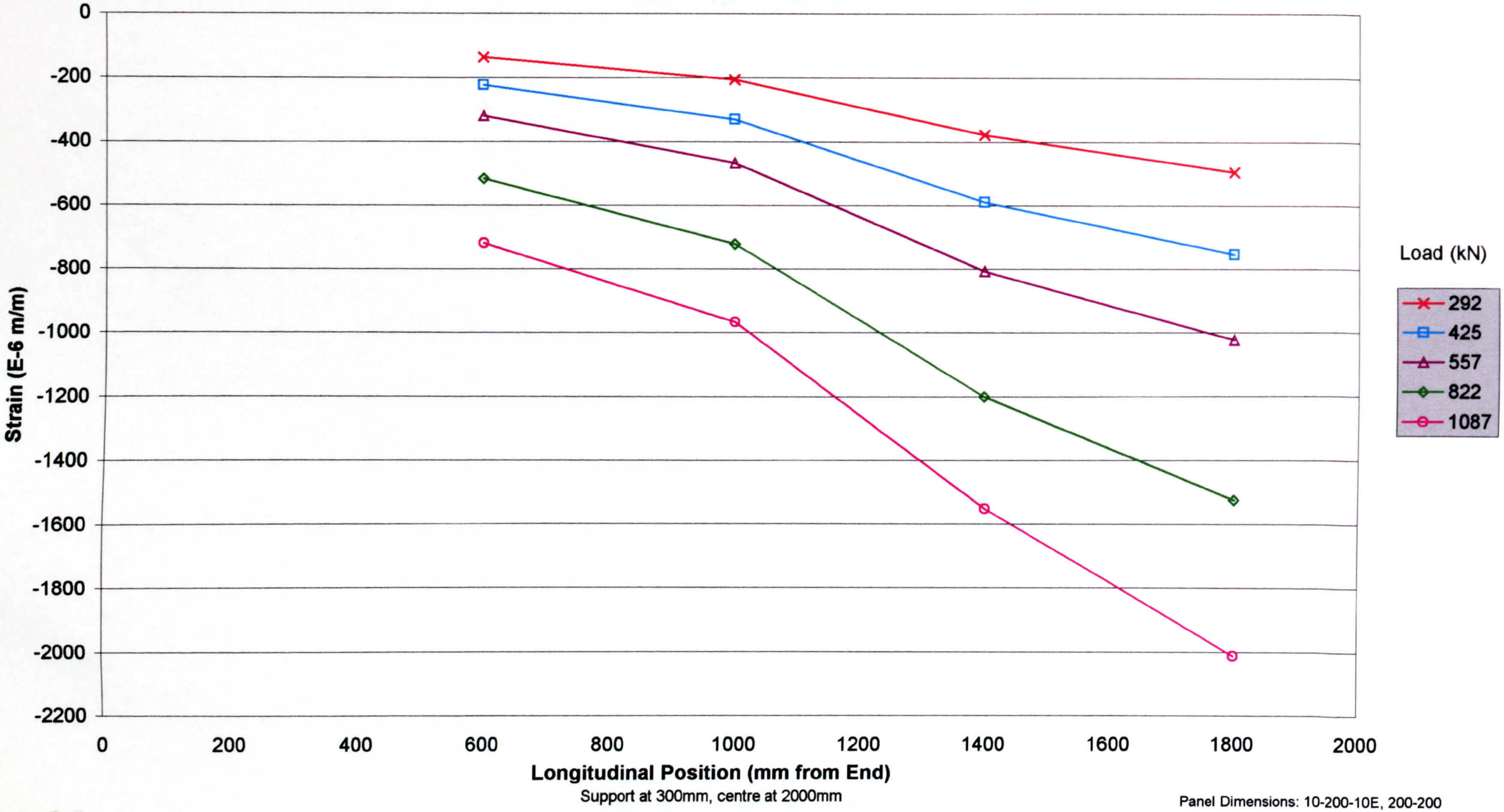
Longitudinal Strains in Tension Plate of City1
(for loads to panel yield load)
Strains averaged over plate depth
0
-200
-400
-600
-800
-1000
-1200
-1400
-1600
-1800
-2000
-2200
Strain (E-6 m/m)
0
200
400
600
800
1000
1200
1400
1600
1800
2000
Longitudinal Position (mm from End)
Support at 300mm, centre at 2000mm
Load (kN)
292
425
557
822
1087
Panel Dimensions: 10-200-10E, 200-200

Figure C.5

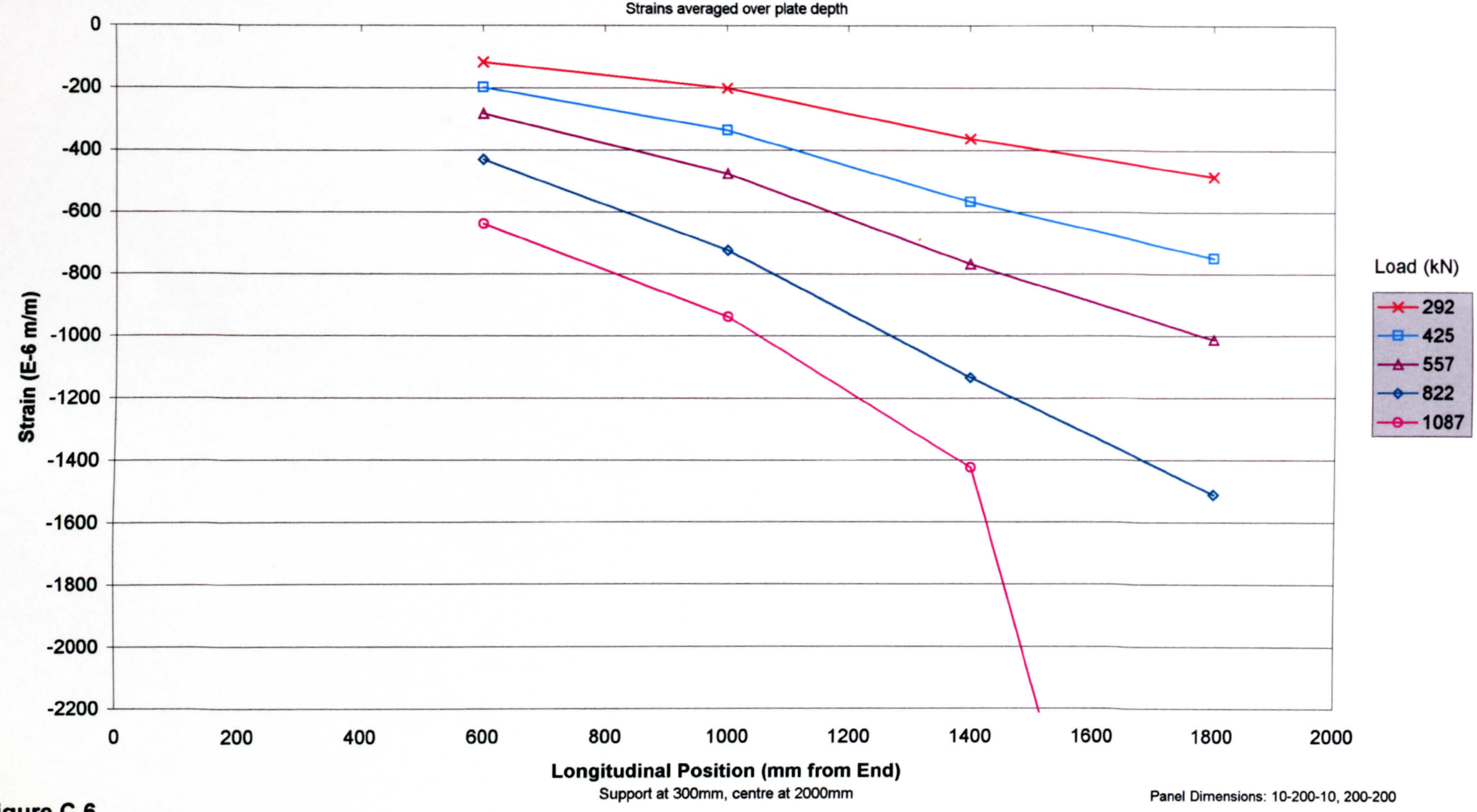
Longitudinal Strains in Tension Plate of City2
(for loads to yield load in equal increments)
Strains averaged over plate depth
Strain (E-6 m/m)
0
-200
-400
-600
-800
-1000
-1200
-1400
-1600
-1800
-2000
-2200
0
200
400
600
800
1000
1200
1400
1600
1800
2000
Longitudinal Position (mm from End)
Support at 300mm, centre at 2000mm
Load (kN)
292
425
557
822
1087
Panel Dimensions: 10-200-10, 200-200

Figure C.6

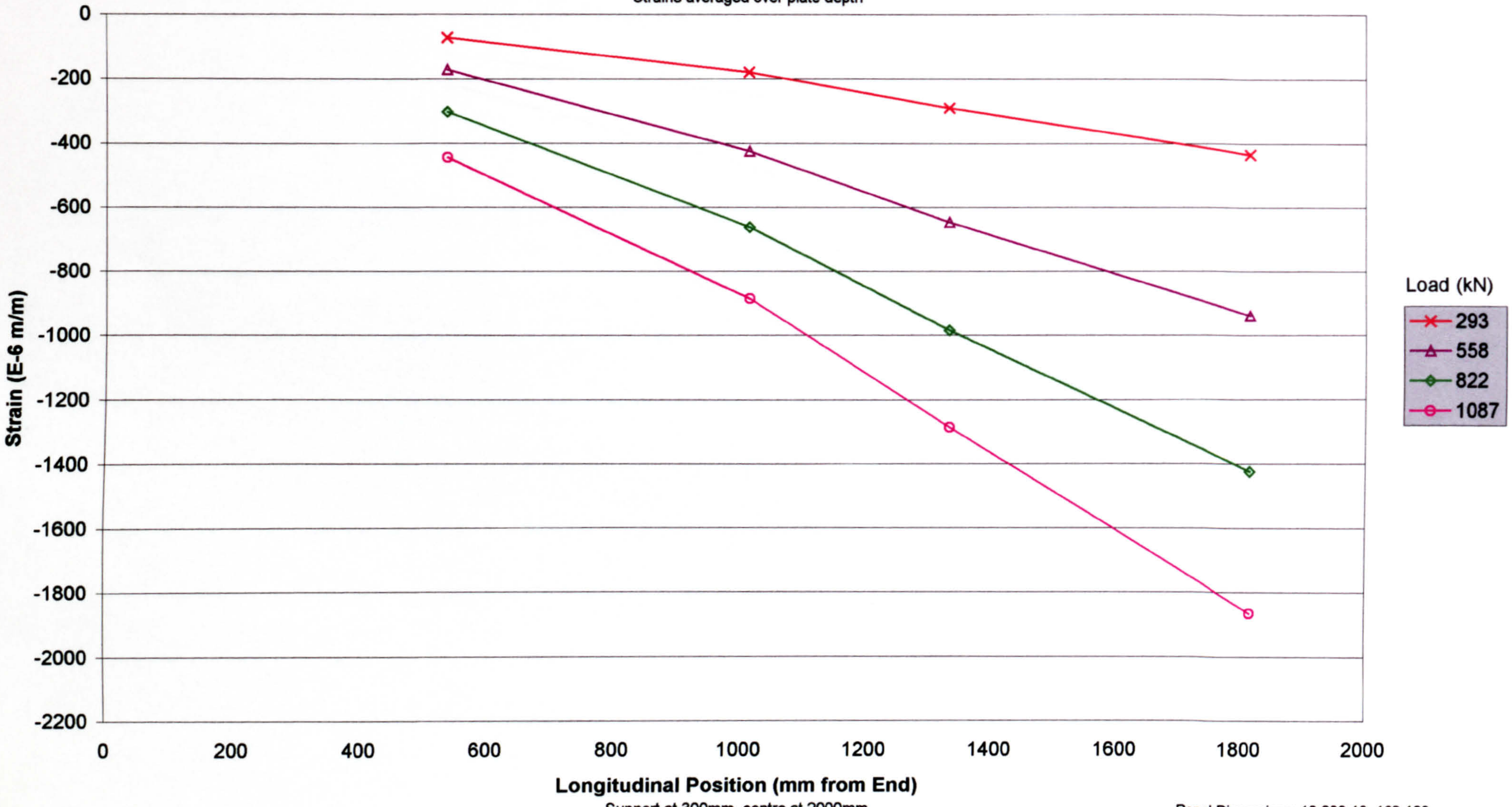
Longitudinal Strains in Tension Plate of Stud2
(for loads to yield load and post yield deflection)
Strains averaged over plate depth
0
-200
-400
-600
-800
-1000
-1200
-1400
-1600
-1800
-2000
-2200
Strain (E-6 m/m)
0
200
400
600
800
1000
1200
1400
1600
1800
2000
Longitudinal Position (mm from End)
Support at 300mm, centre at 2000mm
Load (kN)
293
558
822
1087
Panel Dimensions: 10-200-10, 160-133

Figure C.7

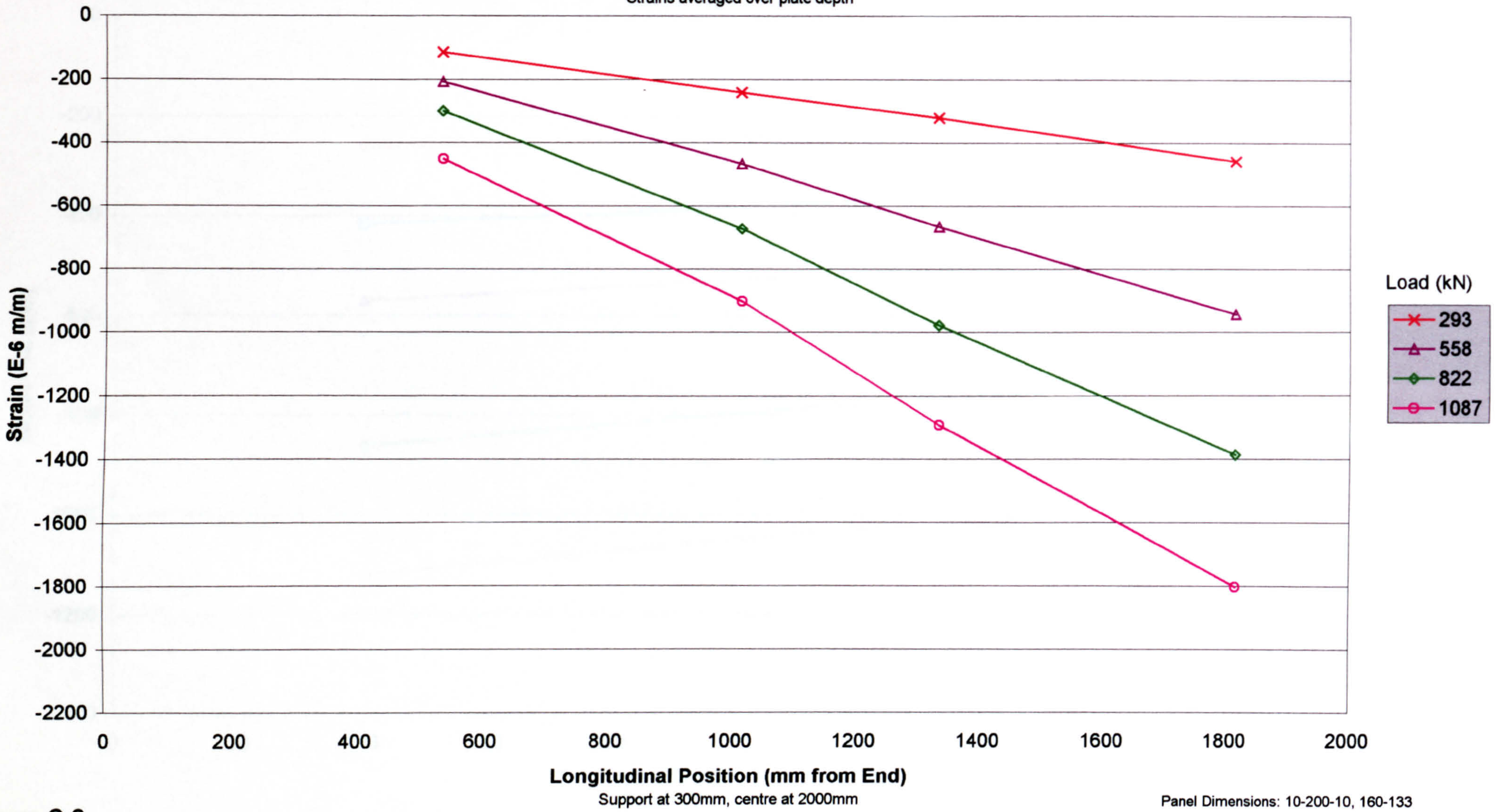
Longitudinal Strains in Tension Plate of Stud2b
(for loads to yield load and post yield deflection)
Strains averaged over plate depth
Strain (E-6 m/m)
0
-200
-400
-600
-800
-1000
-1200
-1400
-1600
-1800
-2000
-2200
0
200
400
600
800
1000
1200
1400
1600
1800
2000
Longitudinal Position (mm from End)
Support at 300mm, centre at 2000mm
Load (kN)
293
558
822
1087
Panel Dimensions: 10-200-10, 160-133

Figure C.8

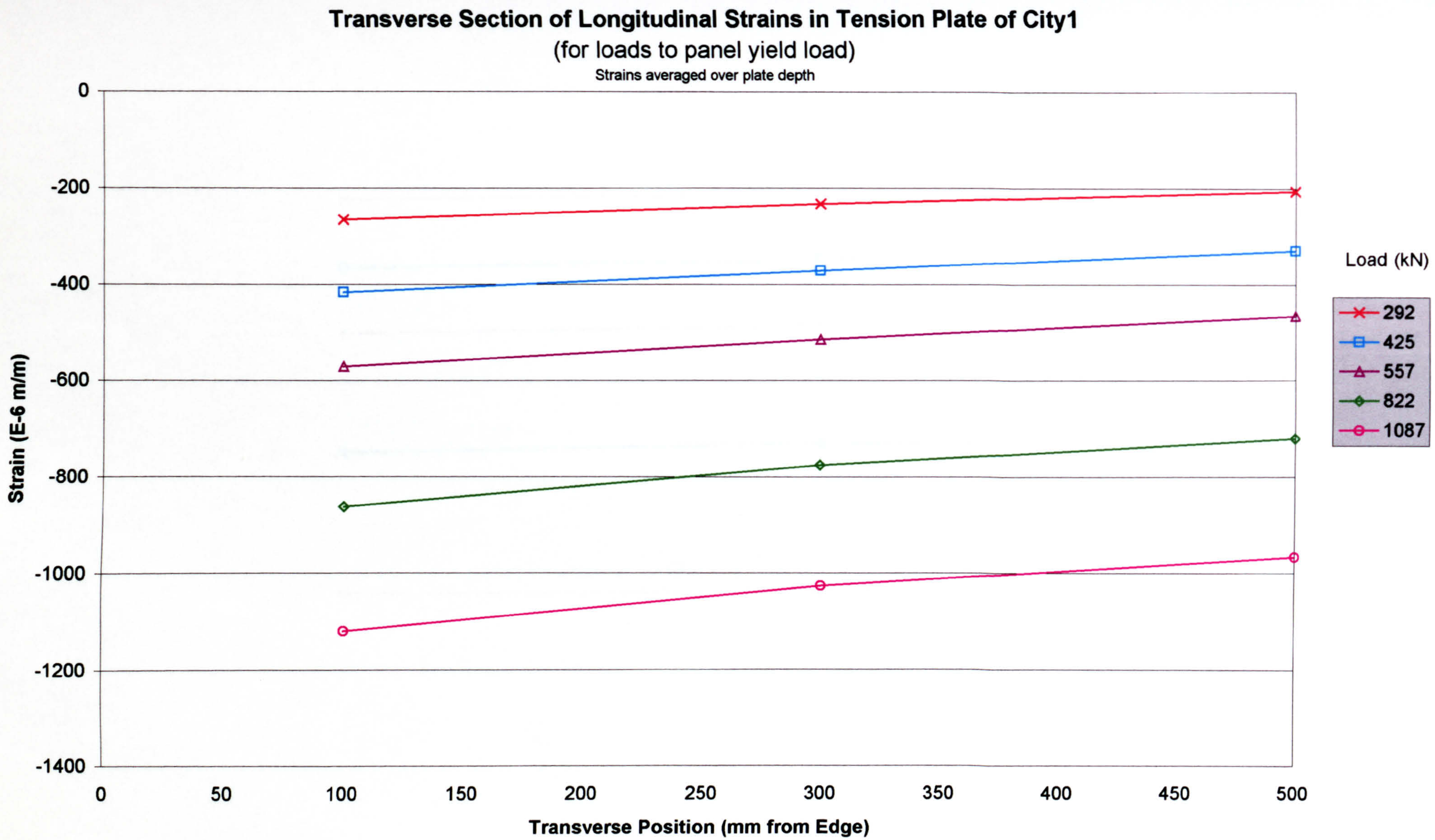
Transverse Section of Longitudinal Strains in Tension Plate of City1
(for loads to panel yield load)
Strains averaged over plate depth
0
-200
-400
-600
-800
-1000
-1200
-1400
Strain (E-6 m/m)
0
50
100
150
200
250
300
350
400
450
500
Transverse Position (mm from Edge)
Edge at 0mm, centre at 500mm
Load (kN)
292
425
557
822
1087
Panel Dimensions: 10-200-10E, 200-200

Figure C.9

Transverse Section of Longitudinal Strains in Tension Plate of City2

(for loads to panel yield load)

Strains averaged over plate depth

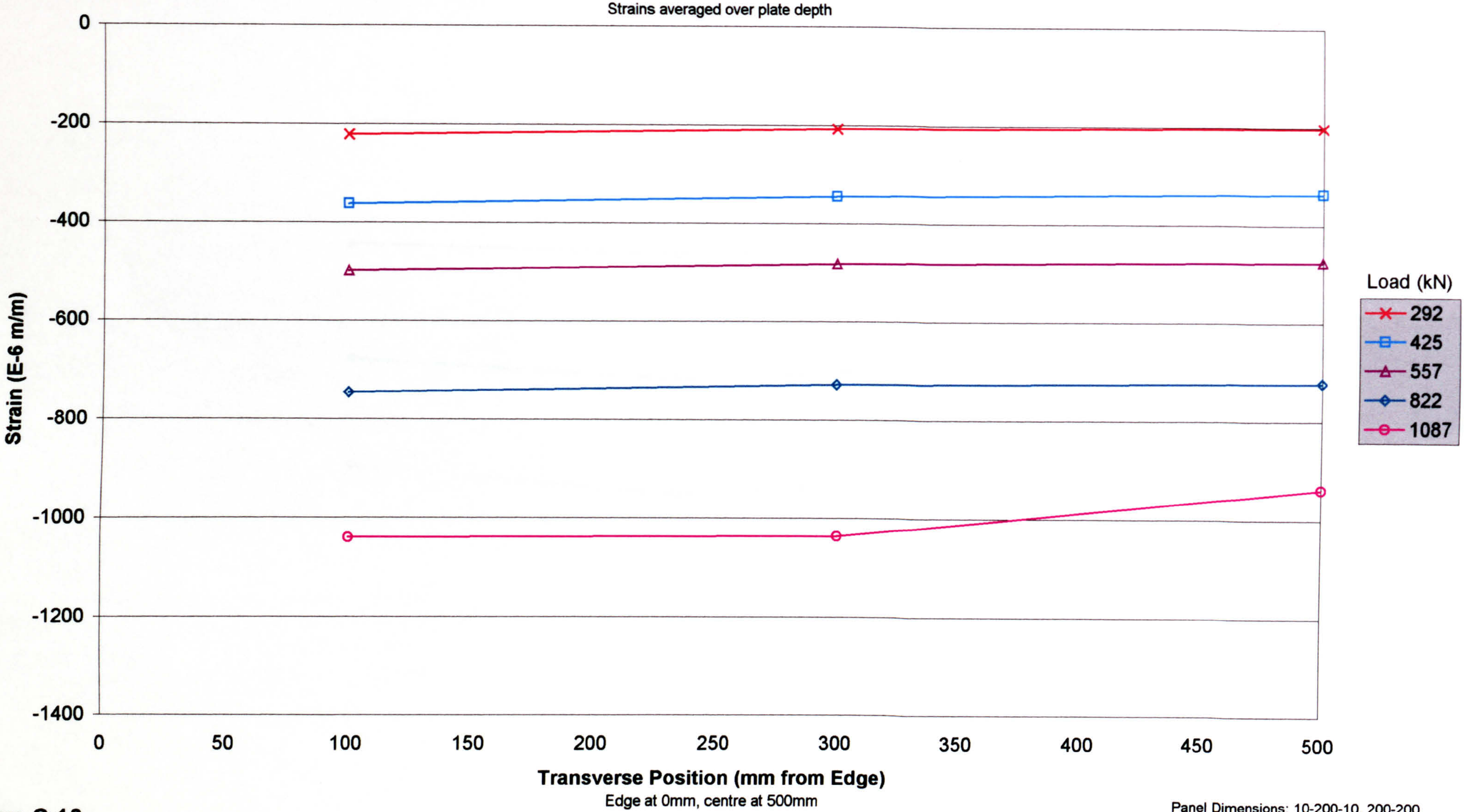

Panel Dimensions: 10-200-10, 200-200

Figure C.10

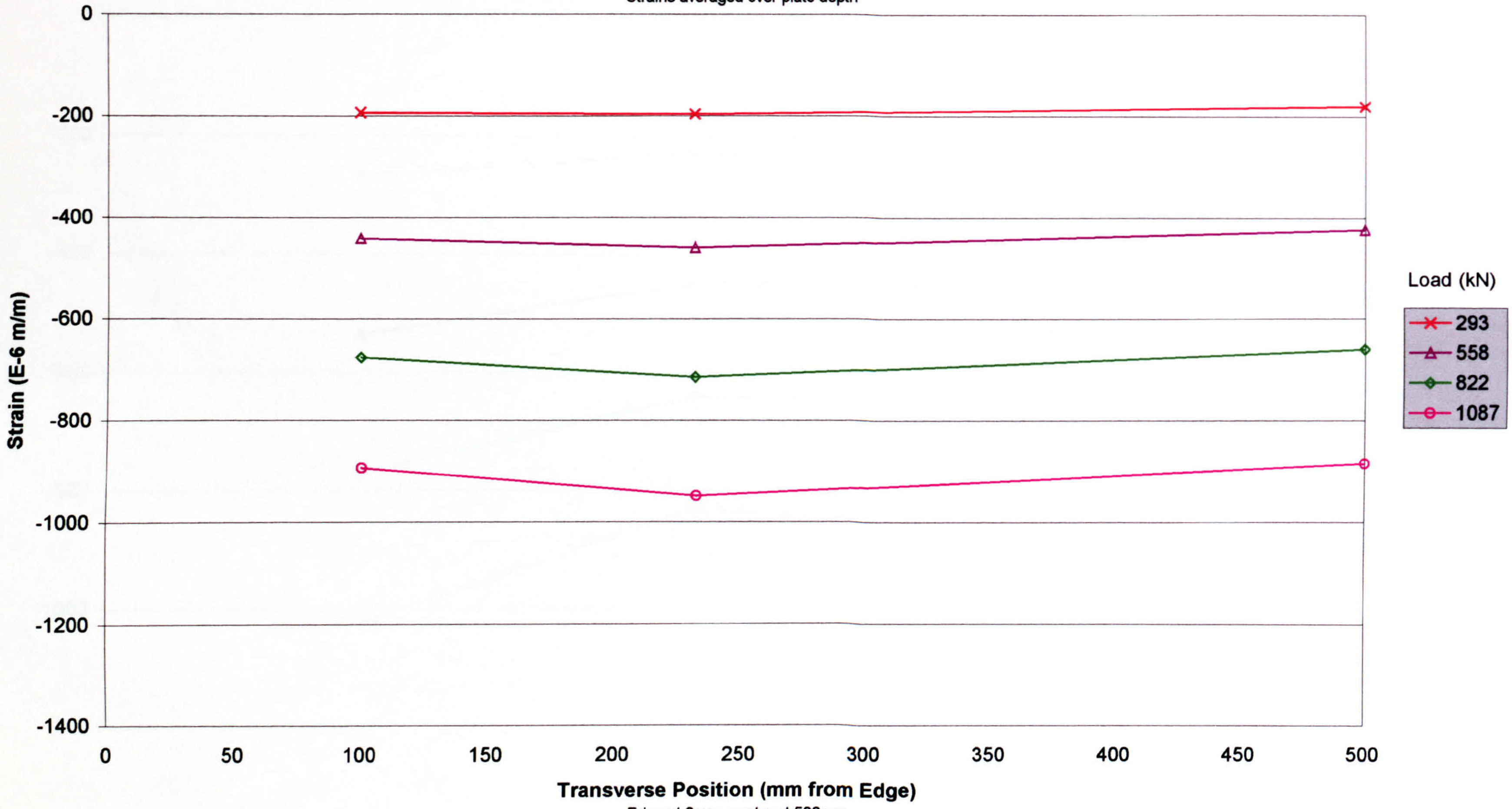
Transverse Section of Longitudinal Strains in Tension Plate of Stud2
(for loads to panel yield load)
Strains averaged over plate depth
0
-200
-400
-600
-800
-1000
-1200
-1400
Strain (E-6 m/m)
0
50
100
150
200
250
300
350
400
450
500
Transverse Position (mm from Edge)
Edge at 0mm, centre at 500mm
Load (kN)
293
558
822
1087
Panel Dimensions: 10-200-10, 160-133

Figure C.11

Transverse Section of Longitudinal Strains in Tension Plate of Stud2b

(for loads to panel yield load)

Strains averaged over plate depth

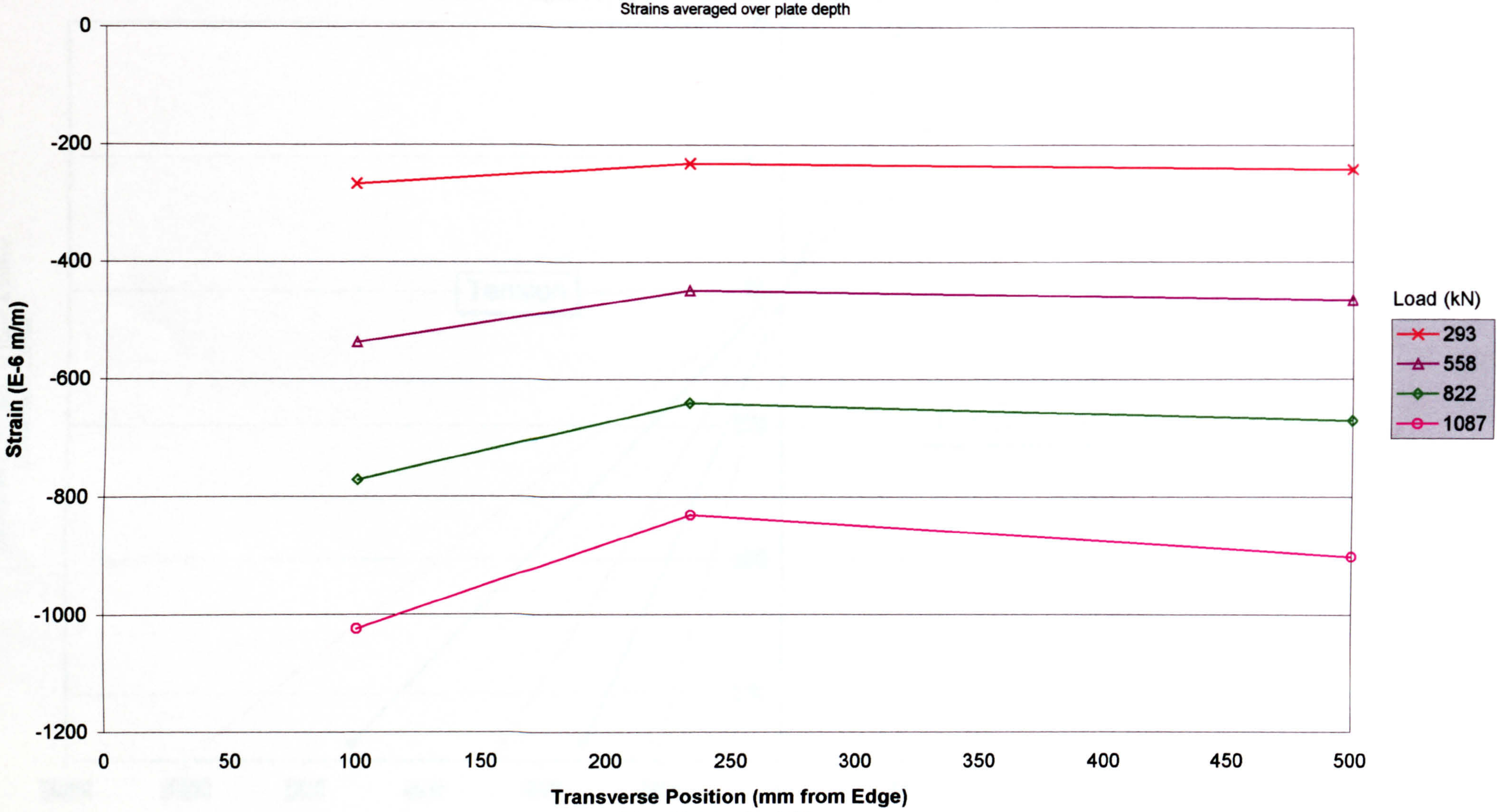

Figure C.12

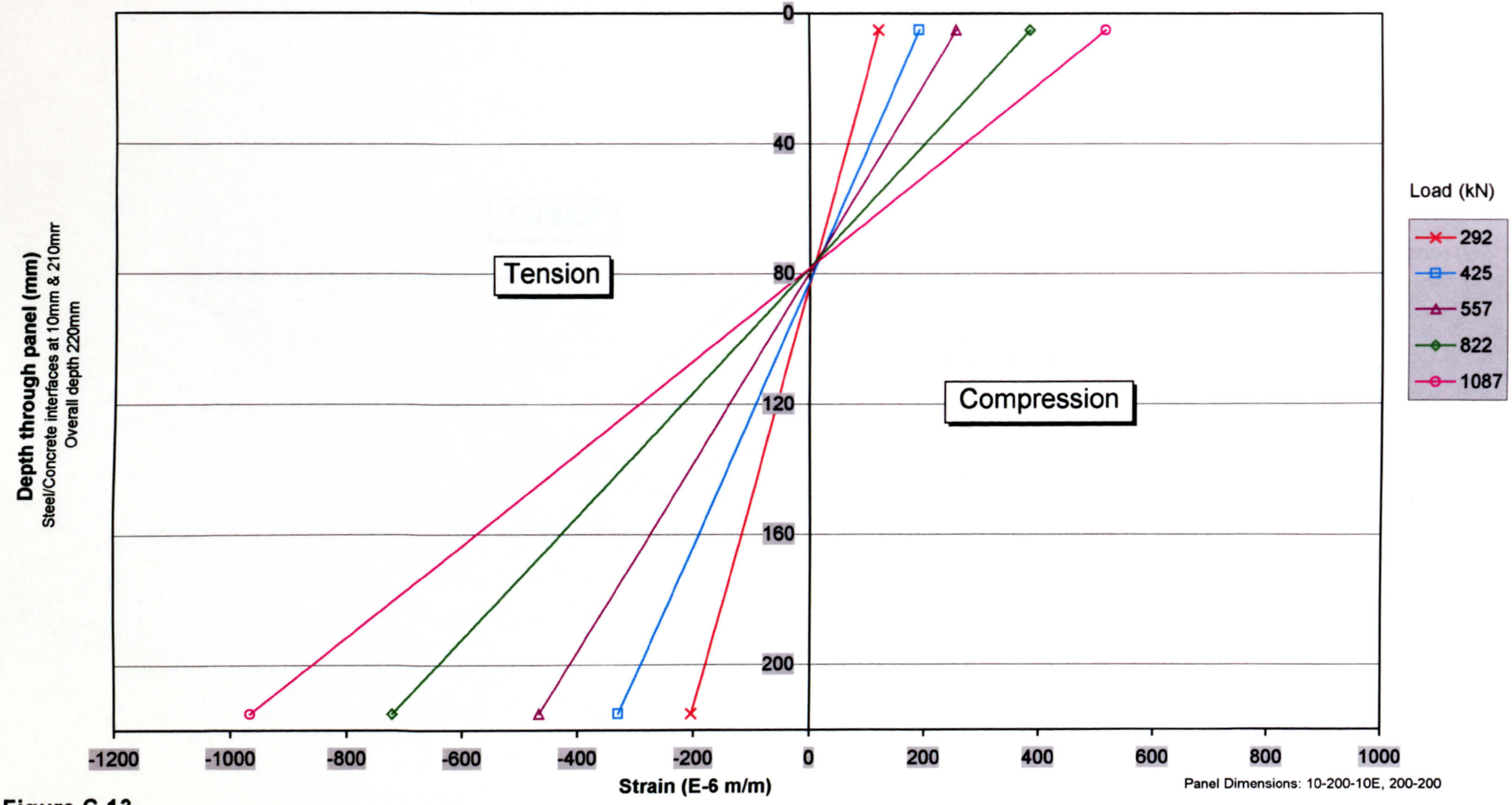
Vertical Section of Longitudinal Strains of City1
(for loads upto panel yield)
Strains averaged over plate depth at a location 700mm from support
Depth through panel (mm)
Steel/Concrete interfaces at 10mm & 210mm
Overall depth 220mm
0
40
80
120
160
200
Tension
Compression
-1200
-1000
-800
-600
-400
-200
0
200
400
600
800
1000
Strain (E-6 m/m)
Load (kN)
292
425
557
822
1087
Panel Dimensions: 10-200-10E, 200-200

Figure C.13

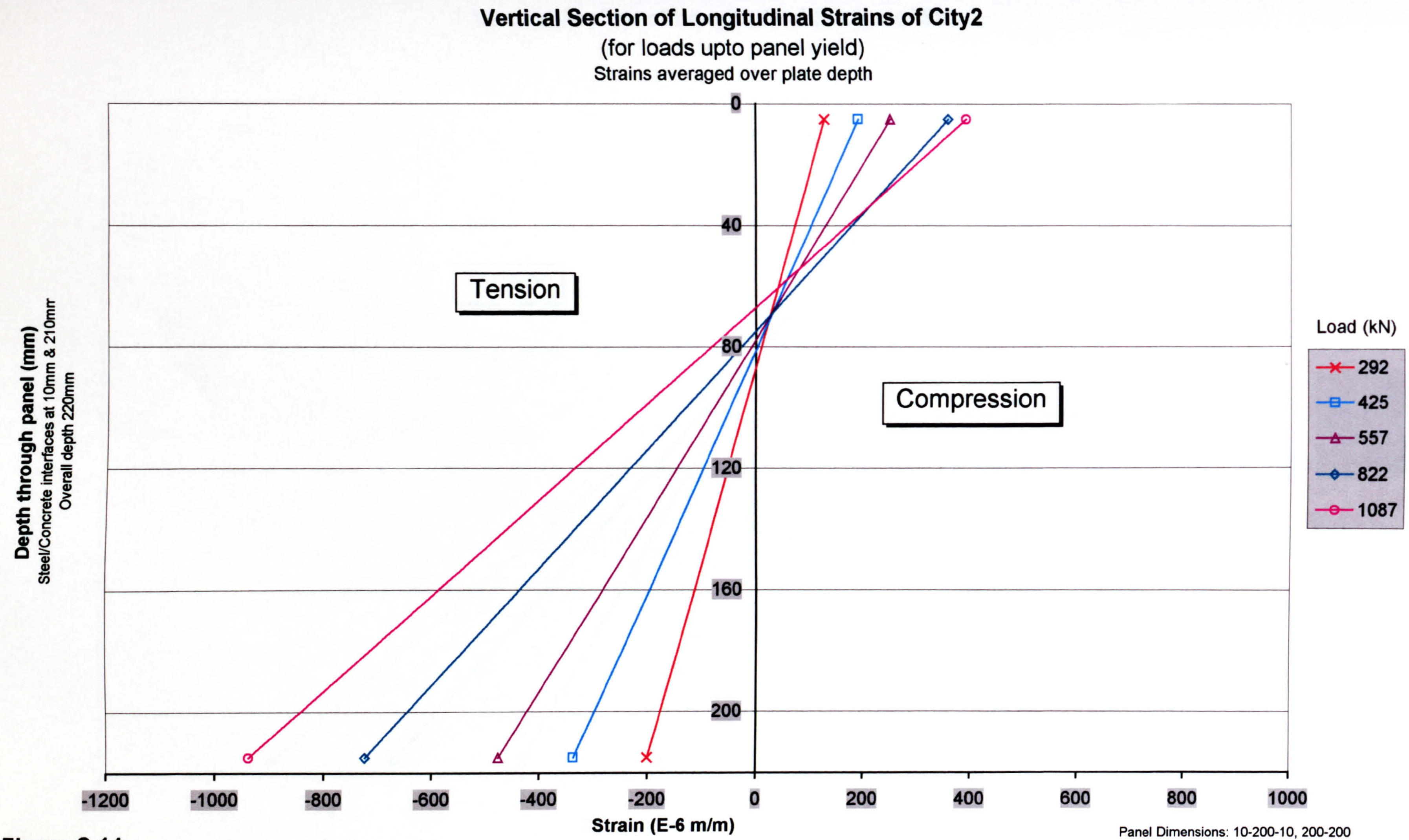
Vertical Section of Longitudinal Strains of City2
(for loads upto panel yield)
Strains averaged over plate depth
Depth through panel (mm)
Steel/Concrete interfaces at 10mm & 210mm
Overall depth 220mm
0
40
80
120
160
200
Tension
Compression
-1200
-1000
-800
-600
-400
-200
0
200
400
600
800
1000
Strain (E-6 m/m)
Load (kN)
292
425
557
822
1087
Panel Dimensions: 10-200-10, 200-200

Figure C.14

Vertical Section of Longitudinal Strains of Stud2

(for loads upto panel yield)

Strains averaged over plate depth

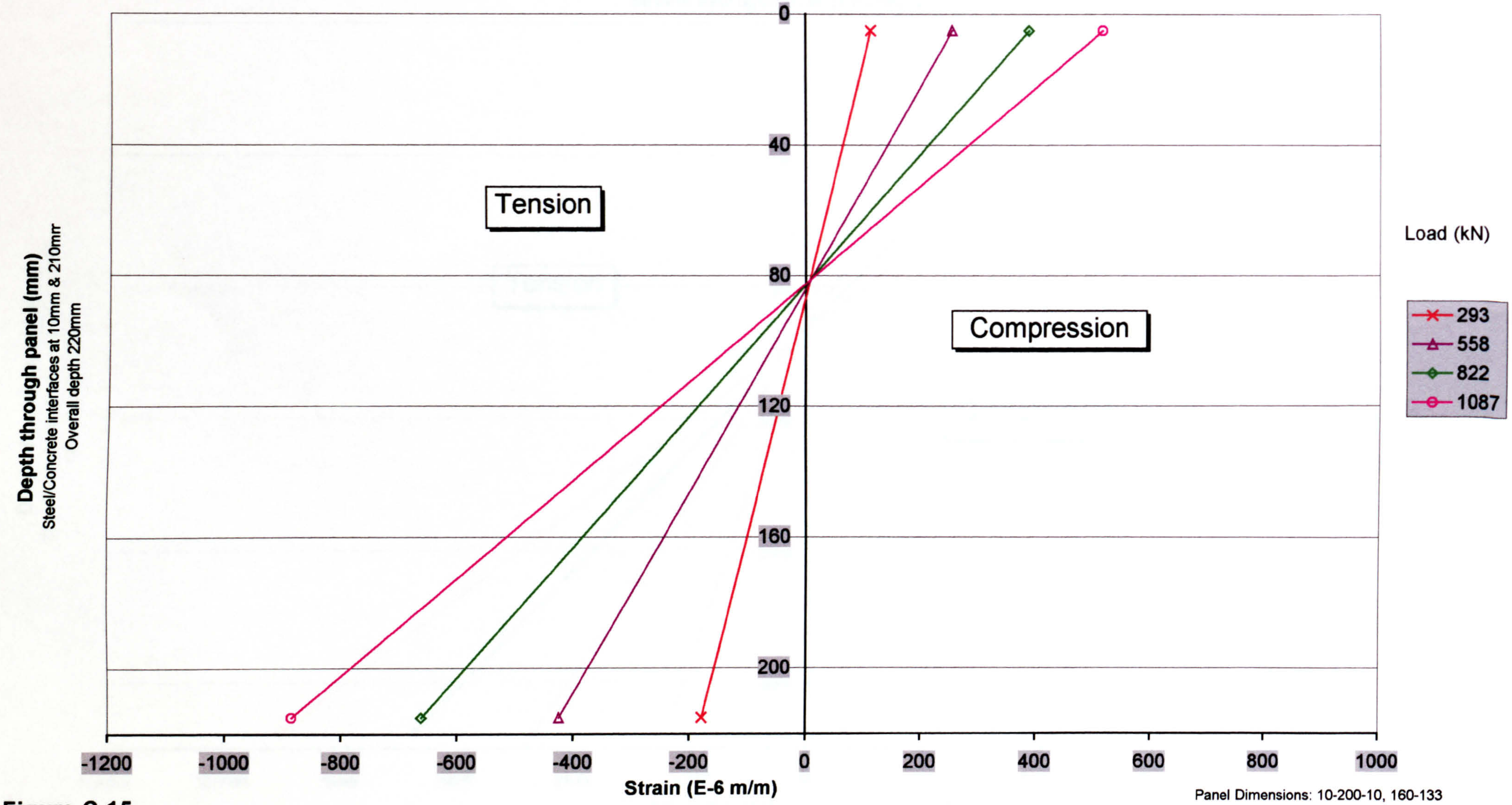

Panel Dimensions: 10-200-10, 160-133

Figure C.15

Vertical Section of Longitudinal Strains of Stud2b

(for loads upto panel yield)

Strains averaged over plate depth

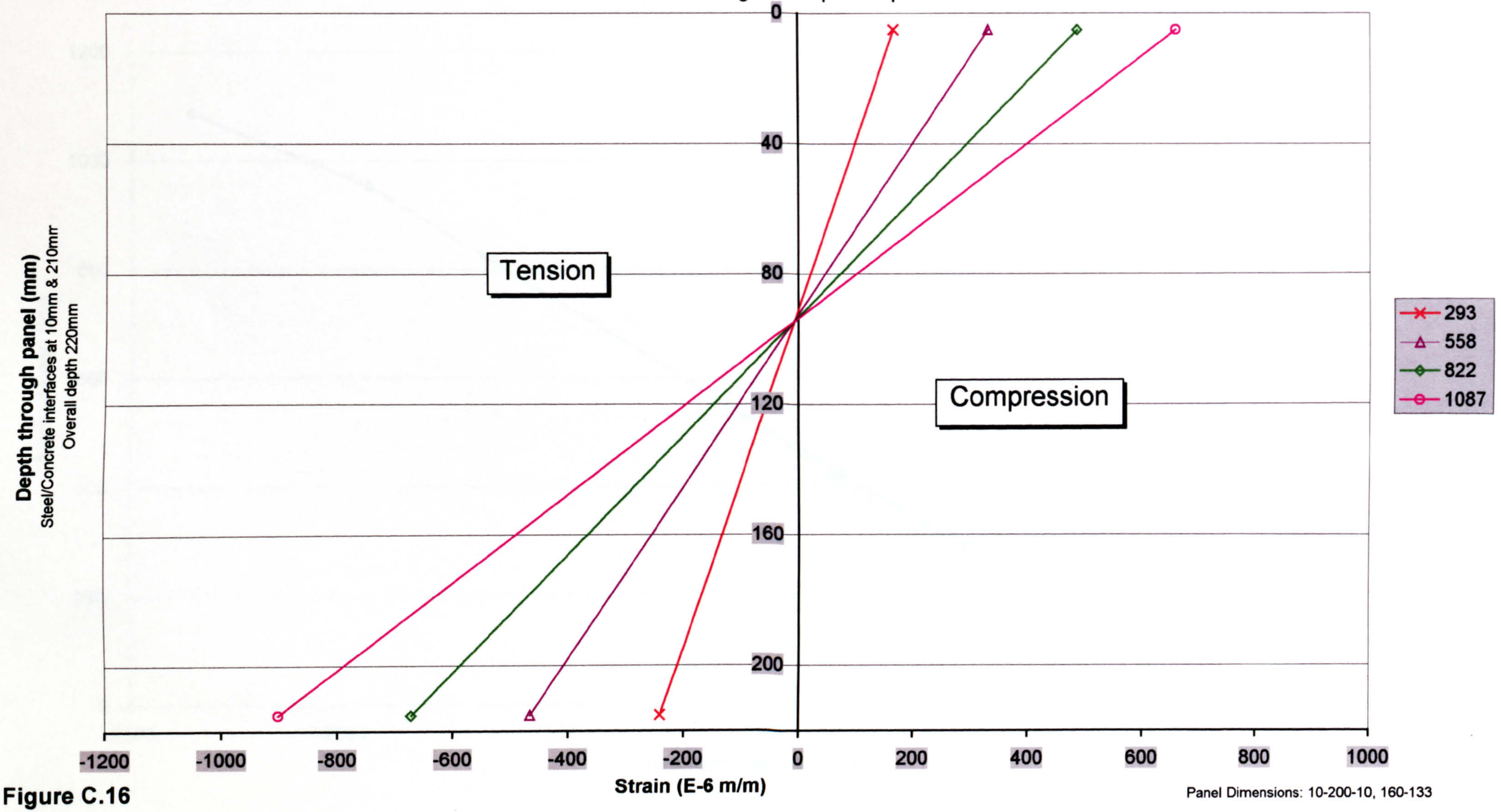

Figure C.16

Panel Dimensions: 10-200-10, 160-133

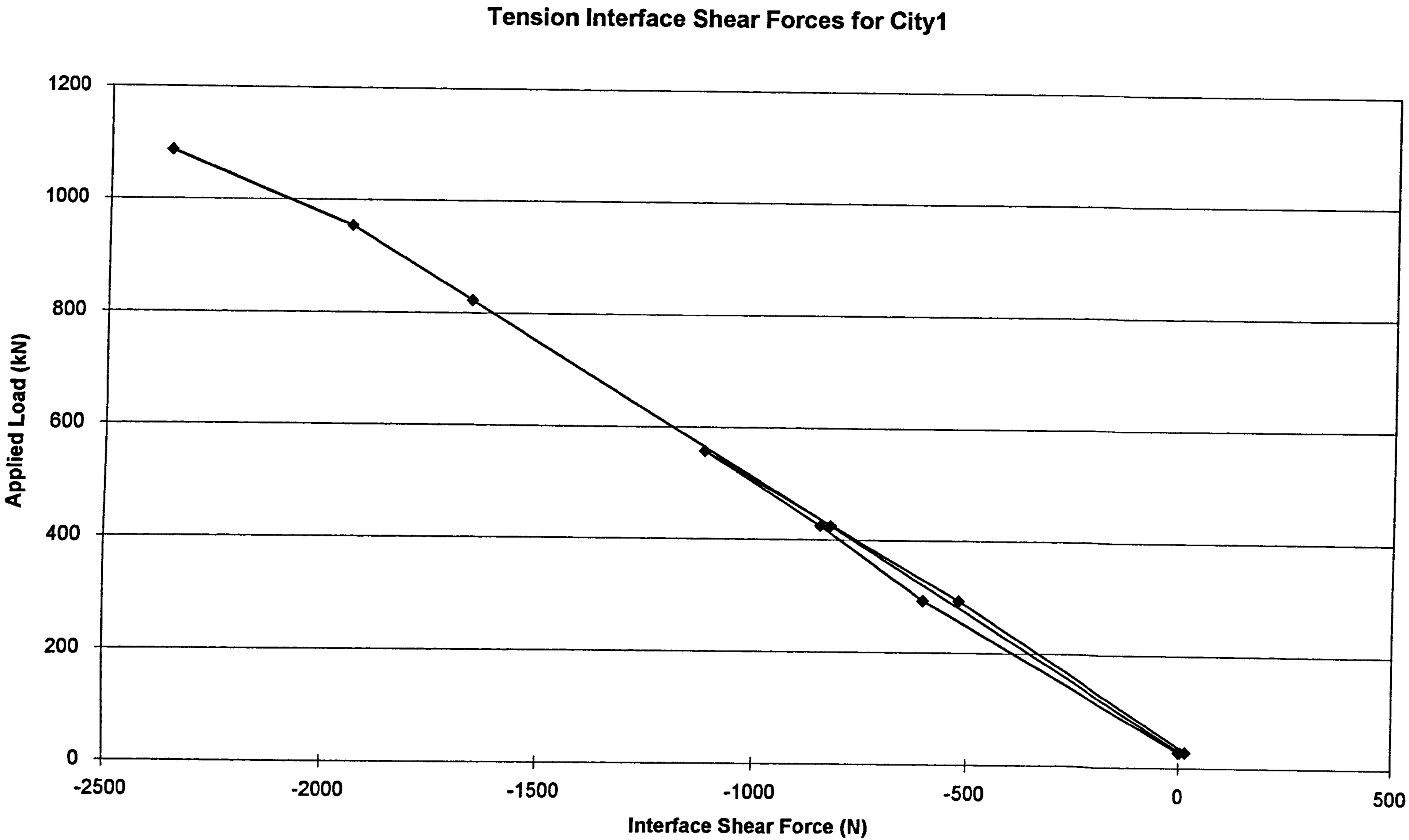
Tension Interface Shear Forces for City1
Applied Load (kN)
1200
1000
800
600
400
200
0
-2500
-2000
-1500
-1000
-500
0
500
Interface Shear Force (N)

Figure C.17

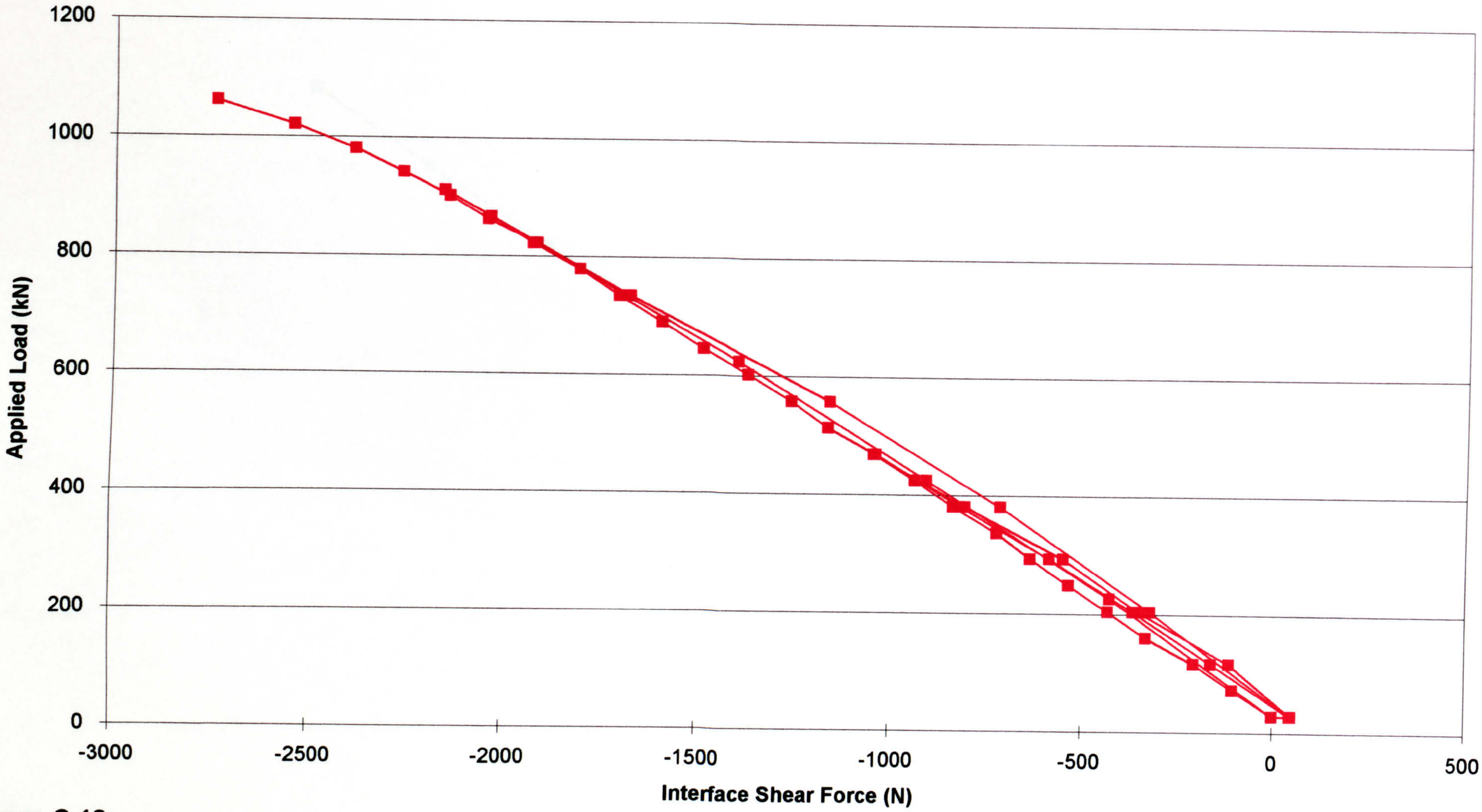
Tension Interface Shear Forces for City2
Applied Load (kN)
1200
1000
800
600
400
200
0
-3000
-2500
-2000
-1500
-1000
-500
0
500
Interface Shear Force (N)

Figure C.18

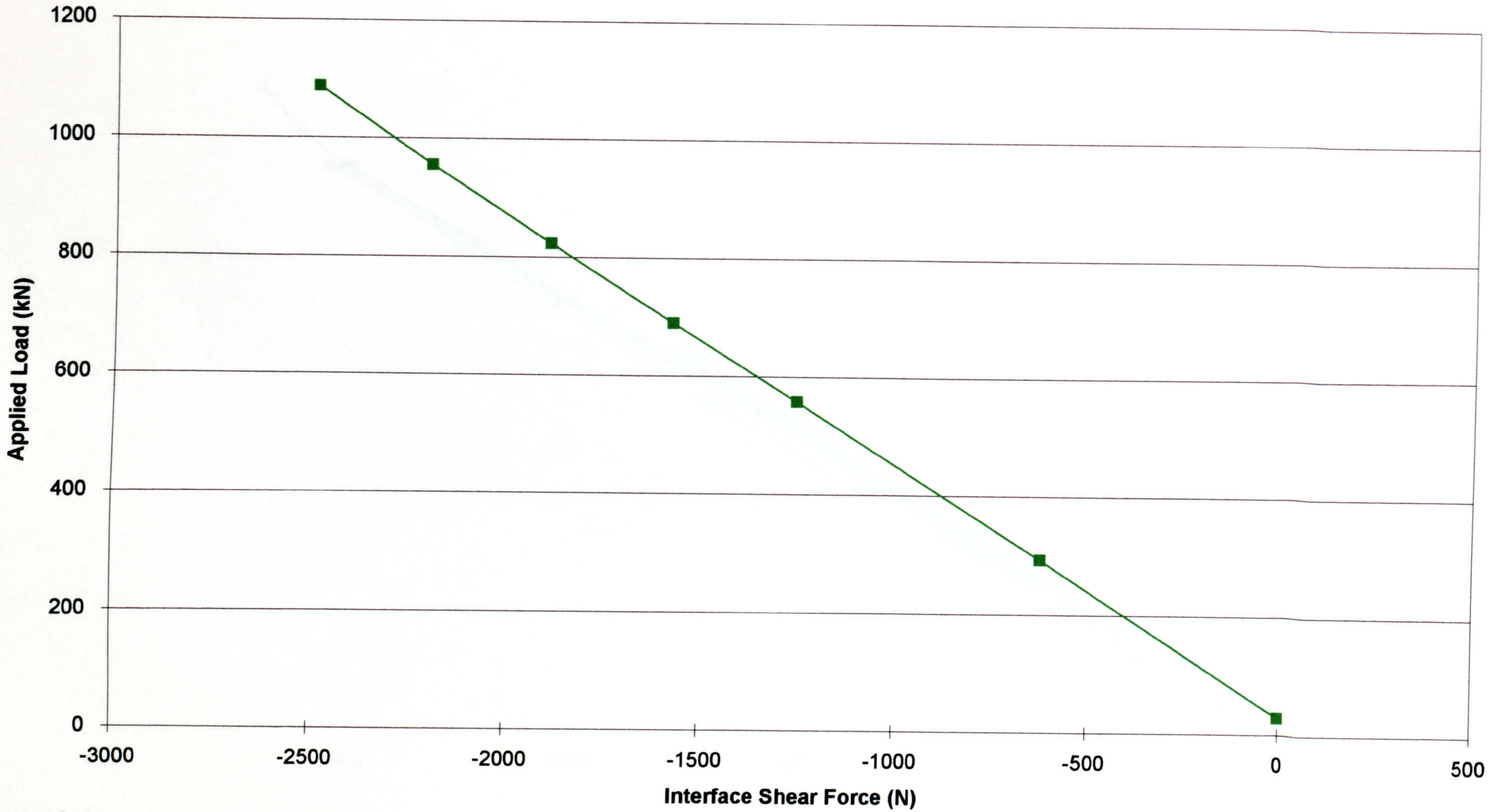
Tension Interface Shear Forces for Stud2
Applied Load (kN)
1200
1000
800
600
400
200
0
-3000
-2500
-2000
-1500
-1000
-500
0
500
Interface Shear Force (N)

Figure C.19

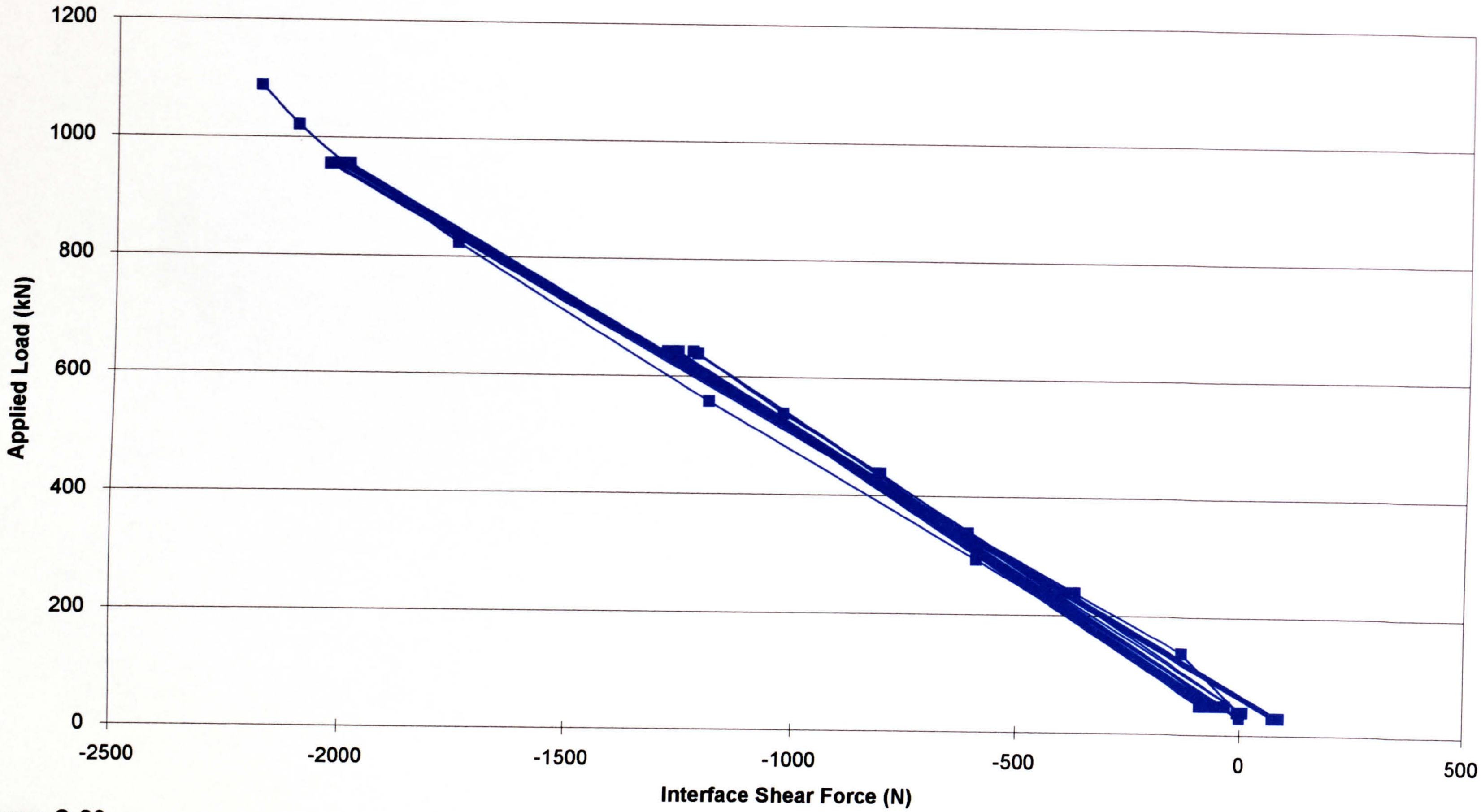
Tension Interface Shear Forces for Stud2b
Applied Load (kN)
1200
1000
800
600
400
200
0
-2500
-2000
-1500
-1000
-500
0
500
Interface Shear Force (N)

Figure C.20

Appendix D Series 2 (parts 1 and 2) Test Results

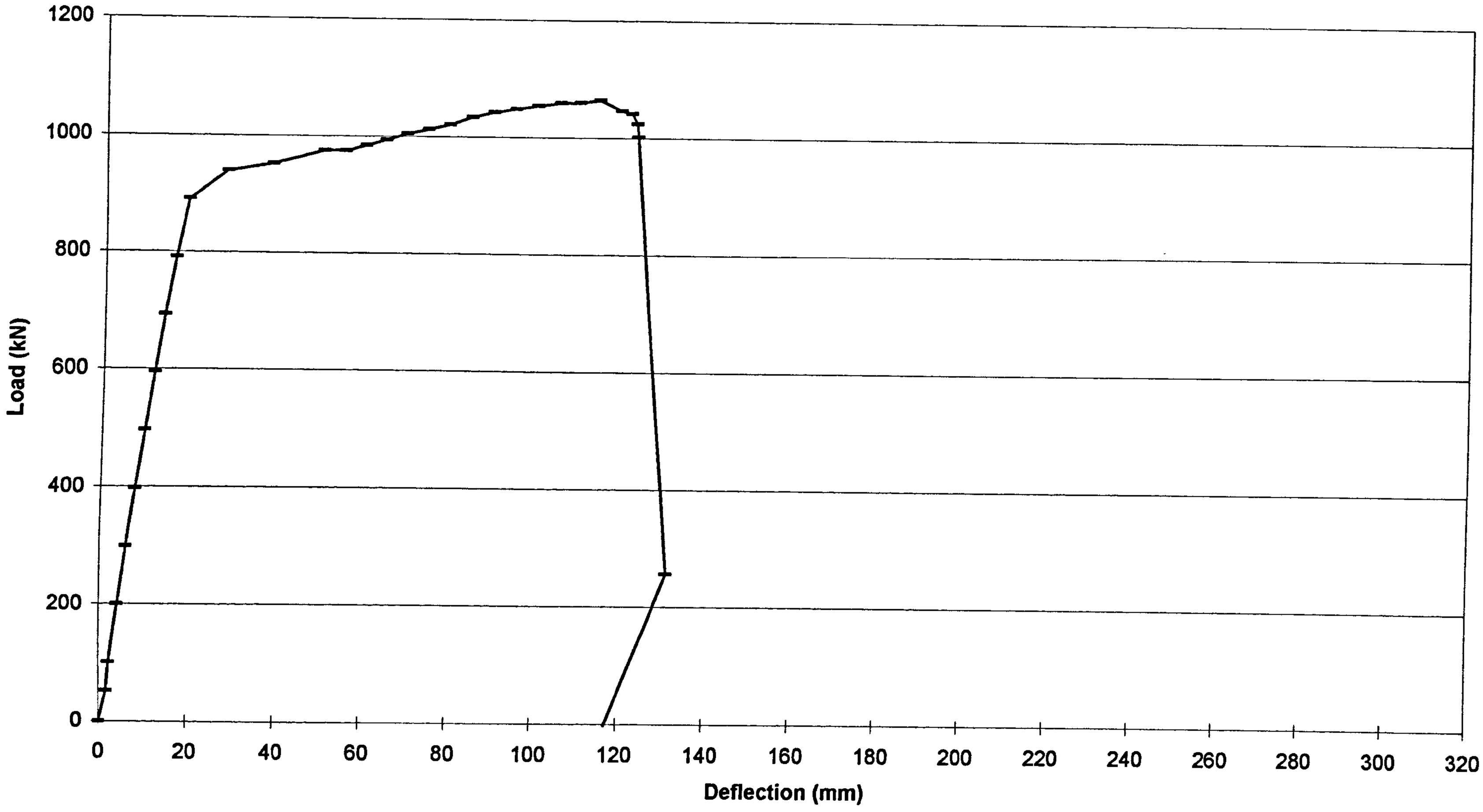
Load/deflection curve for City3
Load (kN)
1200
1000
800
600
400
200
0
0
20
40
60
80
100
120
140
160
180
200
220
240
260
280
300
320
Deflection (mm)

Figure D.1

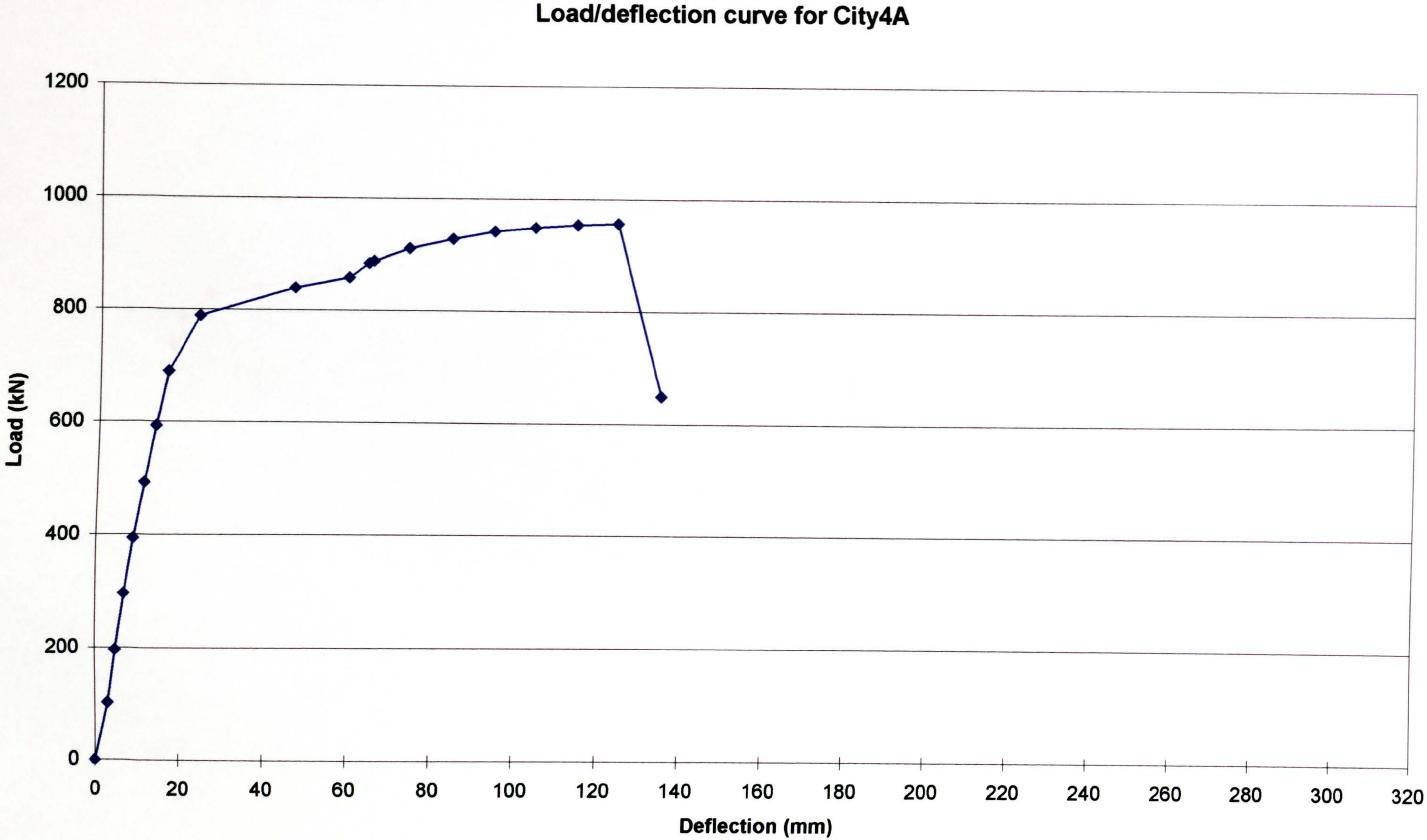
Load/deflection curve for City4A
Load (kN)
1200
1000
800
600
400
200
0
0
20
40
60
80
100
120
140
160
180
200
220
240
260
280
300
320
Deflection (mm)

Figure D.2

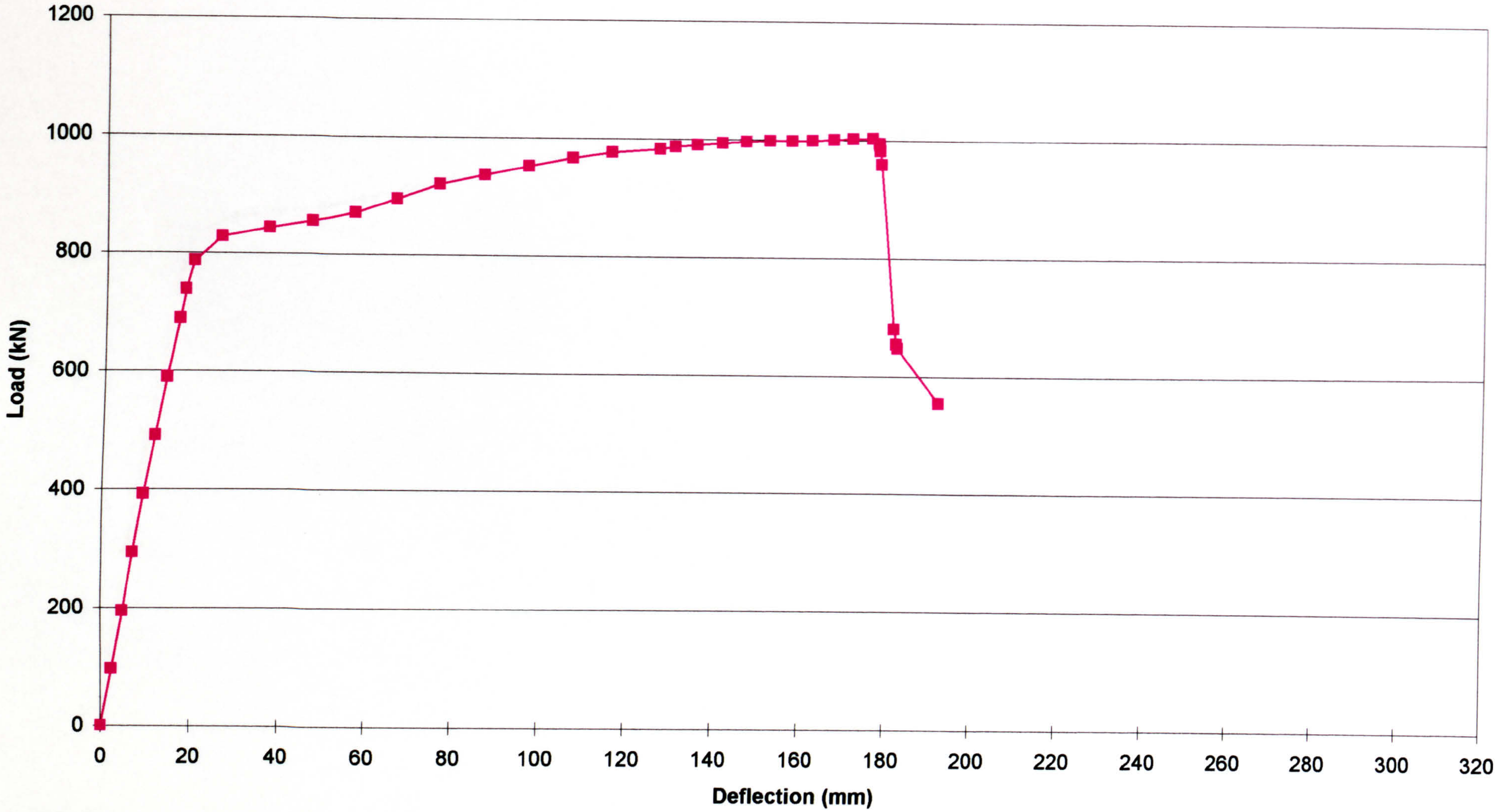
Load/deflection curve for City4b
Load (kN)
1200
1000
800
600
400
200
0
0
20
40
60
80
100
120
140
160
180
200
220
240
260
280
300
320
Deflection (mm)

Figure D.3

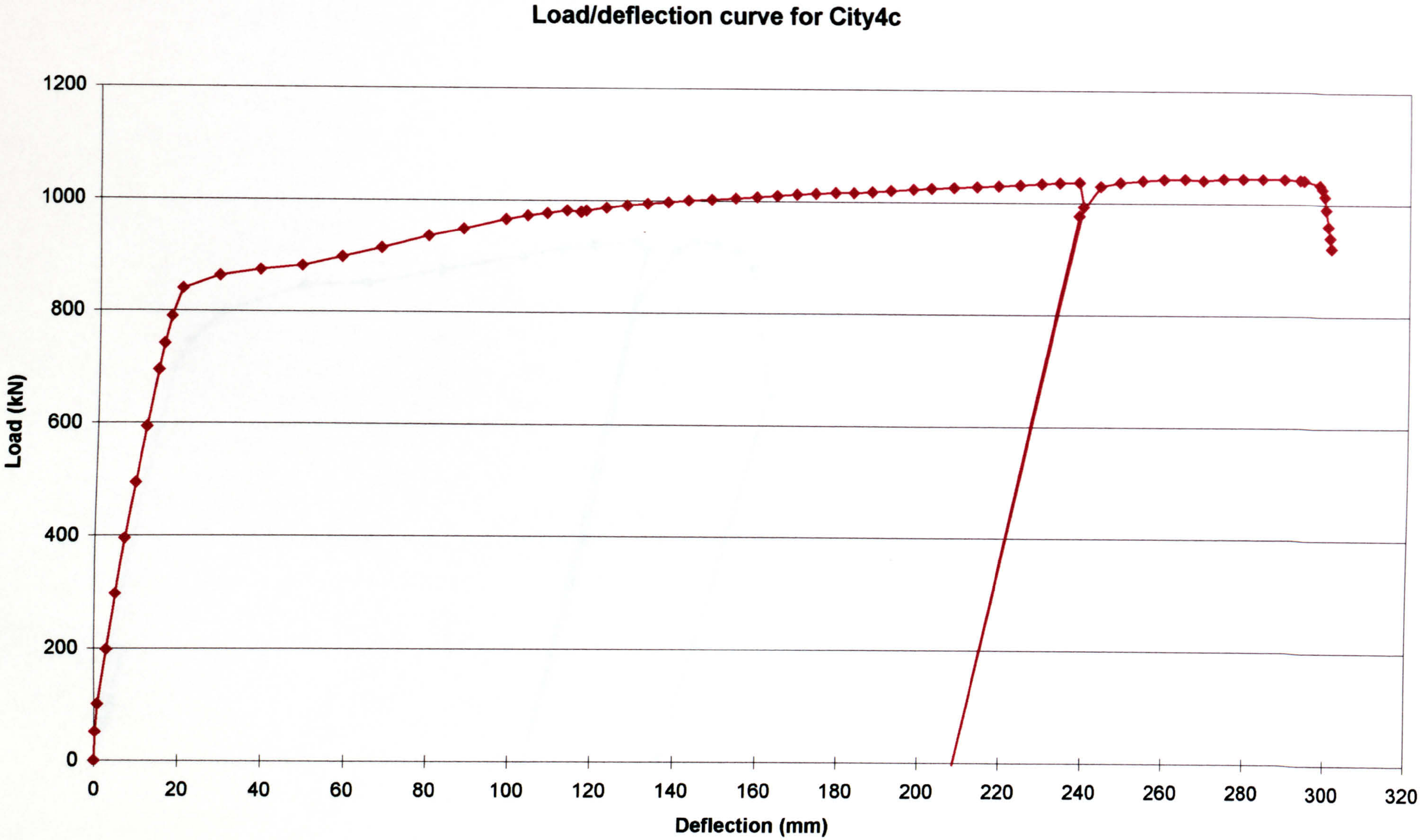
Load/deflection curve for City4c
Load (kN)
1200
1000
800
600
400
200
0
0
20
40
60
80
100
120
140
160
180
200
220
240
260
280
300
320
Deflection (mm)

Figure D.4

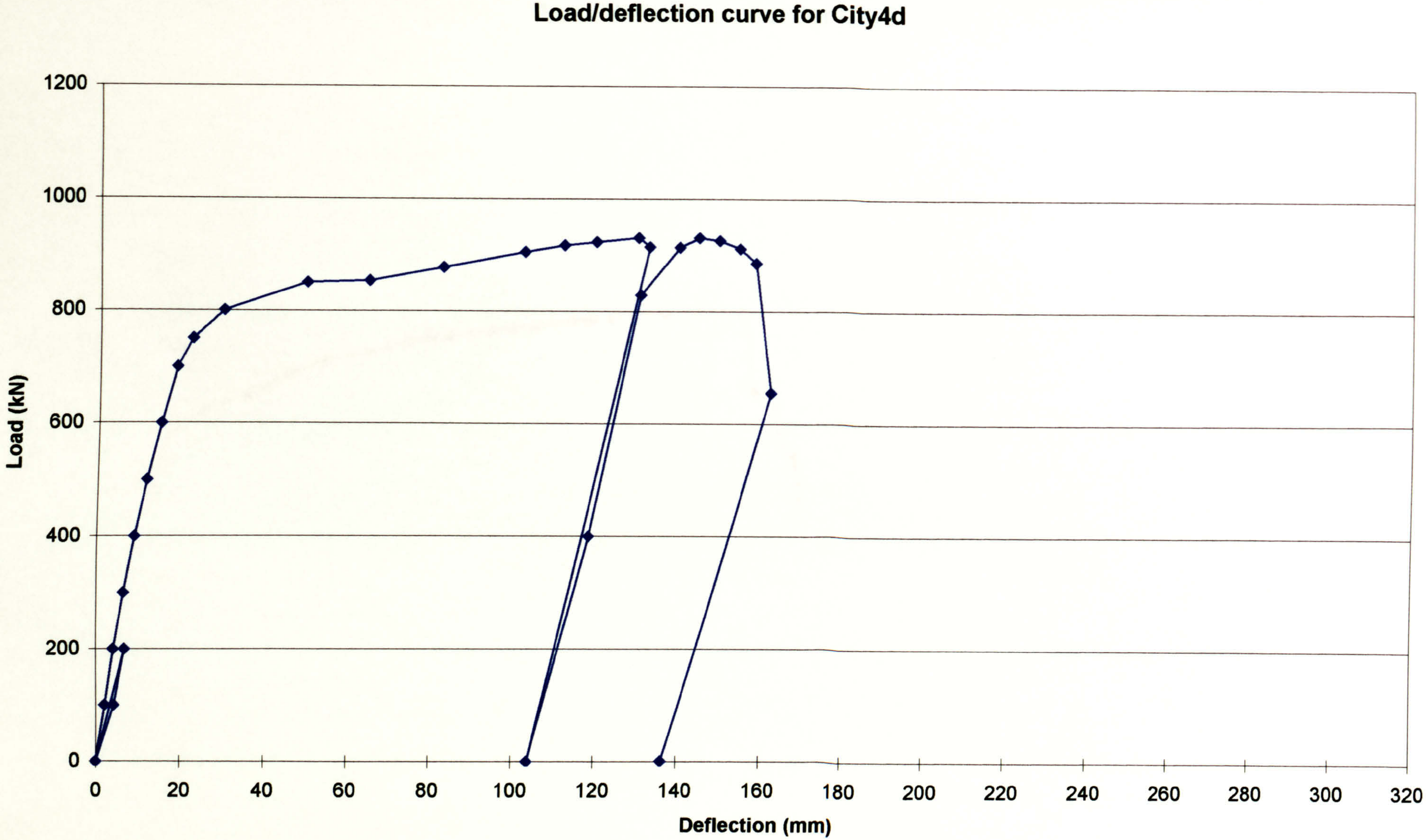
Load/deflection curve for City4d
Load (kN)
1200
1000
800
600
400
200
0
0
20
40
60
80
100
120
140
160
180
200
220
240
260
280
300
320
Deflection (mm)

Figure D.5

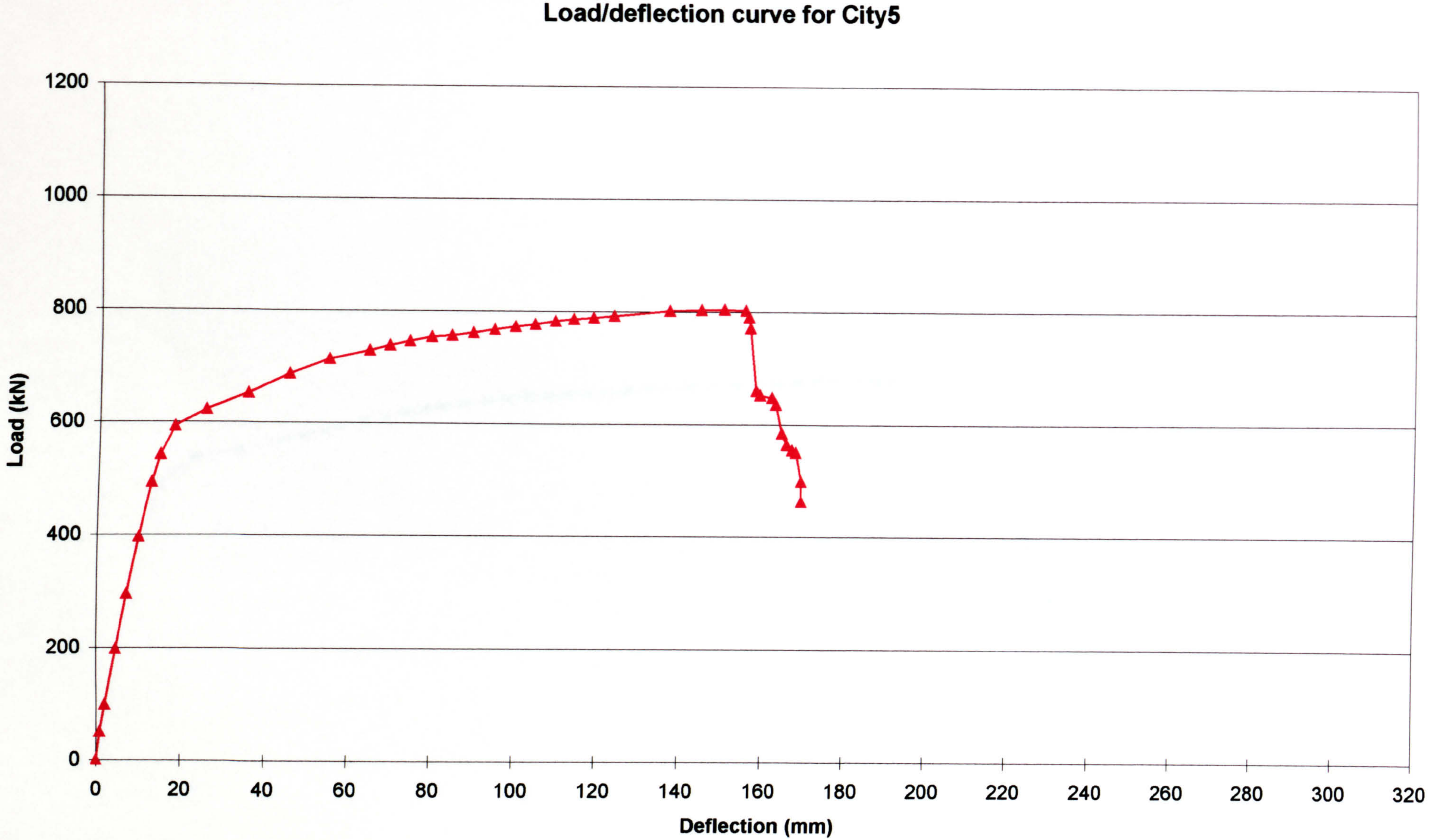
Load/deflection curve for City5
Load (kN)
1200
1000
800
600
400
200
0
0
20
40
60
80
100
120
140
160
180
200
220
240
260
280
300
320
Deflection (mm)

Figure D.6

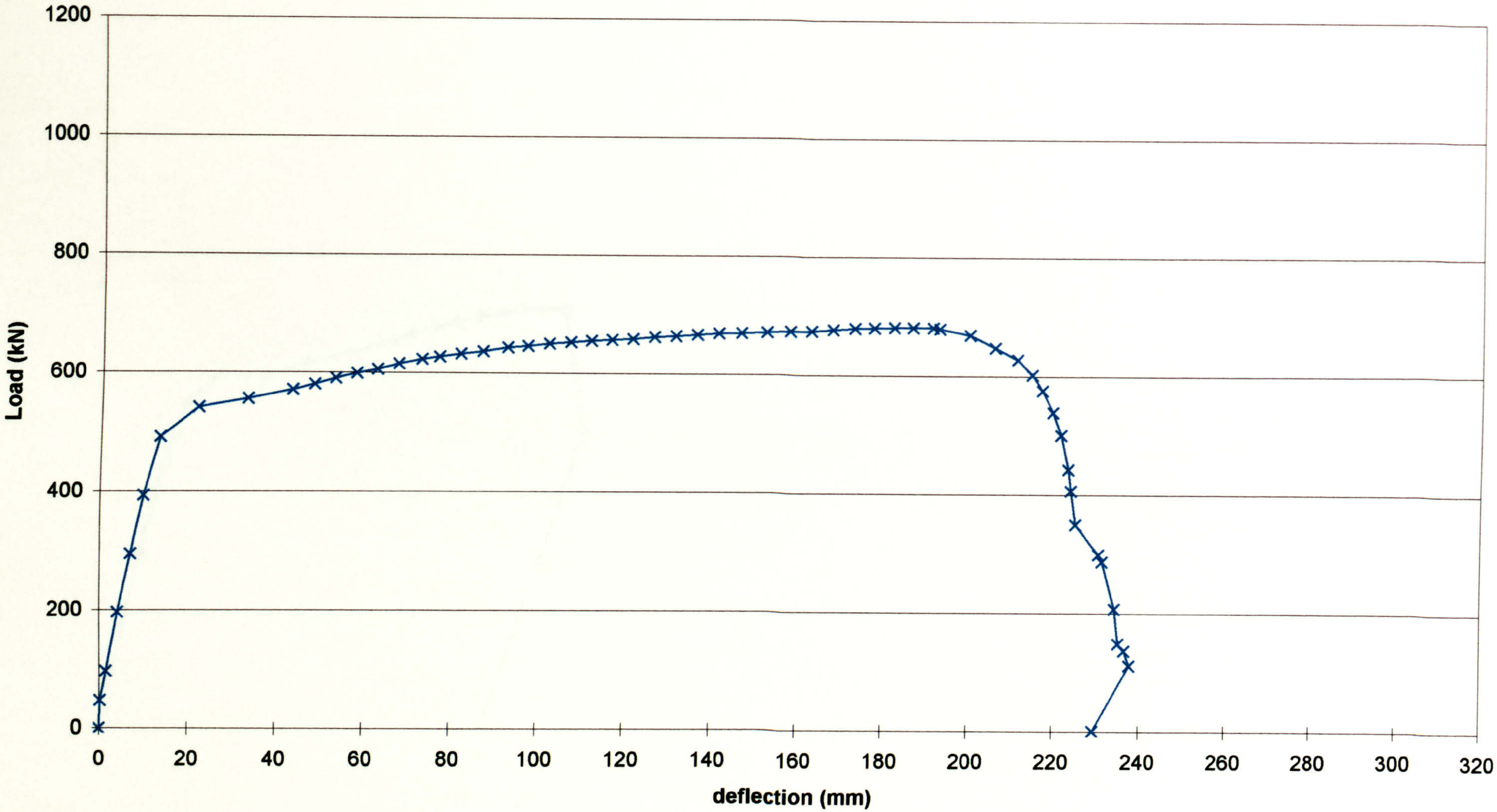
Load/deflection curve for City6
Load (kN)
1200
1000
800
600
400
200
0
0
20
40
60
80
100
120
140
160
180
200
220
240
260
280
300
320
deflection (mm)

Figure D.7

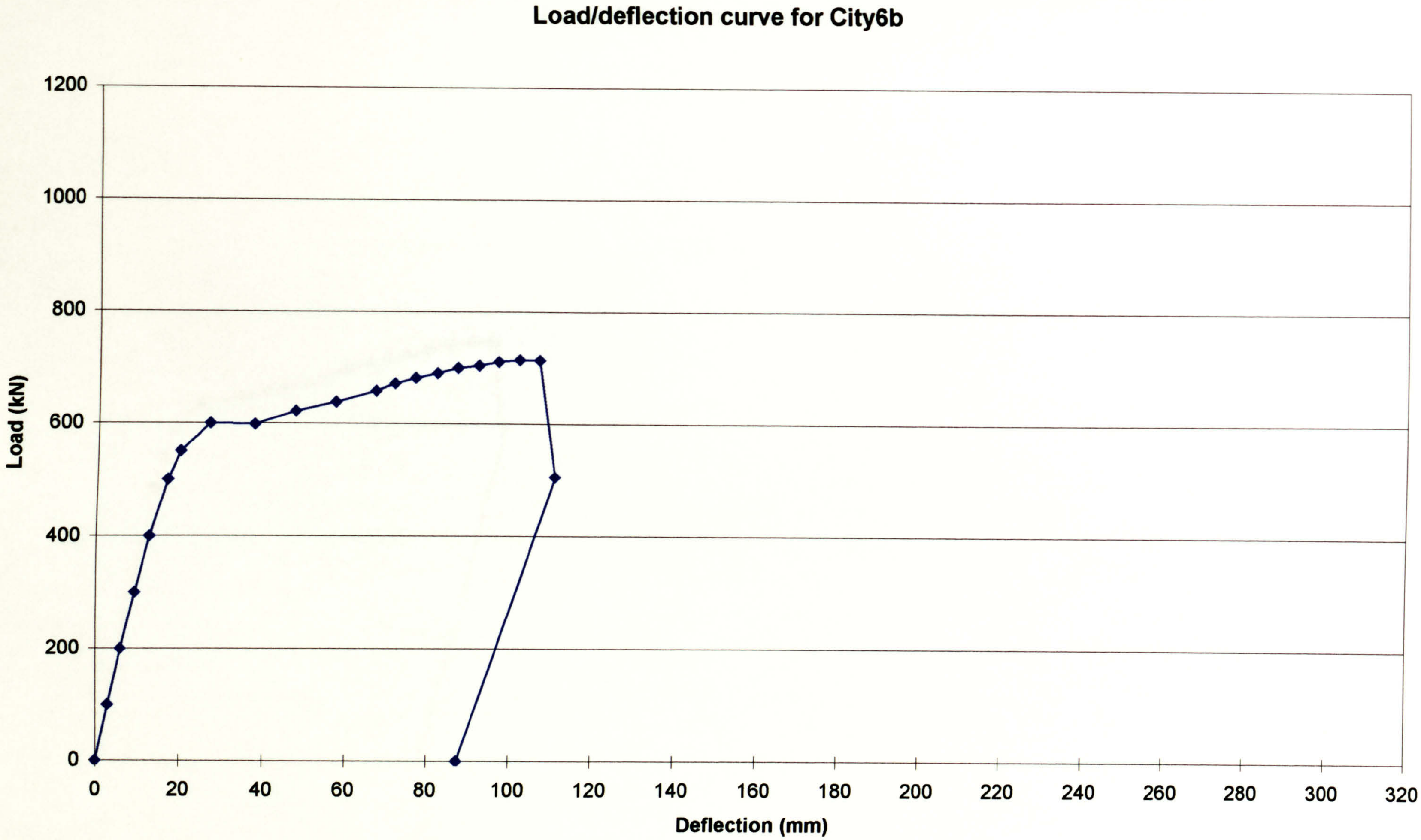
Load/deflection curve for City6b
Load (kN)
1200
1000
800
600
400
200
0
0
20
40
60
80
100
120
140
160
180
200
220
240
260
280
300
320
Deflection (mm)

Figure D.8

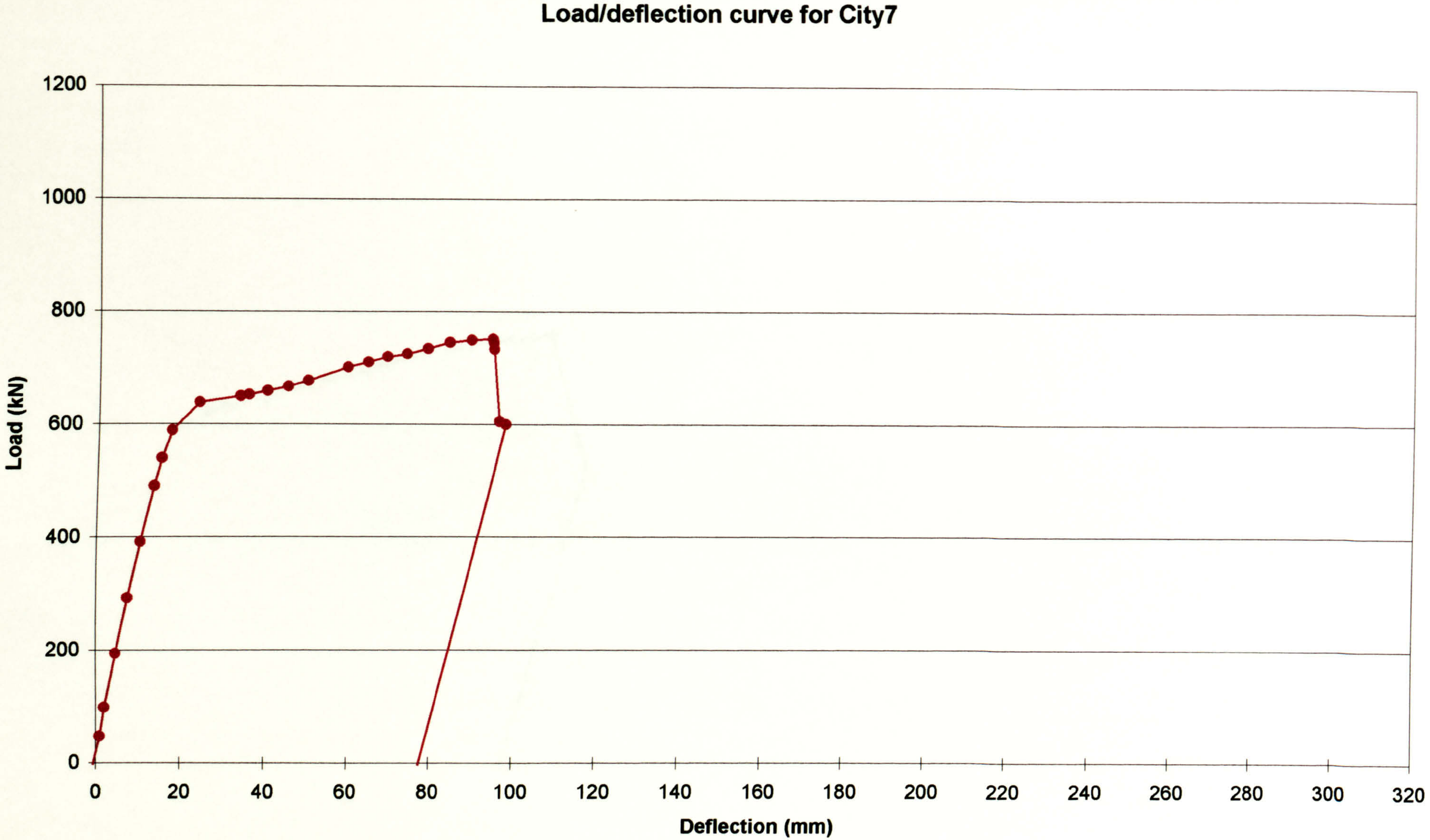
Load/deflection curve for City7
Load (kN)
1200
1000
800
600
400
200
0
0
20
40
60
80
100
120
140
160
180
200
220
240
260
280
300
320
Deflection (mm)

Figure D.9

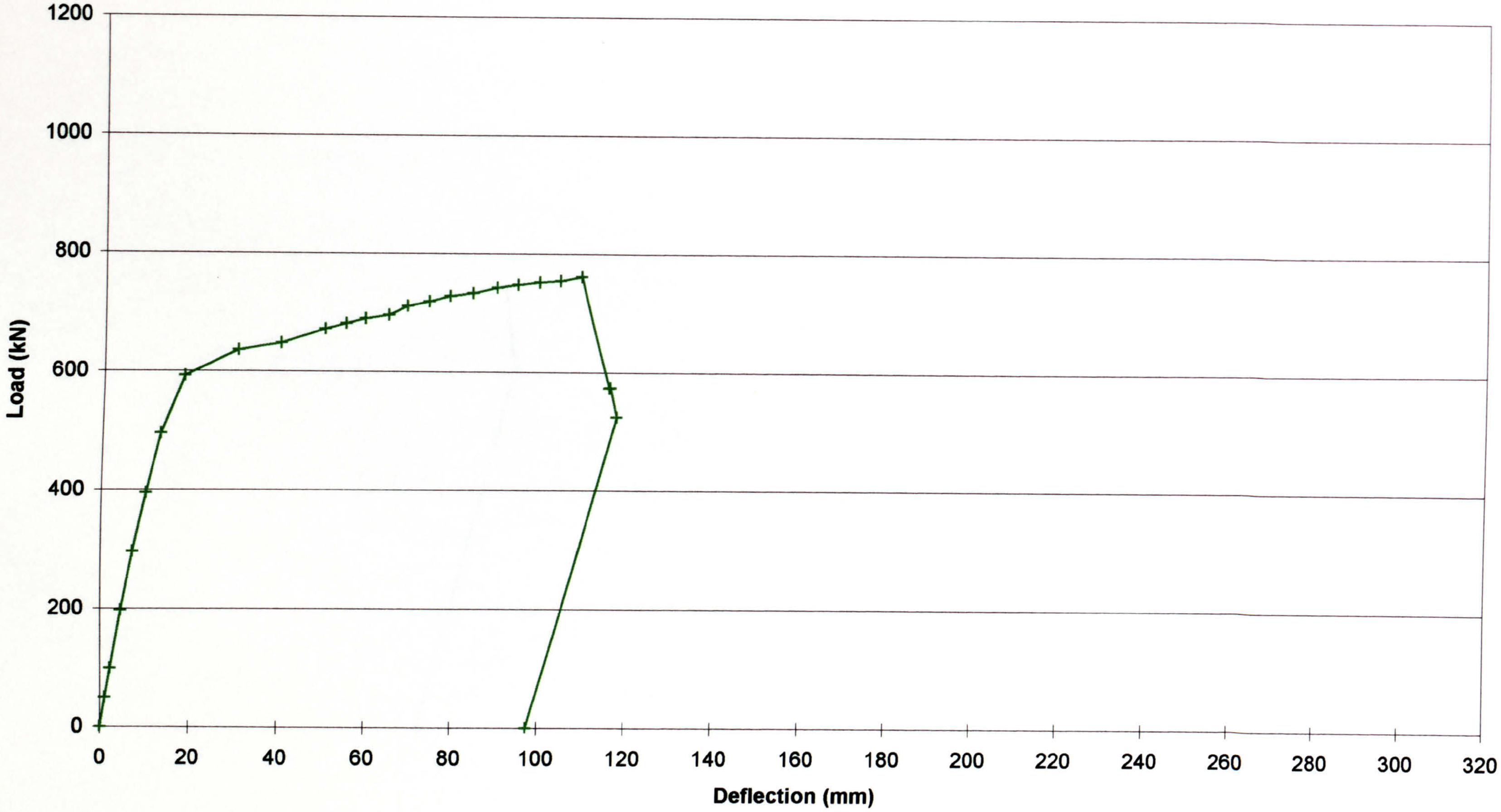
Load/deflection curve for City8
Load (kN)
1200
1000
800
600
400
200
0
0
20
40
60
80
100
120
140
160
180
200
220
240
260
280
300
320
Deflection (mm)

Figure D.10

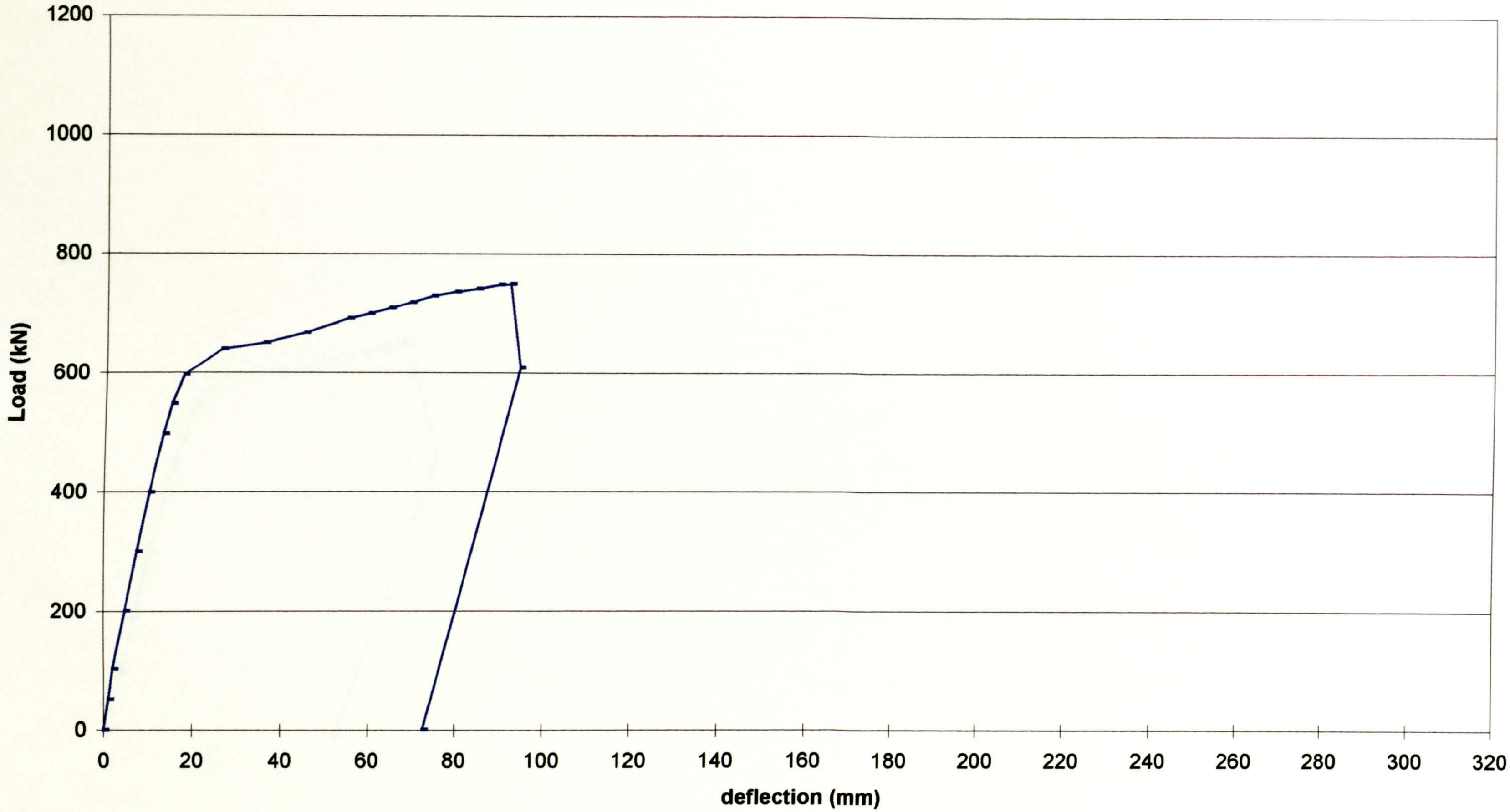
Load/deflection curve for City9
1200
1000
800
600
400
200
0
Load (kN)
0
20
40
60
80
100
120
140
160
180
200
220
240
260
280
300
320
deflection (mm)

Figure D.11

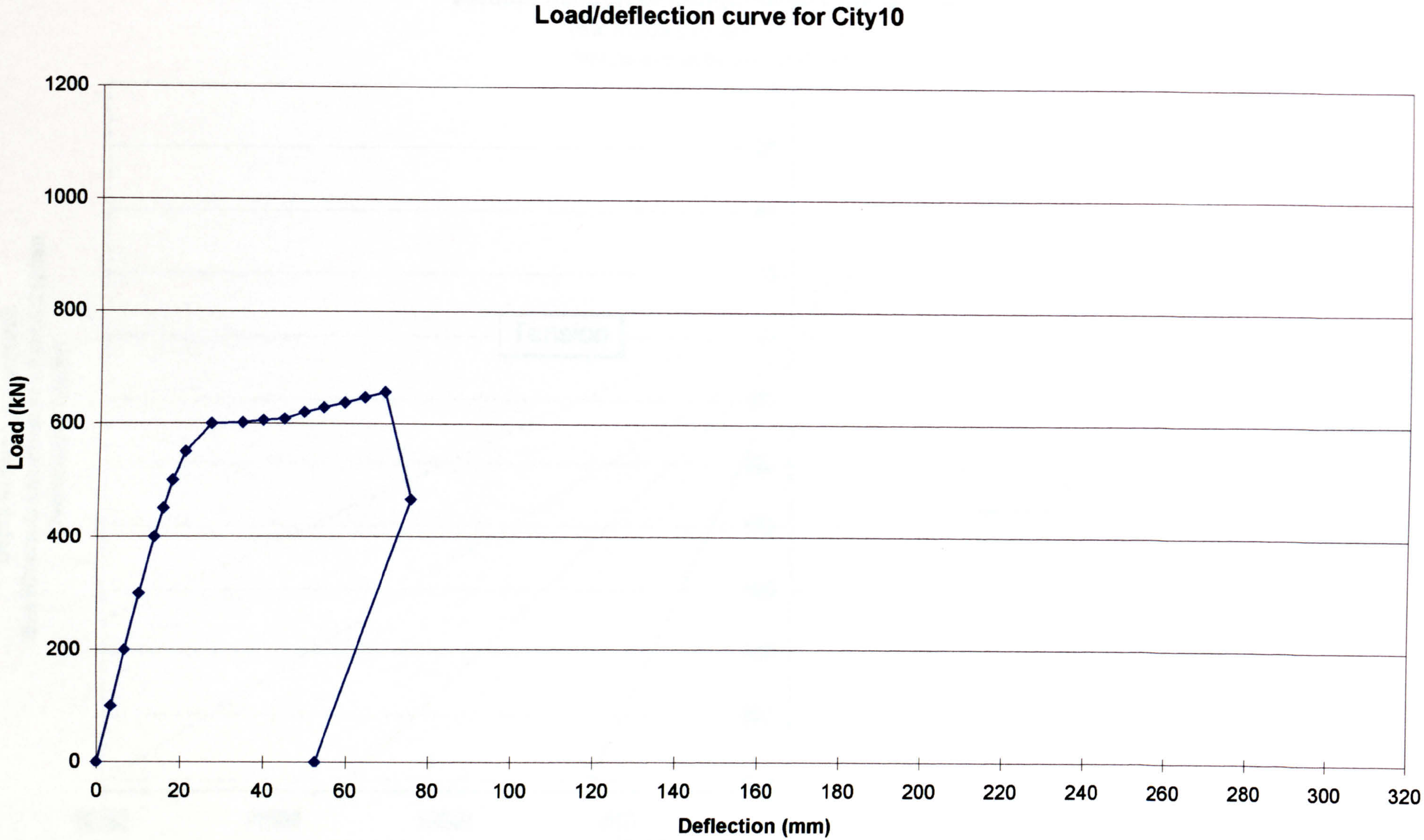
Load/deflection curve for City10
Load (kN)
1200
1000
800
600
400
200
0
0
20
40
60
80
100
120
140
160
180
200
220
240
260
280
300
320
Deflection (mm)

Figure D.12

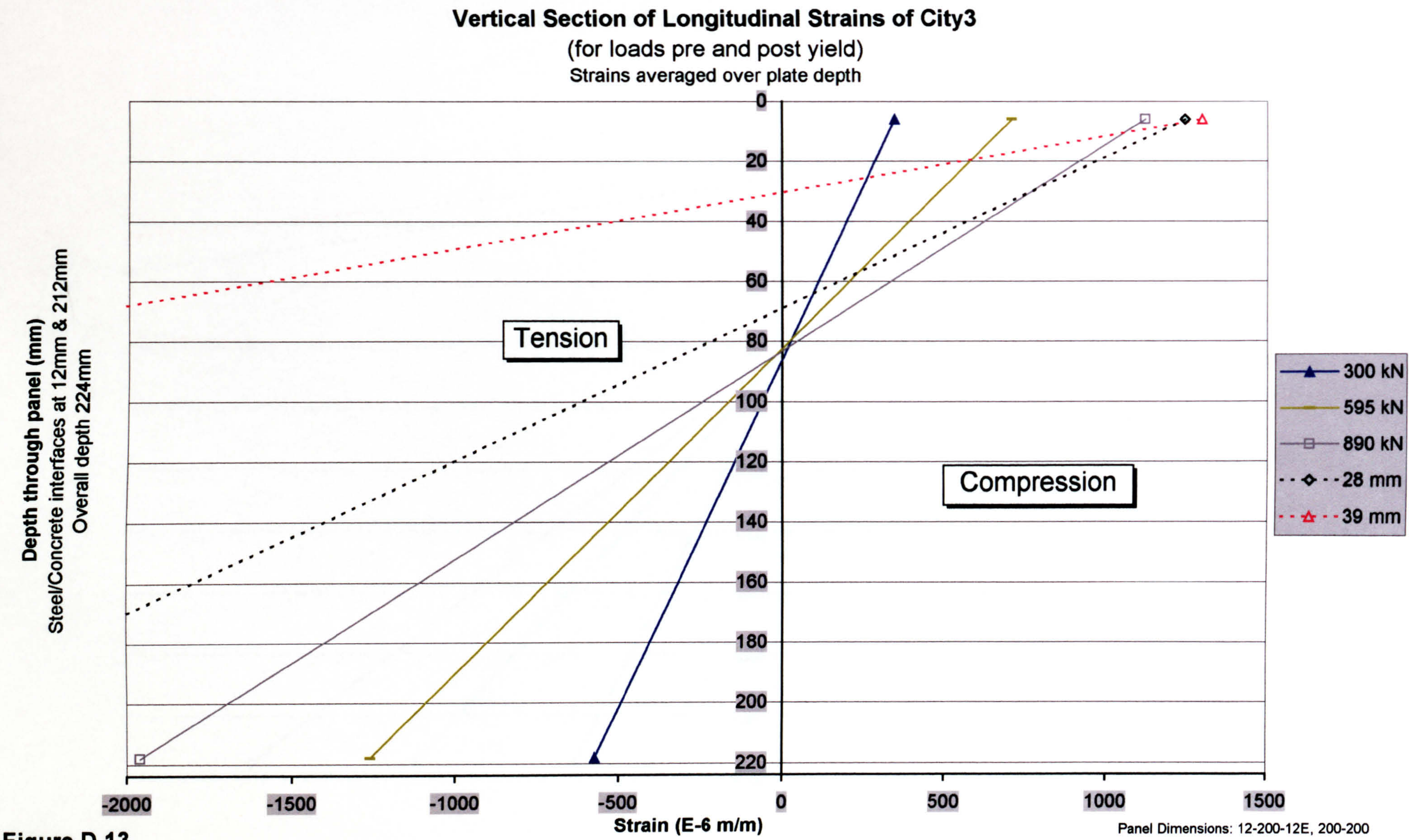
Vertical Section of Longitudinal Strains of City3
(for loads pre and post yield)
Strains averaged over plate depth
Depth through panel (mm)
Steel/Concrete interfaces at 12mm & 212mm
Overall depth 224mm
Tension
Compression
0
20
40
60
80
100
120
140
160
180
200
220
-2000
-1500
-1000
-500
0
500
1000
1500
Strain (E-6 m/m)
300 kN
595 kN
890 kN
28 mm
39 mm
Panel Dimensions: 12-200-12E, 200-200

Figure D.13

Vertical Section of Longitudinal Strains of City4a

(for loads pre and post yield)

Strains averaged over plate depth

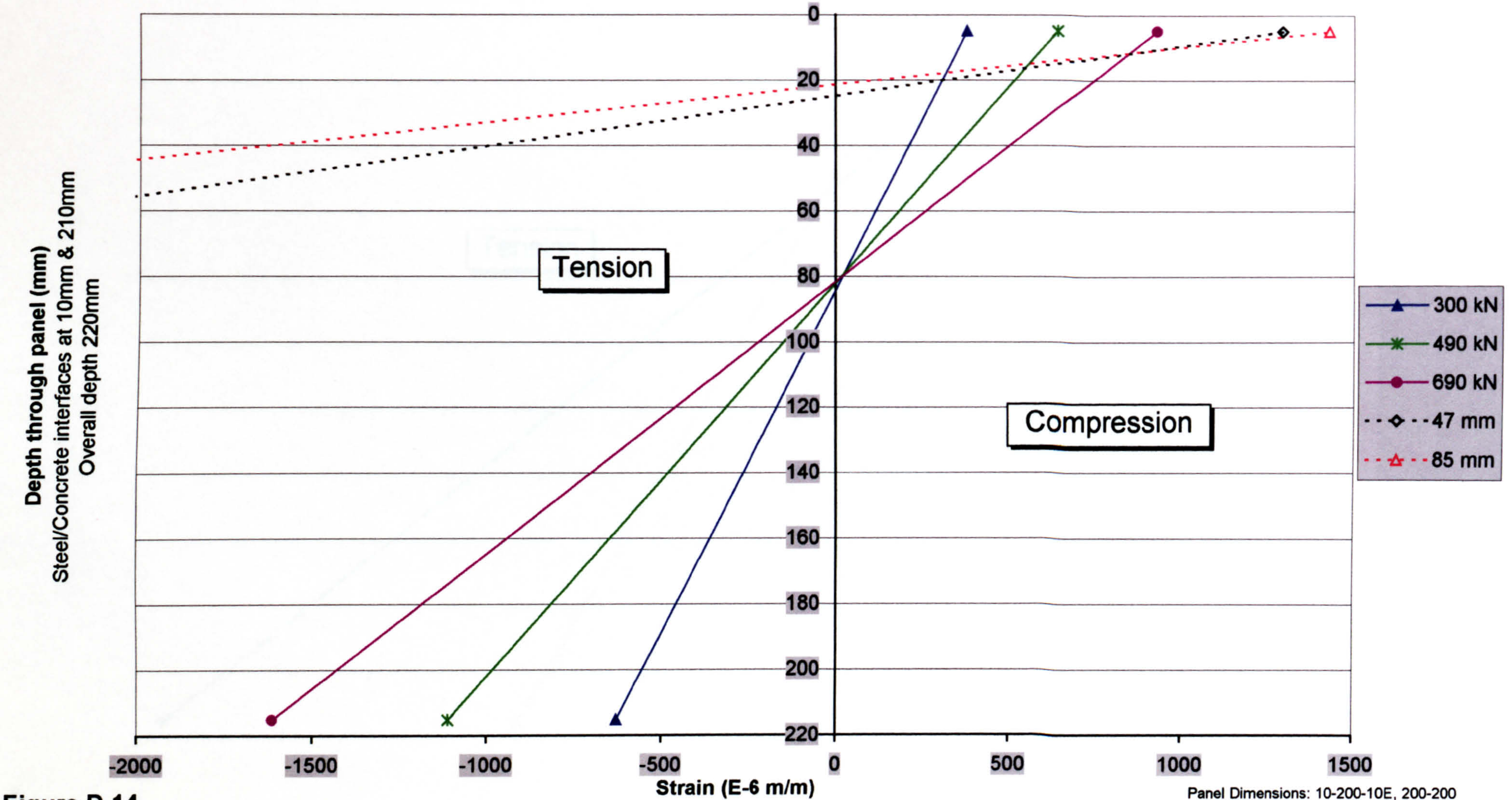

Panel Dimensions: 10-200-10E, 200-200

Figure D.14

Vertical Section of Longitudinal Strains of City4b

(for loads pre and post yield)

Strains averaged over plate depth

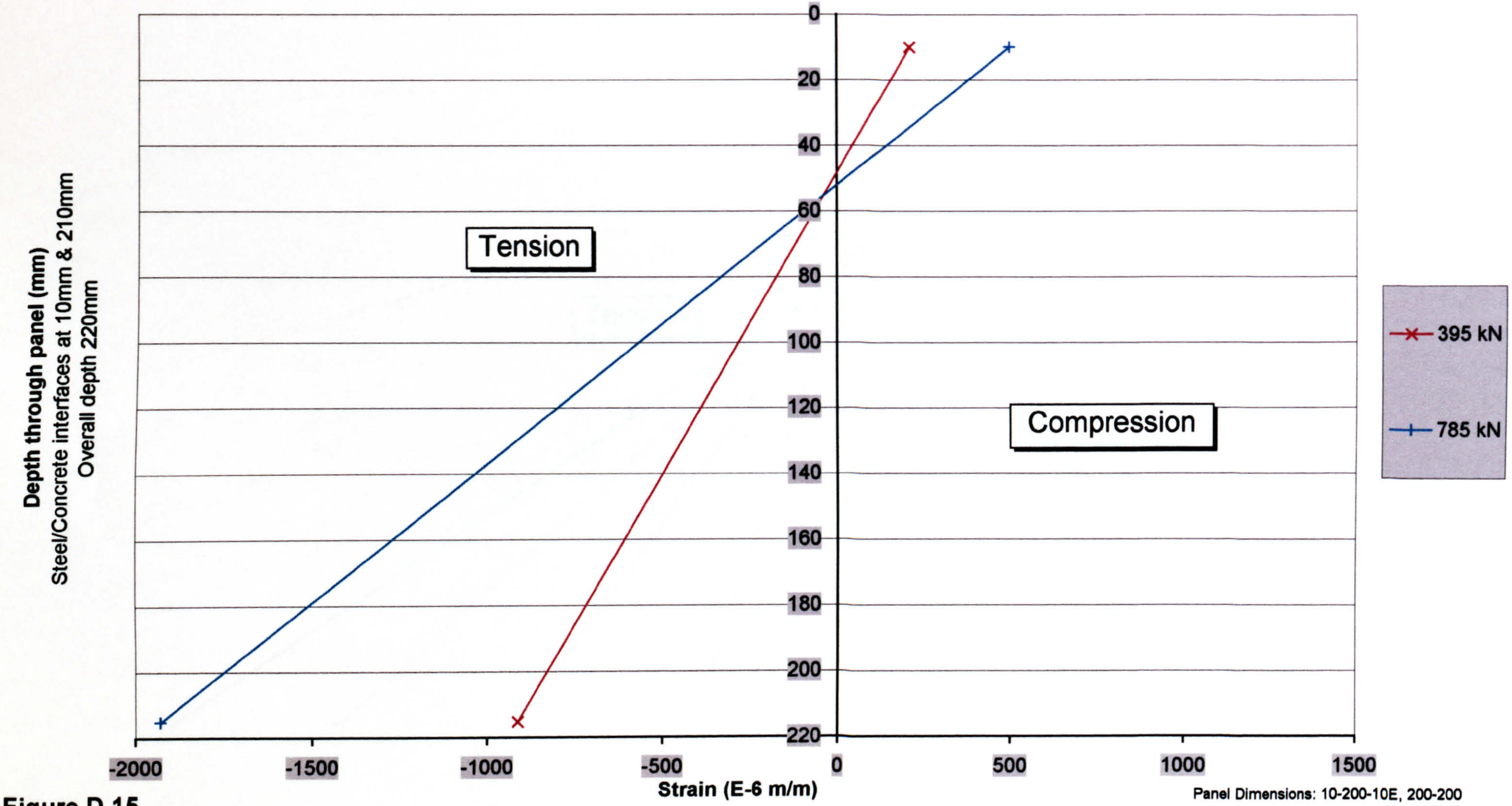

Figure D.15

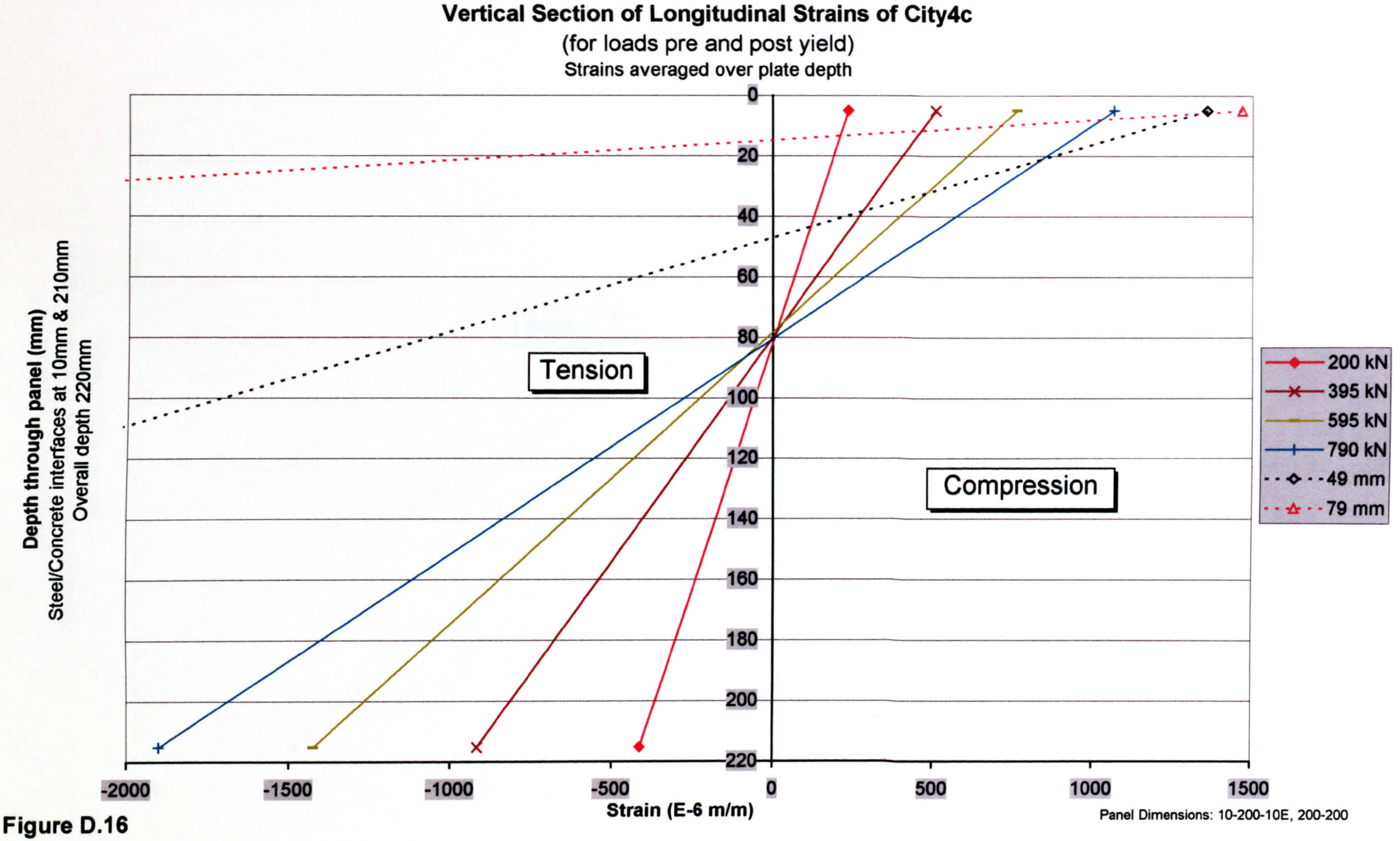
Vertical Section of Longitudinal Strains of City4c
(for loads pre and post yield)
Strains averaged over plate depth
Depth through panel (mm)
Steel/Concrete interfaces at 10mm & 210mm
Overall depth 220mm
0
20
40
60
80
100
120
140
160
180
200
220
Tension
Compression
200 kN
395 kN
595 kN
790 kN
49 mm
79 mm
-2000
-1500
-1000
-500
0
500
1000
1500
Strain (E-6 m/m)
Panel Dimensions: 10-200-10E, 200-200

Figure D.16

Vertical Section of Longitudinal Strains of City4d

(for loads pre and post yield)

Strains averaged over plate depth

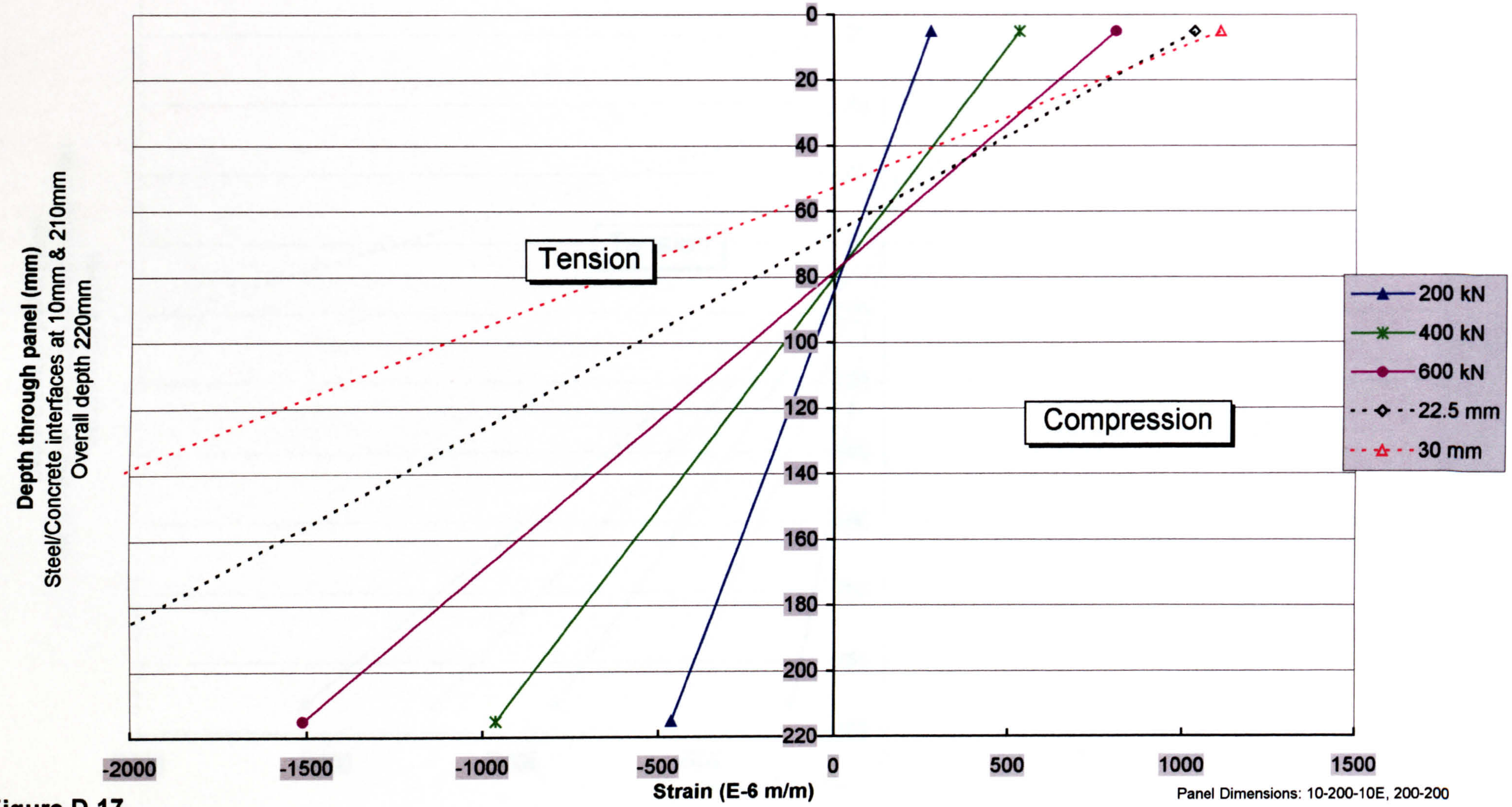

Figure D.17

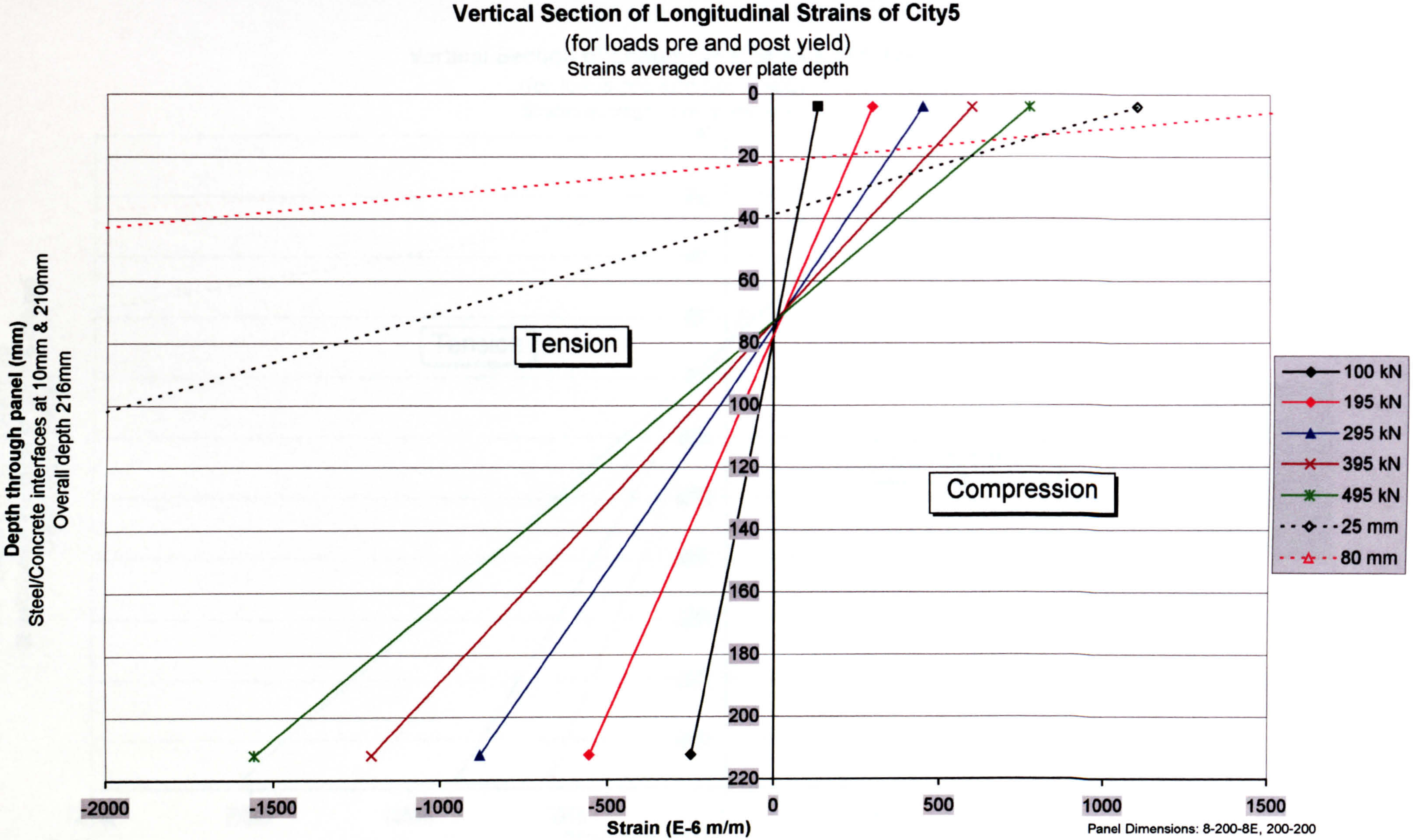
Vertical Section of Longitudinal Strains of City5
(for loads pre and post yield)
Strains averaged over plate depth
Depth through panel (mm)
Steel/Concrete interfaces at 10mm & 210mm
Overall depth 216mm
Tension
Compression
0
20
40
60
80
100
120
140
160
180
200
220
-2000
-1500
-1000
-500
0
500
1000
1500
Strain (E-6 m/m)
100 kN
195 kN
295 kN
395 kN
495 kN
25 mm
80 mm
Panel Dimensions: 8-200-8E, 200-200

Figure D.18

Vertical Section of Longitudinal Strains of City6

(for loads pre and post yield)

Strains averaged over plate depth

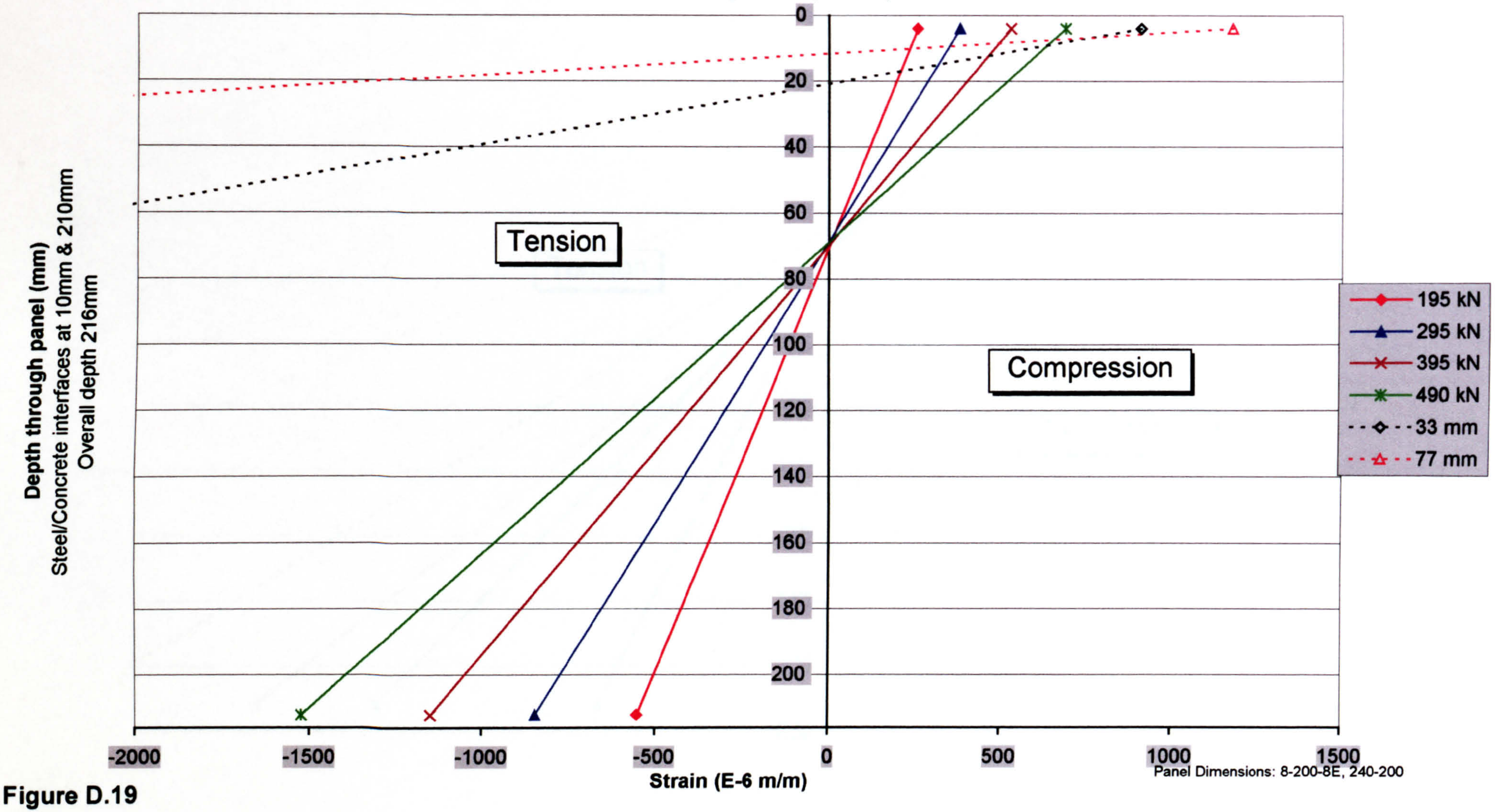

Figure D.19

Vertical Section of Longitudinal Strains of City6b

(for loads pre and post yield)

Strains averaged over plate depth

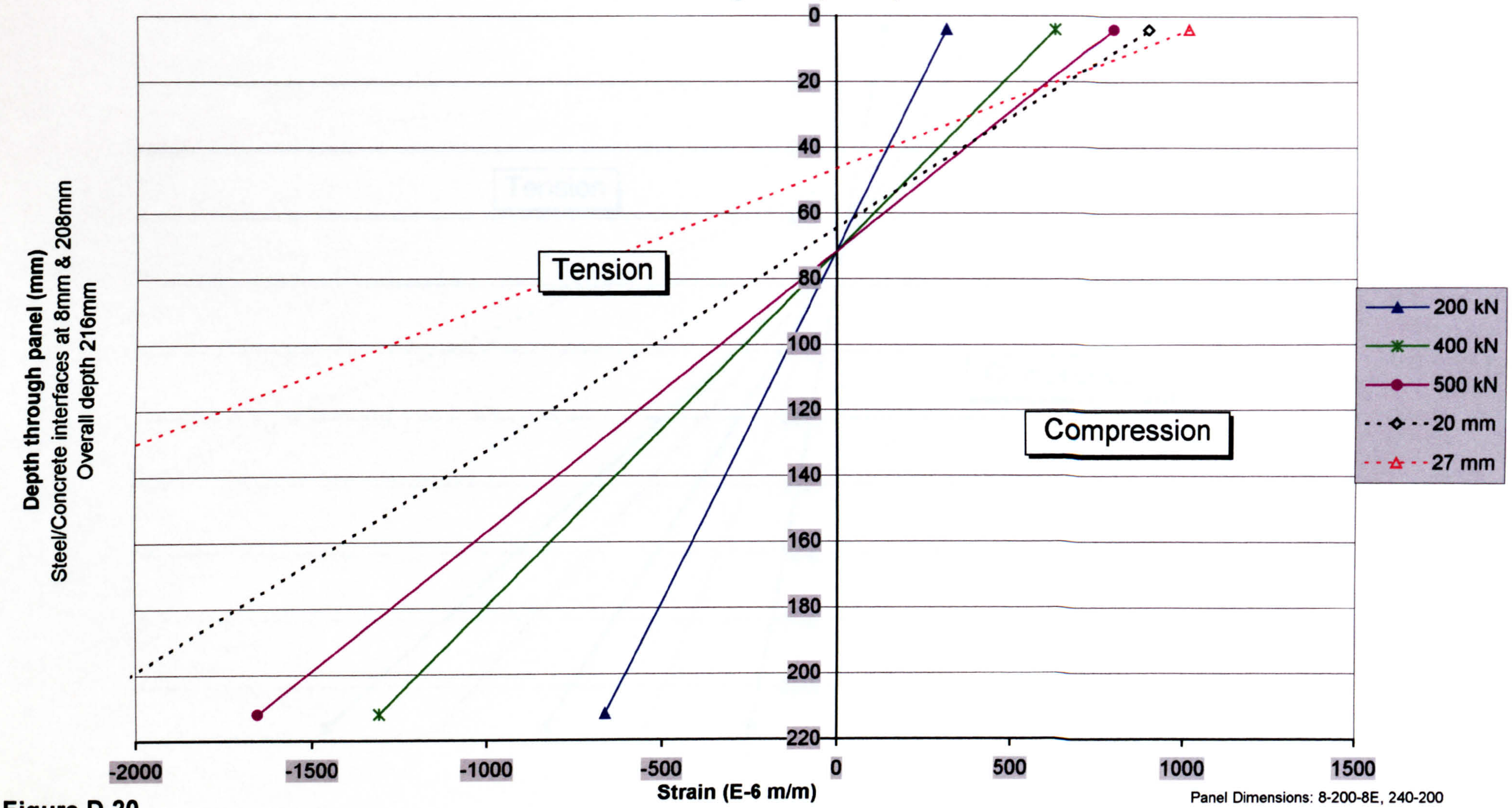

Panel Dimensions: 8-200-8E, 240-200

Figure D.20

Vertical Section of Longitudinal Strains of City7

(for loads pre and post yield)

Strains averaged over plate depth

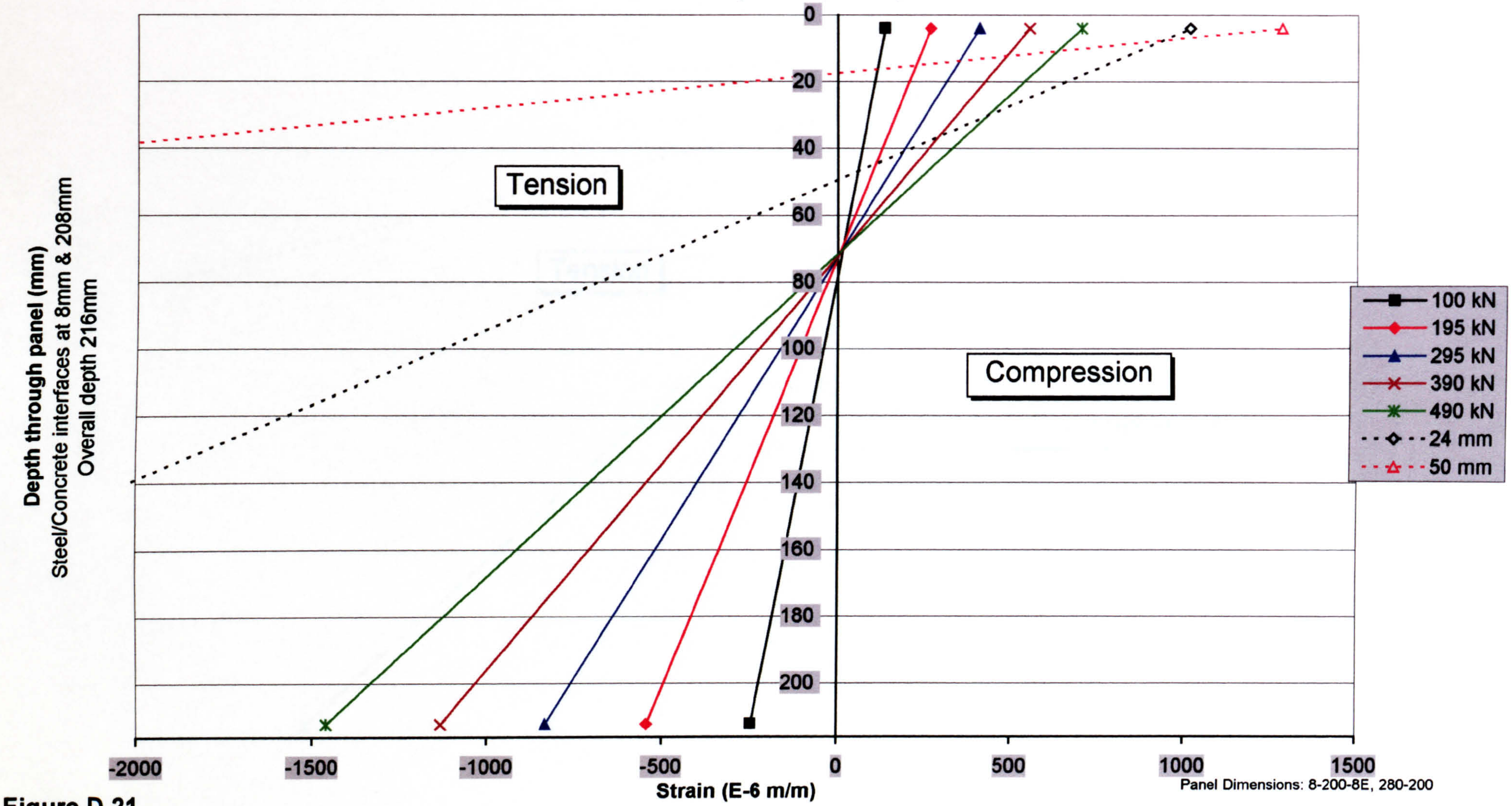

Figure D.21

Vertical Section of Longitudinal Strains of City8

(for loads pre and post yield)

Strains averaged over plate depth

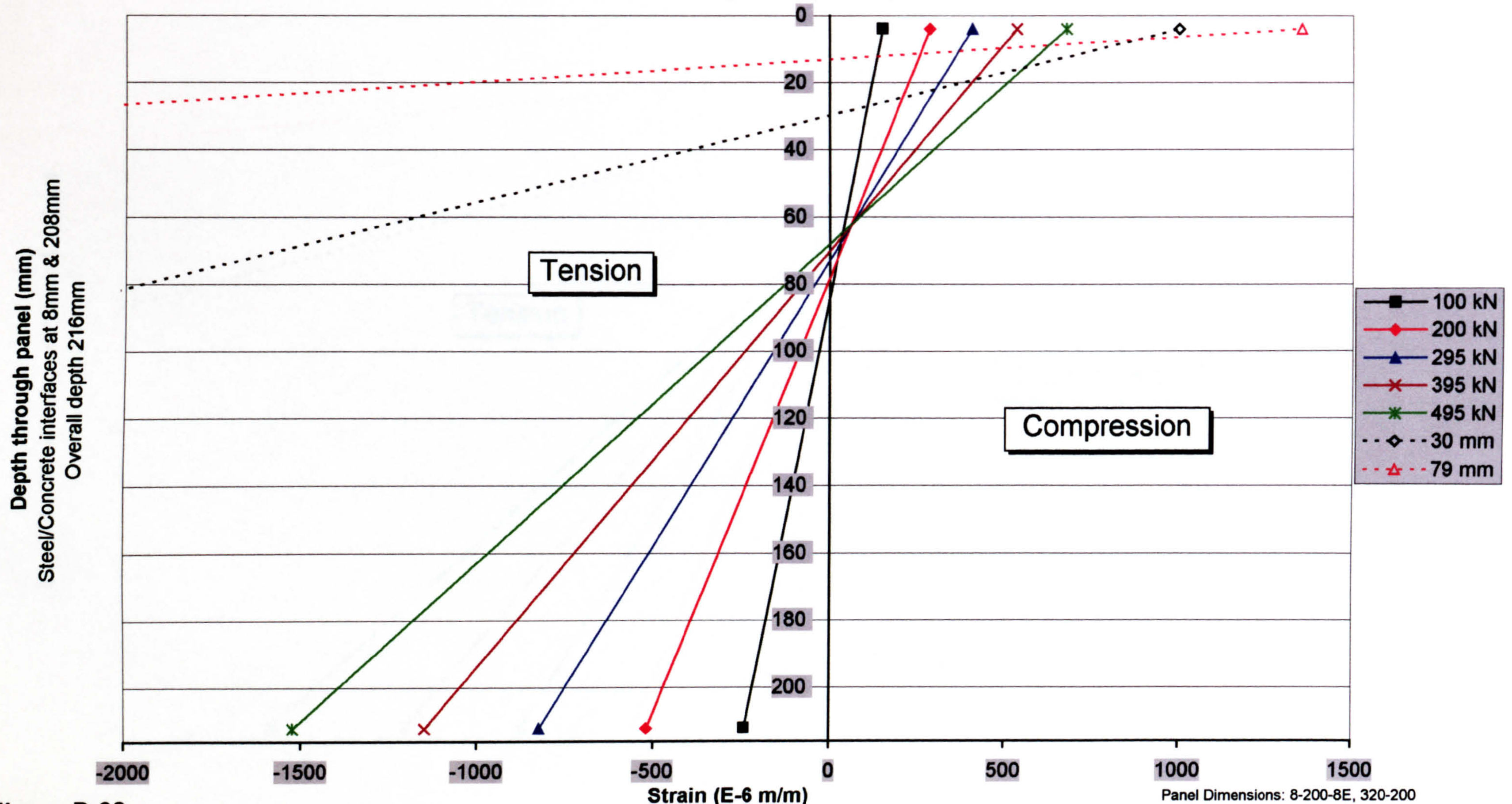

Figure D.22

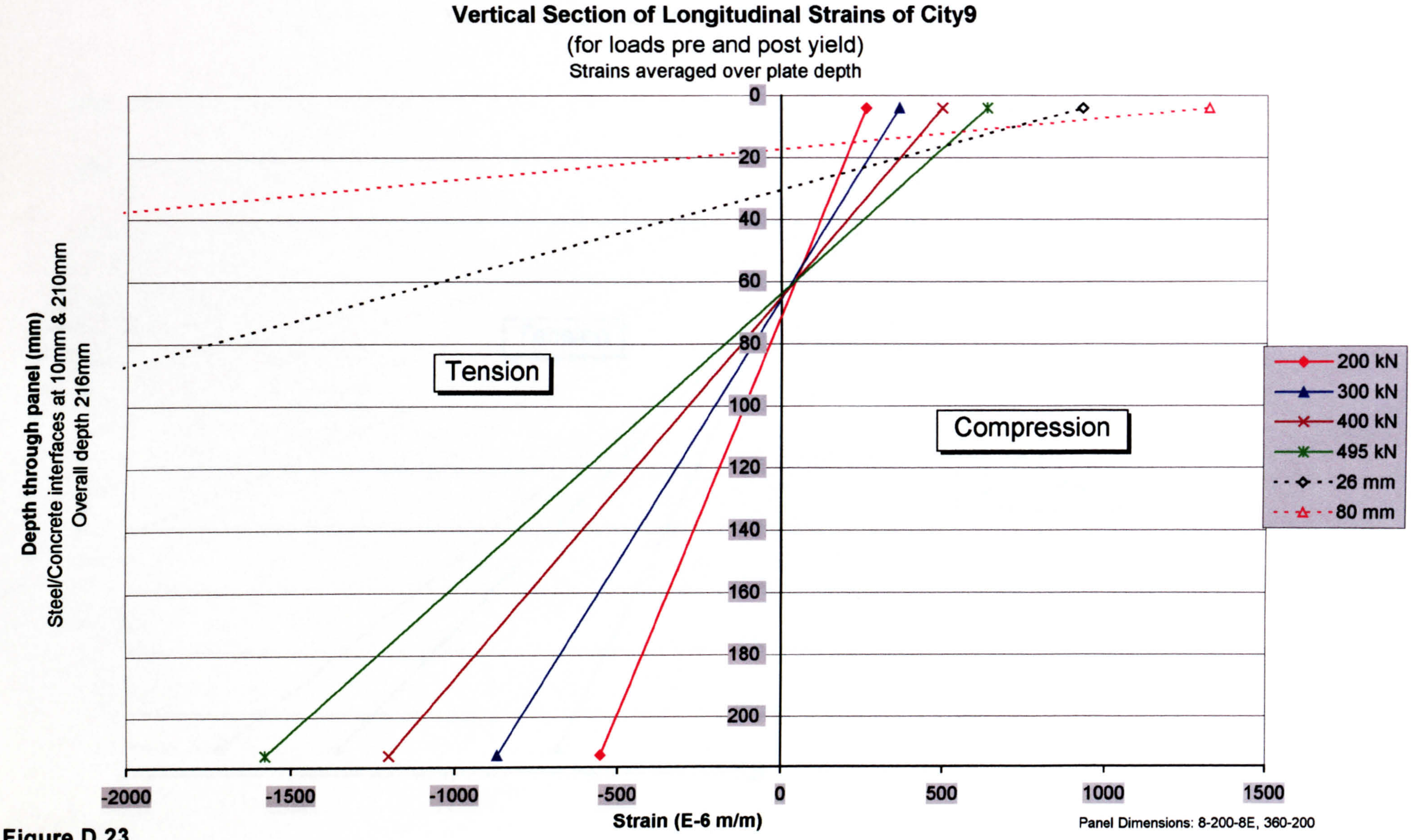
Vertical Section of Longitudinal Strains of City9
(for loads pre and post yield)
Strains averaged over plate depth
Depth through panel (mm)
Steel/Concrete interfaces at 10mm & 210mm
Overall depth 216mm
0
20
40
60
80
100
120
140
160
180
200
Tension
Compression
200 kN
300 kN
400 kN
495 kN
26 mm
80 mm
-2000
-1500
-1000
-500
0
500
1000
1500
Strain (E-6 m/m)
Panel Dimensions: 8-200-8E, 360-200

Figure D.23

Vertical Section of Longitudinal Strains of City10

(for loads pre and post yield)

Strains averaged over plate depth

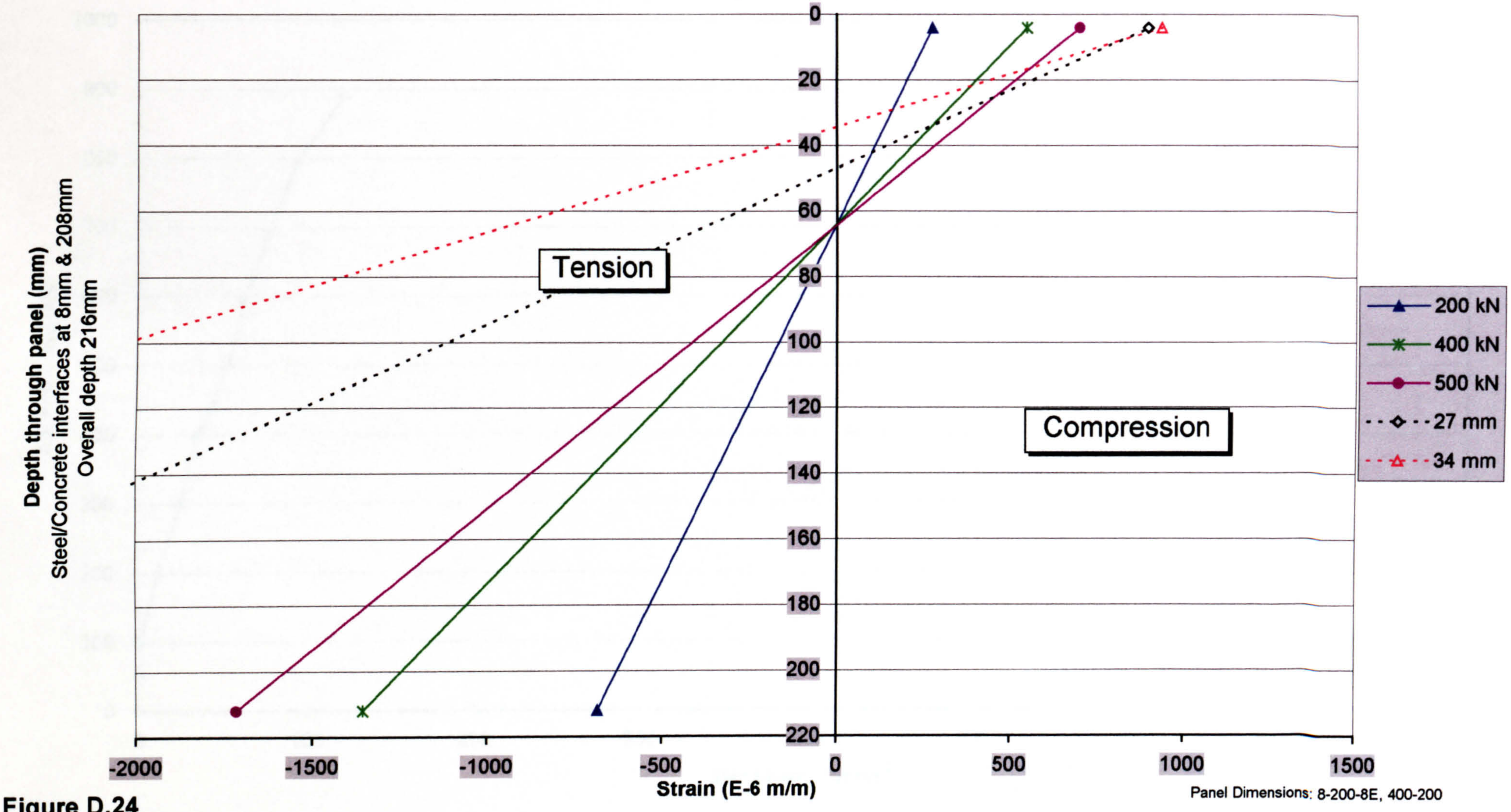

Figure D.24

Tensile Axial Bar Stresses in City3
(for applied loads in the elastic region)

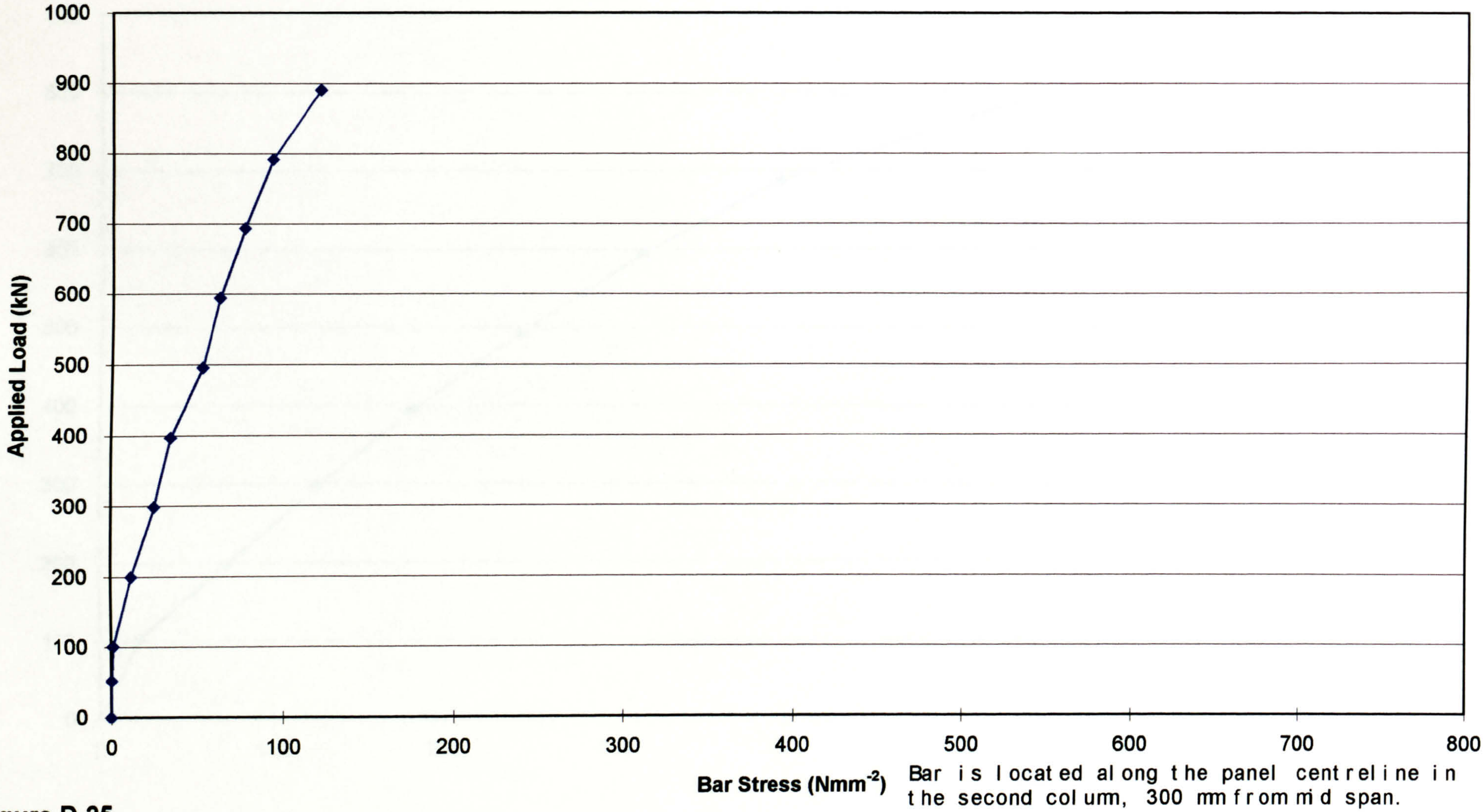

Figure D.25

Tensile Axial Bar Stresses in City4a
(for applied loads in the elastic region)

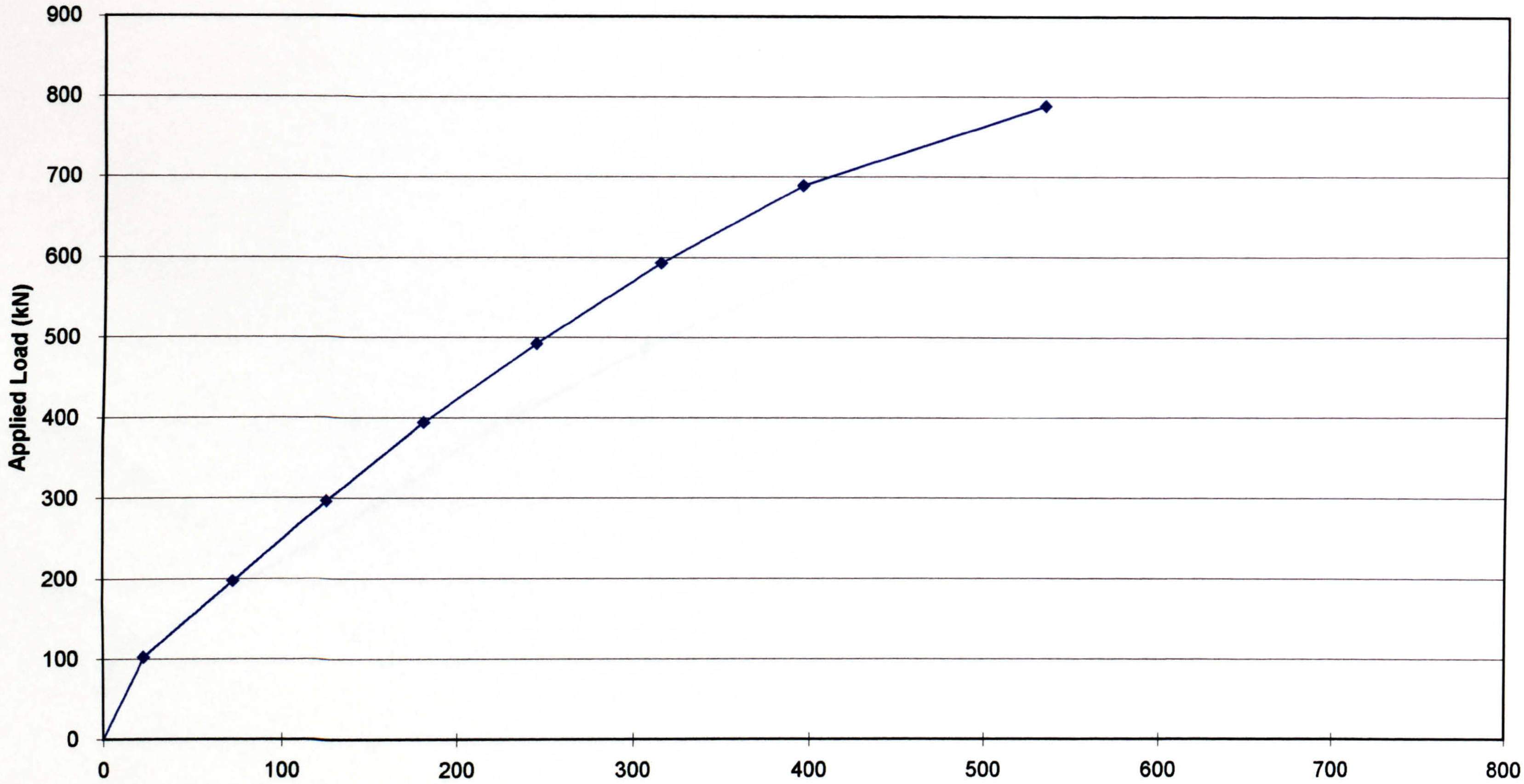

Bar is located along the panel centreline in the second column, 300 mm from mid span.

Figure D.26

Tensile Axial Bar Stresses in City4b
(for applied loads in the elastic region)

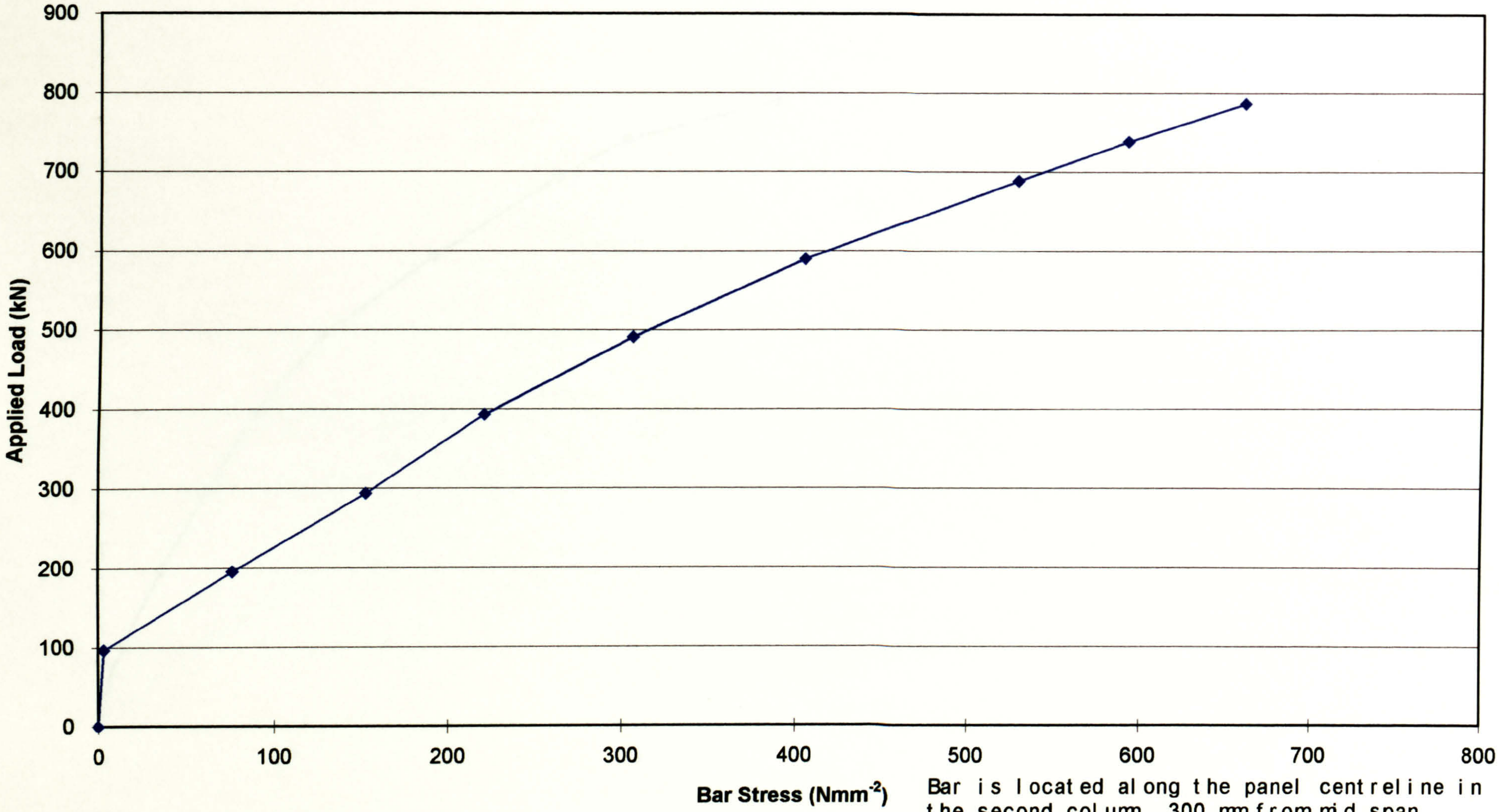

Bar is located along the panel centreline in the second column, 300 mm from mid span.

Figure D.27

Tensile Axial Bar Stresses in City4c
(for applied loads in the elastic region)

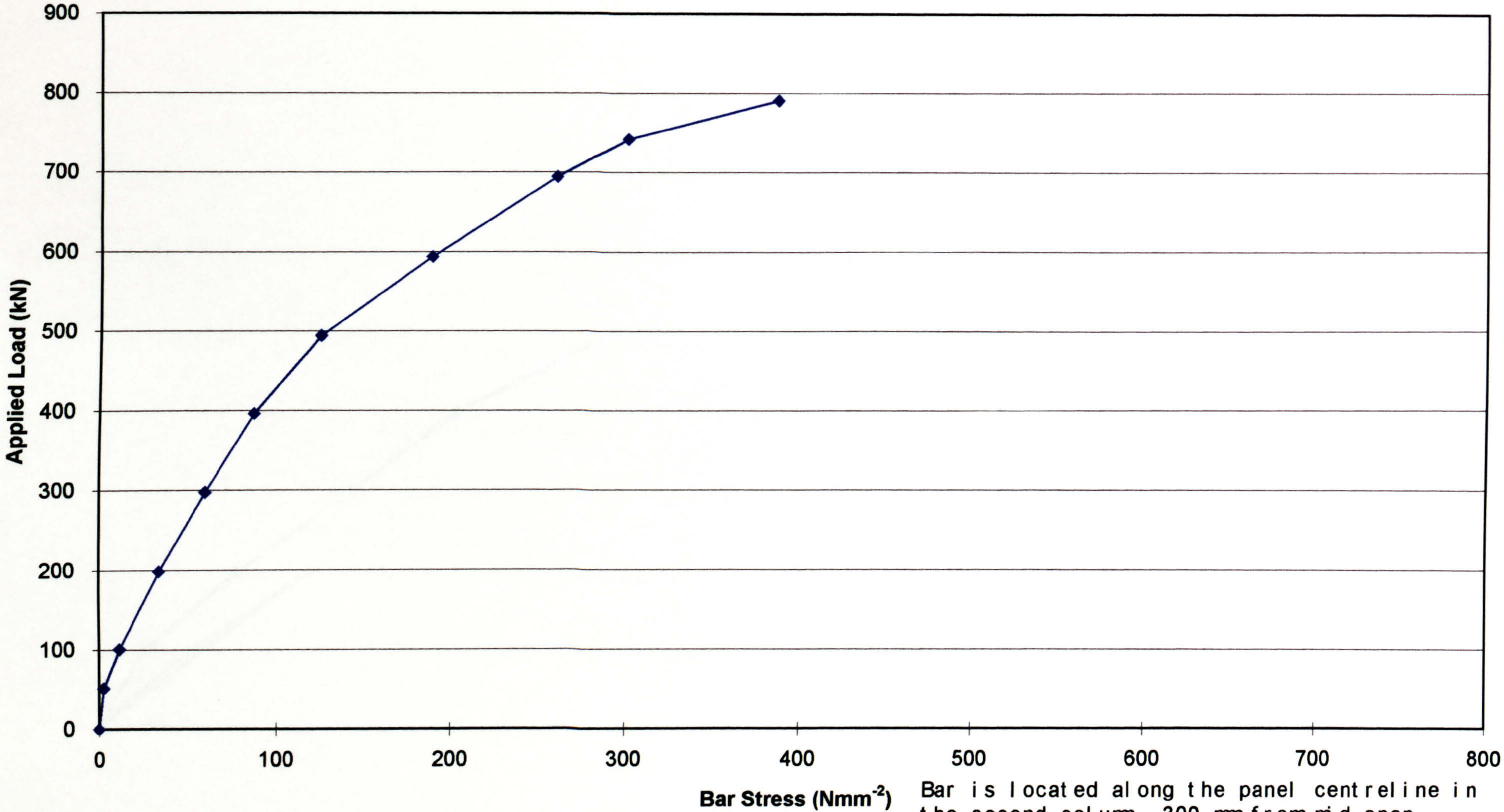

Bar is located along the panel centreline in the second column, 300 mm from mid span.

Figure D.28

Tensile Axial Bar Stresses in City4d
(for applied loads in the elastic region)

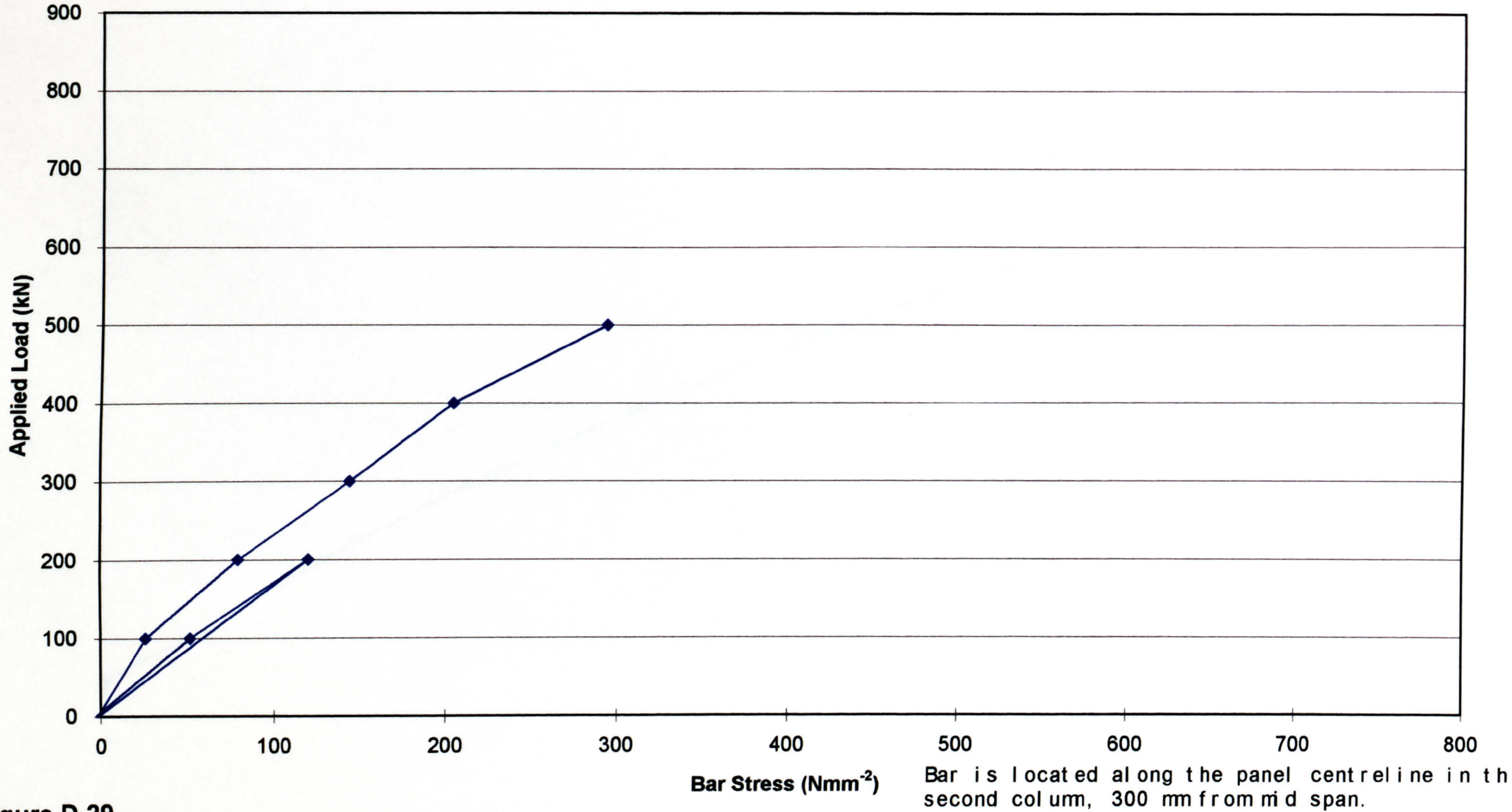

Figure D.29

Tensile Axial Bar Stresses in City5
(for applied loads in the elastic region)

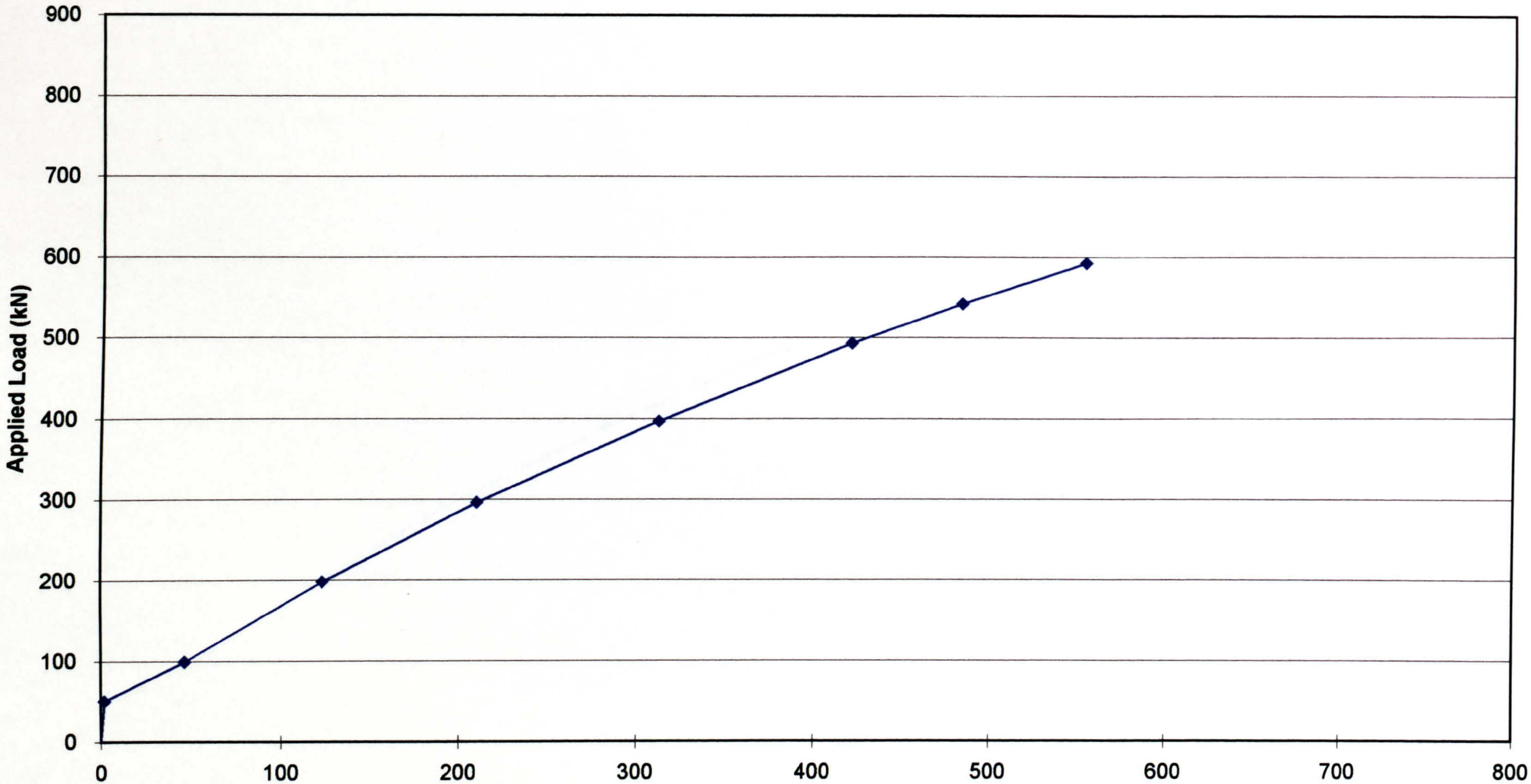

Bar is located along the panel centreline in the second column, 300 mm from mid span.

Figure D.30

Tensile Axial Bar Stresses in City6
(for applied loads in the elastic region)

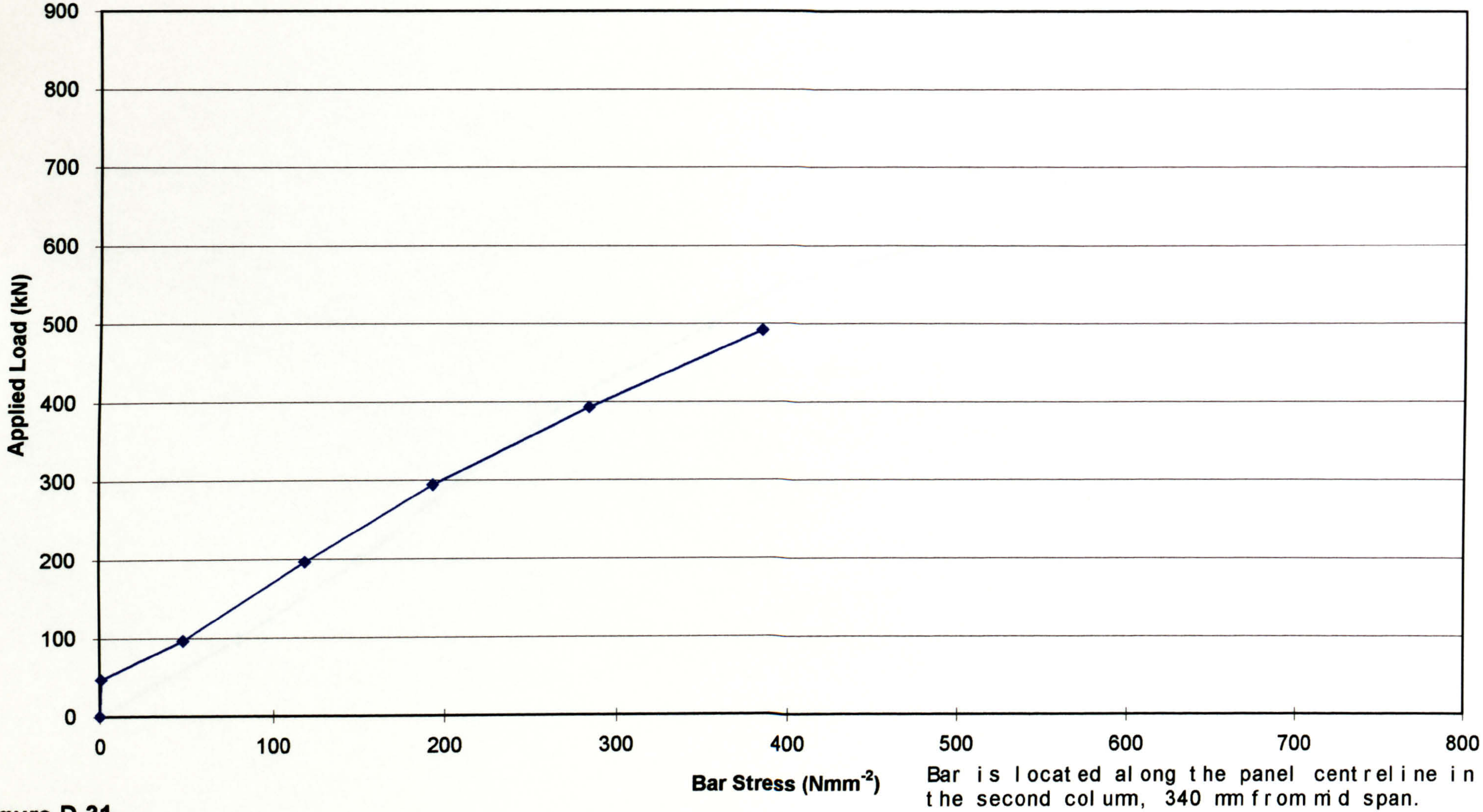

Bar is located along the panel centreline in the second column, 340 mm from mid span.

Figure D.31

Tensile Axial Bar Stresses in City6b
(for applied loads in the elastic region)

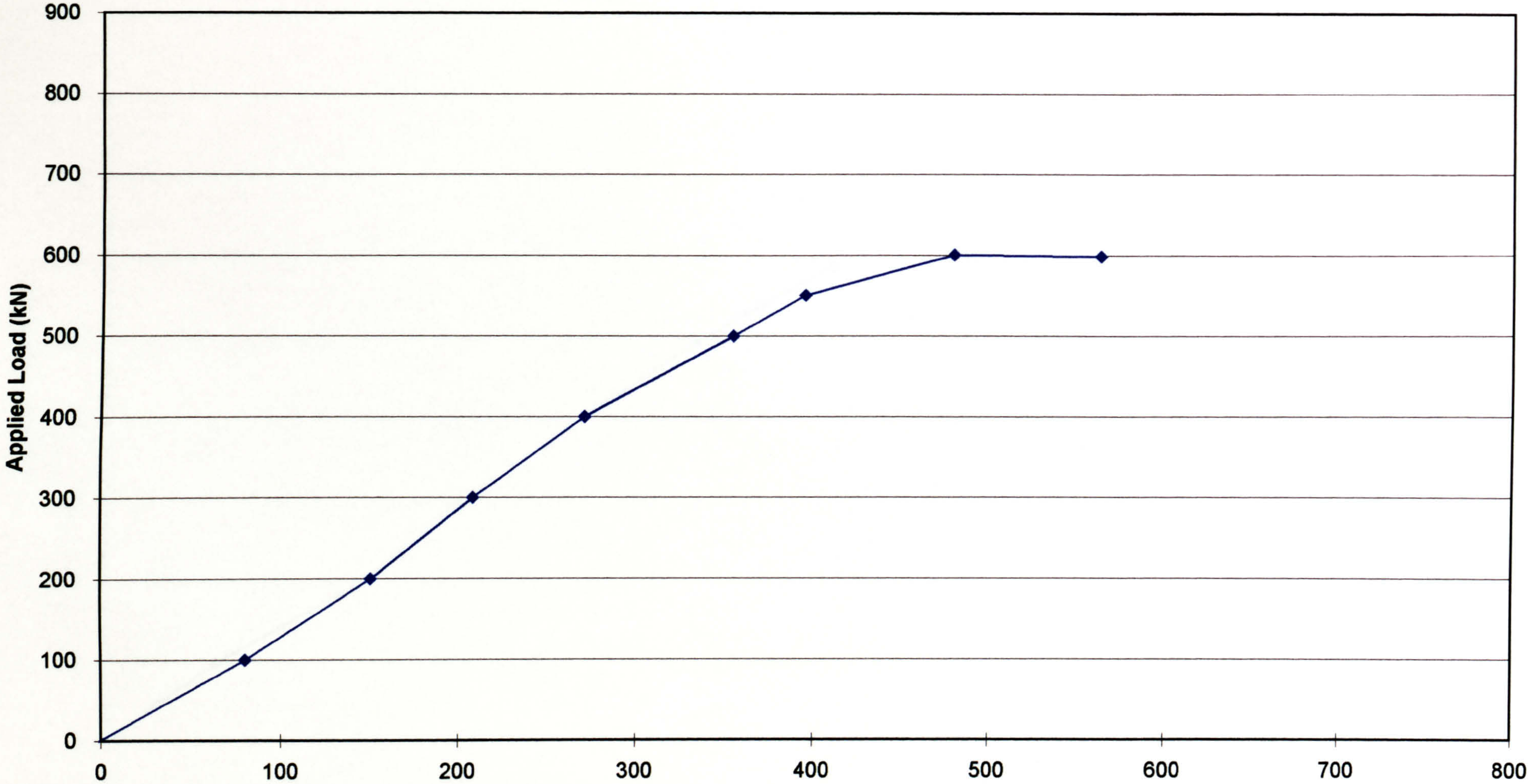

Bar is located along the panel centreline in the second column, 340 mm from mid span.

Figure D.32

Tensile Axial Bar Stresses in City7
(for applied loads in the elastic region)

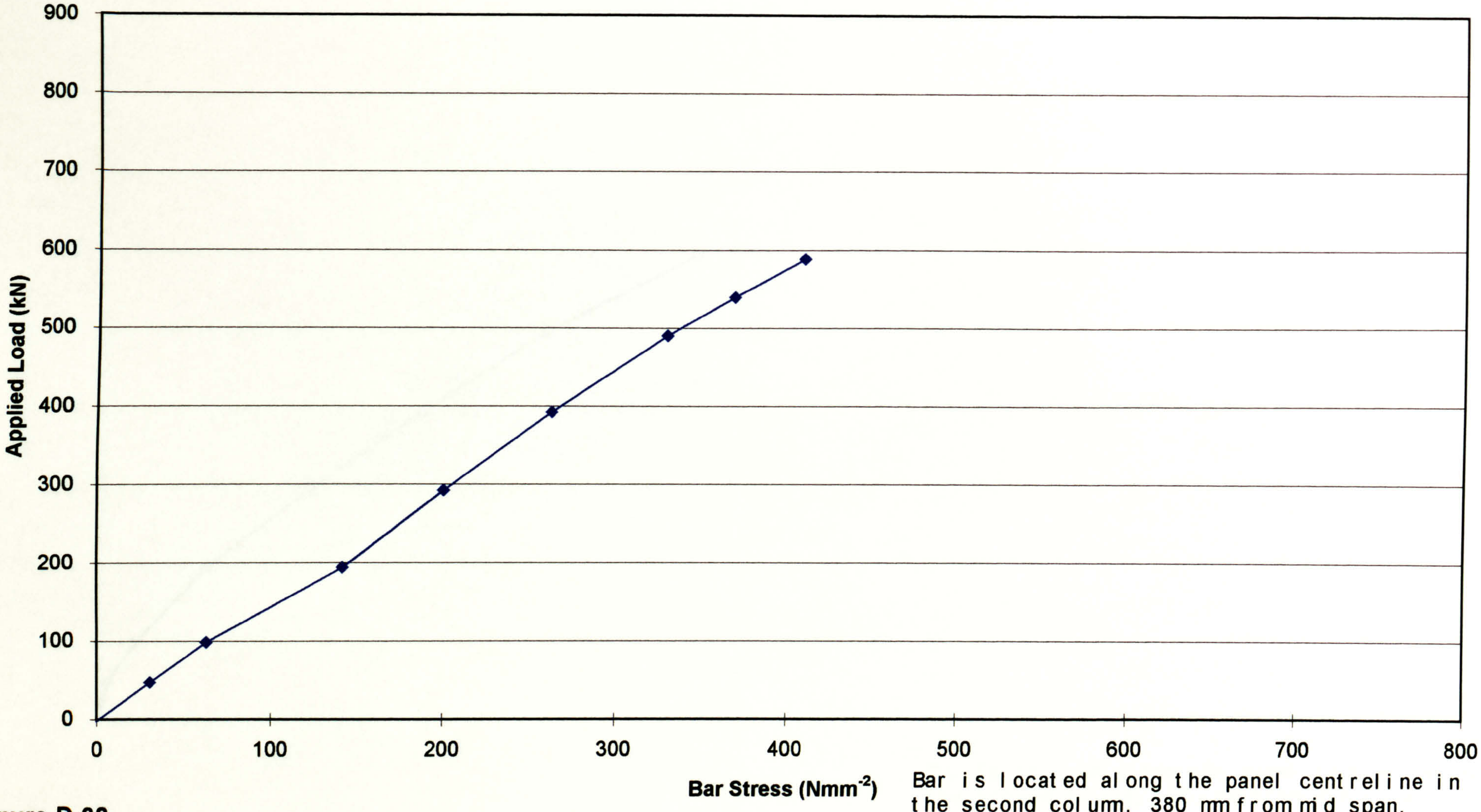

Bar is located along the panel centreline in the second column, 380 mm from mid span.

Figure D.33

Tensile Axial Bar Stresses in City8
(for applied loads in the elastic region)

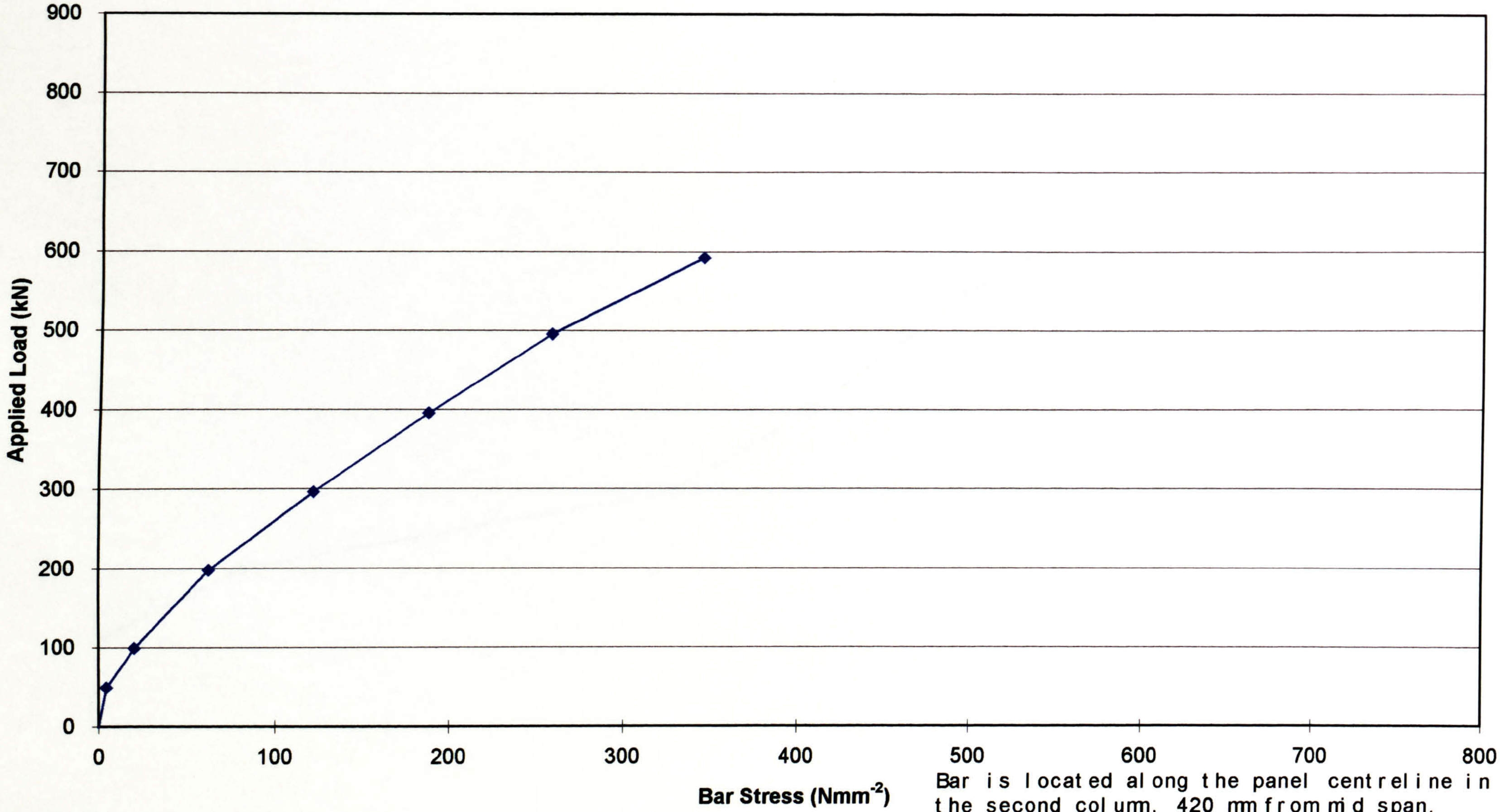

Bar is located along the panel centreline in the second column, 420 mm from mid span.

Figure D.34

Tensile Axial Bar Stresses in City9
(for applied loads in the elastic region)

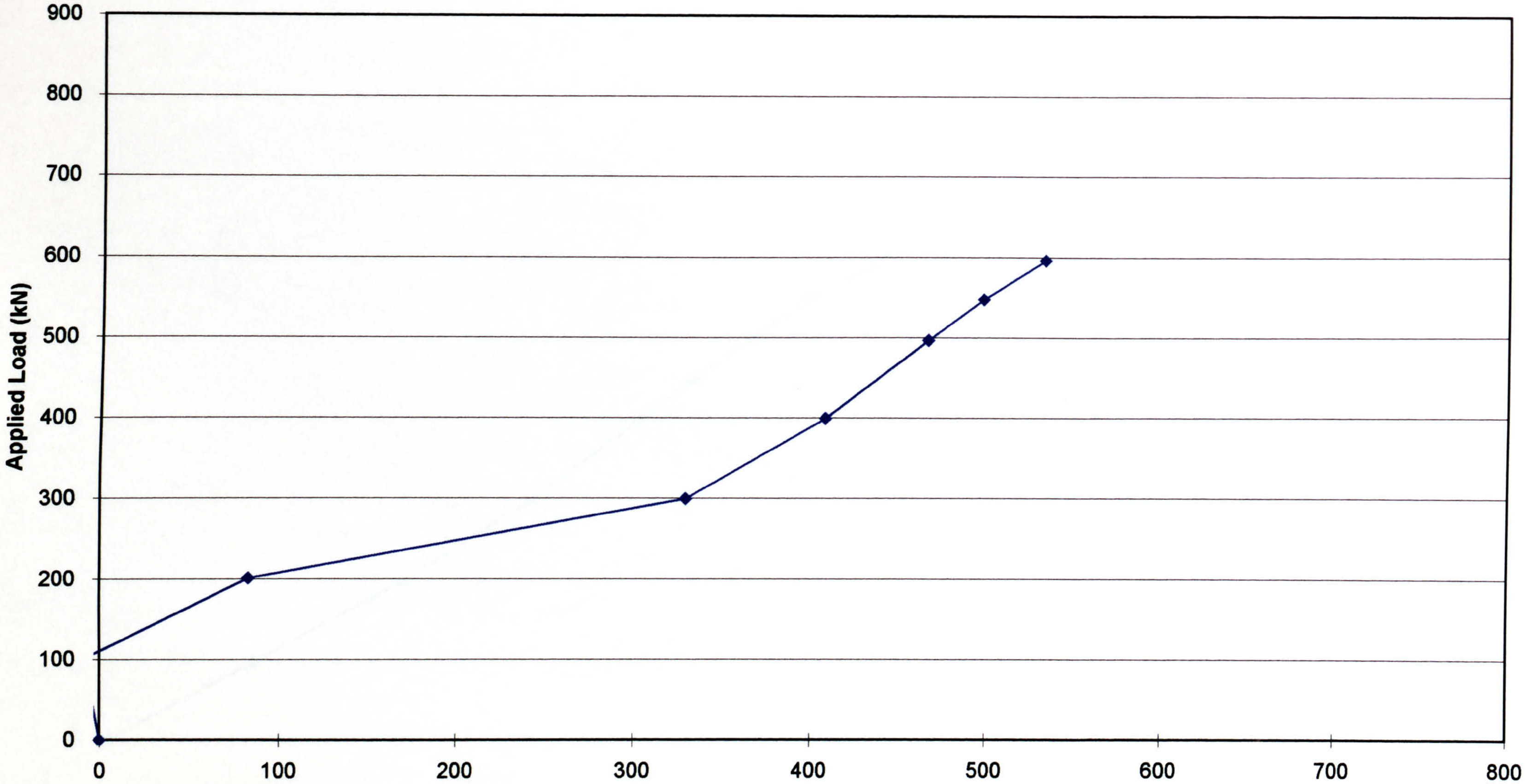

Bar is located along the panel centreline in the second column, 460 mm from mid span.

Figure D.35

Tensile Axial Bar Stresses in City10
(for applied loads in the elastic region)

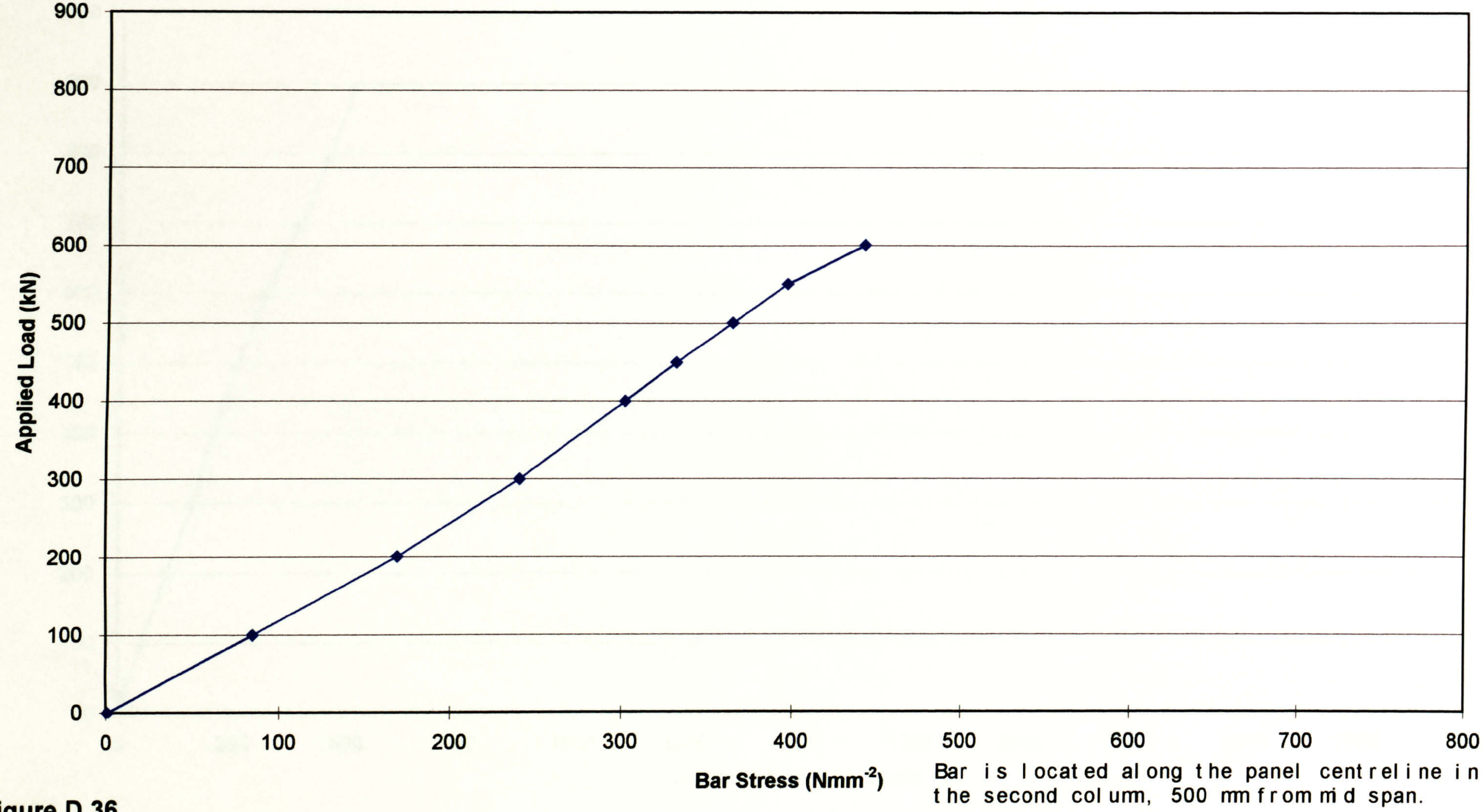

Bar is located along the panel centreline in the second column, 500 mm from mid span.

Figure D.36

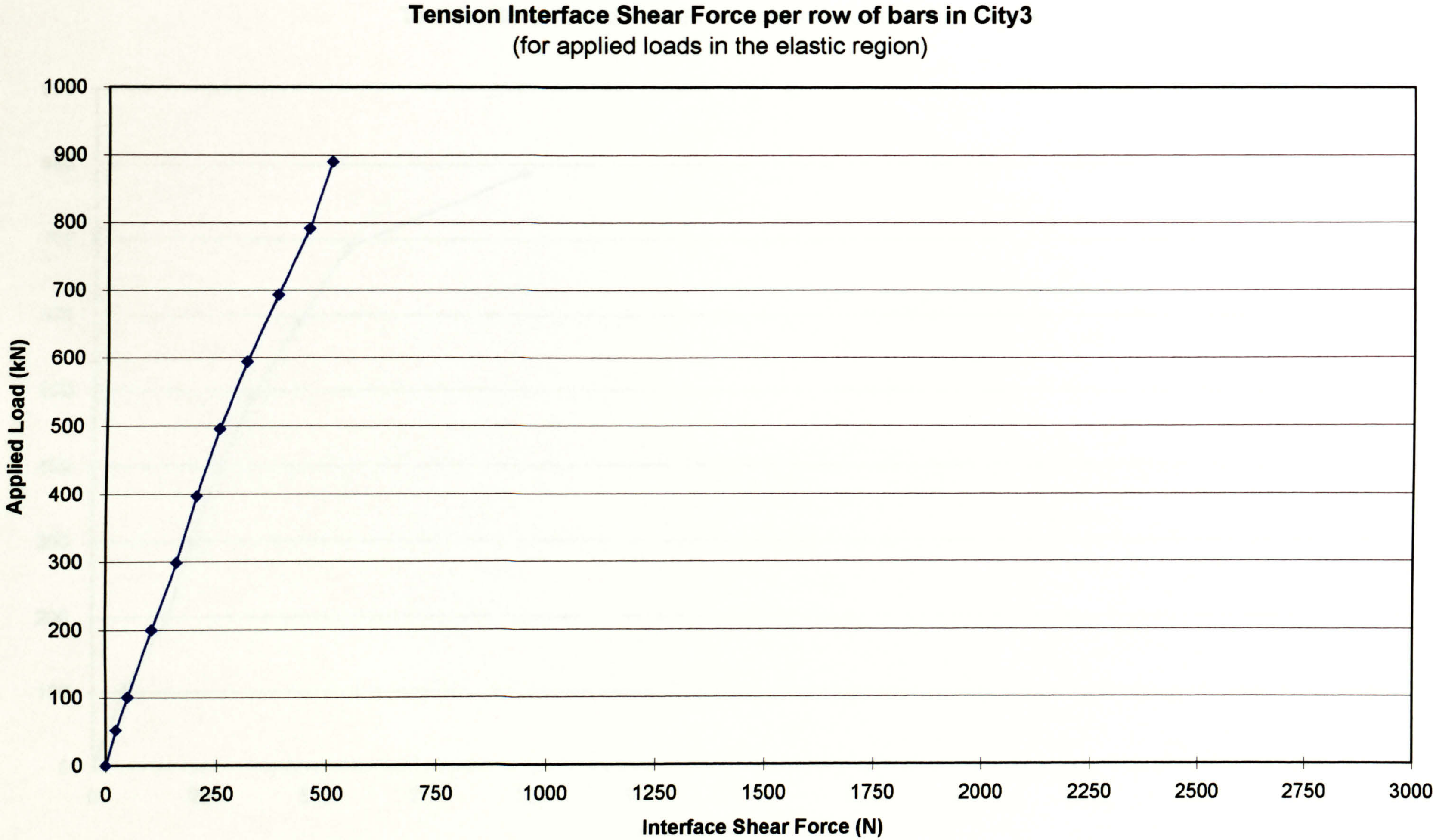
Tension Interface Shear Force per row of bars in City3
(for applied loads in the elastic region)
Applied Load (kN)
1000
900
800
700
600
500
400
300
200
100
0
0
250
500
750
1000
1250
1500
1750
2000
2250
2500
2750
3000
Interface Shear Force (N)

Figure D.37

Tension Interface Shear Force per row of bars in City4a
(for applied loads in the elastic region)

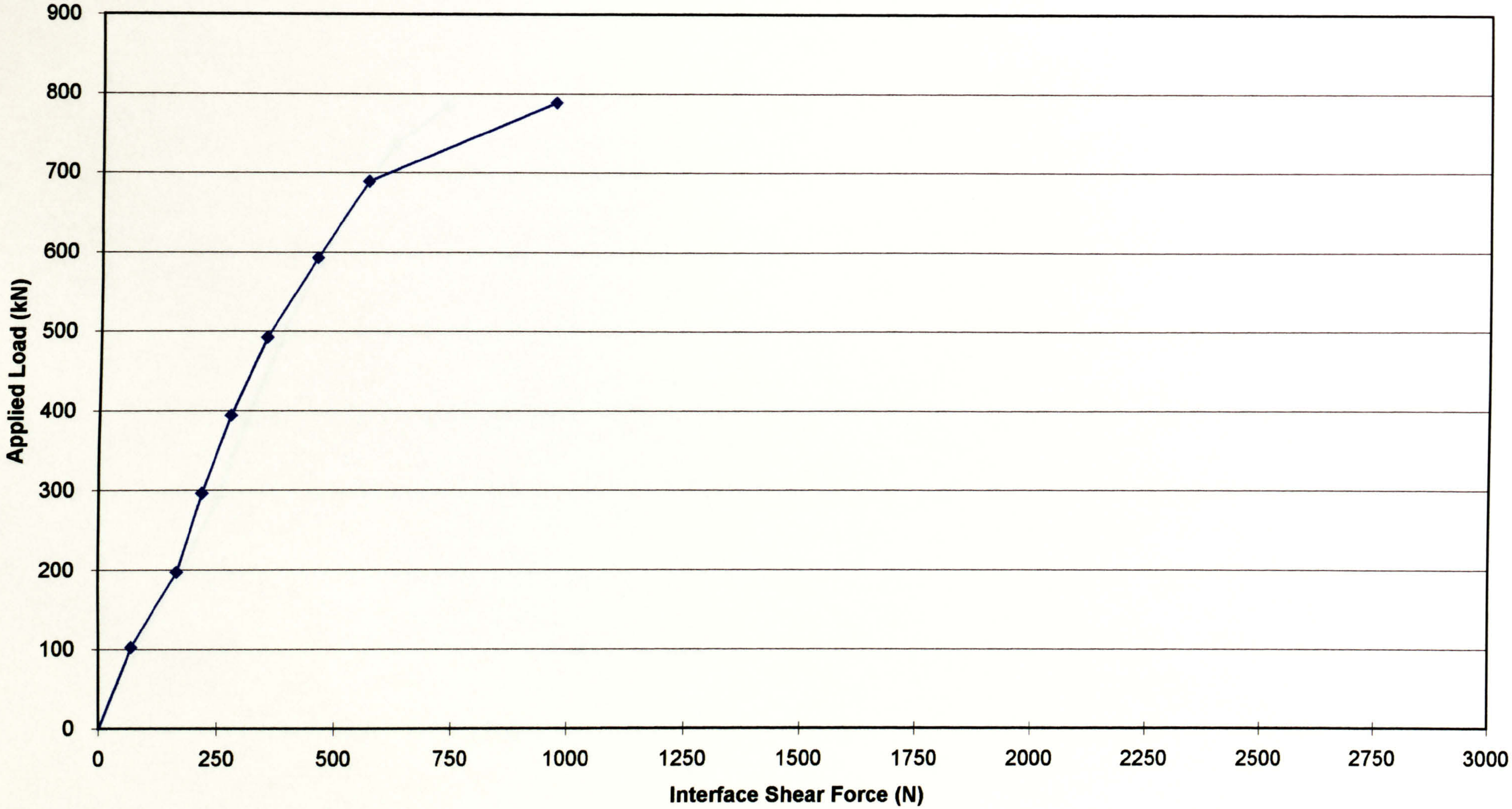

Figure D.38

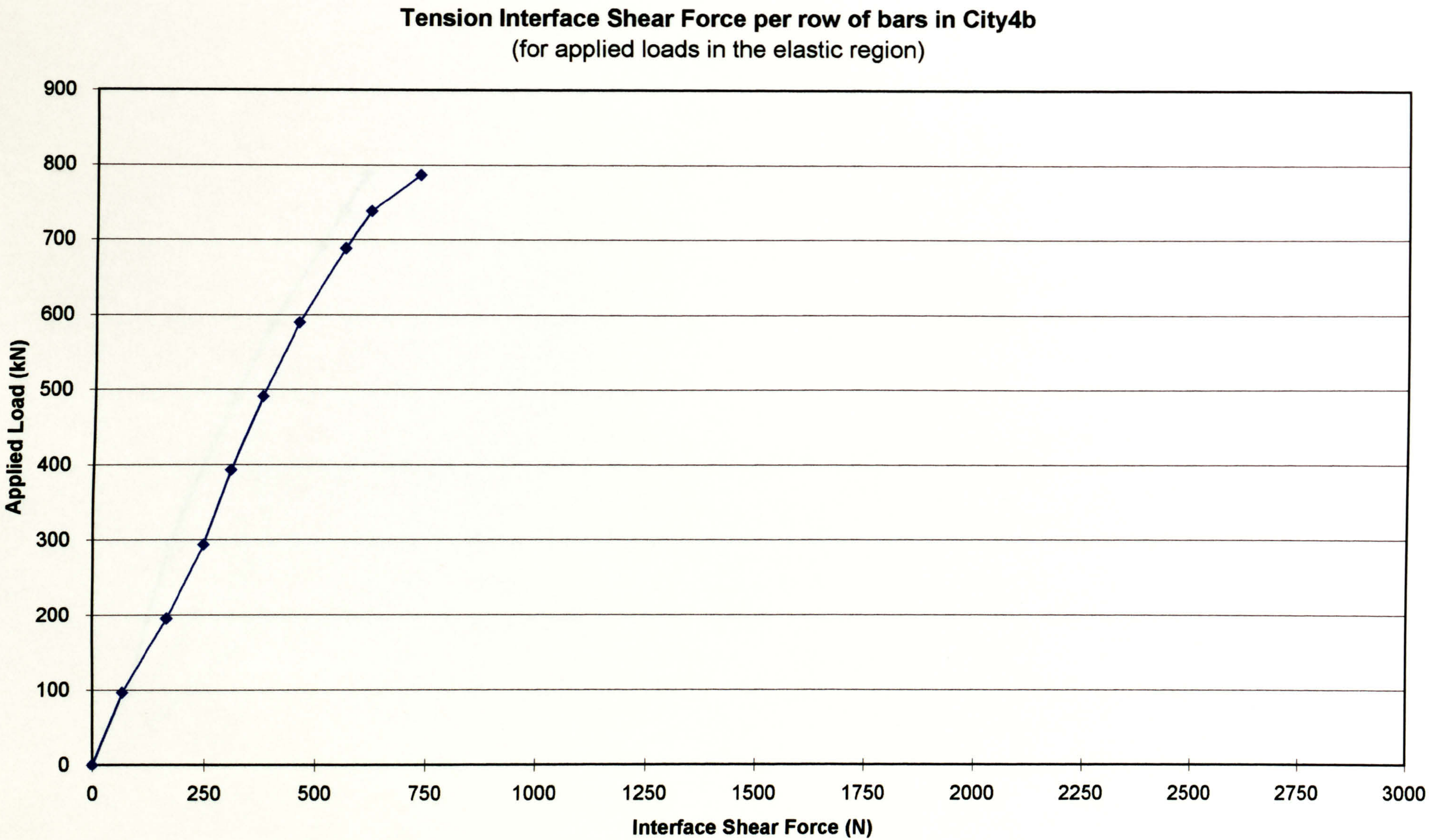
Tension Interface Shear Force per row of bars in City4b
(for applied loads in the elastic region)
Applied Load (kN)
900
800
700
600
500
400
300
200
100
0
0
250
500
750
1000
1250
1500
1750
2000
2250
2500
2750
3000
Interface Shear Force (N)

Figure D.39

Tension Interface Shear Force per row of bars in City4c
(for applied loads in the elastic region)

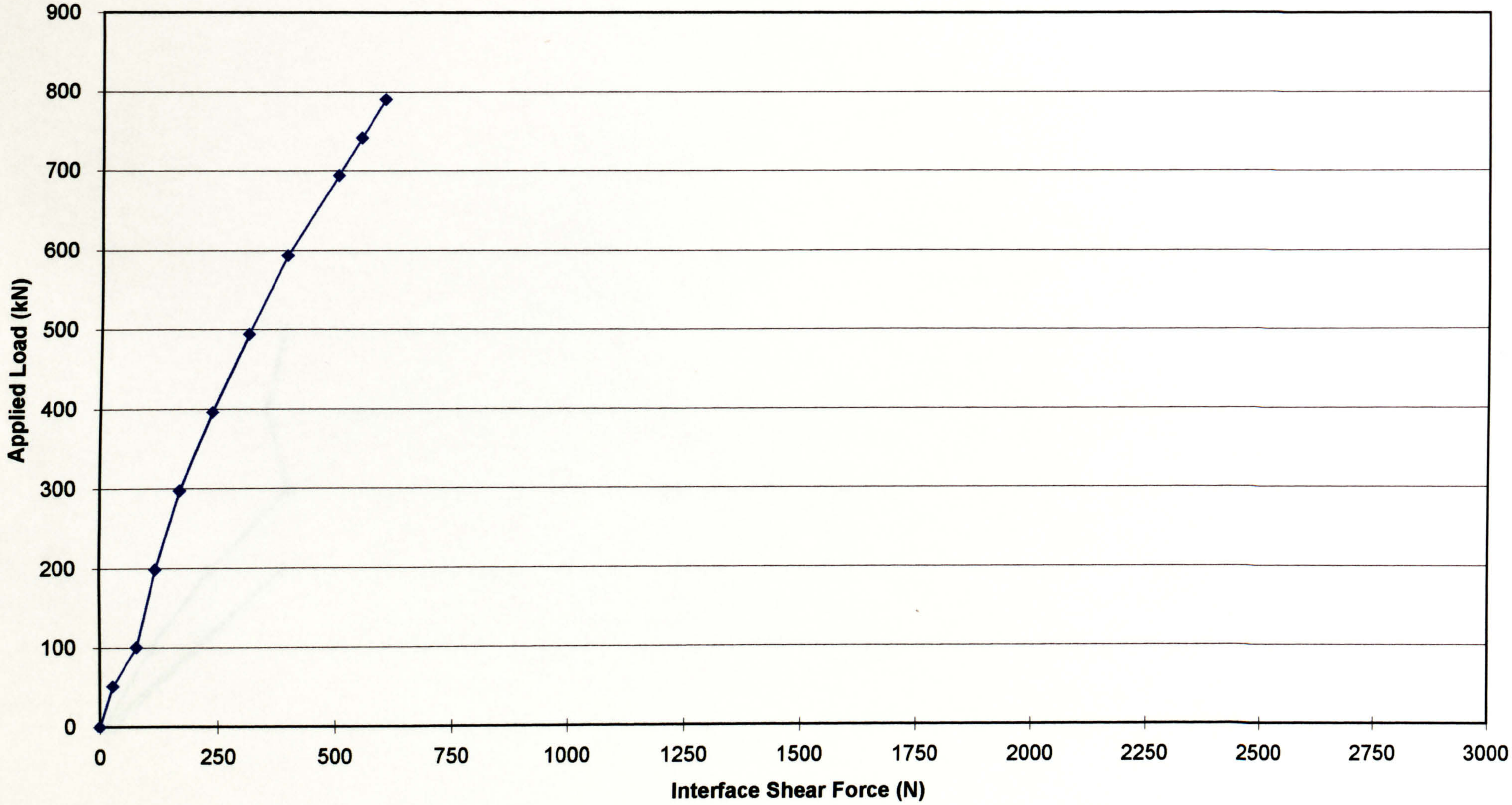

Figure D.40

Tension Interface Shear Force per row of bars in City4d
(for applied loads in the elastic region)

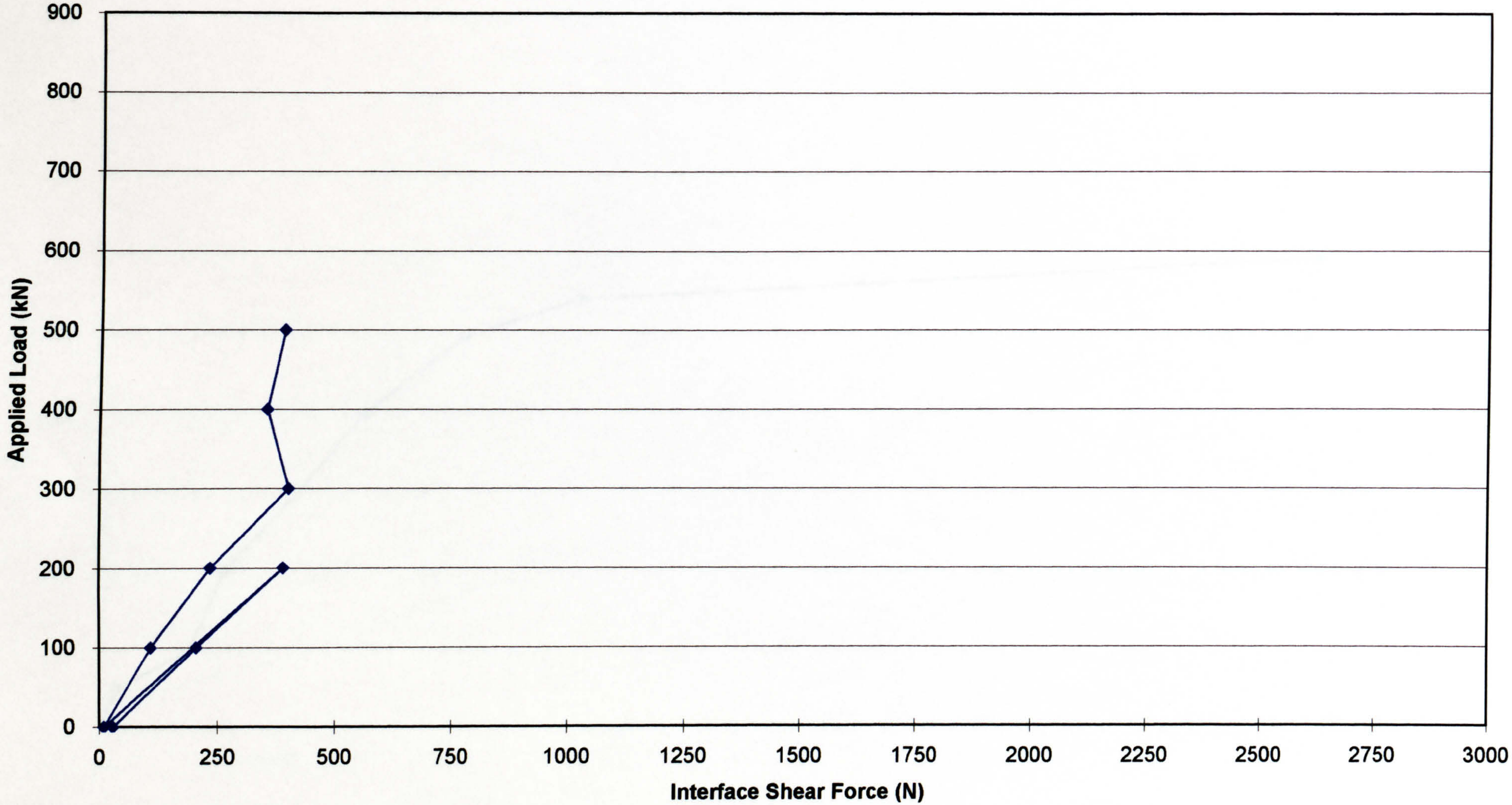

Figure D.41

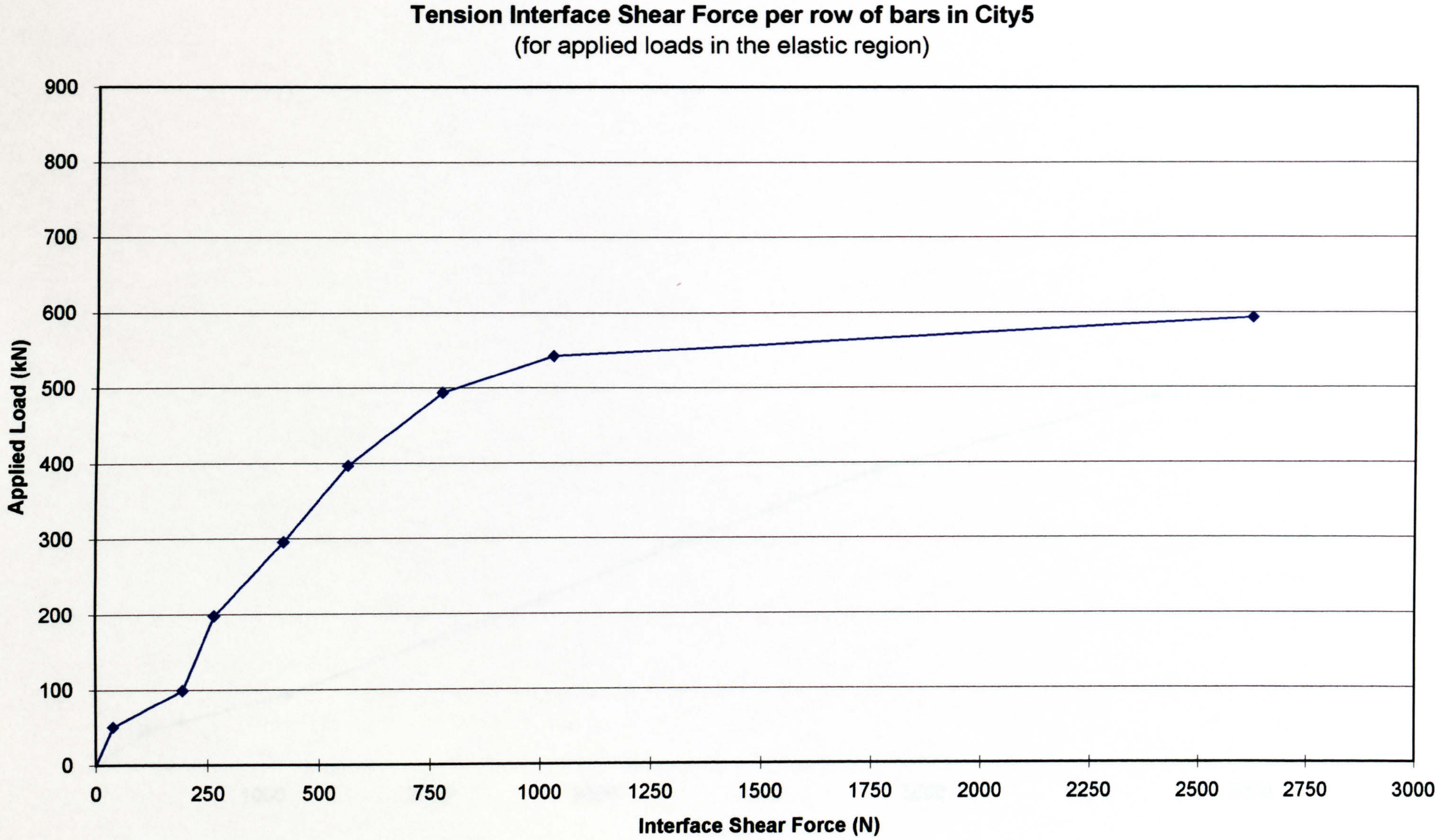
Tension Interface Shear Force per row of bars in City5
(for applied loads in the elastic region)
Applied Load (kN)
900
800
700
600
500
400
300
200
100
0
0
250
500
750
1000
1250
1500
1750
2000
2250
2500
2750
3000
Interface Shear Force (N)

Figure D.42

Tension Interface Shear Force per row of bars in City6
(for applied loads in the elastic region)

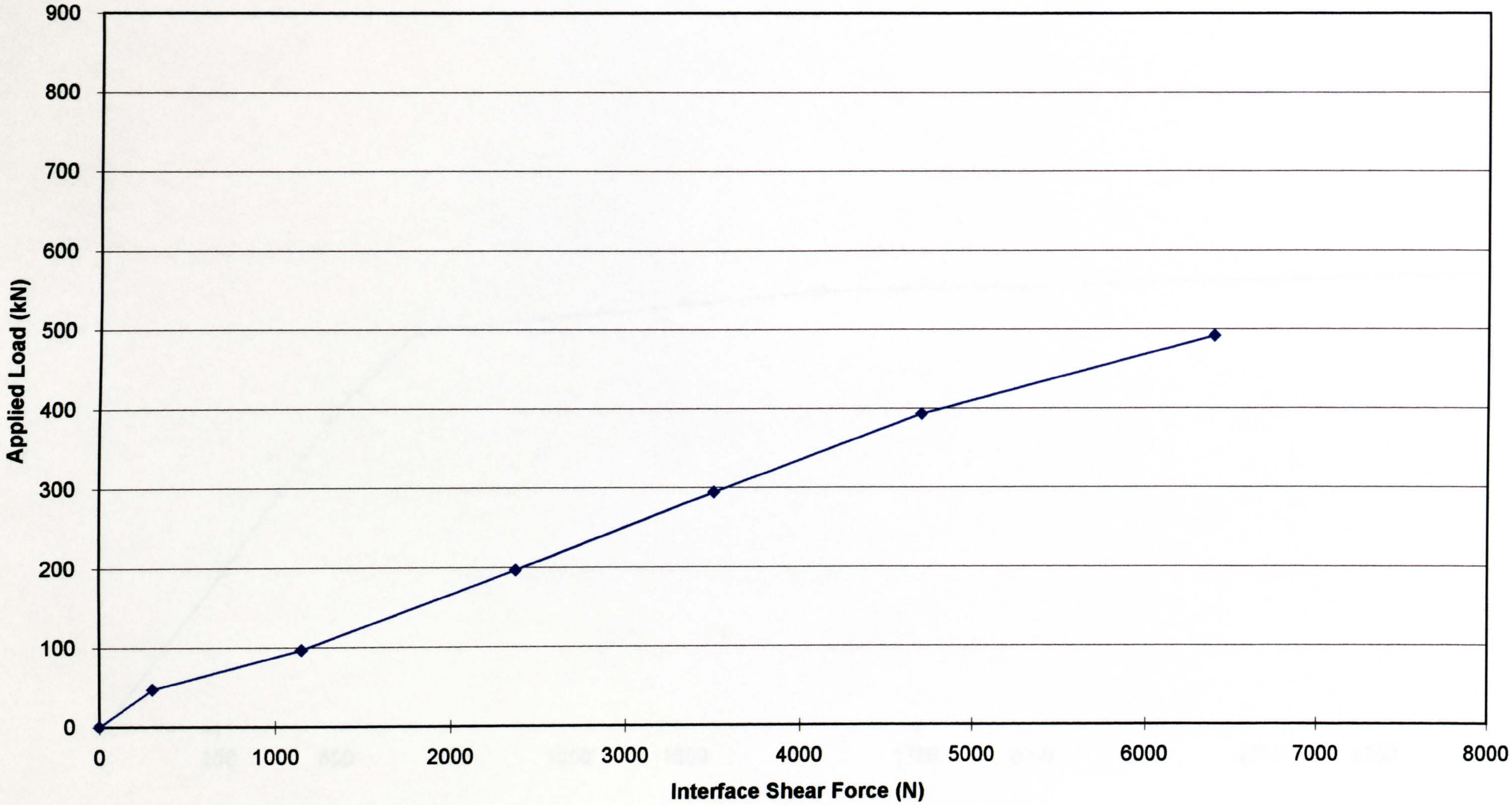

Figure D.43

Tension Interface Shear Force per row of bars in City6b
(for applied loads in the elastic region)

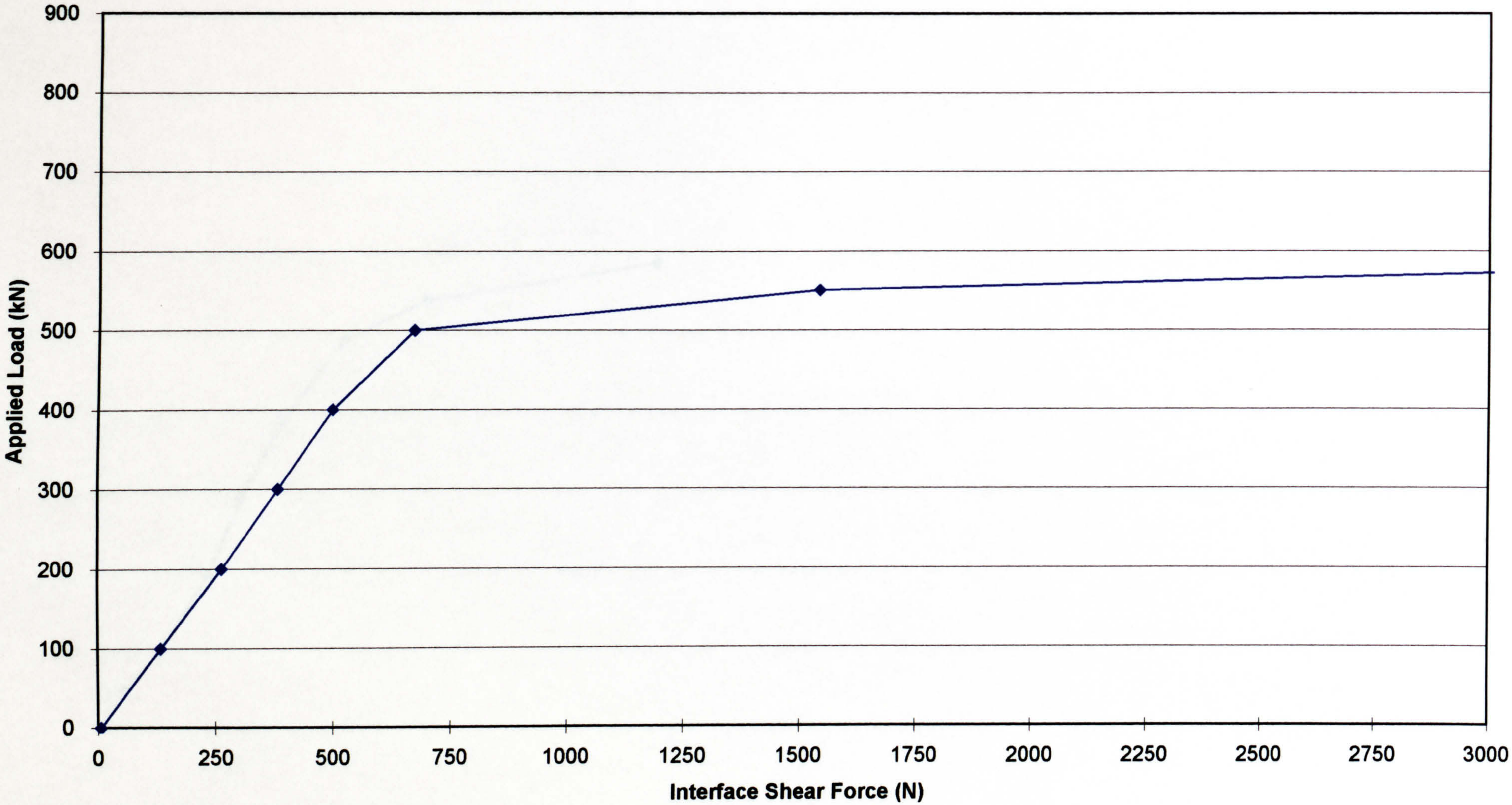

Figure D.44

Tension Interface Shear Force per row of bars in City7
(for applied loads in the elastic region)

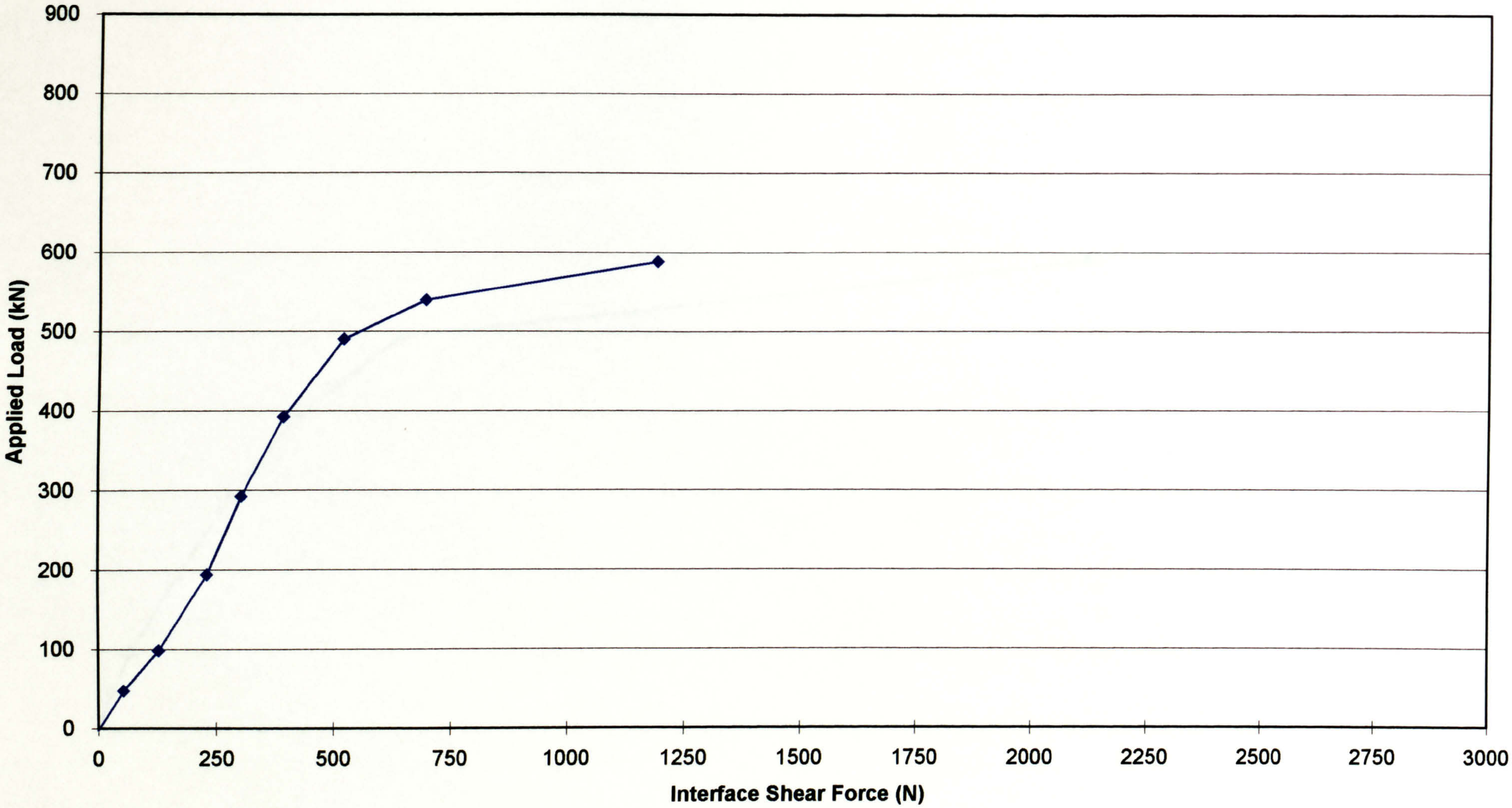

Figure D.45

Tension Interface Shear Force per row of bars in City8
(for applied loads in the elastic region)

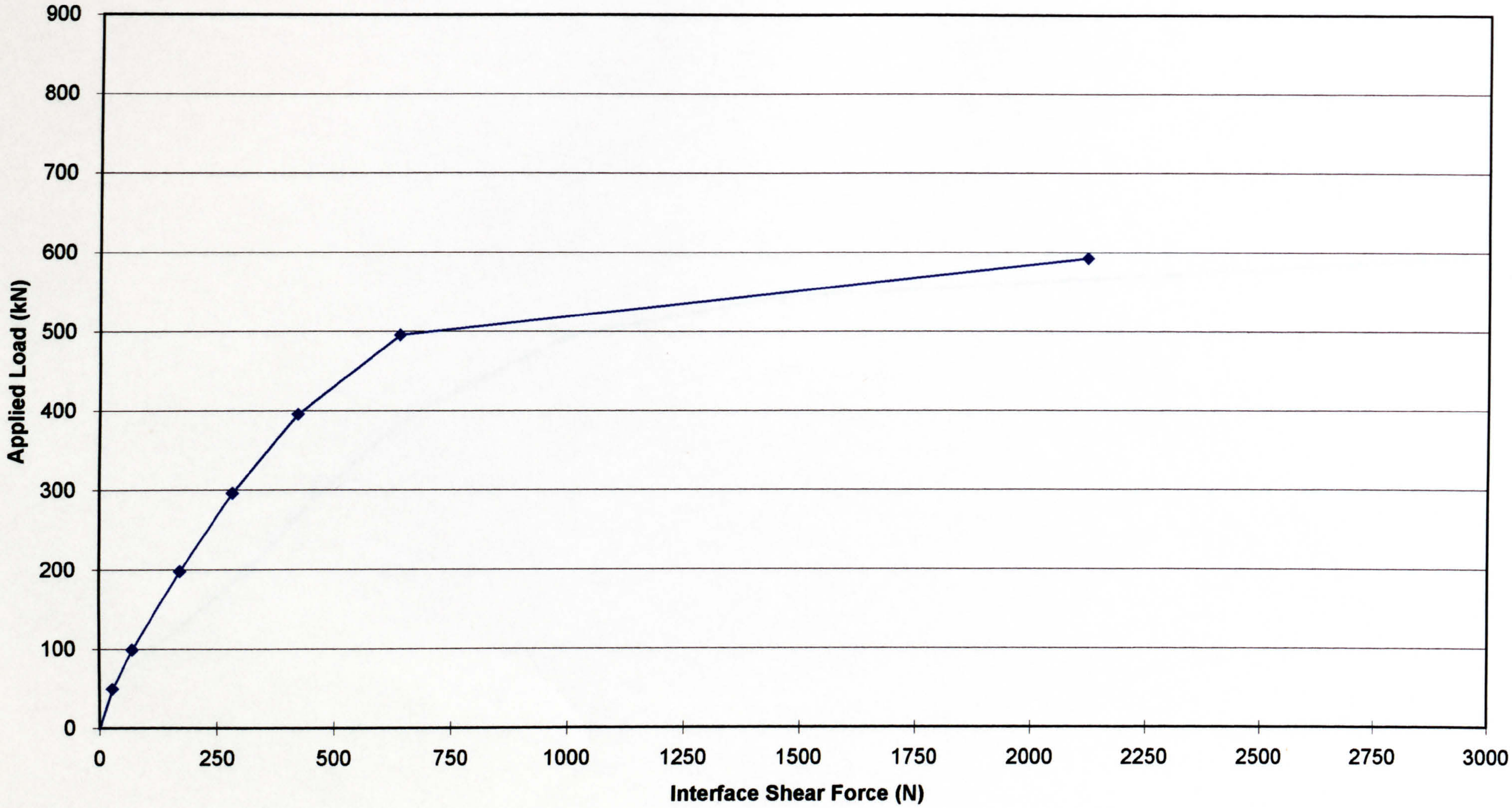

Figure D.46

Tension Interface Shear Force per row of bars in City9
(for applied loads in the elastic region)

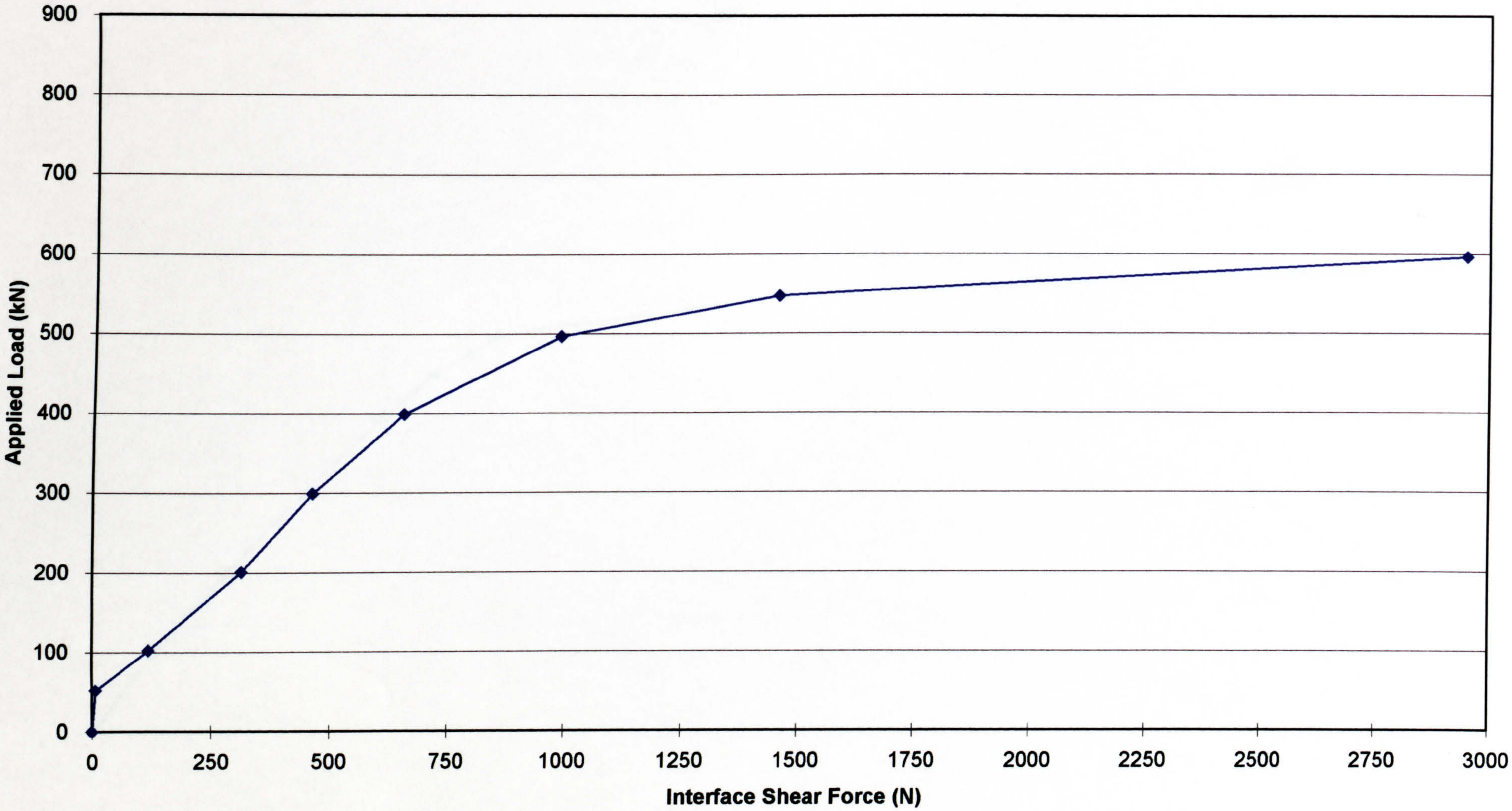

Figure D.47

Tension Interface Shear Force per row of bars in City10
(for applied loads in the elastic region)

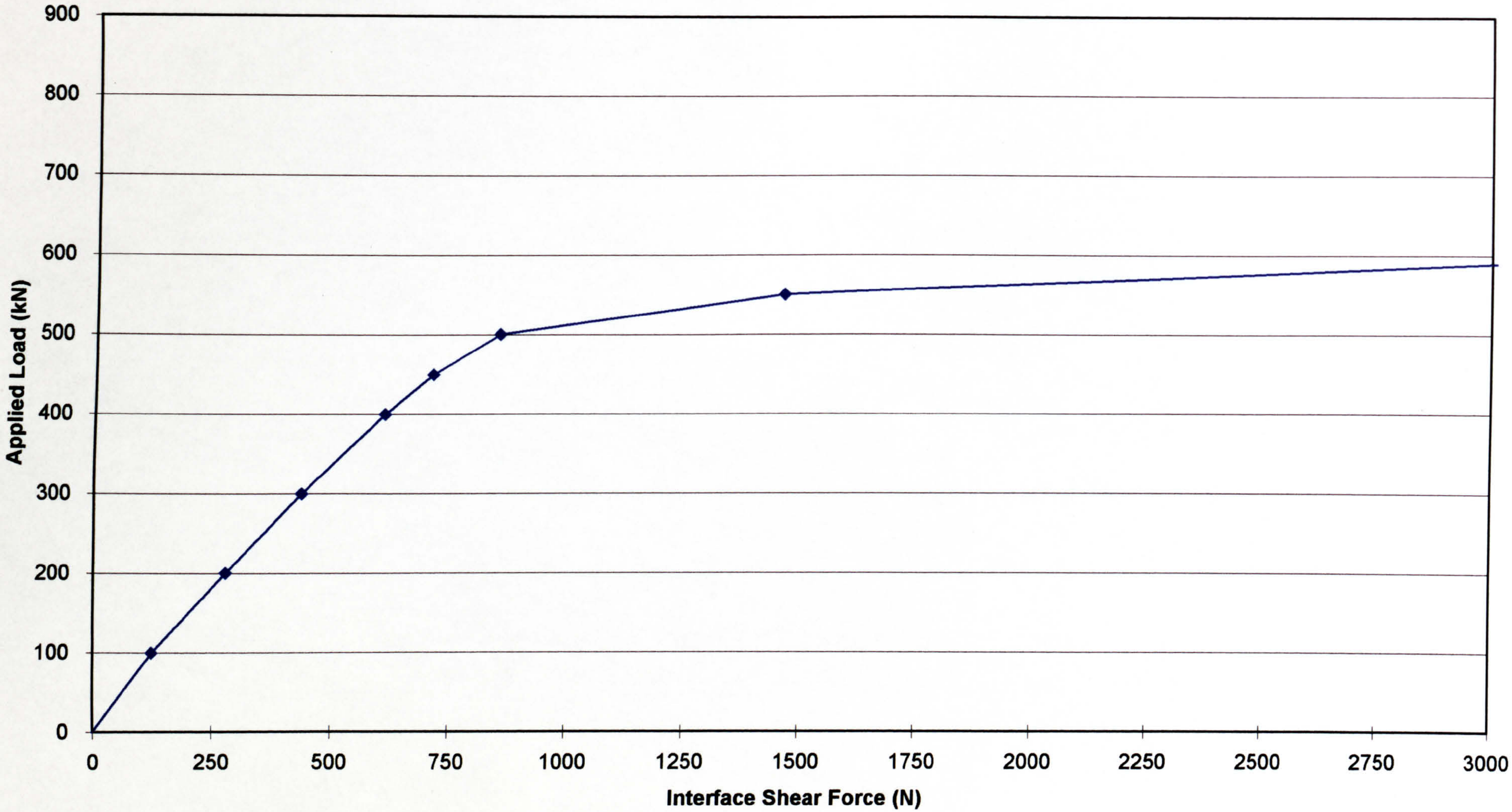

Figure D.48